Interpretation of the aeromagnetic anomalies of mainland Scotland using pseudogravimetric transformation and other methods

Samsudin Hj. Taib

INTERPRETATION OF THE AEROMAGNETIC ANOMALIES OF MAINLAND SCOTLAND USING PSEUDOGRAVIMETRIC TRANSFORMATION AND OTHER METHODS

by

Samsudin Hj. Taib

A thesis submitted for the degree of

Doctor of Philosophy in the University of Durham

Graduate Society March 1990

ABSTRACT

A procedure to upward continue magnetic anomalies observed on an irregular surface onto a horizontal plane has been developed and applied to the aeromagnetic map of Great Britain. Pseudogravimetric transformation was then carried out on this reduced anomaly and both data sets have been used for analysis and interpretation of several prominent anomalies in Scotland along the Great Glen fault and over the Midland Valley.

A prominent linear positive magnetic anomaly occurring along the Great Glen fault has been modelled as due to a locally magnetized outward dipping body almost symmetrical about its apex beneath the fault line, together with a magnetized crustal slab to the northwest of the fault. The outward dipping body has its top lying within the upper crust, a magnetization of greater than about 1.0 A/m, a half-width of about 40 km at its base and a thickness of the order of 7-18 km. The origin of the outward dipping magnetized body may possibly be explained by metamorphism produced by frictional heating resulting from the transcurrent fault movement. Alternatively the metamorphism may be associated with some other fault related process such as crustal fluid flow. Thermal modelling has been used to demonstrate this. The magnetization contrast across the fault may be the direct result of blocks of differing magnetization on opposite side, juxtaposed as a result of transcurrent movement.

The modelling along a profile over the Clyde Plateau (Midland Valley of Scotland) using a well-constrained lava body reveals the presence of a long wavelength anomaly component due to a deeper crustal source. The basement anomaly is conspicuous on the pseudogravimetric map but not on the aeromagnetic map. A near circular magnetic anomaly near Bathgate in the Midland Valley can be explained by an unexposed intrusive body superimposed on the deep crustal source as above.

ACKNOWLEDGMENTS

I am most grateful to my supervisor Professor M. H. P. Bott for his invaluable suggestions, criticism and advice throughout the the course of this project.

I would like to thank:

The British Geological Survey for providing the aeromagnetic, topographic and borehole data, and the staff who have assisted in the data acquisation, Dr. D. M. McCann, Mr. R. Gillanders and especially Mr Ian Smith for his numerous help particularly in arranging access to the BGS geophysical databank.

The staff in the Department of Geological Sciences, University of Durham, Dr. J. G. Holland and Dr. C. H. Emeleus, and colleagues.

The University of Malaya for providing the study grant and allowing me to remain on leave throughout the course of this study.

I am grateful to my family, my wife for her patience, encouragement and assistance in typing and reading the manuscript.

CONTENT

CHAPTER 1

Introduction

1.1 Scope of studies

The main objective of the project is to study the origin of some of the long and medium wavelength magnetic anomalies of northern Great Britain. These may be caused by either deep subsurface structures or shallow sources having a wide lateral extend. Some of these anomalies can be correlated to near surface features such as the Carboniferous lavas of the Clyde Plateau. Some may be related to deep features associated with surface structure such as the Great Glen fault. Others have no obvious association with the surface geology such as the medium wavelength anomaly over Bathgate. The study aims to contribute to an understanding of the magnetic crust underlying northern Great Britain and particularly concentrates on the major anomalies associated with the Great Glen fault and the Midland Valley of Scotland.

Magnetic anomalies have a complicated relationship to their source bodies. This is partly because of the oblique dip direction of the total field and the magnetization which produces asymetry. Furthermore, the magnetization is dipolar. The dipole nature of the magnetic source results in a more complicated field than a monopole source as in gravity. These factors prevent direct correlation of the causative body to the magnetic anomaly. Shallow magnetic sources produce unduly prominent short wavelength anomalies and these add to the complexity and may make the identification and interpretation of the medium and long wavelengths anomalies difficult. For these reasons, it has been found useful to use the simpler pseudogravimetric anomalies to assist interpretation of the longer wavelength anomalies. As the aeromagnetic data was observed at variable height, it needs to be reduced to a plane at constant

height prior to the pseudogravimetric transformation.

There has been some previous interpretation of medium and long wavelength aeromagnetic anomalies of northern Britain. Powell (1970) and Hall and Dagley (1970) studied some of the anomalies of the aeromagnetic map of Great Britain and Northern Ireland (scale 1:250000). Powell (1970) correlated the aeromagnetic anomalies of northern Great Britain to the surface magnetization, thus identifying the near surface sources and the deeper sources. Hall and Dagley (1970) digitised the contour map on a 3.5 km grid spacing, interpolating between contour lines where necessary. A general correlation of the magnetic highs and structural features was made. Based on this map, Powell (1978a) suggested a regional magnetic basement for northern Britain and described the sources for some of the broader anomalies. Bott et al. (1972) interpreted a positive long wavelength anomaly in the Scourie-Durness region as due to shallowing of the Scourian basement rocks. Hossain (1976) presented two different models to explain the Bathgate anomaly, a body near the surface and a body within the middle crust.

This thesis describes the data retrieval and treatment, gives the background of the interpretation methods used and reports on the analysis and interpretation of (1) the linear positive long wavelength anomaly along the Great Glen fault and (2) the medium and long wavelength anomalies over the Midland Valley of Scotland.

1.2 The pseudogravimetric transformation

The pseudogravimetric transformation was first introduced by Baranov (1957). He used a surface integral method to convert a magnetic anomaly to a pseudogravimetric anomaly. The pseudogravimetric transformation is based on the Poisson relation between gravity and magnetic potential. The Poisson relation is valid provided that the density to magnetization ratio is constant and the magnetization is in a

constant direction. The method requires knowledge of the direction of magnetization which has been taken as the present field direction in most of this work (as is justified later).

Baranov (1957) recognised the advantages of using the method to overcome some of the problems related to interpretation of magnetic data. The skewness of the anomaly is removed and the resulting pseudogravimetric anomaly is symmetrical with respect to the causative body. Another advantage of the pseudogravimetric transformation is that the troublesome short wavelength components of the magnetic anomaly are suppressed. This avoids the necessity of filtering out the large amplitude anomalies caused by the smaller but strongly magnetized shallower sources. The transformed data emphasizes the longer wavelength components. The pseudogravimetric anomalies are symmetrical about the causative body and monopole in character, so that they have the same relationship to the source as does the gravity anomaly. The specified constant ratio of density to magnetization enables the conversion of the magnetization contrast to a fictitious density contrast for use with gravity interpretation methods. For bodies which are wide in comparison to their depth extent, the simple slab formula of gravity can be used to give a quick estimate of the product of thickness and magnetization of the causative body (i.e. the magnetic moment per unit area).

Fourier methods have been used to compute the pseudogravimetric anomalies in this project, as described by Cordell and Taylor (1971). The Fourier method as applied here makes use of the fast Fourier transform (Cooley and Tukey 1965), which provides a fast and efficient computer-based method particularly suitable for large data sets. The potential field formulae such as for the pseudogravimetric transformation are less cumbersome in the frequency domain than in the spatial domain. Another advantage of the frequency domain method is the similarity of the formulae for the two and three-dimensional transformations.

The procedure developed to upward continue the aeromagnetic anomaly observed on an irregular surface onto a horizontal plane also utilises the the fast Fourier transform. It is a further development of the Cordell (1985) procedure for upward continuation from a horizontal plane onto an irregular surface.

1.3 Data handling and modelling

This work is based on digitised aeromagnetic data provided by the British Geological Survey (BGS). The digitised data were observed along flight lines and have been resampled onto a regular grid. The gridding is required by the fast Fourier transform procedures used in the subsequent data treatment, including the upward continuation of the magnetic data onto a horizontal level and the pseudogravimetric transformation of the magnetic data. The map of the gridded data upward continued onto a horizontal plane and the pseudogravimetric map are shown in figures 1.1 and 1.2 respectively for the whole Britain.

The digitised data provided by BGS is archived in the BGS geophysical data bank in Keyworth. The digitisation has been carried out by BGS directly from survey data along the flight lines at 10 nT interval. During the earlier part of the project the digitisation at BGS was still in progress so that the data has been retrieved progressively. The Joint Academic Network, an inter site computer link, was used to transfer the data to Durham.

The gridding to a regular 2x2 km^2 grid has been carried out using the Surface2 packages (Sampson 1975) prior to analysis. The data which was acquired at variable absolute height was then upward continued onto a horizontal plane using the reduction procedure developed. The pseudogravimetric transformation has been carried out on this upward continued data (figure 1.1) giving the pseudogravimetric map in figure 1.2.

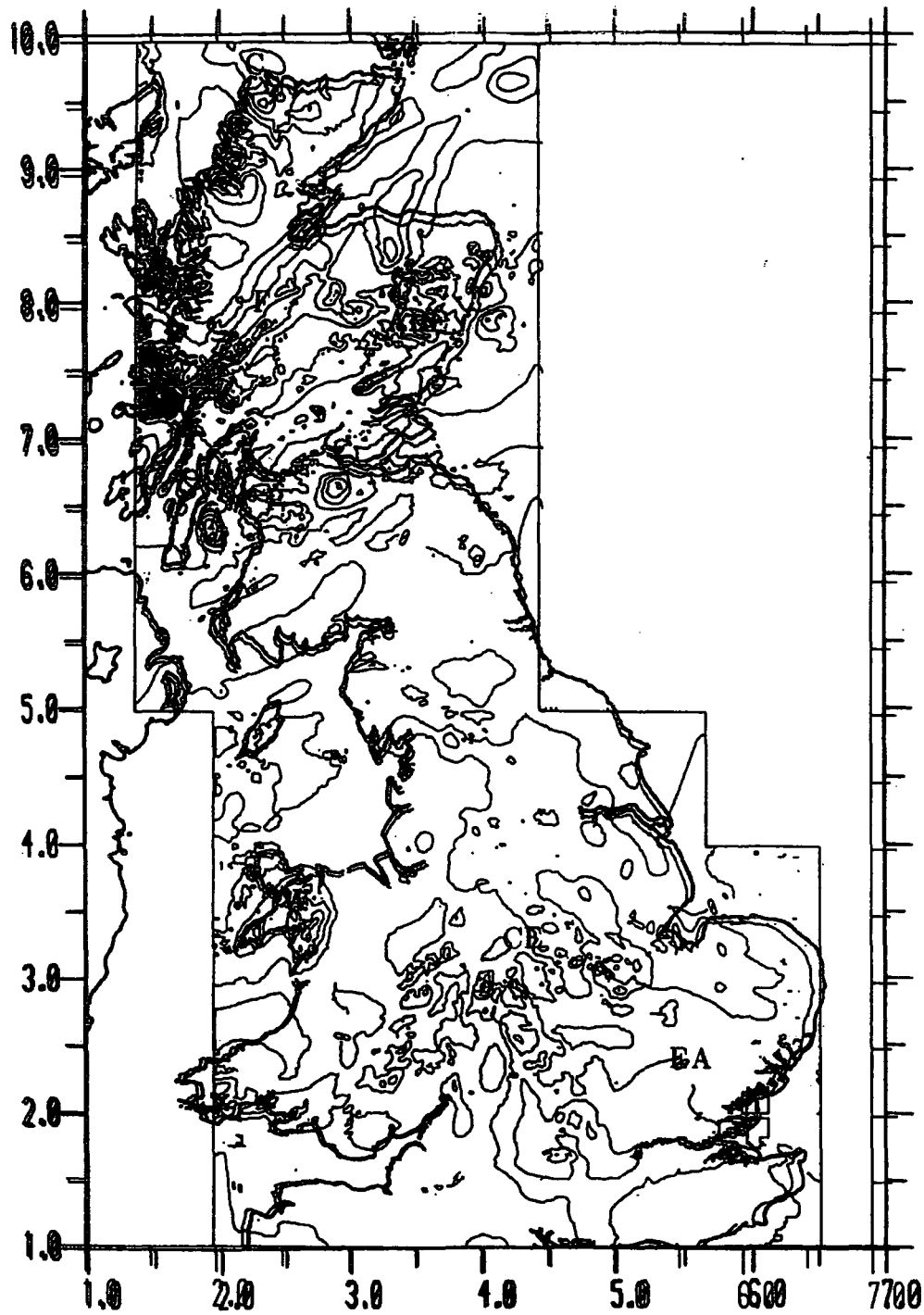

C-Cape Wrath, G-Gruinard Bay, F-Great Glen fault, ABE-Aberdeenshire, A-Arran, P-Clyde Plateau, CE-Central England, W-North Wales, EA-East Anglia

Figure 1.1 Aeromagnetic map of Great Britain digitised on a 2x2 km^2 grid. The contour in 100 nT. The coordinates are in 10^2 km British National grid.

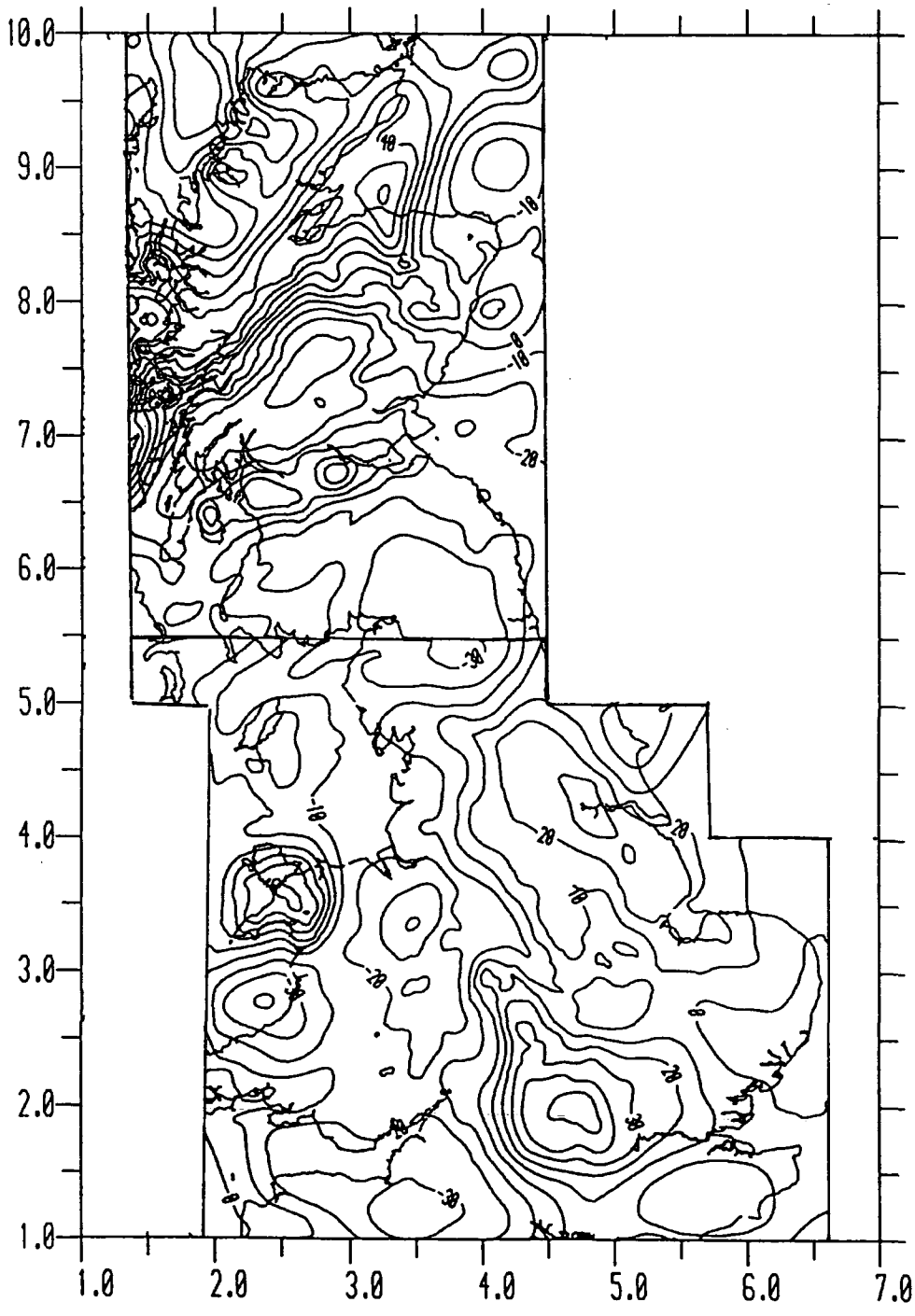

Figure 1.2 Pseudogravimetric map of Great Britain transformed from the aeromagnetic map in figure 1.1. The transformation has been carried out in two different blocks (north and south) with an overlap region between the 500 and 600 km north. The background values for the two blocks are different. The density (kg/m^3) to magnetization (A/m) ratio is 150:1.0. The inclination and declination for the magnetization and the earth's magnetic field are 70.3^o and -10.4^o respectively. The contour interval is 10 mGal. The coordinates are in 10^2 km British National grid (BNG).

Modelling has been mostly carried out using two-dimensional methods. The pseudogravimetric anomaly has been modelled using standard two-dimensional modelling of the gravity effect. This is only applicable for sources having a wide extent along strike. Two dimensional modelling with an end correction factor has been used where the along strike extent of the causative body is limited. Non-linear optimisation methods (James and Roos 1969) have been used to speed up the modelling and to obtain more accurate fit.

1.4 The magnetic and pseudogravimetric map of Britain

The magnetic map of Great Britain (Figure 1.1) shows areas of high magnetization indicated by positive magnetic anomalies. The magnetic anomalies are of varied wavelengths and display different shapes indicating the varied nature of the sources. The regional trend of the anomalies generally follows the basement structural trend of the area.

Along the northwest coast of mainland Scotland, a slightly elongated long wavelength anomaly occurs south of Cape Wrath. This has been associated with shallow granulites (Scourian assemblage, Bott et al. 1972). The positive anomaly over Gruinard Bay is probably caused by a similar source. The two anomalies are complicated by the presence of shorter wavelength anomalies between them. Southeast of these anomalies, a linear positive anomaly trending northeast-southwest superimposed by short and medium wavelength anomalies occurs along the line of the Great Glen fault. To the east and south of this linear positive anomaly, short to medium wavelength anomalies dominate the area. These are mainly attributed to shallow lying sources such as the ultra basic rocks in Aberdeenshire. Over the Midland Valley of Scotland a chain of positive short to medium wavelength anomalies traverses the region. Over Arran and the Clyde Plateau area, the anomalies are associated with the Tertiary volcanic centre and the Carboniferous lavas respectively. Between the

Midland Valley of Scotland and Central England, the magnetic features are mainly represented by low amplitude long wavelength anomalies. South of this region the magnetic feature cause short to long wavelength anomalies, some of which are associated with shallow volcanic rocks (e.g. North Wales) and magnetic basement (East Anglia, Allsop, 1985).

The pseudogravimetric transformation clearly results in a simpler map compared to the magnetic map (figure 1.2). The short wavelength anomalies are suppressed and the long wavelength components enhanced. The two slightly elongated magnetic anomalies along the northwest coast of mainland Scotland become less complicated. The linear positive magnetic anomaly along the Great Glen fault is enhanced, the short wavelength anomalies are suppressed. Over the Midland Valley of Scotland the pseudogravimetric transformation reveals an elongated long wavelength anomaly not obviously present on the magnetic map. Shorter wavelength anomalies caused by the lavas over the Clyde Plateau are superimposed. In England, regions of high magnetization in the crust produce substantial pseudogravimetric anomalies. The pseudogravimetric anomalies give a much better indication of major deep-seated magnetization than the magnetic map.

1.5 Pattern of the thesis

The method of data retrieval from the BGS data bank is described in the earlier part of chapter two. This is followed by the theory and procedure for upward continuation of the aeromagnetic anomalies onto a horizontal plane. The tests and limitations of the method are then described. Chapter three gives the derivation of the pseudogravimetric method and discusses the results of tests on the method and its limitations. A brief description of the other interpretation methods used is then given.

The interpretation of some major Scottish magnetic and pseudogravimetric anomalies forms the subject of chapters four and five. Chapter four describes the analysis and interpretation of the conspicuous linear positive magnetic anomaly along the Great Glen fault. The magnetic and pseudogravimetric modelling is first discussed. A brief description of heat generation along a transcurrent fault and and the associated temperature distribution in the crust are then given. The theory of the finite difference procedure used in the calculation of the temperature field is given. The thermal modelling is applied to the Great Glen fault in an attempt to explain the origin of the anomaly. Other possible modes of origin, such as crustal fluid flow are also discussed.

Chapter 5 describes the analysis and interpretation of the medium and long wavelength magnetic and pseudogravimetric anomalies of the Midland Valley of Scotland. Modelling of the well-constrained Clyde Plateau lavas reveals the presence of a supplementary deeper crustal source. The result has been used to assist the modelling of the local Bathgate anomaly. Chapter six gives a summary of the work done and discusses possible extension.

CHAPTER 2

Aeromagnetic data and the upward continuation of magnetic anomaly from an irregular surface onto a horizontal plane

2.1 Data sources

The aeromagnetic data of Great Britain has been obtained from the British Geological Survey (BGS), Keyworth. The data is in digitised form and is archived in the BGS geophysical data bank. The data was digitised from the aeromagnetic survey made with flight line separation of about 2 km apart and tie lines at about 10 km apart. The digitisation has been carried out along the flight lines at 10 nT interval. The data as obtained from the data bank contains the flight line numbers, the values of the aeromagnetic anomalies, the coordinates and the average flight heights above the topography. The coordinates of the data points are with respect to the British National Grid and are in units of metres east and north of the origin. The anomalies are total field anomalies in nanotesla above a linear regional field for the British Isles which increases 2.1728 nT/km northward and 0.259 nT/km westward. A reference datum value of 47033 nT at the grid reference origin of epoch 1955.5 has been used (Hall and Dagley 1970). The average flight height is about 1000 ft (300 m) above the topography.

The transfer of data from the geophysical data bank to the Durham computer centre was carried out by firstly signing on at Durham. The connection with the BGS computer was established through the JANET link. A successful connection to the BGS computer enables retrieval of the aeromagnetic data from the data bank. The retrieved data was placed in a file at BGS. The transfer of data from the BGS computer to the Durham computer was then carried out using the program SUBMIT which is an inter-site file transfer utility available in the Durham computer centre.

The data was transferred and archived in blocks of either 110 km by 110 km, or 210 km by 210 km where the data is sparse. The hundred kilometre National Grid square is the basic block used. The outer 5 km strip of data surrounding the basic blocks was needed for the gridding and for combining the data. Data was progressively transferred as the digitisation at BGS progressed.

2.2 Gridding of the data

As the data are distributed along profiles, gridding has been carried out to give values on a regular square grid. A major difficulty in gridding this aeromagnetic data is to retain the frequency content of the original data. The short wavelength nature of some aeromagnetic anomalies and the irregular distribution of values along profiles results in a variable data point distribution which can severely affect the accuracy of the gridding. The large amount of data involved and the limited computer time and space also add to the problem.

A number of gridding routines available at Durham have been tested. As the data are digitised along almost parallel lines about 2 km apart, a digitising interval of 2 km might be expected to give the best result. Intervals of 1 km to 4 km were used for testing. The gridding routines tested include Ghost80, GinoF, Surface2 and NAG packages. The results from various tests have been compared with hand drawn contours, random points contours and published aeromagnetic maps. The routine GRID from the Surface2 packages which uses the radial averaging method, gives good results with 2 km sample interval within reasonable time and is easy to use. The routine INTERP2 from Ghost80 which interpolates using a mean weighted inversely as fourth power of the distance also gives good results and is suitable for parallel data points. This routine, however, uses a large amount of computing time. It was therefore decided to use the routine GRID from the Surface2 package to grid the aeromagnetic data.

The gridding has been carried out in rectangular or square blocks. Where the data are sparse, it has been possible to combine a number of blocks together for the gridding. The gridded data of the surrounding 5 km data strip is removed leaving only gridded data within the hundred kilometre squares. This is archived. The final archived data set contains the topographic height data (discussed in the next section), the values of the aeromagnetic anomalies, and the national grid coordinates of the data points. The digitised aeromagnetic map of Great Britain can then be obtained by combining the gridded blocks together. The 5 km strip surrounding each block serves as an overlap and is sufficiently wide to remove any edge error caused by the gridding. Tests have been carried out which confirm that the edge errors have been effectively removed.

2.3 Topographic height data

Knowledge of the topographic height is essential for the interpretation and analysis of the aeromagnetic anomalies. This is because the anomalies have been acquired at a constant height above the topography and the height is needed for the upward continuation of the aeromagnetic anomalies onto a horizontal plane.

The height data used in this project has been acquired from the compilation of Woollett (1988). Topographic data from the BGS data bank has also been made available. However, the digitised data in the data bank does not cover the whole of Great Britain. The procedure for retrieving the data is similar to that for the aeromagnetic anomalies. The data can be retrieved as an average height either for 1x1 or 5x5 km^2 squares. The 1x1 km^2 data needs regridding to a 2 km interval for use with the digitised aeromagnetic data and the 5x5 km^2 data already gives a smoothed topography. The height data of Woollett (1988) used in this work has been gridded to yield an average height over 2x2 km^2 squares. Comparison with the BGS height data has been carried out to check the accuracy of the gridded height data. The

average flight height (300 m above the topography) used in the aeromagnetic survey is assumed to be 300 m above the smoothed topographic height. This is because the aeromagnetic data set obtained from the BGS data bank does not have the actual flight height measurement. The only height information is the 300 m average height above the topography.

2.4 Previous methods on the upward continuation of magnetic anomaly from an irregular surface onto a horizontal plane

Acquisition of aeromagnetic data can either be at a horizontal level or at a constant height above the topography. These different methods of acquiring data over the same area produce slightly different anomaly maps particularly at short wavelengths. The differences may give rise to problems in the analysis and interpretation of the aeromagnetic anomalies obtained at variable absolute height. Among the problems are :

(1) The short wavelength content varies with height above the magnetization sources, and if these sources are shallow there will be substantial differences between the aeromagnetic maps at constant and variable heights above the surface.

(2) Most direct interpretation methods require the observed anomalies to be on a horizontal plane. Direct application of these methods to data observed on a surface of variable height will result in erroneous interpretation. The processing of aeromagnetic data acquired on an irregular surface to yield values on a horizontal plane is thus an important prior stage to application of direct methods such as the pseudogravimetric transformation.

Various procedures have been developed by previous workers to reduce potential field data from an irregular surface onto a horizontal surface and also from a horizontal surface onto an irregular surface and between irregular surfaces. The main methods are based on equivalent sources or harmonic series.

2.4.1 The equivalent source methods

The magnetic anomaly $F(x, y, z)$ at a field point $P(x, y, z)$ on or above the XY-plane caused by a distribution of magnetization $J(x', y', z')$ beneath the plane between upper and lower depth limit z_1 and z_2 (Bott 1973) is,

$$F(x, y, z) = \int_{-\infty}^{\infty} \int_{-\infty}^{\infty} \int_{z_1}^{z_2} J(x', y', z') K(x' - x; y' - y; z' - z; \underline{s}; \underline{j}) dz' dy' dx'$$

where $\underline{j}$ and $\underline{s}$ are unit vector in the direction of magnetization and the measured field respectively, K is the kernal function which depends on the field component and on direction of magnetization and z is positive downwards. If the shape of the magnetised body is known the problem is to determine the magnetization distribution from the field anomalies and if the magnetization distribution and one of the depths are known the problem is to deduced the undefined surface (Bott 1973). The main idea of the equivalent source technique is to determine the nature of the source according to the first criterion mentioned such that the equivalent source anomalies fit the observed anomalies. Simple models are usually used for the equivalent sources. The sources can be a distribution of poles or dipoles. The distribution of magnetic pole strength or magnetic moment is initially determined to fit the observed anomalies. Having obtained the equivalent sources, the anomalies at any point outside the sources can then be determined by forward calculation from the specified magnetic distribution. Even though the source is not unique, the fit of the equivalent source anomalies to the observed anomalies provides an almost exact method for calculating the anomalies at other points above the plane of observation. The equivalent source method for continuing potential fields is not concerned with the physical ambiguity of the final source distribution but with the stability of the source distribution and the reliability of the fit between the theoretical anomalies and the observed anomalies. This method can be used to determine the anomaly field on a plane surface when the observed anomalies are on a surface of varying height.

The earlier work on the reduction of the potential field on an uneven surface

to a plane surface deals only with gravity field. Most of the early work on gravity data used iterative techniques based on the linear Fredholm intergral of the first kind. The approach has subsequently been extended to solve the linear Fredholm integral of the second kind (e.g. Tsirulskiy and Ospishcheva 1968). Dampney (1969) carried out the reduction for three dimensional gravity data by assuming a series of discrete masses for the source. With N data points and N equivalent masses, he used the matrix method to solve for the density distribution. Knowing the density distribution, a direct calculation gives the anomalies at other points. The approximation of the discrete masses is only a valid representation of the anomalies if the masses are sufficiently deep below the surface relative to the sample spacing Δ but are not so deep that they show instability (Emilia 1973). Limits of $2.5\Delta > d > 6\Delta$ have been given by Dampney where d is the depth of the mass.

The application to magnetic anomalies using a similar method to Dampney's has been done for two-dimensional anomalies by Emilia (1973). He used a system of lines of dipoles in place as the magnetization distribution. The magnetic dipoles are perpendicular to the profile and are placed on a plane parallel to the observation surface. As with Dampney, he used linear inversion by fixing the location of each line of dipoles and varying the individual magnetic moment per unit length. Courtillot et al. (1974) applied a similar procedure but used a geometrical distribution of sources for the observed magnetic anomalies. This involves non-linear inversion to obtain the source.

Bhattacharyya and Chan (1977) used the Fredholm integral of the second kind. The total field $F(x, y, z)$ is

$$F(x, y, z) = 2\pi\mu(x, y, z) - \int\int \mu(a, b, c)\frac{d}{dn}(\frac{1}{R})dS$$

where μ is the gradient of the magnetization distribution in the direction of the total field and $\frac{d}{dn}(\frac{1}{R})$ is the kernal of the integration. The observed anomaly $F(x, y, z)$ is on an irregular surface S. They used a dipole distribution perpendicular to surface S.

An iterative scheme is used to determine the distribution of magnetization μ on the observation surface. Knowing the equivalent source, a forward procedure is then used to determine the anomalies on other planes or surfaces. Nakatsuka (1981) pointed out that the Bhattacharyya and Chan (1977) derivation used an approximation that the observation surface is not so irregular. He improved the method by using a distribution of vertical magnetic moments instead of a distribution of dipoles perpendicular to the observation surface. He reported that his modification improves the results and the speed is thirty percent faster. Pedersan (1989) pointed out an error in one of the equations used by Bhattacharyya and Chan but this does not affect the validity of the procedure (Chan 1989).

Hansen and Miyasaki (1984) and Hansen (1985) made a further improvement to the method. The equivalent layer is placed close below the observation surface. The method was initially restricted for continuation to regions above the observation surface. The improvement enables the continuation to be carried out below the observation surface but above the source. The iteration is reported to converge faster and the results are improved.

Ray and Friedberg (1985) introduced a generalised convolution method. The convolution coefficients are calculated using transformation methods and vary from point to point. The method assumes a locally horizontal observation surface. Zhou et al. (1985) applied a similar equivalent source method where calculation of the magnetic moment and strength of the equivalent source involves the use of either the steepest descent or damped least square Marquardt method.

Ivan (1986) used an approximation of the Dirichlet integral problem where the knowledge of values at the boundary of a closed surface enables calculation of values at other points within the volume. His derivation reduces to solution of the Fredholm equation. He applied the method to gravity anomalies and indicated that its use can be extended to magnetic anomalies. His approximation gives good result when the

observation surface is not unduly irregular and when the continued surface is at a relatively high elevation above the topography and the source body. His method is computationaly faster than that of Bhattacharyya and Chan (1977).

2.4.2 The Fourier Transform methods

The Fourier representation of magnetic anomalies takes a different form from that of the equivalent source. Instead of relating the anomalies to the variable parameters of the source body, the anomalies are represented by a superposition of a finite number of linearly independent harmonic functions. This direct representation of the field anomalies avoids the necessity of relating to the source and, therefore, does not need any assumptions concerning the source body. In practice the anomalies are known only at discrete points and are approximated by using the sum of the relevant functions. The earlier methods applying the Fourier series also used matrix inversion. The fast discrete Fourier transform is used in later applications.

One of the earliest applications of Fourier series for reducing magnetic anomalies observed on an irregular surface to a horizontal plane was given by Nagata (1939). He represented both the magnetic anomalies and the height using Fourier series. The Fourier series for the height is incorporated into the Fourier series for the magnetic anomalies. This is used to determine the Fourier series for the magnetic anomalies on the horizontal reference plane. As the Fourier coefficients of the height and of the observed anomalies are known, the solution of simultaneous equations can be used to calculate the coefficients of the anomalies on the plane surface. To simplify the method Nagata assumed the Fourier coefficients of the anomalies observed on the irregular surface could be treated as the Fourier coefficients of anomalies on a horizontal plane, so that they can be upward continued. The method was only applied to the two-dimensional case.

Tsuboi (1965) used Fourier analysis and successive approximation to reduce evenly-spaced two-dimensional gravity data to a horizontal plane. The method was extended by Hagiwara (1966) to deal with three-dimensional evenly-spaced data. Henderson and Cordell (1971) applied a similar approach to unevenly spaced gravity data observed on an irregular surface. The observed anomalies F_k are represented in matrix form

$$F_k = \sum_{k=1}^{2m+1} \alpha_k C_{i,k} + \epsilon_{i,m}$$

where $C_{i,k}$ is a product of cosine or sine function with the height function. The Fourier coefficients α_k are obtained by using matrix inversion and minimising the error term $\epsilon_{i,m}$. Having obtained the Fourier coefficients the anomalies on the plane $z = 0$ are determined by synthesising the Fourier series. Both two and three dimensional data can be reduced using this method but the procedure needs a relatively large amount of computer time as it involves the inverting of a large number of matrices especially for the three dimensional case.

Syberg (1972) presented a method based on a generalised two dimensional continuation operator. The operator which is derived in the spatial domain is converted to the frequency domain using the Fourier transform. The continuation operator is basically a function of the differences in the position of the observation points and the reduction surface. The observed anomalies are multiplied by the operator to obtain the anomalies at the horizontal level. The operator developed is not applicable directly to total intensity. Resolving to give the horizontal and vertical components enables the reduction of the total field to be carried out. The application to the total field anomalies is therefore quite involved despite operating in the frequency domain because of the necessity of resolving to give the components, reducing the anomalies and resolving back to the total field anomalies. Granser (1983) pointed out some misprinting and inaccuracy in the derivation of the continuation operator.

A similar approach has been used by Courtillot et al. (1973) for two-dimensional

data and Ducruix et al. (1974) for three-dimensional data. The method represents the magnetic anomalies, $F_0(x, y)$, as

$$F_0(x, y) = \sum_{k=-\infty}^{\infty} \sum_{l=-\infty}^{\infty} F_0(k, l) K_0(x - k, y - l)$$

where K_0 is the classic sinc function and is an approximation of the Green function at $z = 0$. The anomalies $F_h(x, y)$ at level h have a corresponding operator K_h. The operator K_h is calculated using a modified sinc function . The resulting formulation is represented in matrix form $F_h = F_0.K_h$ and is solved using the generalised inverse matrix. Similar restrictions on the relief and computing times hold.

Another method which uses the harmonic function but applies the Schwarz Christoffel transformation has been developed by Parker and Klitgord (1972). The method is mainly used to deal with deep tow survey. The transformation only deals with two dimensional data and has no three dimensional equivalent. The method has also been described by Wendorff (1985).

A simple and systematic procedure has been developed by Tsay (1976) to reduce total field anomaly observed along a profile of constant gradient to a horizontal plane above. The basic method is restricted to data measured at constant elevation differences along the profile, when using the fast Fourier transform method. However, extrapolation of data obtained at irregular elevation to values at regular constant height may be carried out. Not many data are measured along profiles of constant gradient and extrapolation may introduce significant errors.

2.4.3 Comparison of equivalent layer and Fourier methods

In all the above methods the theoretical formulation deals with an infinite surface. In practice all the methods use a finite data range and discrete data points, and assume that the discrete data duplicates the continuous field exactly.

In the matrix methods, using discrete point sources, the total number of points used should not be so large as to make the matrix inversion unmanageable. The advantage of the matrix method is that the field and the reduced points need not be equally spaced and this gives the versatility of the method (Bott 1973).

The reduction scheme using the equivalent source methods needs a relatively large amount of computer time particularly in the three dimensional case and for larger data set. This is because of the necessity to compute an equivalent source prior to calculating the anomalies on the horizontal surface.

The Fourier series method operates directly on the anomalies and uses the frequency domain. The method assumes repetition of data outside the region used. In practice data repetition seldom occurs. It may therefore be desirable to surround the anomaly by a border of zero values before carrying out the analysis to avoid consequent distortion near the margins of the region used (Bott 1973). The Fourier method enables the use of the fast Fourier algorithm. The fast Fourier transform greatly speeds up the computation particularly on large data sets. The formulation for the two and three dimensional problems is similar when using the Fourier transformation. With the aid of the fast Fourier transform, an iterative scheme becomes possible. Such a scheme has been used in this work as described in the following section.

2.5 The method used for the upward continuation of magnetic anomaly from an irregular surface onto a horizontal plane

The method used in this thesis for reducing aeromagnetic anomalies observed on an irregular surface onto a horizontal plane is discussed in this section. With the apparent advantages of using the fast Fourier transform and its availability in the NAG subroutine packages at Durham, a method based on this has been used.

Cordell (1985) developed a method to upward or downward continue the aeromagnetic anomalies observed on a horizontal plane onto an irregular surface. In the upward continuation, he first upward continued the anomalies to a number of horizontal planes using the fast Fourier transform. The anomalies at each point on the irregular surface can then be obtained by interpolation. The method needs the initial anomalies to be observed on a horizontal plane. The procedure described below for upward continuing anomalies observed on an irregular surface onto a horizontal plane above is a further development of the Cordell (1985) procedure.

2.5.1 Derivation of the present procedure

The procedure initially assumes that the observed anomalies are on a horizontal plane. The iterative method used is based on a series of downward and upward continuations. In the upward continuation process a reference horizontal plane where the anomalies are to be calculated is first defined above the irregular observation surface. The height differences between the two surfaces are determined at each point. The observation surface is initially assumed to be a horizontal plane and the reference surface is then irregular. The observed anomalies are then upward continued from the assumed horizontal observation plane onto the irregular surface using the Cordell (1985) procedure. These upward continued anomalies are taken as the initial approximate solution.

The downward continuation process is next used to test the correctness of the solution. The initial solution is downward continued from the reference surface (which is now assumed to be horizontal) onto the true irregular observation surface using Cordell's procedure. The downward continued anomalies are compared to the observed anomalies on the irregular observation plane. The differences give the residual anomalies. The residual anomalies are then upward continued using the upward continuation process described earlier. The upward continued residual anomalies are

added to the solution to give a new solution. Testing is again carried out on the solution by using the downward continuation process. The upward and the downward continuation processes are repeated until the residual anomalies become negligible. The solution then gives the correct upward continued anomalies from the irregular surface onto the horizontal plane. The theoretical background of the Fourier method used for the downward and upward continuation of the anomalies is described below.

Gravity and magnetic potentials satisfy Laplace equation $\nabla^2 U = 0$ in free space. In the study of local total field magnetic anomalies, the sea level surface of the earth can be assumed to be horizontal and the Cartesian coordinate system can be used. Taking the xy-plane to be horizontal, x as the north direction, y as the east direction and z as the vertical direction positive downwards, the potential U in Cartesian coordinates satisfies

$$\nabla^2 U = \frac{d^2U}{dx^2} + \frac{d^2U}{dy^2} + \frac{d^2U}{dz^2} = 0. \tag{2.1}$$

The total field magnetic anomaly ΔF is derivable from the magnetic potential of the causative body

$$\Delta F = -\mu_o \frac{dU}{d\tilde{r}} \tag{2.2}$$

where $\tilde{r}$ is the unit vector in the direction of the field and μ_o is the susceptibility. We assume $\tilde{r}$ is a constant vector, although this is an approximation for total field anomalies, but is sufficiently good for our purpose provided ΔF is small in relation to the earth's magnetic field. The Laplacian operator ∇^2 applied to both side of the equation 2.2 gives

$$\begin{aligned} \nabla^2(\Delta F) &= \nabla^2(-\mu_o \frac{dU}{d\tilde{r}}) \\ &= -\mu_o \frac{d(\nabla^2 U)}{d\tilde{r}} \\ &= 0 \qquad (\nabla^2 U = 0). \end{aligned} \tag{2.3}$$

Under the conditions mentioned, the total field magnetic anomaly also satisfies the Laplace equation. In the study of a local anomaly F_l due to a magnetized

body, F_l must be much smaller than the earth's magnetic field F_e so that ΔF and F_e can be assumed to be in the same direction. The general form of the total field magnetic anomaly can be obtained by solving equation 2.3 using the method of separation of variables. A simple particular solution can be taken as product of three function $X_i(x), Y_i(y)$ and $Z_i(z)$ each dependent only on one variable x, y or z respectively,

$$\Delta F_i = X_i(x)Y_i(y)Z_i(z) \tag{2.4}$$

Substituting equation 2.4 into equation 2.3 and dividing by ΔF_i gives,

$$\frac{1}{X_i(x)}\frac{d^2X_i(x)}{dx^2} + \frac{1}{Y_i(y)}\frac{d^2Y_i(y)}{dy^2} + \frac{1}{Z_i(z)}\frac{d^2Z_i(z)}{dz^2} = 0.$$

This is the sum of three terms each dependent on one variable. Each term is therefore constant and can be separated,

$$\frac{d^2X_i(x)}{dx^2} = -k_x^2X_i(x),$$

$$\frac{d^2Y_i(y)}{dy^2} = -k_y^2Y_i(y) \tag{2.5}$$

and

$$\frac{d^2Z_i(z)}{dz^2} = (k_x^2 + k_y^2)Z_i(z),$$

where k_x and k_y are arbitrary constants. The integrals for the different terms can be written as

$$X_i(x) = A_i \cos k_x x + B_i \sin k_x x,$$

$$Y_i(y) = C_i \cos k_y y + D_i \sin k_y y \tag{2.6}$$

and

$$Z_i(z) = E_i e^{|K|z}$$

where $|K| = \sqrt{k_x^2 + k_y^2}$. $k_x = 2\pi/\lambda_x$ and $k_y = 2\pi/\lambda_y$ are the wavenumbers in the x and y directions respectively. λ_x and λ_y are the wavelengths. The particular solution related to one set of wavenumbers k_x and k_y can be written as

$$\Delta F_i(x, y, z) = (A_i \cos k_x x + B_i \sin k_x x)(C_i \cos k_y y + D_i \sin k_y y)e^{|K|z}. \tag{2.7}$$

This can be used to represent a simple anomaly containing only a single wavenumber pair (k_x, k_y). The anomaly at $z = 0$ can be written as

$$\Delta F_i(x, y, 0) = (A_i \cos k_x x + B_i \sin k_x x)(C_i \cos k_y y + D_i \sin k_y y). \qquad 2.8$$

Anomalies at any level above or below $z = 0$ may be obtained by multiplying the anomaly at $z = 0$ by the continuation operator

$$K_O = e^{|K|z}. \qquad 2.9$$

Total field anomalies are generally made up of more than one term of this type. They may be approximated by combining a finite number of simple anomalies of the above type each satisfying Laplace's equation. The wavenumbers in the x and y directions may vary independently. The total field anomaly $\Delta F(x, y, z)$ may then be written in the form

$$\Delta F(x, y, z) = \sum_m \sum_n (A \cos k_m x + B \sin k_m x)(C \cos k_n y + D \sin k_n y) e^{|K|z} \qquad 2.10$$

where $m = 0, 1, 2...\infty$ and $n = 0, 1, 2...\infty$.

In practice the total field anomaly is measured over a finite length and at discrete sampling intervals. The wavenumbers present are thus governed by the longest and shortest wavelengths (figure 2.1). Consider data lengths L_x and L_y sampled at $2N_x + 1$ and $2N_y + 1$ points in the x and y directions respectively. The longest wavelengths are L_x and L_y and the shortest wavelength are L_x/N_x and L_y/N_y. The total field may also contain a component of infinite wavelength (background value). The maximum wavenumbers in the x and y directions are $2\pi N_x/L_x$ and $2\pi N_y/L_y$ respectively. As the anomaly is measured at discrete equally spaced points, k_m and k_n can only be multiples of the values corresponding to the fundamental wavelengths L_x and L_y where $k_m = 2\pi m/L_x$, $m = 0, 1, 2....N_x$ and $k_n = 2\pi n/L_y$, $n = 0, 1, 2....N_y$.

The total field anomaly can be written as

$$\Delta F(x, y, z) = \sum_m \sum_n (A \cos 2\pi \frac{m}{L_x} x + B \sin 2\pi \frac{m}{L_x} x)(C \cos 2\pi \frac{n}{L_y} y + D \sin 2\pi \frac{n}{L_y} y) e^{|K|z} \qquad 2.11$$

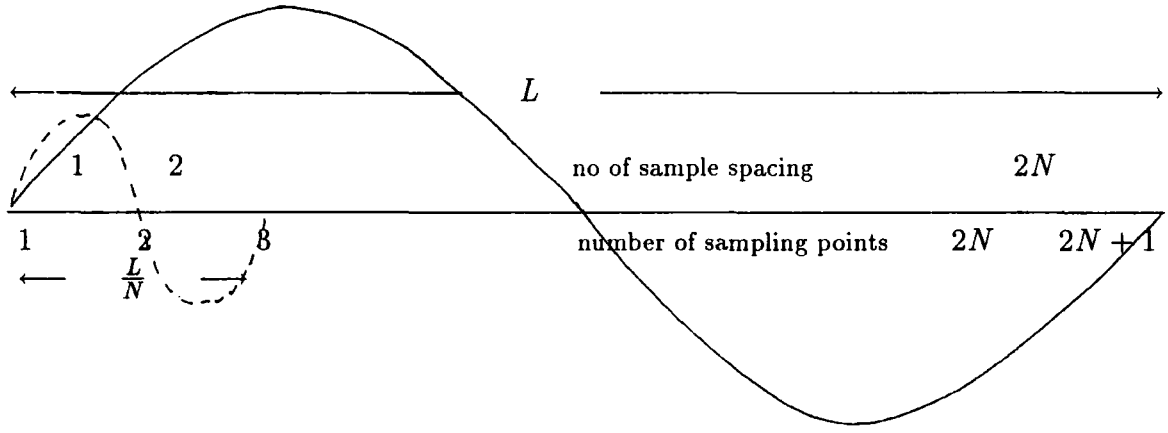

Figure 2.1 The shortest $2(\frac{L}{2N})$ and the longest wavelengths $2N(\frac{L}{2N})$ in a finite data length L sampled at $2N + 1$ sampling points.

and can also be written in the complex form as

$$\Delta F(x,y,z) = \sum_m \sum_n F(k_m, k_n) e^{i(2\pi m x/L_x + 2\pi n y/L_y)} e^{|K|z} \qquad 2.12$$

$F(k_m, k_n)$ is complex and is the partial amplitude of each wavenumber set.

It is possible to upward or downward continue the total field anomaly from one level to another. The amplitudes of each term are first determined by Fourier analysis. Each anomaly component is continued separately using the continuation operator (equation 2.9). These are recombined to obtain the total field anomaly. The observed anomaly may be expressed in the form required by the fast Fourier transform.

A two dimensional function $F(x,y)$ has its Fourier transform pair defined as (eg. Båth 1974),

$$F(k_x, k_y) = \frac{1}{(2\pi)^2} \int\int_{-\infty}^{\infty} F(x,y) e^{-i(k_x x + k_y y)} dx dy \qquad \text{direct transform} \qquad 2.13a$$

$$F(x,y) = \int\int_{-\infty}^{\infty} F(k_x, k_y) e^{i(k_x x + k_y y)} dk_x dk_y \qquad \text{inverse transform} \qquad 2.13b$$

The equivalent discrete form may be written as follows,

$$F(m,n) = \frac{1}{(2N)^2} \sum_{v=-N}^{N} \sum_{w=-N}^{N} F(v,w) e^{-i(k_x v + k_y w)} \qquad 2.14a$$

$$F(v,w) = \sum_{m=-N}^{N} \sum_{n=-N}^{N} F(m,n) e^{i(k_x v + k_y w)} \qquad 2.14b$$

where m,n,v and w are integers and the total number of data points are $(2N+1)^2$. When applied to a total field anomaly measured within a square area with sides L^2 and sampled at $(2N+1)^2$ grid points, v and w may be replaced by x and y sampling values respectively and $k_x = 2\pi m/L$ and $k_y = 2\pi n/L$.

In upward and downward continuation using the Fourier method, the anomaly is first analysed using the discrete form of the Fourier transform. The Fourier coefficients of each component are modified using the continuation operator. Synthesis of

the new Fourier coefficients gives the anomaly at the needed level. The upward and downward continuation of the total field anomaly observed on a horizontal plane onto an irregular surface (Cordell 1985) uses this method and an interpolation procedure. This procedure of Cordell is next described.

Consider two surfaces a_o and b with surface b at a higher elevation (figure 2.2). Take the surface b to be the horizontal xy-plane (z=0) The anomaly on this surface is $B(x, y, 0)$. Let surface a_o be the irregular surface and the anomaly on this surface is $A_o(x, y, h)$. h is the height difference between the two surfaces with the lower and upper limit of $z = 0$ and $z = h_{max}$ respectively. The anomaly $B(x, y, 0)$ observed on the horizontal surface is to be downward continued onto the irregular surface a_o.

The anomaly $B(x, y, 0)$ is first downward continued to a number of equally spaced horizontal levels L_i from $L_i = 0$ to $L_i = h_{max}$. This is carried out by obtaining the Fourier coefficients of the anomaly $B(x, y, 0)$ using equation 2.14a. The Fourier coefficients are multiplied by the continuation operators (equation 2.9) at the specified levels L_i. The anomalies at the different levels $B_i(x, y, L_i)$ are obtained by carrying out the inverse Fourier transform on the modified coefficients. The anomaly at each point on the irregular surface can then be obtained by interpolation using the anomalies at the known levels. A similar procedure can be applied if the irregular surface a_o is at a higher level than surface b. The anomaly $B(x, y, 0)$ is first upward continued to a number of levels. The anomaly on the irregular surface can then be determined from these upward continued values.

This procedure gives the exact anomaly on the irregular surface upward continued from the horizontal plane. The procedure is used in the iterative scheme to upward continue anomalies observed on an irregular surface onto a horizontal plane above as described earlier. The implementation in the fortran program written (REDUCE, Appendix 2.1) follows the scheme described below.

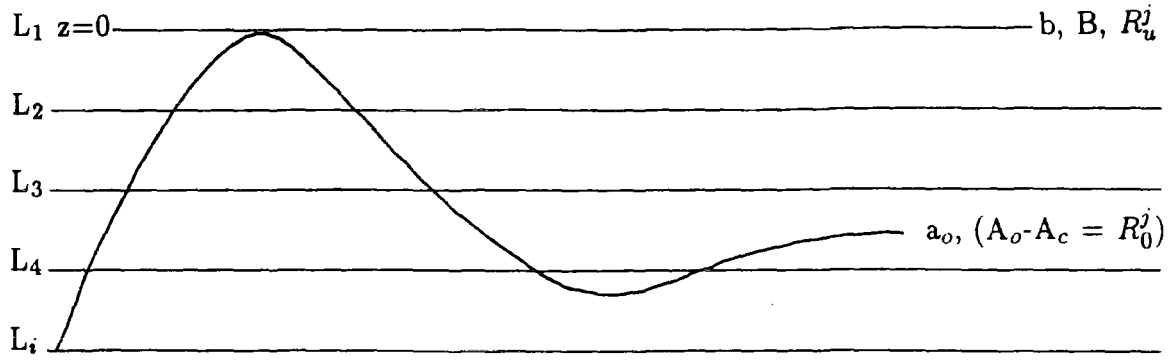

Figure 2.2 Parameters used in Cordell (1985) and the downward continuation procedure of the iterative scheme. b-horizontal surface, a_o-irregular surface, B-anomaly on horizontal plane b, A_o-anomaly on irregular surface a_o, A_c-anomaly interpolated on surface a_o, h-depth of surface a_o from surface b, R_o^j-residual anomaly after j^{th} iterations, R_u^j-upward continued value of R_o^j.

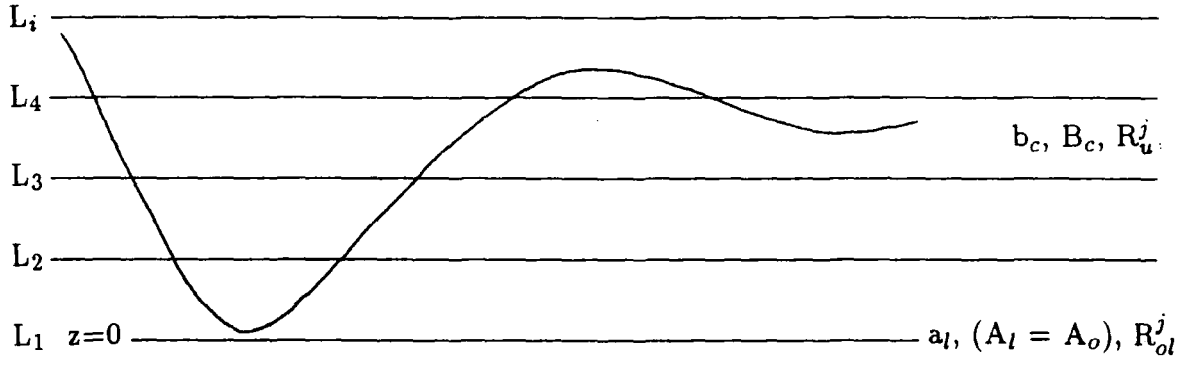

Figure 2.3 Parameters used in the upward continuation procedure of the iterative scheme a_l-assumed horizontal surface, b_c-irregular surface, A_l-anomaly A_o on horizontal plane a_l. B_c-anomaly A_l upward continued onto the irregular surface b_c, R_{ol}^j-residual anomaly assumed to be on a_l.

Take the situation where the observed anomaly $A_o(x, y, h)$ is on the irregular surface a_o. The anomaly $A_o(x, y, h)$ is to be continued upwards onto the horizontal surface b to give anomaly $B(x, y, 0)$. The first step in the iterative scheme is to obtain an initial estimate of the solution. The anomaly $A_o(x, y, z)$ is initially assumed to be on a horizontal plane a_l (figure 2.3). With this assumption and by using the relevant height differences a surface b_c is defined by the height differences above surface a_l. The anomaly $A_o(x, y, z)$ is upward continued onto surface b_c using the Cordell (1985) procedure. The upward continued anomaly $B_c(x, y, h)$ is the initial estimate of the upward continued anomaly (the solution) on the horizontal plane b. The anomaly $B(x, y, 0)$ takes the values of anomaly $B_c(x, y, z)$.

The residuals are determined by downward continuing $B(x, y, 0)$ onto the true observation surface a_o using the Cordell (1985) procedure. This gives the calculated anomaly $A_c(x, y, h)$. The calculated anomaly should be equal to the observed anomaly $A_o(x, y, h)$ if the observed anomaly has been correctly continued from the irregular surface onto the horizontal plane above. The residual anomaly $R_o^j(x, y, h) = A_o(x, y, h) - A_c(x, y, h)$ is used to check the correctness of the reduction. A large residual sum ($\sum R_o^j(x, y, h)$) indicates that further improvement of the solution is necessary.

If further improvement is necessary the residual anomaly is assumed to be on the horizontal plane a_l. Upward continuation of the residual anomaly is carried out as for the observed anomaly described earlier. The upward continued residual anomaly $R_u^j(x, y, 0)$ is added to the solution to obtain a new solution $B(x, y, 0) = B(x, y, 0) + \sum_{j=2} R_u^j(x, y, 0)$. The new solution is again tested and the iteration is carried out until the residual anomaly is negligible. j is the number of iterations. A flow chart of the scheme is given in figure 2.4.

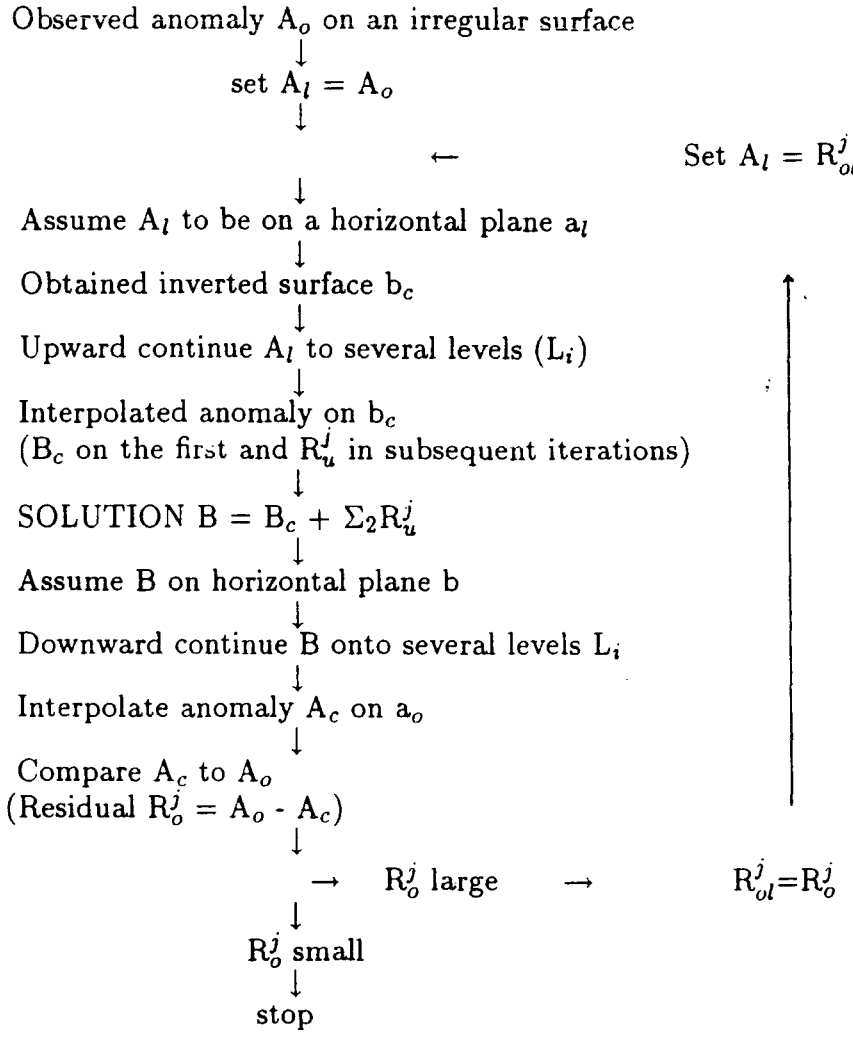

Figure 2.4 Flow chart of the iterative scheme

a_o-irregular surface, A_o-anomaly on irregular surface a_o, A_c-anomaly interpolated on surface a_o, A_l-anomaly A_o assumed on horizontal plane a_l, a_l-assumed horizontal surface, b-horizontal surface, B-anomaly on horizontal plane b, b_c-irregular surface, B_c-anomaly A_l upward continued onto the irregular surface b_c, R^j_o-residual anomaly after j^{th} iterations, R^h_u-upward continued value of R^h_o, R^j_{ol}-residual anomaly assumed to be on a_l.

2.5.2 The interpolation method

A simple quadratic interpolation method is used. The anomalies $F(L)$ at any level L can be represented using the quadratic equation of the form $F(L) = aL^2 + bL + c$. In the upward and downward continuation procedures the anomalies at a number of heights are known. The anomalies at points in between the levels can be evaluated using the anomaly values at the three nearest levels. The anomalies at the three appropriate levels at any particular observation point are substituted in the equation. With three set of equations and three unknowns the coefficients a, b and c can be evaluated. Knowing the coefficients, the anomalies at any height within the range can be determined for the particular observation point.

The accuracy of the interpolation method is dependent on the three sets of values used for the interpolation. The gradient defined by the three values can range from high to low. A high rate of change in the gradient may increases errors in the interpolation. Spherical models have been used to test the accuracy of the interpolated values. Magnetic anomalies due to the models have been calculated for upward and downward continuation heights from 0 to 2400 metres at 200 metre downward continuation height interval. Using the anomalies at the 400 metre upward and downward continuation height interval, the anomalies at the 200 metre interval have been calculated using the interpolation method. Comparison between the interpolated values and the calculated values from the models shows only a slight difference. Table 2.1 shows an example of such comparison. This indicates the suitability of the interpolation method. A more accurate result can be obtained by using a smaller continuation height interval particularly where the rate of change of the gradient is large.

2.6 Testing the iterative scheme

The upward continuation procedure has been tested independently using

Level (m)	Calculated anomaly (nT)	Interpolated anomaly (nT)	Differences (nT)
2400	-690.5		
2200	-738.9	-740.5	1.6
2000	-790.8		
1800	-846.1	-845.5	.5
1600	-904.9		

Table 2.1 Comparison of the calculated magnetic anomaly values due to a spherical model with the interpolated values. The interpolation has been carried out for the anomalies on the 2200 m and 1800 m levels using the calculated anomalies at 2400, 2000 and 1600 m levels. Interpolation on the lower levels result in smaller differences.

known models. This is to ensure the correctness of the procedure and the programme written. The programme REDUCE for the reduction of the aeromagnetic anomalies from an irregular surface onto a horizontal plane has been written for three-dimension anomalies. The anomalies for the test are generated using programme SPHEREM (Appendix 2.2), which calculates magnetic anomalies of a single or a number of spheres on both horizontal and irregular surfaces. A programme to obtain an exact magnetic profile (Appendix 2.3) from the data set have also been written. Problems are expected to arise from the high frequency content of the anomalies and the degree of irregularities of the topographic heights on which the aeromagnetic anomalies are observed, both of which may introduce instability in downward continuation. These problems may set limitation to the reduction procedure. The tests have been carried out as below.

An irregular surface was first generated. Using the same source model, magnetic anomalies were calculated on the irregular surface and on a horizontal surface above. The anomalies calculated on the irregular surface were then upward continued onto the horizontal plane using the program REDUCE. The upward continued anomalies and the anomalies calculated on the same horizontal plane were compared. Tests were initially carried out on two-dimensional topography using a system of ridges and valleys. Anomalies were calculated over structures such as valleys, hills and slopes. Anomalies of different wavelengths were obtained by placing models at different depths. The anomalies were then calculated on a square area and the upward continuation were carried out on this data. Similarly the anomalies on the horizontal plane above the irregular topography were calculated on the same square area. Comparison of the calculated and upward continued anomalies were carried out along profiles traversing the structural features. The effect of true three-dimensional features were also tested. A system of domes and basins were generated. Anomalies calculated for these features were similarly upward continued on to a horizontal plane. The upward continued anomalies across various profiles were then compared to the anomalies calculated on the horizontal plane from the same source.

Figure 2.5 shows a test result for the convergence of the procedure. Magnetic anomalies of spherical bodies placed at 5, 6 and 7 km depth below a reference level have been calculated on the two-dimensional topography shown in figure 2.5a. The maximum continuation height is 2 km. The results of the first, second, third and seventh iterations are given in figure 2.5b. The test shows that the results converged to stable values with a few iterations when applied to relatively long wavelength anomalies and topography. Most off the anomalies converged by the third iteration (figure 2.5b). The results from greater than six iterations do not change significantly. Comparison of the upward continued anomalies with the anomalies calculated on the horizontal continuation plane 2 km above the reference datum shows that there are only slight differences (figure 2.5c). These differences are not likely to cause serious error when used with interpretation methods requiring anomalies on a horizontal plane as compared to using the observed anomalies on the irregular surface. Short wavelength instabilities limit the use of the procedure as described below.

The problems due to the wavelength of the anomalies and the continuation heights arise from the use of the continuation operator K_O. Equation 2.9 shows that, in the upward or downward continuation procedure, the partial amplitude of any particular wavelength is amplified by a factor of $e^{|K|z}$. Taking the wavelength in the x and y direction to be the same ($\lambda_x = \lambda_y$) the amplification factor can be written as $e^{2\pi z\sqrt{2}/\lambda}$. For downward continuation of half a wavelength the amplification factor is $e^{\pi\sqrt{2}}$(=85.0) while upward continuation by half a wavelength the amplification factor is $e^{-\pi\sqrt{2}}$ (=0.012). The upward continuation is a stable process while downward continuation is not. Therefore, downward continuation can only be carried out to a limited depth otherwise short wavelength instabilities caused by high amplification of error dominates the data (Bott 1973).

Figure 2.6 is a sample test result using a topographic wavelength of 8 km and of variable amplitude. The magnetic sources are placed at 5 km depth below the structural low where the continuation heights are large. The wavelengths of the

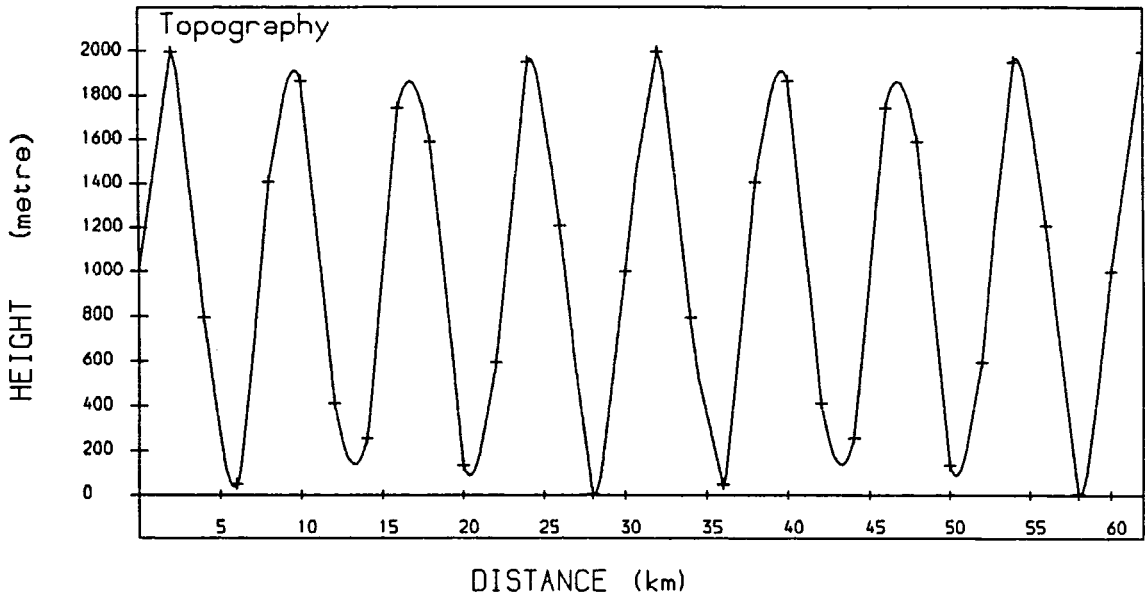

Figure 2.5a Two-dimensional topography used to test the convergence of the the upward continuation procedure.

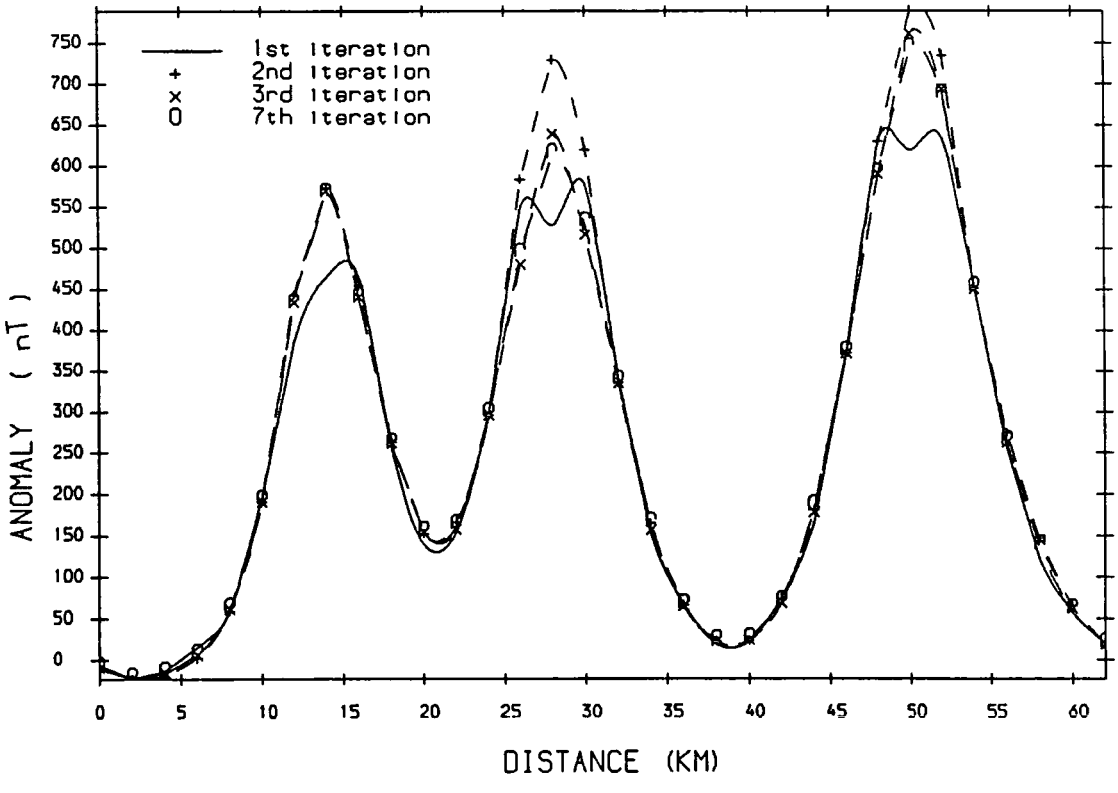

Figure 2.5b Upward continued anomalies onto a horizontal plane from the magnetic anomaly shown in figure 2.5c. Only the results from the first, second, third and seventh iterations are shown. The upward continuation level is 2 km above the reference datum.

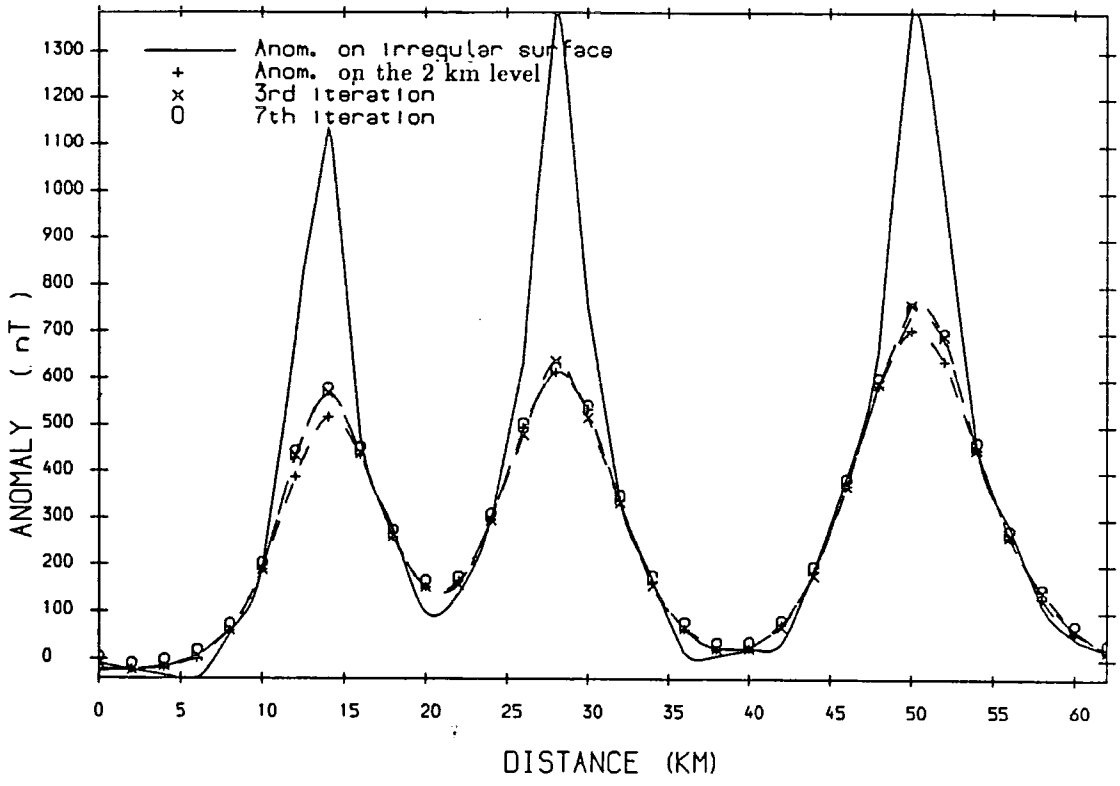

Figure 2.5c Comparison of the upward continued anomalies from the third (x) and seventh (o) iterations to the magnetic anomaly calculated on the upward continuation level (+). The magnetic anomaly calculated on the irregular surface (line) of figure 2.5a is also shown. The anomaly are calculated from bodies placed at 5, 6 and 7 km depth using magnetization of 2.0 A/m. The earth's magnetic field and body magnetization declinations and inclinations are -10.4 and 70.3 ^{o}

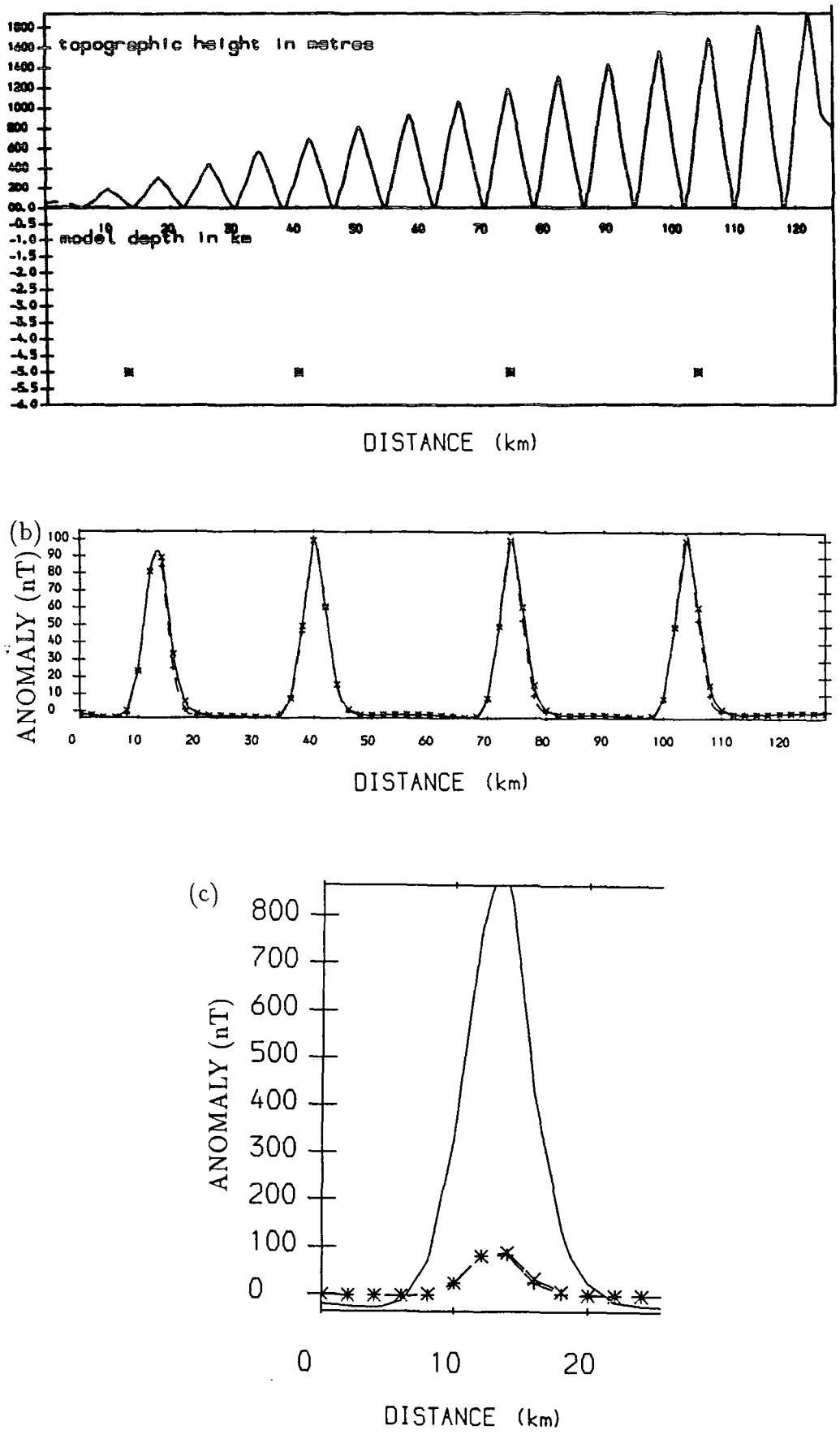

Figure 2.6 (a) Topopgraphy, depth and location of the point masses. (b) The upward continued anomaly (+) and calculated anomaly (x) on the 2 km continuation height. (c) Enlargment of the anomaly at the 10-20 km distance. Bold line is the anomaly calculated on the irregular surface.

anomalies are about 10 km. The result shows that the procedure is able to upward continue medium to long wavelength anomalies observed on an irregular surface onto a horizontal plane above successfully (figures 2.6b). One of the anomalies calculated on the irregular surface is shown in figures 2.6c.

Figure 2.7 is a result of an upward continuation test carried out using magnetic anomalies calculated over topographic surface of different wavelengths (about 6 to 12) km. The sources are placed at 3 km depth (figure 2.7a). The upward continuation was carried to a height of 2 km. The procedure is still able to reduce such short wavelength anomalies (figure 2.7b). However, slight differences started to appear between the upward continued anomaly and the anomaly calculated at the 2 km level (figure 2.7c) even over the long wavelength topographic features. Tests using shorter wavelength topography and shallower sources (shorter anomaly wavelengths), indicated increasing difference between the upward continued anomalies and the anomalies calculated on the continuation plane. Short wavelength instabilities were also introduced. Figure 2.8 shows the test result using topographic wavelength of about 5 to 15 km, source depth of 2 km and a maximum continuation height of 2.3 km. The short wavelength instabilities are pronounced at the region of short wavelength topography.

The tests indicate that the upward continuation procedure can successfully upward continue magnetic anomalies observed on an irregular surface onto a horizontal plane above. The continuation procedure, however, is limited by the short wavelength components of the anomalies and topography, and the continuation heights. The short wavelength anomalies particularly with high amplitude may not be totally reduced whilst short wavelength topography and large continuation height may cause high amplification of errors. Using a sampling interval of 2 km in the x and the y directions, the safe limit for the continuation height is about 2 km. The smoothed topographic height data used to continue the aeromagnetic data on to a horizontal plane above has a maximum height difference of less than this limiting continuation height. Therefore instability due to continuation height is not likely to be a serious problem.

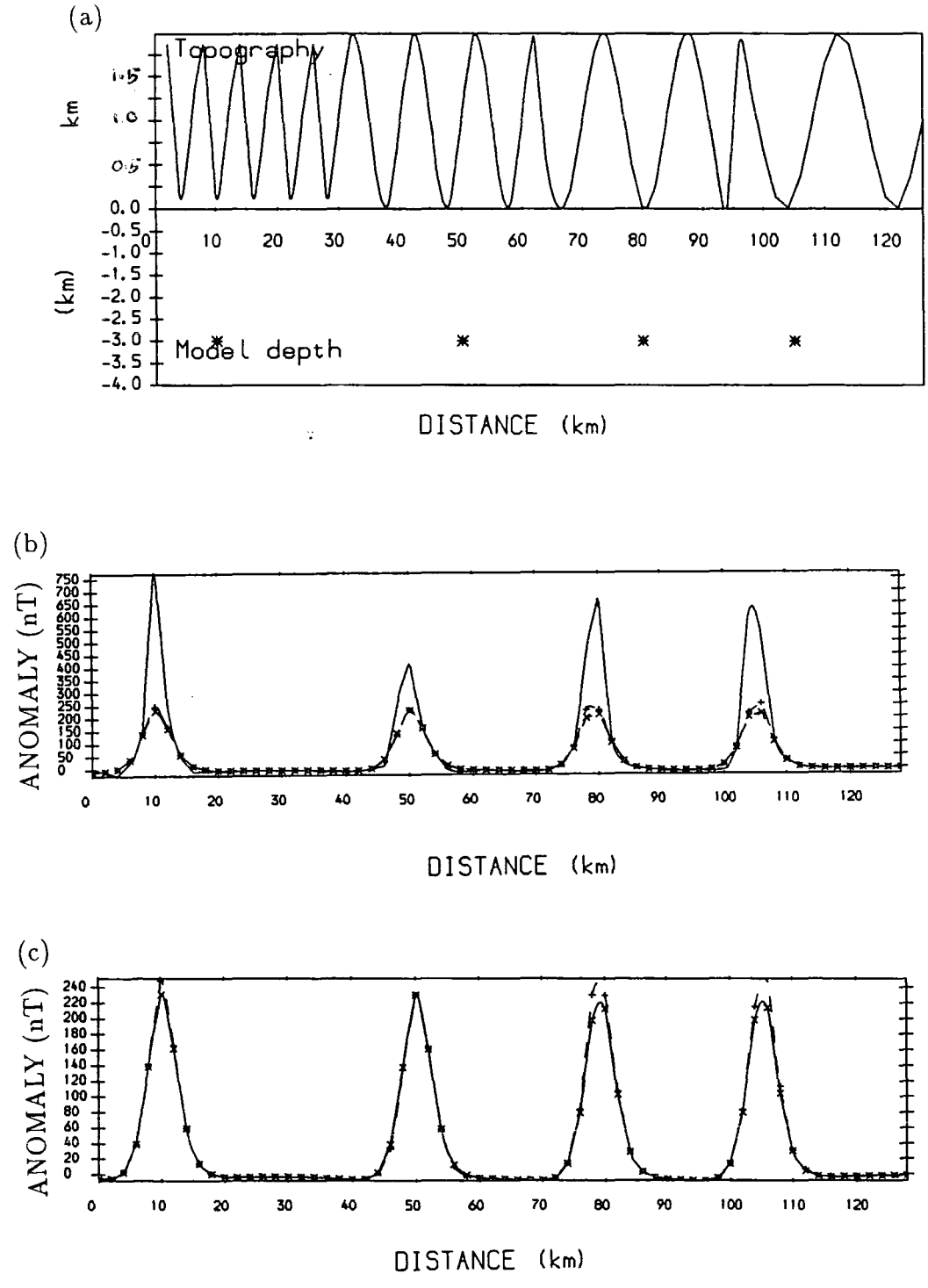

Figure 2.7 (a) Topopgraphy, depth and location of the point masses. (b) The upward continued anomaly (+) and calculated anomaly (x) on the 2 km continuation height and the anomaly calculated on the irregular surface (line). (c) The upward continued anomaly (+) and calculated anomaly (x) on the 2 km continuation height of figure (b).

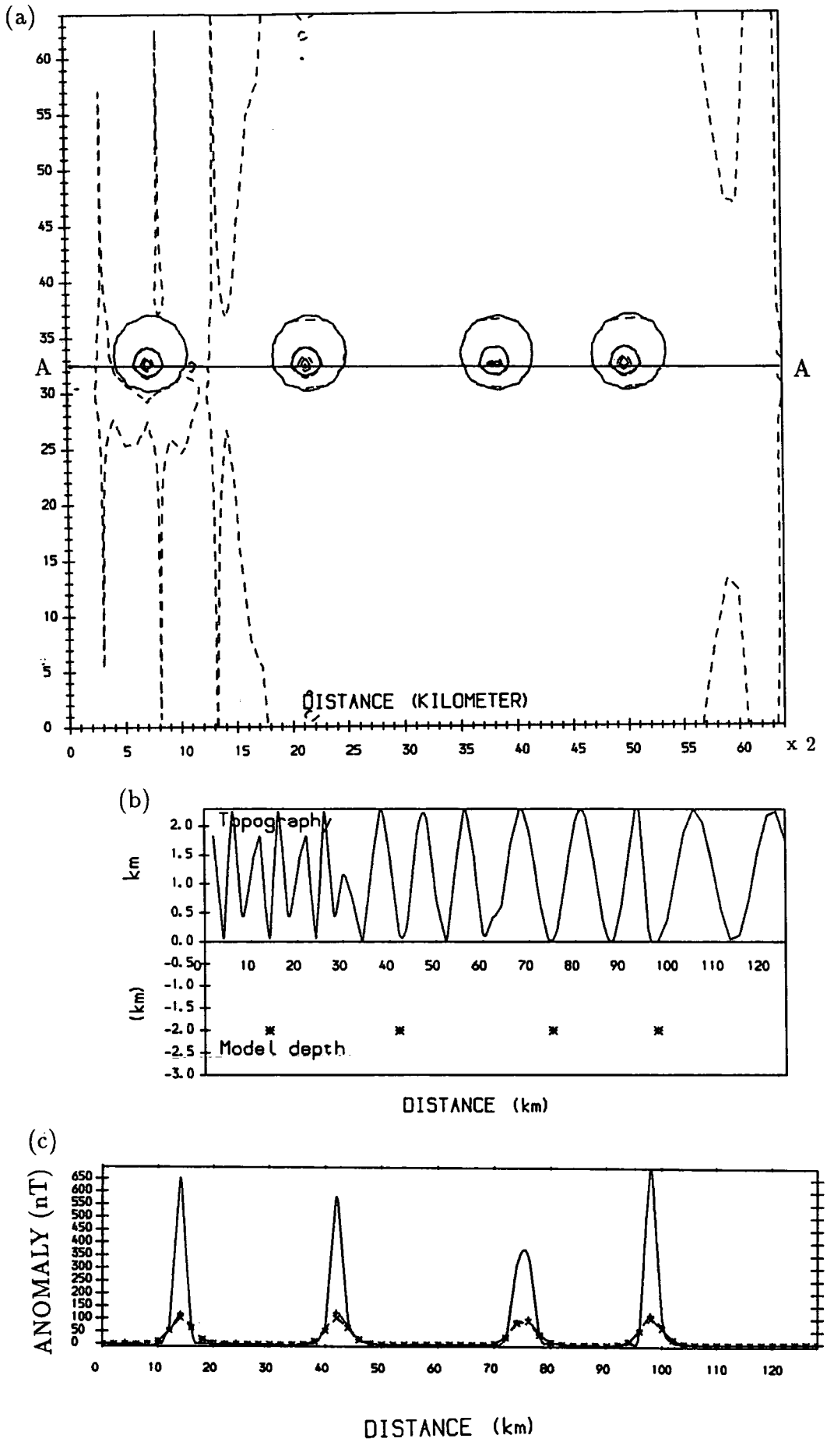

Figure 2.8 (a) Map showing the upward continued anomalies (dashed) and the anomalies calculated on the 2.3 km continuation level (line). (b) The topography, location and depth of the sources. (c) The upward continued anomaly (+) and calculated anomaly (x) on the 2 km continuation height, and the anomaly calculated on the irregular surface (line) along AA′ in figure (a).

The tests also indicate that at this continuation height topographic wavelengths of less than 5 km and short wavelength anomalies of the same order as produced by a point source at a depth of 2 km may give rise to instability. The aeromagnetic data and the height data used in this thesis have been smoothed which reduces the high frequency contents during the gridding process. The instability effect of the high frequency contents is not expected to be large. The reduction procedure can therefore be used to reduce the aeromagnetic data effectively.

2.7 Problems related to the use of the Fourier method

The problems related to Fourier series and the use of the discrete Fourier transform include the aliasing effect and the edge effect. The aliasing effect can occur when a continuous function is sampled at an interval greater than half the shortest wavelength. To obtain a more exact representation of the function any wavelength shorter than twice the sampling interval must be removed or filtered out. Alternatively the data may be sampled using smaller sampling intervals so as to include more of the higher frequency components to give a better approximation to the true data. The original aeromagnetic data digitised at 10 nanotesla interval by BGS contains shorter wavelength components than twice the sampling interval used in the gridding. The gridding of the data using the radial averaging method has already smoothed the aeromagnetic anomalies. This has a similar effect to filtering out the higher frequency contents. The aliasing effect arising from the filtered data is not therefore expected to be severe.

The Fourier method assumes periodicity outside the region of the representation. In practice the anomalies are assumed to repeat outside the study area. This may give rise to discontinuities at the edges of the area used. Synthesis using the Fourier method causes the anomaly to oscillate about the discontinuities. This is known as the edge effect. Data affected by the edge effect cannot validly be used for

analysis. In practice the edge effect can be reduced and avoided in a number of ways. One method is to reduce the discontinuities at the edges. One way of doing this is to apply a cosine series (Tsay 1975) to the edges of the data or to add extrapolated values surrounding the study area (Gupta and Ramani 1978). The cosine method tapers the values near the edges to a mean value. This necessitates the use of the edge data and these data still cannot be used for analysis. Extrapolating values surrounding the study area is useful where the behavior of the anomalies outside the region is known. Padding the surrounding regions with zero also helps reduces the edge effect. Padding the data with zeroes has been carried out where necessary. Richard and Blakely (1988) used a technique in which they rotate the magnetic data about an origin, then Fourier transform and rotate back by the same amount. By stacking the results of a number of rotations the edge effect can be reduced significantly.

The easiest and most effective way of avoiding the edge effect within the study area is to used an area larger than the area of interest. As the edge effect only affects areas near the discontinuities the area studied is then free of the edge effect. This is only possible if data surrounding the study area are available. Avoiding taking the edges through anomalous areas reduces the discontinuities and this also helps to reduce the edge effect.

CHAPTER 3

Pseudogravimetric transformation and other interpretation methods

3.1 Pseudogravimetric transformation method

This chapter describes the method used for transformation of a magnetic anomaly map to a pseudogravimetric anomaly map. This is followed by description of the interpretation methods used later in the thesis. The derivation of the pseudogravimetric transformation procedure follows Tantrigoda (1982). The transformation routine implemented by Tantrigoda has been upgraded to use the more efficient fast Fourier transform routine from the Numerical Analysis Group subroutine packages (NAG) available in the University of Durham Computer Centre.

The pseudogravimetric transformation as first introduced by Baranov (1957) used a double integration method. It is based on the Poisson relation between gravity and magnetic potentials and is valid under the conditions of constant density to magnetization ratio and constant magnetization direction. The relationship between the pseudogravimetric anomaly $g(M)$ at any point M above a surface S due to the total field $T(P)$ at any point P on the surface is

$$g(M) = -\frac{1}{2\pi} \int\int_{\pi} H(M,P)T(P)dS_p,$$

where $H(M,P)$ is the kernal of the transformation. With the magnetization direction pointing downwards, the kernal involves line integrals along the opposite directions to both the magnetization and the earth's magnetic field. Baranov assumed the direction of magnetization to be in the direction of the total field.

Bott et al. (1966) extended the procedure to the case where the direction of magnetization is not along the direction of the earth's magnetic field. The magnetic and gravity potentials were treated as complex functions. The transformation used the Cauchy-Riemann equations. The transformation was applied to the two-

dimensional case. The method was used to estimate remanent magnetization.

Bott and Ingles (1972) used the equivalent layer theorem to carry out the two-dimensional pseudogravimetric transformation. The equivalent layer is divided into units of rectangular cross section where the magnetization of each block is specified in direction and its value is calculated by matrix linear inversion. Using a constant ratio of density to magnetization, each block is assigned a uniform density contrast proportional to the calculated magnetization distribution. The pseudogravimetric anomaly can then be calculated from the equivalent source. Both two and three-dimensional transformations can be carried out using this method.

A method applying the Weiner filter has been used by Gunn (1972). The coefficients used in the transformation are generally specific to the models. The method, therefore, needs some knowledge of the causative body to carry out the transformation.

Shuey (1972) carried out the two-dimensional pseudogravimetric transformation using the Hilbert transform. The pseudogravimetric anomaly is derived by combining the reduction to pole transformation with vertical integration. The numerical computation is carried out using the Hilbert transform which transforms the vertical integration to horizontal integration. The calculation using the the horizontal integration is reportedly performed with greater numerical efficiency and stability than the vertical integration. The method, however, is dependent on the efficiency of the programme for carrying out the Hilbert transformation.

The Fourier method was first used by Cordell and Taylor (1971) to carry out the pseudogravimetric transformation. Using the Poisson relation they obtained a relationship between the magnetic anomaly and the gravity anomaly. Fourier transformation gives frequency domain relationship between the magnetic anomalies and the pseudogravimetric anomalies.

Tantrigoda (1982) implemented a transformation operator in the frequency

domain which is basically similar to that of Cordell and Taylor (1971). Tantrigoda used two different approaches to obtain the theoretical relationship for the pseudo-gravimetric transformation. Both approaches produce the same final expression. The first approach integrated the magnetic potential in form of a Fourier series to recover the pseudogravimetric potential. The second approach used a differentiation procedure which has also been used in this thesis to derive the pseudogravimetric transformation.

3.2 The three-dimensional transformation

The gravity potential U and magnetic potential V of a body with density proportional to intensity of magnetization at each point and magnetization in a constant direction are related by the Poisson equation

$$V = -\frac{1}{4\pi G}\frac{J}{\rho}(\underline{c}.\nabla U), \qquad \frac{J}{\rho} = \text{constant}, \tag{3.1}$$

where

J = intensity of magnetization,

$\underline{c}$ = unit vector in the direction of magnetization,

ρ = density of the mass,

and G = gravitational constant.

The magnetic field component F in the direction of the unit vector $\underline{s}$ can be derived from the potential as follows,

$$F = -\mu_o(\underline{s}.\nabla V) \tag{3.2}$$

where μ_o is the permeability. Substituting equation 3.1 into equation 3.2 gives the following expression relating gravity potential and magnetic field

$$F = \frac{\mu_o}{4\pi G}\frac{J}{\rho}\underline{s}.\nabla(\underline{c}.\nabla U). \tag{3.3}$$

The gravity potential can thus be obtained from the magnetic field by the integrals along $\underline{s}$ and $\underline{c}$. The gravity field can then be derived from the gravity potential by

differentiation. A constant ratio between density and magnetization must be assumed for the pseudogravimetric transformation.

The actual formulation of the programme as written assumes a square grid of data with side L, digitised at $(2N+1)^2$ data points. Taking x as the north direction, y as the east direction, z as the vertical direction positive downwards, $\underline{j}$, $\underline{k}$ and $\underline{l}$ as the unit vectors in x, y and z directions, I_s and D_s as the the inclination and declination of the earth's magnetic field and I_c and D_c as the the inclination and declination of the magnetization, then $\underline{c} = \cos I_c \cos D_c \underline{j} + \cos I_c \sin D_c \underline{k} + \sin I_c \underline{l}$ and $\underline{s} = \cos I_s \cos D_s \underline{j} + \cos I_s \sin D_s \underline{k} + \sin I_s \underline{l}$. D_s and D_c are measured from the positive x axis.

The anomalous magnetic field component $F(x,y,z)$ in a constant direction and the gravity potential $U(x,y,z)$ satisfy Laplace's equation and can be represented by Fourier series in the xy-plane and by the solution of Laplace's equation in three-dimensional space as described in chapter 2. The gravity potential and the magnetic field can be written as

$$U(x,y,z) = \sum_{m=-N}^{N} \sum_{n=-N}^{N} U(m,n,0) e^{i(2\pi mx/L + 2\pi ny/L)} e^{|K|z} \qquad 3.4a$$

and

$$F(x,y,z) = \sum_{m=-N}^{N} \sum_{n=-N}^{N} F(m,n,0) e^{i(2\pi mx/L + 2\pi ny/L)} e^{|K|z} \qquad 3.4b$$

where $|K| = \frac{2\pi}{L}(m^2+n^2)^{\frac{1}{2}}$. Differentiating the gravity potential (equation 3.4a) gives

$$\nabla U(x,y,z) = \sum_{m=-N}^{N} \sum_{n=-N}^{N} U(m,n,0)(i\frac{2\pi m}{L}\underline{j} + i\frac{2\pi n}{L}\underline{k} + |K|\underline{l}) e^{i2\pi(mx+ny)/L} e^{|K|z}.$$

The derivative in the direction of magnetization $\underline{c}$ is

$$\underline{c}.\nabla U(x,y,z) = \sum_{m=-N}^{N} \sum_{n=-N}^{N} U(m,n,0) e^{i2\pi(mx+ny)/L} e^{|K|z} (i\frac{2\pi m}{L} \cos I_c \cos D_c$$

$$+ i\frac{2\pi n}{L} \cos I_c \sin D_c + |K| \sin I_c). \qquad 3.5$$

The magnetic potential $V(x,y,z)$ from equations 3.1 and 3.5 is

$$V(x,y,z) = -\frac{1}{4\pi G}\frac{J}{\rho}\sum_{m=-N}^{N}\sum_{n=-N}^{N} U(m,n,0)e^{i2\pi(mx+ny)/L}e^{|K|z}\sin I_c(iT_c+|K|) \quad 3.6$$

where

$$T_c = \frac{2\pi}{L}\frac{\cos I_c}{\sin I_c}(m\cos D_c + n\sin D_c).$$

The magnetic anomaly is obtained by differentiating the potential as in equation 3.2 giving

$$\mu_o \nabla V(x,y,z) = -\sum_{m=-N}^{N}\sum_{n=-N}^{N} AU(m,n,0)e^{i2\pi(mx+ny)/L}e^{|K|z}\sin I_c(iT_c+|K|)(i\frac{2\pi m}{L}\underline{\mathrm{j}}$$

$$+i\frac{2\pi n}{L}\underline{\mathrm{k}} + |K|\underline{\mathrm{l}})$$

where $A = (\mu_o/4\pi G)(J/\rho)$. The derivative in the direction $\underline{\mathrm{S}}$ is

$$-\mu_o \underline{\mathrm{S}}.\nabla V(x,y,z) = \sum_{m=-N}^{N}\sum_{n=-N}^{N} AU(m,n,0)e^{i2\pi(mx+ny)/L}e^{|K|z}\sin I_c(iT_c+|K|)$$

$$(i\frac{2\pi m}{L}\cos I_s\cos D_s + i\frac{2\pi n}{L}\cos I_s\sin D_s + |K|\sin I_s)$$

$$= \sum_{m=-N}^{N}\sum_{n=-N}^{N} AU(m,n,0)e^{i2\pi(mx+ny)/L}e^{|K|z}\sin I_c\sin I_s(iT_c+|K|)(iT_s+|K|) \quad 3.7$$

where

$$T_s = \frac{2\pi}{L}\frac{\cos I_s}{\sin I_s}(m\cos D_s + n\sin D_s).$$

Equating equations 3.7 and 3.4*b* gives the modified Fourier coefficients of the gravity potential in term of those of the magnetic anomaly:

$$U(m,n,0) = \frac{1}{A}\frac{F(m,n,0)}{\sin I_c\sin I_s}\frac{1}{(iT_c+|K|)(iT_s+|K|)}. \quad 3.8$$

The gravity anomaly $g(x,y,z)$ can be obtained by differentiating the gravity potential with respect to the vertical direction $\underline{\mathrm{l}}$,

$$g(x,y,z) = \frac{dU(x,y,z)}{dz}.$$

Replacing the gravity potential with its Fourier series expression (equation 3.4a) and differentiating to obtain the gravity anomaly, the pseudogravimetric anomaly may be written as

$$g(x,y,z) = \sum_{m=-N}^{N} \sum_{n=-N}^{N} \frac{1}{A} \frac{F(m,n,0)}{\sin I_c \sin I_s} \frac{|K|}{(iT_c + |K|)(iT_s + |K|)} e^{i2\pi(mx+ny)/L} e^{|K|z}. \quad 3.9$$

This can be rewritten as

$$g(x,y,z) = \sum_{m=-N}^{N} \sum_{n=-N}^{N} g'(m,n,0) e^{i2\pi(mx+ny)/L} e^{|K|z} \quad 3.10$$

where

$$g'(m,n,0) = F(m,n,0)A'K',$$

$$A' = \frac{1}{A} = \frac{4\pi G}{\mu_o} \frac{\rho}{J}, \qquad \text{(density to magnetization ratio)}$$

and $$K' = \frac{|K|^3 - T_s T_c |K| - i(T_s + T_c)|K|^2}{\sin I_c \sin I_s (T_c^2 + |K|^2)(T_s^2 + |K|^2)} \qquad \text{(transformation operator).}$$

The pseudogravimetric anomaly is then expressed as a Fourier series having coefficients $g'(m,n,0)$. The pseudogravimetric transformation may be carried out as described below.

The inclination and declination of the magnetization are initially determined from known sources or may be assumed to be along the earth's magnetic field. The IGRF routine (Barraclough and Malin 1971) has been used to determine the direction of the earth's magnetic field. The density to magnetization ratio may be set such that reasonable amplitudes are obtained for the pseudogravimetric anomalies. The height z is the height at which the pseudogravimetric anomalies are needed or they may be obtained at the same level as the magnetic anomalies by putting z=0. When the height $z = 0$, the function $e^{|K|z}$ becomes unity. The two-dimensional Fourier analysis is then applied to the magnetic anomaly. Each coefficient is modified by the height function, density to magnetization ratio and the transformation operator. Inverse Fourier transformation using the modified coefficients $g'(m,n,z)$ then gives the pseudogravimetric anomalies. The three-dimensional pseudogravimetric transformation programme PSGRA3D is given in Appendix 3.1.

3.3 The two-dimensional transformation

The two-dimensional relationship between gravity g_2 and magnetic field F_2 may be derived from the Poisson relation and Laplace's equation. It can be written as (Bott 1969)

$$F_2 = \frac{\mu_o f' |J|}{4\pi G\rho}(\sin\beta\frac{\partial g_2}{\partial x} - \cos\beta\frac{\partial g_2}{\partial z}), \qquad 3.11$$

where

$$f' = (\sin^2 I_c + \cos^2 I_c \cos^2 \alpha_c)^{\frac{1}{2}}(\sin^2 I_s + \cos^2 I_s \cos^2 \alpha_s)^{\frac{1}{2}}$$

and

$$\beta = \arctan(\frac{\tan I_c}{\cos \alpha_c}) + \arctan(\frac{\tan I_s}{\cos \alpha_s}).$$

α_c and α_s are the azimuth of the directions of magnetization and the earth's magnetic field respectively, measured with respect to the positive x direction. x is the direction perpendicular to strike of the body (y direction) and z is vertical downwards. Other notation follows the three-dimensional case. In the two-dimensional case $|K| = |k|$.

Taking a profile of length L with $2M + 1$ data points, the discrete two-dimensional Fourier series representation of the magnetic and gravity anomalies may be written as

$$F_2(x,z) = \sum_m F_{2m}(k,0)e^{ikx}e^{|k|z} \qquad 3.12a$$

and

$$g_2(x,z) = \sum_m g_{2m}(k,0)e^{ikx}e^{|k|z} \qquad 3.12b$$

where the wavenumber $k = 2\pi m/L$, $m = -M...1,0,1...M$, L is the fundamental wavelength in the x direction and $|k| = |2\pi m/L|$. Equation 3.11 may be rewritten as

$$F_2(x,z) = \frac{\mu_o f' |J|}{4\pi G\rho}\Big(\sin\beta\frac{\partial g_2(x,z)}{\partial x} - \cos\beta\frac{\partial g_2(x,z)}{\partial z}\Big).$$

Expressing the gravity anomaly as a Fourier series (equation 3.12b) and differentiating, and substituting in 3.11 gives

$$F_2(x,z) = \frac{\mu_o f' |J|}{4\pi G\rho}(\sin\beta\sum_m g_{2m}(k,0)ike^{ikx}e^{|k|z} - \cos\beta\sum_m g_{2m}(k,0)e^{ikx}|k|e^{|k|z}) \qquad 3.13$$

From equations 3.12a and 3.13

$$\sum_m F_{2m}(k,0)e^{ikx}e^{|k|z} = \frac{\mu_o f'|J|}{4\pi G\rho}(\sin\beta\sum_m g_{2m}(k,0)ike^{ikx}e^{|k|z}$$

$$-\cos\beta\sum_m g_{2m}(k,0)e^{ikx}|k|e^{|k|z}\rangle.$$

The individual terms in the series may be equated as

$$F_{2m}(k,0) = \frac{\mu_o f'|J|}{4\pi G\rho}ikg_{2m}(k,0)\sin\beta - \frac{\mu_o f'|J|}{4\pi G\rho}|k|g_{2m}(k,0)\cos\beta \qquad 3.14$$

and may be rewritten as

$$g_{2m}(k,0) = \frac{4\pi G\rho}{\mu_o f'|J|}F_{2m}(k,0)\frac{1}{(ik\sin\beta - |k|\cos\beta)}$$

$$= -F_{2m}(k,0)\frac{4\pi G\rho}{\mu_o f'|J|}\Big(\frac{\cos\beta}{|k|} + \frac{i\sin\beta}{k}\Big). \qquad 3.15$$

The two-dimensional pseudogravimetric anomaly can then be written as

$$g_{2m}(x,z) = \sum_m g'_{2m}(k,0)e^{ikx}e^{|k|z} \qquad 3.16$$

where

$$g'_{2m}(x,0) = -F_{2m}(k,0)A'_2K'_2,$$

$$A'_2 = \frac{4\pi G}{\mu_o}\frac{\rho}{|J|} \qquad \text{(density to magnetization ratio)}$$

and $$K'_2 = \Big(\frac{\cos\beta}{|k|} + \frac{i\sin\beta}{k}\Big)\frac{1}{f'} \qquad \text{(transformation operator).}$$

A similar procedure to that of the three-dimensional case may be used to carry out the pseudogravimetric transformation. The magnetic anomaly is first Fourier analysed and each coefficient is modified by the height function, density to magnetization ratio and the transformation operator. Fourier synthesis of the new coefficients gives the two-dimensional pseudogravimetric anomaly. The two-dimensional pseudogravimetric programme PSGRA2D is given in Appendix 3.2.

3.4 The Numerical Analysis Group Fourier transformation subroutines

The fast Fourier transform subroutines available in the Numerical Analysis Group (NAG) package calculate the finite discrete Fourier transform $\hat{a}_o$ (DFT) of a sequence of N real or complex values a_j. j and o are 0,1,2,....,N-1. $\hat{a}_o$ is periodic with period N. The DFT is implemented in the one-dimensional problems. Three type of transformation subroutines are available. They are for (1) real, (2) Hermitian and (3) general complex sequences. Each type comprises three routines, named as groups 1, 2 and 3.

Group 1 routines compute the Fourier transform without use of extra work space. Group 2 routines compute the Fourier transform using additional work storage. As a consequence the group 2 routines are much more efficient. The group 3 routines can only be implemented on vector-processing machines and are not implemented in the Durham Computer centre. The routines of group 2 for general complex sequences have been used in this thesis.

The one-dimensional transformation group 2 subroutine (CO6FCF) calculates the discrete Fourier transform of a sequence of N complex data. Subroutine CO6FJF is the multidimensional group 2 transformation routine for complex values. The routine calls the subroutine CO6FCF to perform the one-dimensional Fourier transform and repetitive call to the one-dimensional subroutine enable transformation of the multi-dimensional data.

3.5 Testing the transformation method

A programme SPHEREGM (Appendix 3.3) has been written to produce the magnetic and gravity anomalies of spherical bodies. This routine has been used to give anomalies from a specified system of spheres. In order to test the transformation programmes, gravity and magnetic anomalies of the same model were initially calculated. Pseudogravimetric transformation was carried out on the calculated magnetic anomalies using the actual ratio of density to magnetization (150 kg/m^{-1}:1 A/m).

The pseudogravimetric anomalies were then compared with the calculated gravity anomalies. Tests have been carried out for cases where the magnetization is both along and in different directions from that of the earth's magnetic field. The effects of different inclinations at different constant declination have been tested. Regression analysis has been used to test the degree of fit between the pseudogravimetric anomalies and the calculated gravity anomalies of the same model.

Tests for the three-dimensional cases have been carried out for single and multiple sources. The anomaly of a single source can either be represented by a single sphere or by several spheres close together. The regression analysis between the pseudogravimetric and the calculated gravity anomalies has been carried out by removing a strip of ten data points wide surrounding the 64 by 64 data points used for the testing. The data point spacing was 1x1 km^2 square. This is to remove any edge effect present in the pseudogravimetric anomalies caused by use of the Fourier method. Table 3.1 shows the correlation coefficients between the pseudogravimetric and the calculated gravity anomalies of a spherical body of radius 12 km having magnetization of 1.0 A/m along the earth's magnetic field direction and with the centre of gravity at 15 km depth. The tests for different inclinations at the same declination indicate that the transformation results in the highest degree of mismatch at smaller inclination angles (table 3.1). The tests on bodies having magnetization directions different from that of the earth's magnetic field give similar results (table 3.2). The mismatch between the pseudogravimetric and the calculated gravity anomalies becomes significant at inclinations of about 20 degrees for both and may give serious error at smaller inclination angles. This particularly applies when the magnetization and earth's magnetic field inclinations are both small. If one of the inclination components is high, good fit between the pseudogravimetric and the calculated gravity anomalies is still obtained (table 3.2). As the earth's field dips steeply in Great Britain, and the magnetization is probably essentially induced and in the same direction, the transformation should give good results in the region of study. Sample results of the three-dimensional tests using the earth's magnetic field inclination and

EARTH'S FIELD / BODY DECLINATIONS

EARTH'S FIELD / BODY INCLINATIONS	05/05°	10/10°	15/15°	20/20°	25/25°	30/30°	35/35°	40/40°	45/45°	50/50°	85/85°	90/90°
05/05°	0.584	0.917	0.980	0.984	0.962	0.947	0.926	0.744	0.932	0.744	0.584	0.035
10/10°	0.881	0.945	0.982	0.992	0.992	0.985	0.971	0.953	0.954	0.953	0.881	0.897
25/25°	0.978	0.980	0.989	0.994	0.995	0.993	0.990	0.989	0.989	0.989	0.978	0.984
30/30°	0.994	0.993	0.994	0.996	0.997	0.997	0.997	0.997	0.997	0.997	0.994	0.996
35/35°	0.998	0.997	0.997	0.998	0.998	0.998	0.999	0.999	0.999	0.999	0.998	0.998
40/40°	0.999	0.999	0.998	0.999	0.999	0.999	0.999	1.000	1.000	1.000	0.999	0.999
45/45°	1.000	1.000	1.000	1.000	1.000	1.000	1.000	1.000	1.000	1.000	1.000	1.000
50/50°	1.000	1.000	1.000	1.000	1.000	1.000	1.000	1.000	1.000	1.000	1.000	1.000
85/85°	1.000	1.000	1.000	1.000	1.000	1.000	1.000	1.000	1.000	1.000	1.000	1.000
90/90°	1.000	1.000	1.000	1.000	1.000	1.000	1.000	1.000	1.000	1.000	1.000	1.000

Table 3.1 Correlation coefficient (CC) of the transformed pseudogravimetric and calculated gravity anomalies of a spherical body of radius 12 km with the centre at 15 km depth and having magnetization along the earth's magnetic field. The magnetic anomalies were calculated using magnetization of 1.0 A/m. The pseudogravimetric transformation was then carried out using density to magnetization ratio of 150 kg m^{-1}:1.0 A/m. The inclinations and declinations of the earth's field and the body are the same for each CC. The maximum pseudogravimetric value is 32.2 mGal. A symmetry of the CC occurs about the 45° declination.

EARTH'S FIELD / BODY DECLINATIONS

EARTH'S FIELD / BODY INCLINATIONS	05/05°	5/15°	5/30°	5/45°	5/70°	5/85°	45/05°	45/25°	45/45°	45/85°	85/05°	85/85°
05/05 °	0.584	0.884	0.967	0.967	0.998	1.000	0.967	0.911	0.932	0.967	1.000	0.584
05/15°	0.846	0.909	0.967	0.985	0.998	1.000	0.980	0.955	0.934	0.980	1.000	0.846
05/30°	0.963	0.966	0.980	0.990	0.999	1.000	0.990	0.983	0.979	0.990	1.000	0.963
05/45°	0.988	0.988	0.991	0.994	0.999	1.000	0.995	0.993	0.992	0.995	1.000	0.988
05/70°	0.998	0.998	0.998	0.999	1.000	1.000	0.999	0.999	0.999	0.999	1.000	0.998
05/85°	1.000	1.000	1.000	1.000	1.000	1.000	1.000	1.000	1.000	1.000	1.000	1.000
45/05 °	0.988	0.996	0.998	0.995	1.000	1.000	0.994	0.999	0.992	0.994	1.000	0.988
45/25°	0.999	0.999	0.999	0.999	1.000	1.000	0.999	1.000	1.000	0.999	1.000	0.999
45/45°	1.000	1.000	1.000	1.000	1.000	1.000	1.000	1.000	1.000	1.000	1.000	1.000
45/85°	1.000	1.000	1.000	1.000	1.000	1.000	1.000	1.000	1.000	1.000	1.000	1.000
85/05°	1.000	1.000	1.000	1.000	1.000	1.000	1.000	1.000	1.000	1.000	1.000	1.000
85/85°	1.000	1.000	1.000	1.000	1.000	1.000	1.000	1.000	1.000	1.000	1.000	1.000

Table 3.2 Correlation coefficient of pseudogravimetric and calculated gravity anomalies of a spherical body of radius 12 km with the centre at 15 km depth and with the magnetization of the body different from the earth's magnetic field. The magnetic anomalies were calculated using magnetization of 1.0 A/m and the pseudogravimetric transformation was carried out using density to magnetization ratio of 150 kg/ m^{-3}:1.0 A/m. The maximum pseudogravimetric value is 32.2 mGal.

declination of the Scotland region are given below.

Figure 3.1 shows the three dimensional magnetic anomaly due to a system of spheres, of radii 10 and 15 km at depths corresponding to the radii, calculated using a magnetization contrast of 1.0 A/m. The declination D_s and inclination I_s of the earth's magnetic field are -10.4^o and 70.3^o respectively. The magnetization of the spheres is taken to be induced and to have the same declination D_c and inclination I_c as those of the earth's magnetic field. The comparison along profile A-A$'$ indicates that the transformation of the magnetic anomaly results in a pseudogravimetric anomaly similar to the calculated gravity anomaly (figure 3.2). Although the result shows similar shape and amplitude, the pseudogravimetric anomaly is shifted down by an arbitrary constant value relative to the calculated gravity values (figure 3.2). The reason is that the pseudogravimetric anomaly incorporates an arbitrary constant background value, which could be regarded as the anomaly due to an infinite horizontal slab. Such a slab gives a zero magnetic anomaly, but a constant gravity anomaly. Adding the background effect onto the pseudogravimetric anomaly results in a good fit to the calculated gravity anomaly except at the edges (figure 3.3). The differences at the edges are due to the edge effect. The three-dimensional comparison of the pseudogravimetric anomaly with background value of 12 mGal, with the calculated gravity anomaly is given in figure 3.4.

Sources at different depths have been used to test the effects of different wavelengths. Anomalies due to spheres with the centres at 2 to 20 kilometre with depths corresponding to the radii have been calculated using a magnetization contrast of 1.0 A/m, and earth's magnetic field declination and inclination of -10.4^o and 70.3^o respectively (figure 3.5). The magnetization is taken to be induced in the earth's magnetic field direction. The transformation has been carried out using density to magnetization ratio of 150 kg/m^{-3}:1 A/m. Comparison of the pseudogravimetric anomaly with the calculated gravity anomaly along a profile such as B-B $'$ indicates that the transformation is successful (figures 3.6). The shorter wavelength components observed in the magnetic anomaly (figure 3.7) have been suppressed during the

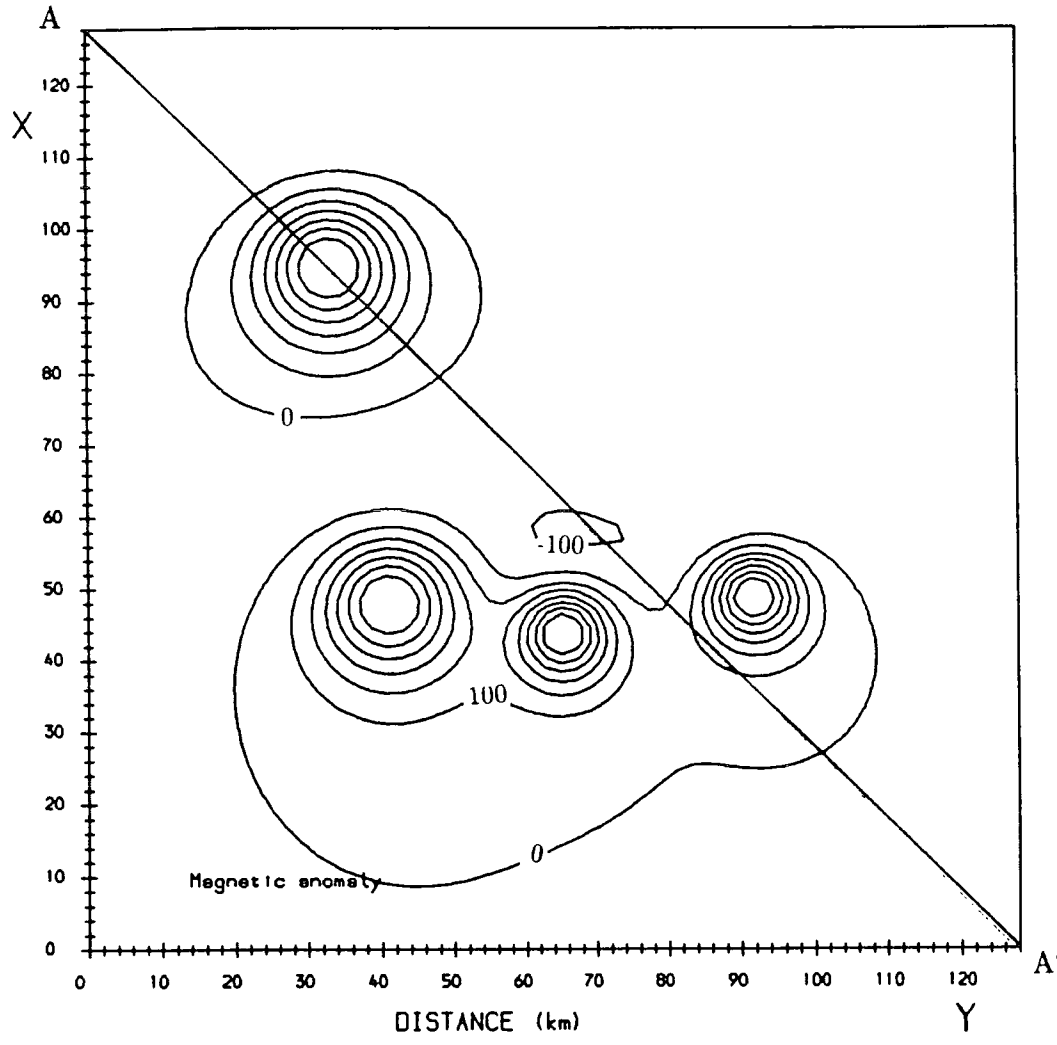

Figure 3.1 Calculated magnetic anomaly for the three-dimensional pseudogravimetric test. Magnetization of the body is 1.0 A/m. Declinations and inclinations: D_s=-10.4, I_s=70.3, D_c=-10.4 and I_c=70.3. Contour interval is 100 nT. The depths of the sources for the anomaly peaking at Y and X coordinates of about 40 and 50, 64 and 45, 32 and 96, and 90 and 50 km are 15, 10, 15 and 10 km respectively. The radii of the spheres correspond to the depths.

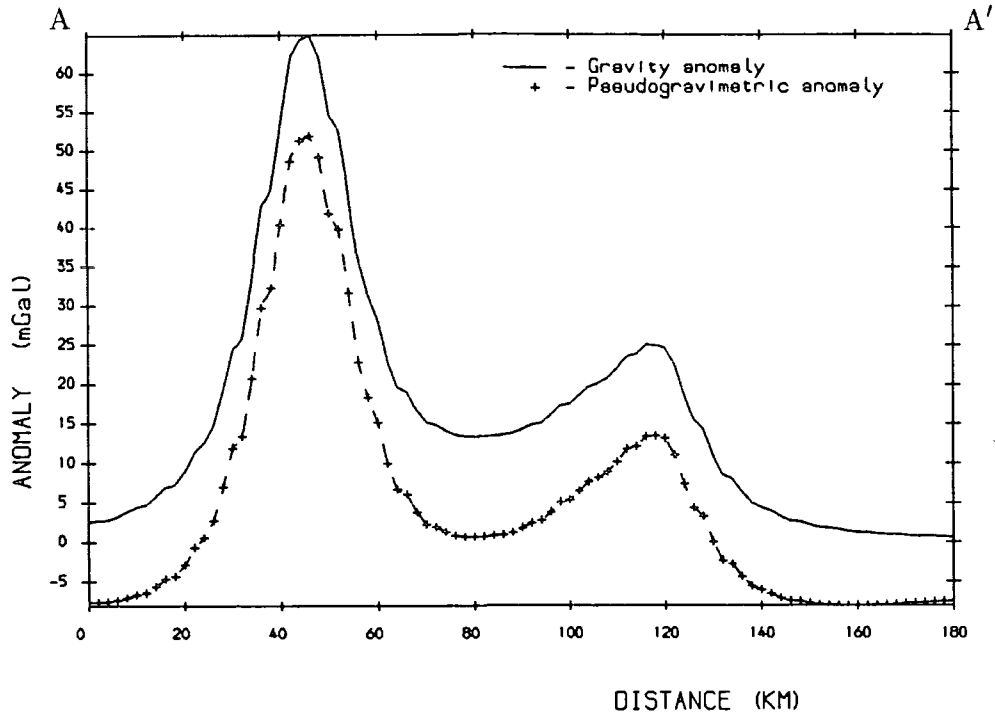

Figure 3.2 Comparison of the pseudogravimetric anomaly without the background value (+) with the calculated gravity anomaly (line) along profile AA′ figure 3.4.

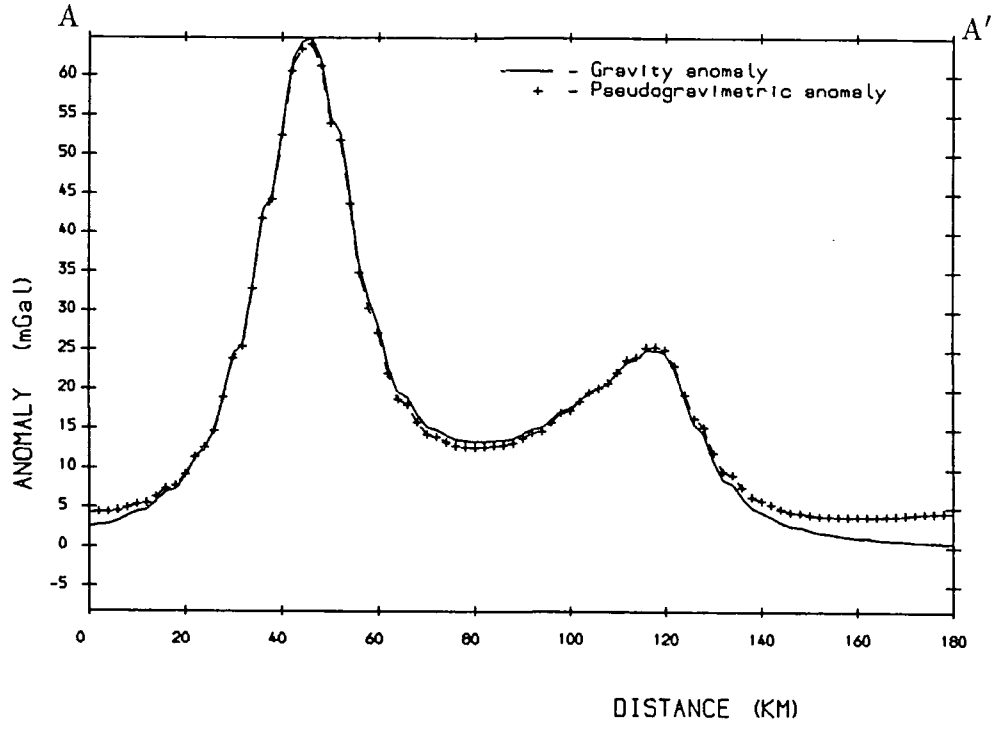

Figure 3.3 Comparison of the pseudogravimetric anomaly with background value (+) of 12 mGal, with the calculated gravity anomaly (line) along profile AA′ figure 3.4.

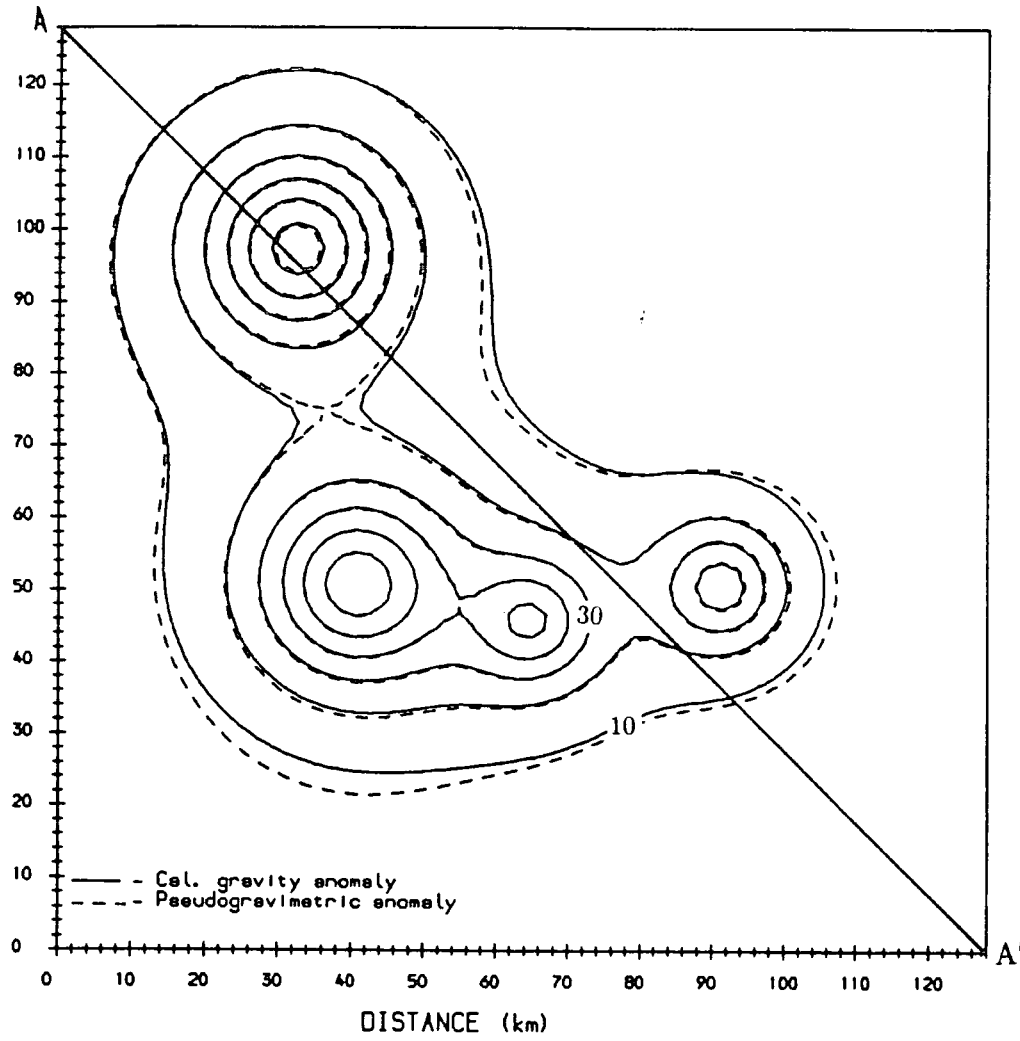

Figure 3.4 Three-dimensional comparison of the pseudogravimetric anomaly (dashed) transformed from the magnetic anomaly in figure 3.1 with a background value of 12 mGal, with the calculated gravity anomaly (line) of the same model. The density (kg/m^2) to magnetisation (A/m) ratio is 150:1.0. The contour interval is 10 mGal.

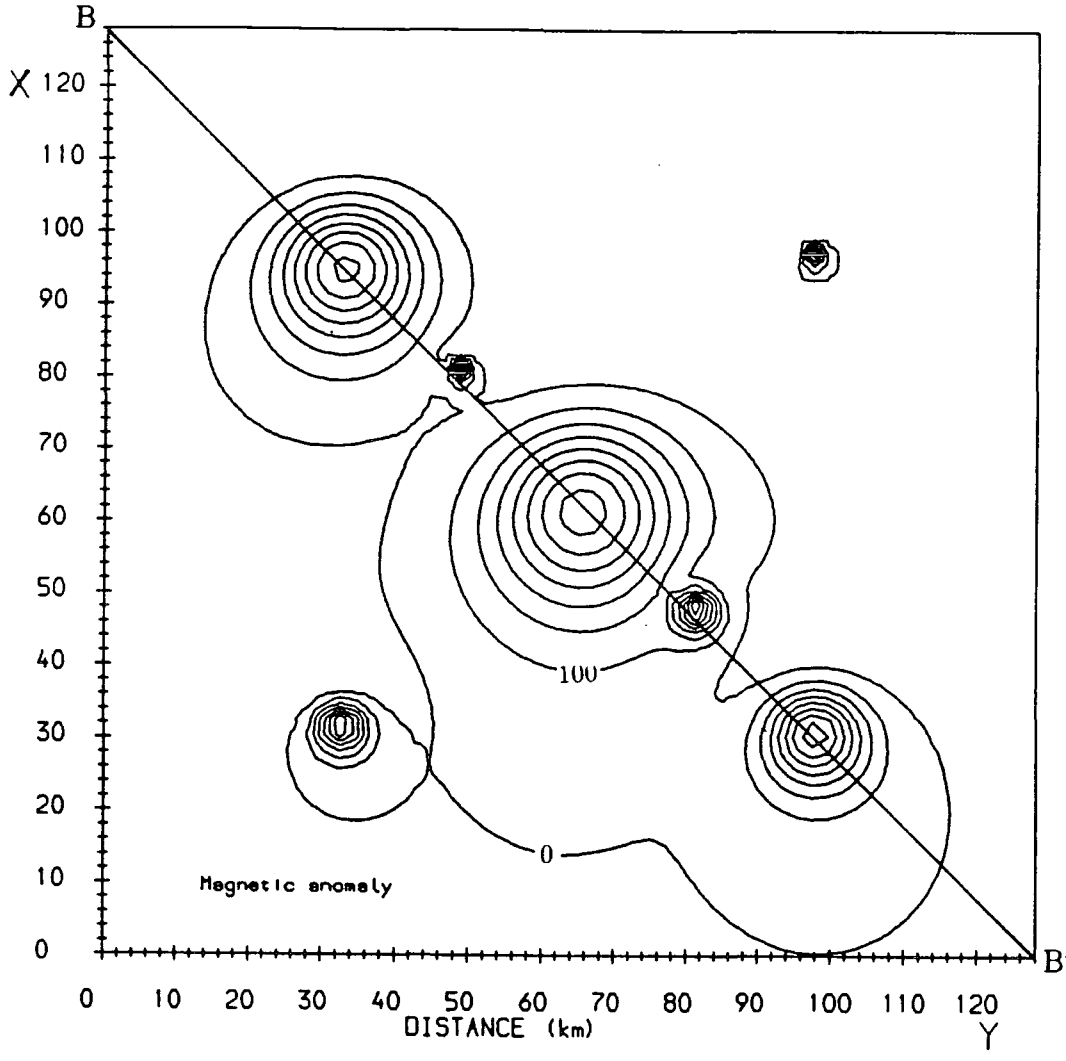

Figure 3.5 Calculated magnetic anomaly for the three-dimensional pseudogravimetric test. Magnetization of the body is 1.0 A/m. Declinations and inclinations : D_s=-10.4, I_s=70.3, D_c=-10.4 and I_c=70.3. Contour interval is 100 nT. The depths of the sources for the anomaly peaking at Y and X coordinated of about 64 and 64, 48 and 80, 32 and 96, 80 and 48, 96 and 32, 32 and 32, and 96 and 96 km are 20, 2, 15, 4, 10, 5, and 2 km respectively. The radii of the spheres correspond to the depths.

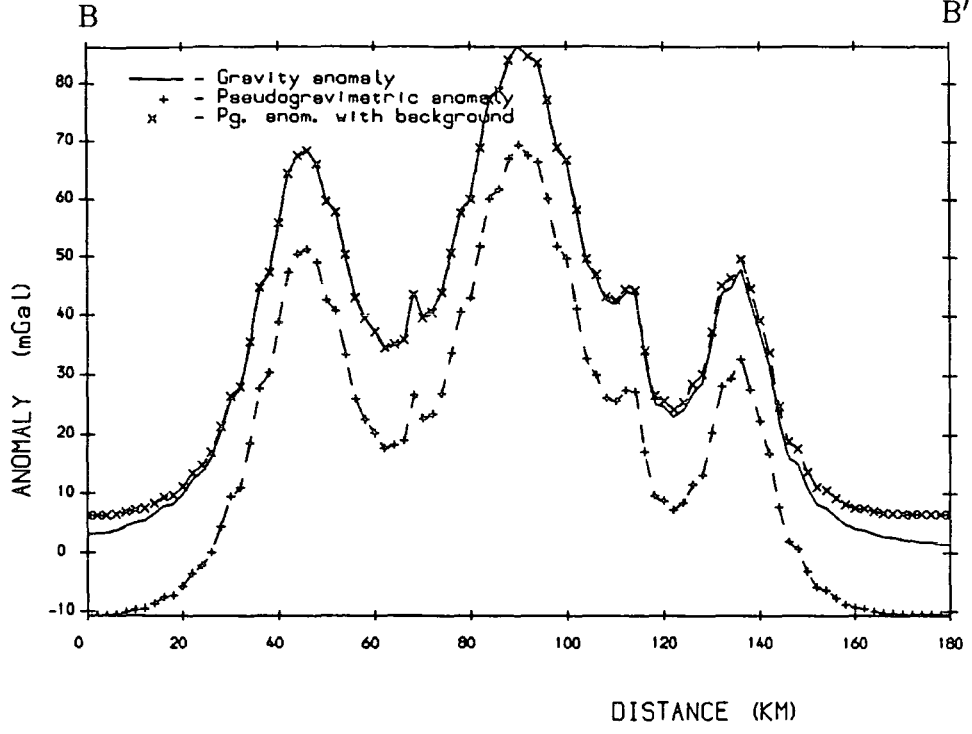

Figure 3.6 Comparison of the pseudogravimetric anomaly without and with (x) background value of 17 mGal transformed from the magnetic anomaly having different wavelength components (figures 3.5), with the calculated gravity anomaly (line) along profile BB′. The density (kg/m^2) to magnetisation (A/m) ratio use in the transformation is 150:1.0.

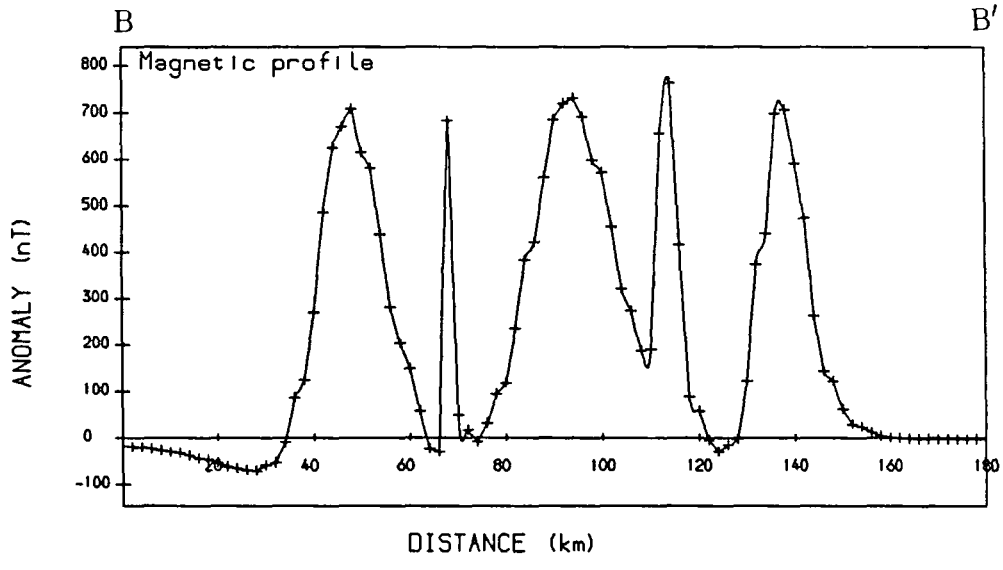

Figure 3.7 Magnetic anomaly along profile BB′ (figure 3.5) showing the prominent short wavelength anomalies but have been suppressed during the transformation (compare with figure 3.6).

transformation. Comparison of the three-dimensional pseudogravimetric anomaly adjusted to a background value of 17 mGal, with the calculated gravity anomaly is given in figure 3.8.

In the two-dimensional tests the gravity and magnetic anomalies of the model, and the pseudogravimetric transformation were calculated using the two-dimensional formulae. In the sample result given here the magnetic anomaly (figure 3.9) was calculated for a body having magnetization of 1.0 A/m. The declination and inclination of the earth's magnetic field and the magnetization are 30^o and 70.3^o respectively, appropriate to the Great Glen anomaly. The declinations are with respect to the positive direction of the profile. As in the three-dimensional cases, the pseudogravimetric anomaly is similarly shifted down by a constant value relative to the calculated gravity anomaly (figure 3.10). Adding a background value to the pseudogravimetric anomaly results in a good fit to the calculated gravity anomaly except at the edges (figure 3.10) .

The tests indicate that both the two and three-dimensional pseudogravimetric transformation can be done successfully except when both the earth's magnetic field and the magnetization are at low inclination angles. Other limitations are related to use of the Fourier method as discussed in Chapter 2. The transformations carried out in subsequent chapters of the thesis invariably use high inclination angles such as used in the examples above because of the high magnetic latitude of Great Britain. Problems related to transforming magnetic anomalies at very low inclination thus do not arise.

3.6 Interpretation methods

The interpretation of gravity and magnetic anomalies involves the determination of the density or magnetization distribution and/or the, shape, size and depth of the subsurface structures causing the anomalies. The shape of the subsurface features causing the anomalies is generally complicated and cannot be modelled without

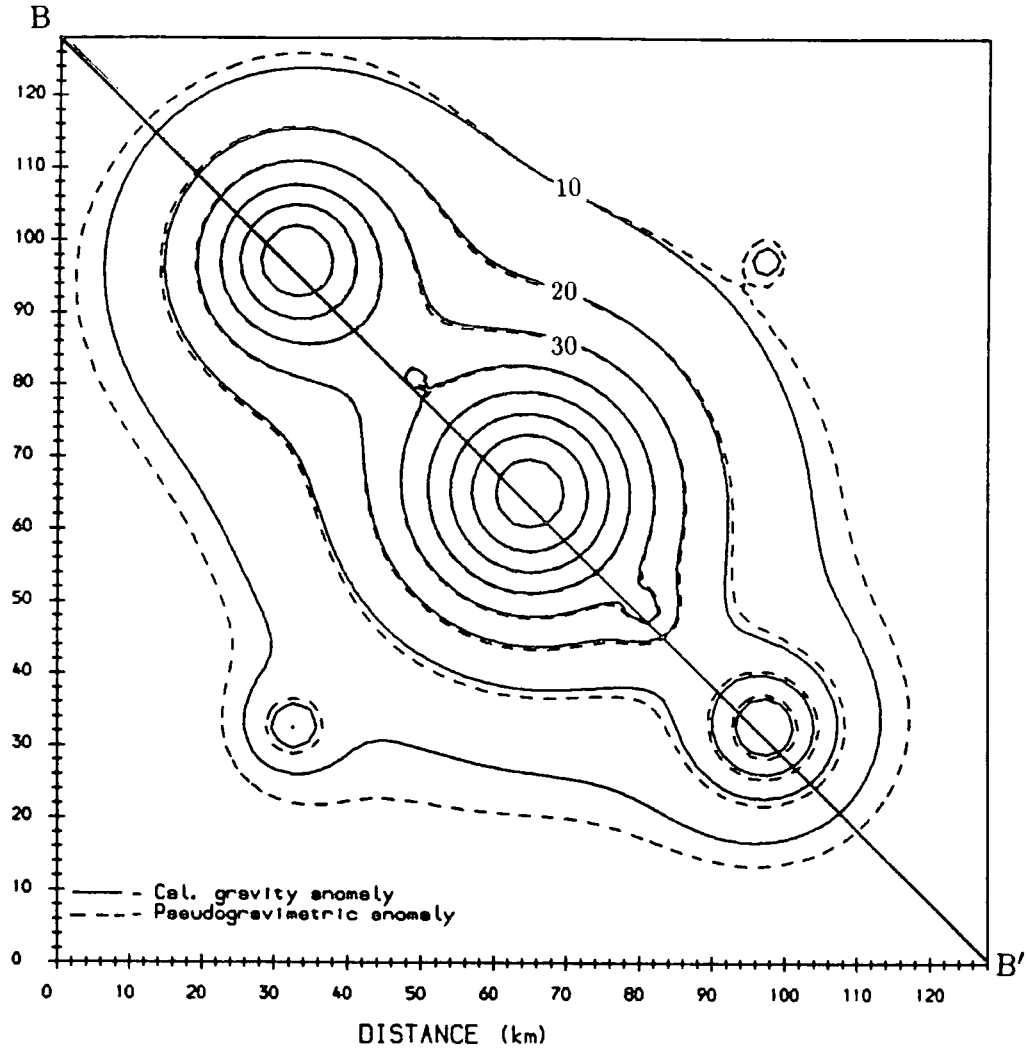

Figure 3.8 Three-dimensional comparison of the pseudogravimetric anomaly (dashed) transformed from the magnetic anomaly in figure 3.5 with background value of 17 mGal, with the calculated gravity anomaly (line) of the same model. The density (kg/m^2) to magnetisation (A/m) ratio is 150:1.0. Contour interval is 10 mGal.

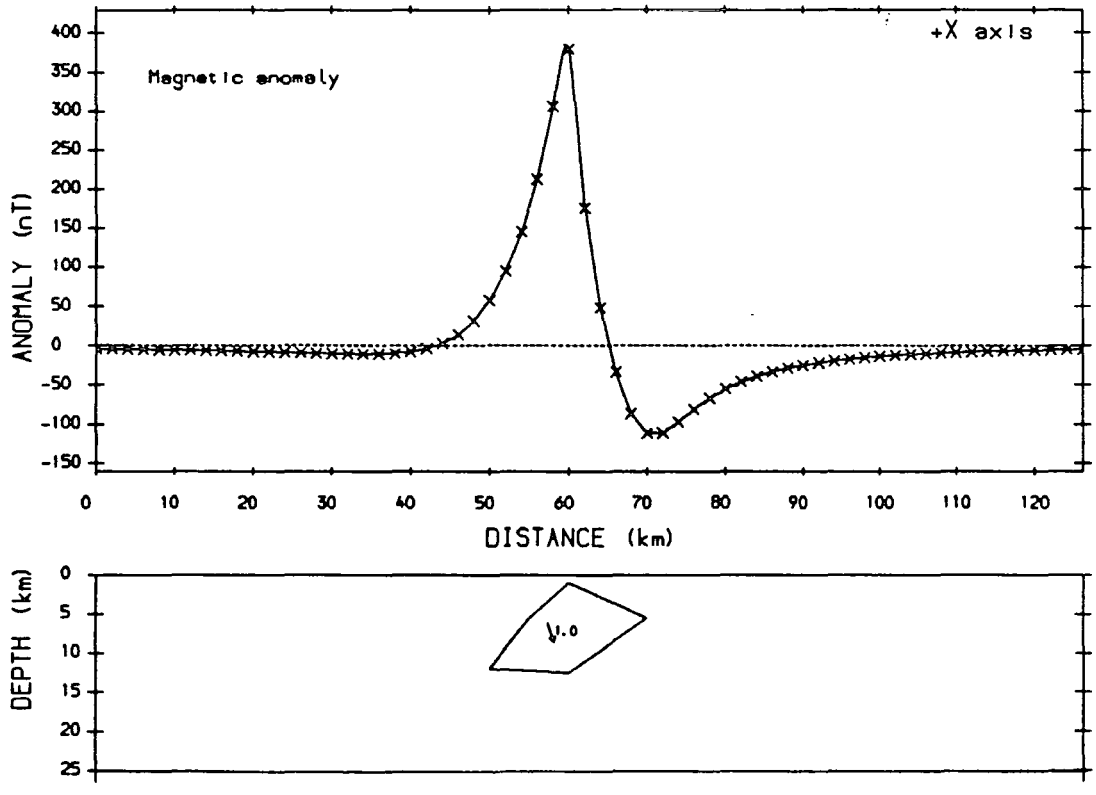

Figure 3.9 Two-dimensional magnetic anomaly calculated from the two-dimensional source shown, using magnetization of 1.0 A/m. Declinations with respect to the positive X and inclinations: D_s=30, I_s=70.3, D_c=30 and I_c=70.3.

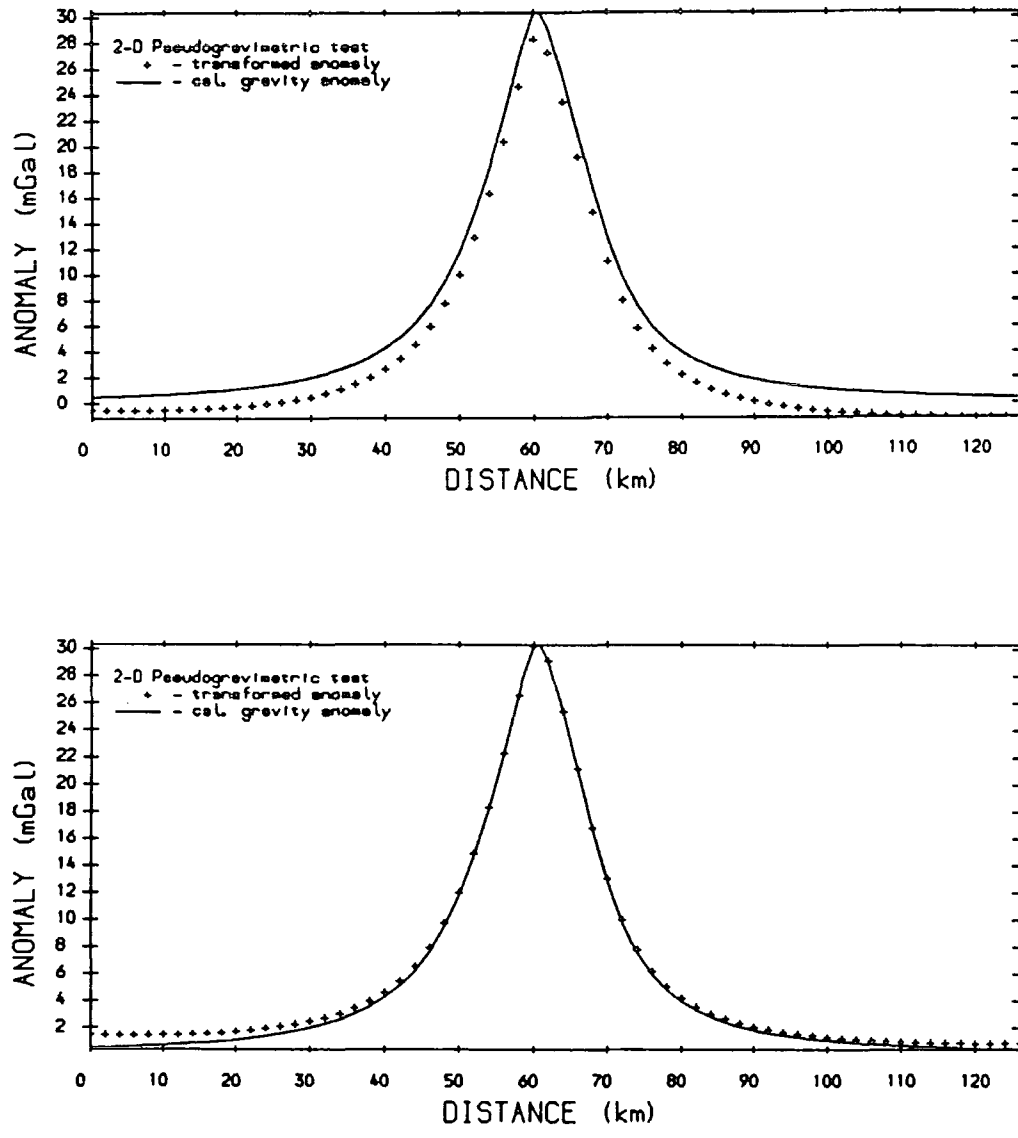

Figure 3.10 Top : Comparison of the pseudogravimetric anomaly (+) with the calculated gravity anomaly (line). Bottom : Comparison of the pseudogravinetric anomaly with background value (+) of 2 mGal, with the calculated gravity anomaly (line). The density to magnetisation ratio is 150 kg/m^2 : 1 A/m.

simplification. Two-dimensional interpretation is a common simplification in the modelling. This greatly reduces the computing time.

The aeromagnetic data obtained from BGS was initially gridded and reduced onto a horizontal plane as described in chapter 2. Pseudogravimetric transformation has been carried out on this reduced data set and the resulting pseudogravimetric anomalies are used for interpretation. The two-dimensional modelling of pseudogravimetric anomalies makes use of existing gravity techniques and modelling routines. The programme GRAV (Bott 1986) has been used to generate the gravity anomalies for the two-dimensional tests and for the initial pseudogravimetric modelling. In pseudogravimetric modelling, the pseudogravimetric anomaly from the expected structure causing the anomaly was first calculated. This was then compared to the observed pseudogravimetric anomaly, obtained from the transformation of the magnetic anomaly. Parameters for the model were changed until a good fit was obtained between the calculated anomaly and the observed pseudogravimetric anomaly. The parameters for the model can be changed manually but this is time consuming. The non-linear optimisation routine MINUIT (James and Roos 1969) has, therefore, been used to speed up the modelling and to obtain more accurate fit. Two-dimensional modelling assumes the source to have great extent along strike. For sources having limited strike extent, modelling has been carried out using the routine GRAVEND (Bott 1984) which incorporates an end correction factor.

The magnetic modelling programme MAG (Bott 1988) has been used to calculate the magnetic anomalies for the two-dimensional tests, for interpretation of magnetic anomaly profiles and for determining the magnetic anomalies across models obtained from the pseudogravimetric modelling. The theory for the modelling methods is described in the following sections.

3.6.1 Standard two-dimensional modelling

The existing modelling routine GRAV calculates the gravity anomaly based

on the gravity effect of semi-infinite slab with a sloping surface at one end. Simple two-dimensional bodies are approximated using polygonal outlines. This is accomplished by repeatedly calculating the effect of slabs with the sloping end coinciding with the polygonal sides. For a closed structure the last body point coincides with the first body point.

The routine MAG uses similar computational procedures. It is based on the magnetic effect of a slab with a sloping surface at one end. In gravity modelling the model parameters are the coordinates of the body and the density contrast. In magnetics, beside the body coordinates and magnetization contrast, the magnetization vector of the body, the earth's magnetic field direction and the angle to the plane of the profile need to be specified.

3.6.2 Modelling with end correction factor

Two-dimensional modelling using the end correction factor is a method to simplify modelling of a three dimensional body. The three-dimensional body may be represented using a two-dimensional source having limited strike extent. The computations thus use standard two-dimensional methods. To calculate the anomaly of a body with limited extent along strike, a correction factor is applied. The method is useful for modelling symmetrical three-dimensional bodies. Use on highly irregular shapes is less satisfactory.

The correction factor may be calculated by assuming the source of the three-dimensional body to be concentrated along the centre of gravity of the cross section (line mass). If the anomaly of the finite line mass is F and the anomaly due to the line mass extended to infinity is F_∞, then the end correction factor EC is F/F_∞. The end correction factor for gravity anomalies as given by Nettlton (1940) is

$$EC = \frac{1}{2}\left(\frac{1}{\sqrt{(1+\frac{R}{Y_1})^2}} + \frac{1}{\sqrt{(1+\frac{R}{Y_2})^2}}\right)$$

where R is the perpendicular distance from the field point to the axis of the polygonal body and Y_1 and Y_2 are the length of the polygonal body on each side of the profile

(figure 3.11). The routine GRAVEND initially calculates the anomaly of the two-dimensional polygonal body and the end correction factor at a field point. The anomaly is then multiplied by the end correction factor to give the approximated anomaly of the three-dimensional body along the profile used. To obtain a good degree of accuracy particularly for a large body, the body may be divided into smaller polygonal bodies and the gravity effects added.

3.6.3 Non-linear optimisation

Optimisation is a process by which an optimal solution to a problem is obtained. The non-linear optimisation technique has been used to obtain an optimised model during two-dimensional modelling. The technique searches for a minimum value of an objective function. In gravity or magnetic modelling the objective function is the sum of squares of the residual values of the observed anomalies minus the calculated anomalies for the model.

The non-linear optimisation programme MINUIT includes three minimising subroutine: (1) subroutine SEEK, a Monte Carlo searching subroutine to start a fit when no reasonable starting point is known. (2) Subroutine SIMPLEX, uses the simplex method of Nelder and Mead (1965). It is safe and reasonably fast when far from the minimum and may also be used to converge to the exact minimum. (3) Subroutine MIGRAD is based on Fletcher's (1970) method and converges very fast in the vicinity of a minimum. The subroutines OPTIGRAV and OPTIMAG (Westbrook 1973) are incorporated in the non-linear optimisation programme MINUIT. The call to the subroutines calculates the model anomaly profile and the objective function. MINUIT carries out self adjusting changes to the variable parameters and searches for the minimum objective function. Both the coordinates and the density or magnetization contrast may be variable parameters. The background value considered as a linear parameter can also be variable. The problem may be floated with all the parameters as variables. The solution obtained in this manner is dependent on the initial model and is not unique. Constraints may be applied by fixing some of the

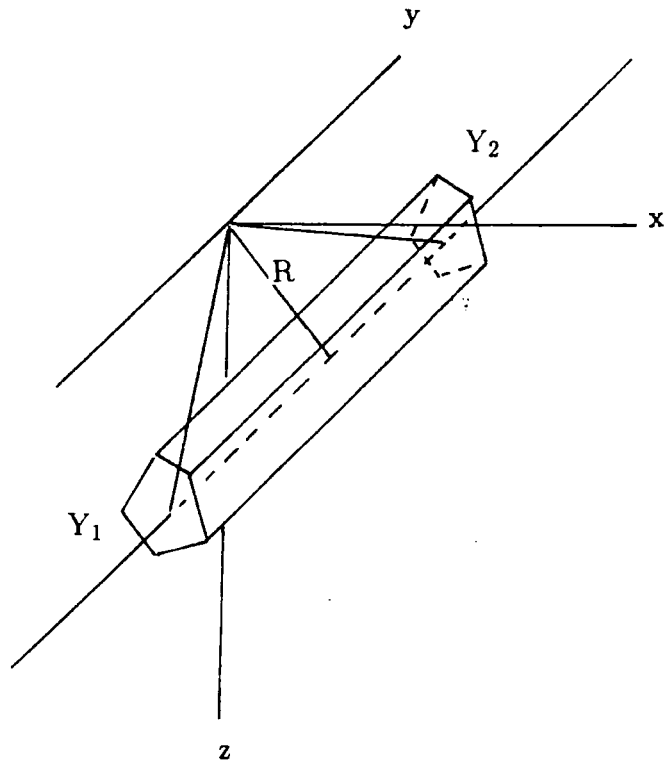

R - perpendicular distance from the field point to the axis of polygon

Y_1 and Y_2 - length of the polygon on each side of the profile

Figure 3.11 Parameters used for calculating the end correction factor.

variables to ensure a unique solution. The method has been described by Westbrook (1973).

3.7 Limitations on the interpretation

3.7.1 Sources of the ambiguity

Determination of the density or magnetization distribution, shape, size and position of the source that can give rise to the observed anomalies in general lacks uniqueness and gives rise to ambiguity in the interpretations (Roy 1962, Al-Chalabi 1971, Ofoegbu 1982). The density or magnetization may sometimes be constrained using existing geological knowledge and other geophysical methods. Constant density or magnetization are normally used to model a particular feature. Although the subsurface is seldom homogeneous, the constant values may be used to represent the average property of the feature. Even after assigning the density or magnetization value, a number of shapes at different depth levels may give rise to the observed anomalies. However, if adequate constraints are applied such as the density and one surface, sometimes a unique solution can be obtained for the assumption adopted.

Other errors in the interpretation may arise from the data itself and from the subsequent process of reduction. The data may contain errors introduced during acquisition and this introduces uncertainty in the interpretation. The data obtained from BGS is assumed to represent the sources correctly but may contain observational error and errors due to diurnal correction and also the heights.

The anomalies are generally acquired at a finite number of field points and for finite data length. The representation is thus incomplete and this introduces a certain degree of uncertainty. In using two kilometre grid spacing, wavelengths of less than four kilometres are not properly represented in the gridded data and their presence can caused aliasing. The medium and long wavelength anomalies studied are probably well represented in the gridded data.

The modelling method may also introduce ambiguity in the interpretation. Ambiguity may arise from the non-linear optimisation technique as it may converge to local minima and define one of the possible shape of the body giving rise to the observed anomalies (Ofoegbu 1982). The use of MINUIT with all parameters variable as mentioned earlier is an example of how such ambiguity can be introduced. If there are sufficient constraints, a unique solution may be obtained subject to the applied assumptions.

Problems in magnetic interpretation are compounded by the fact that the magnetization is directional and may include both remanent and induced components. This causes difficulty when the magnitude and direction of the remanent magnetization are not known. In the study of long wavelength magnetic anomalies from deep sources in the crust, the magnetization is probably induced. The magnitude of the natural remanent magnetization is generally considered to be insignificant from such deep sources (e.g. Schlinger 1985) although exceptions exist (Mutton and Shaw 1979). The reasons for the insignificant magnitude of the remanent magnetization are described below. Large bodies with significant remanent magnetization are generally divided into regions of alternating polarities and these have the effect of reducing the remanent contribution to the long wavelength anomaly (Shive 1989). In the lower crust, chemical remanent magnetization may occur but may only be significant where hydrothermal circulation exist (Arkani-Hamed and Celetti 1989). Viscous remanent magnetization may also occur, giving rise to components along the existing earth's field direction which could reduce the contribution of the remanent magnetization. Magnetic grains can be of single or multiple domains. The multiple domain grains are always at equilibrium with the external field and the single domains are generally fine grained and can acquire viscous remanent magnetization (Worm 1989). In addition, grain growth, and subsequent chemical reactions and geological activities may also reduce the effect of remanent magnetization. Since the present study deals with long and medium wavelength anomalies due to deep or large bodies, the magnetization has been assumed to be induced and along the present earth's magnetic field.

The pseudogravimetric transformation uses a constant earth's field direction and errors may arise if the area involved is large. Tests have been carried out to check errors arising from this. The magnetic data was first transformed using different constant inclination and declination particularly at the corners of the area used. The pseudogravimetric anomalies along profiles were then compared. Figure 3.12 is an example profile of such tests which have been carried out to transform the aeromagnetic anomaly using inclination and declination in the Mull and Moray Firth regions. The differences between the results from the two transformed anomalies are only slight. Use of the average inclination and declination of the region should give acceptable results.

3.7.2 Problems related to two and three-dimensional pseudogravimetric transformation

Two-dimensional modelling requires the strike extent of the body to be large. Analysis dealing with bodies of limited strike extent needs application of end correction factors. Tests on two and three-dimensional pseudogravimetric transformation over bodies of limited and large extent along strike have been carried out.

The theoretical gravity and magnetic anomalies caused by a body of large strike extend may be obtained using the routine SPHEREGM. This was done by superimposing the anomalies of a number of spheres having the same properties aligned sufficiently close together at the same depth. The direction and intensity of magnetization and the direction of the earth's magnetic field were kept constant. Three-dimensional pseudogravimetric transformation was then carried out on the calculated magnetic anomalies. Magnetic profiles were taken perpendicular to the strike of the body and two-dimensional pseudogravimetric transformation was carried out. The two and three-dimensional pseudogravimetric anomalies along the profile and the calculated gravity anomalies for the two-dimensional structure are shown in figures 3.13. For two-dimensional structures both the two and three-dimensional transformations result in similar but not identical pseudogravimetric anomalies. The differences are

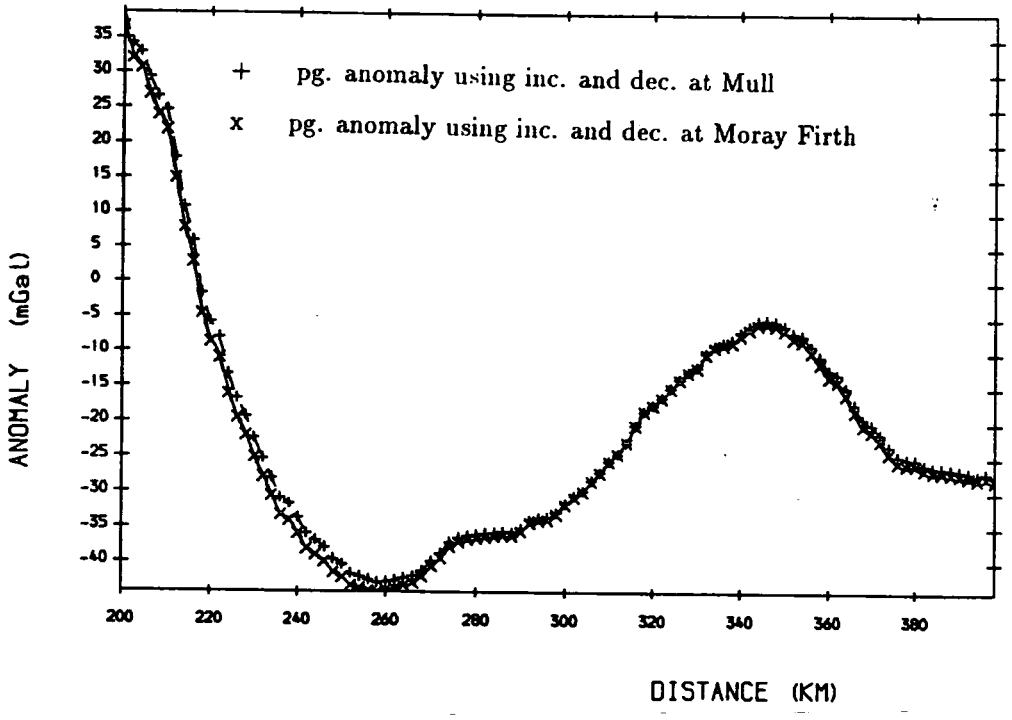

Figure 3.12 Comparison of the pseudogravimetric anomalies transformed using inclinations and declinations at Mull (+) and Moray Firth (x) region. The inclinations and declinations for the two locations are as follows. Mull: 70.2 ^{o} and -11.1 ^{o}, Moray Firth: 71.4 ^{o} and -9.4 ^{o}. The density (kg/m^2) to magnetization A/m ratio has been used (150:1.0).

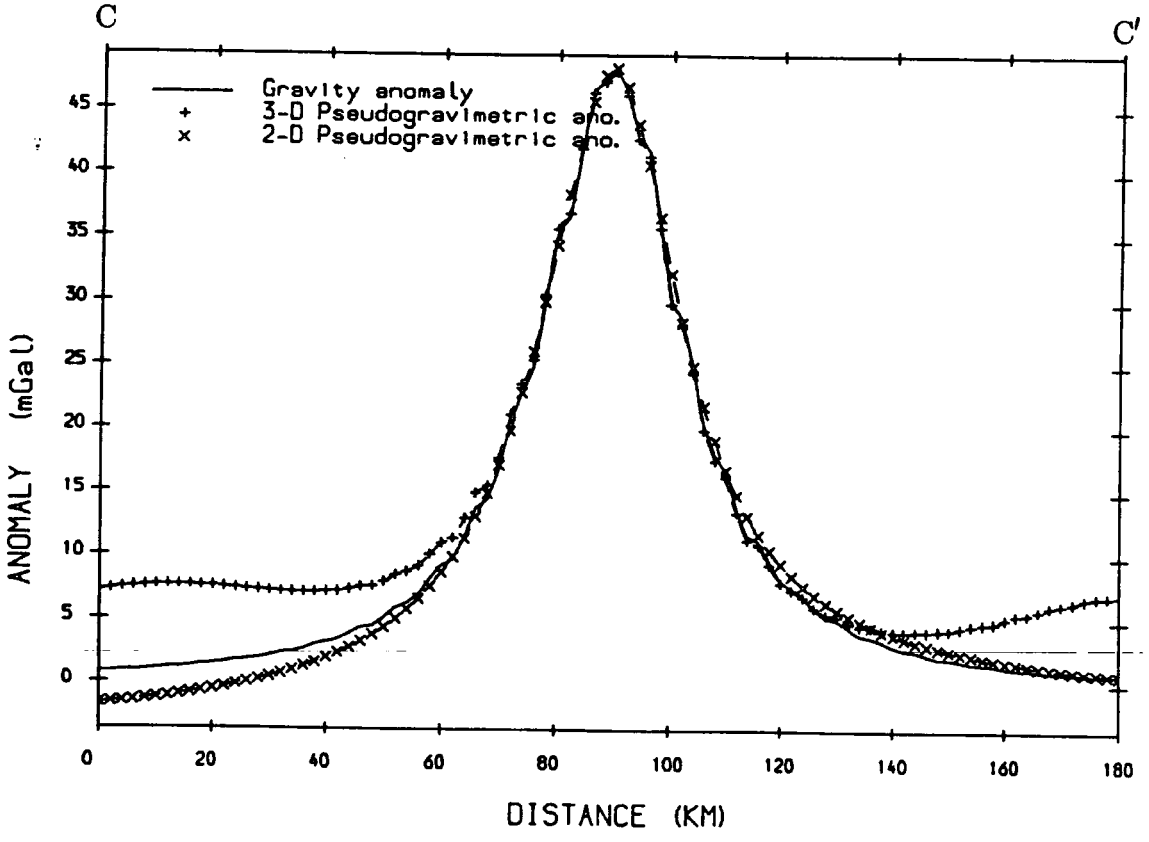

Figure 3.13a Comparison of the two (x) and three-dimensional (+) pseudogravimetric anomalies to the calculated gravity anomaly (line) of the same model across profile CC′ figure 3.13b. The density (kg/m^2) to magnetization (A/m) ratio is 150:1.0.

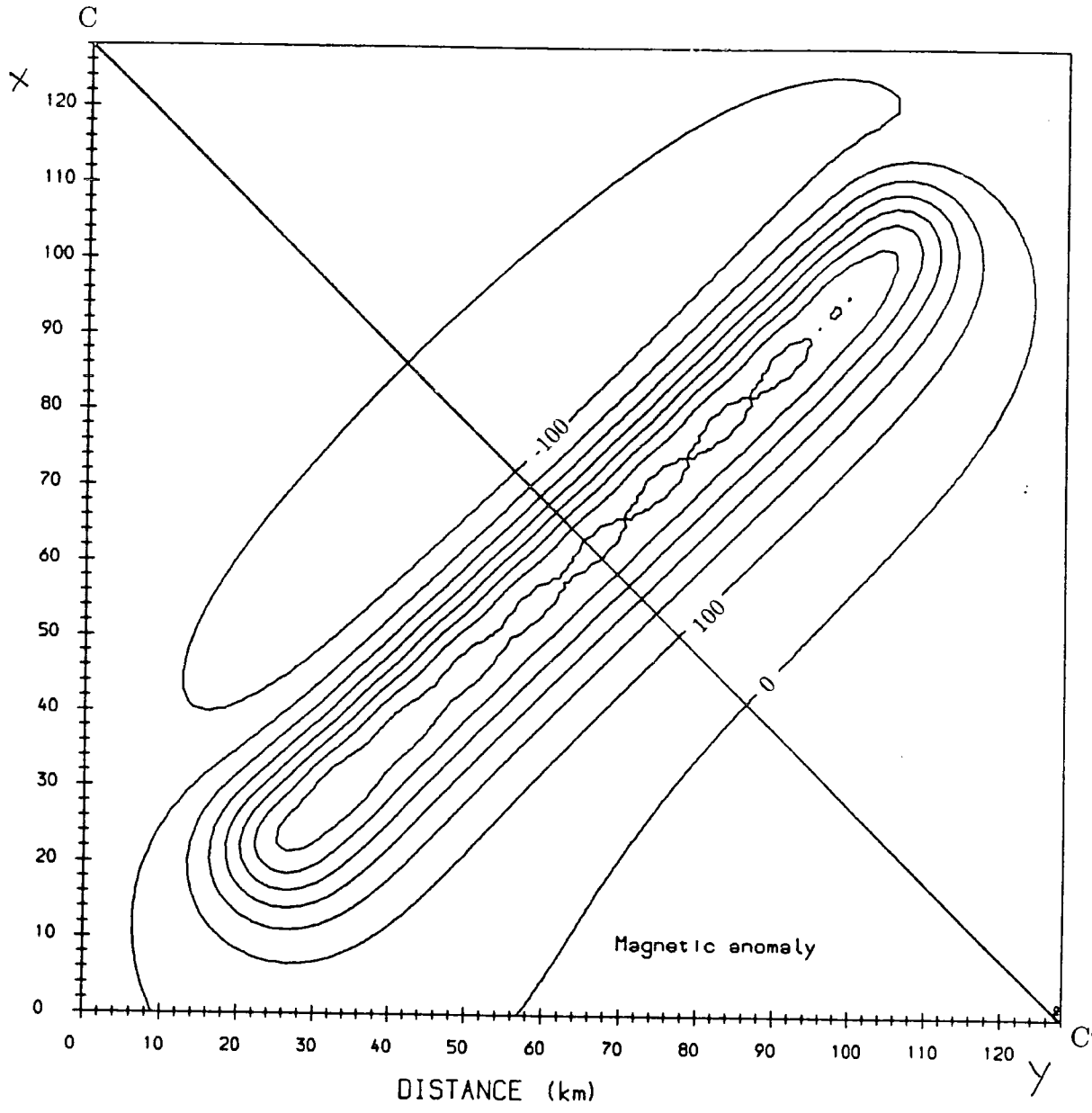

Figure 3.13b Magnetic anomaly of a linear feature. Declination/Inclination are: earth's field -10.6/70.3°C and sources -10.6/70.3°. Magnetization of the source is 1.0 A/m. The contour interval is 100 nT. The sources are spheres of 10 km radii placed at 15 km depth. The x and y coordinates are: (32,32), (48,48), (64,64), (80,80), (96,96) (24,24), (40,40), (56,56), (72,72), (88,88) and (104,104).

attributed to along strike variation, which signigficantly affects the three-dimensional pseudogravimetric anomaly.

Similar tests have been carried out for bodies of more limited strike extent. The gravity and magnetic anomalies have been calculated from spheres aligned for limited extent along strike. Two and three-dimensional transformations along profiles across the elongation of the body were compared. The three-dimensional transformation results in an anomaly similar to the calculated gravity anomaly (figures 3.14a and b). The two-dimensional transformation values differ significantly from the calculated gravity anomalies depending on the profile taken (figures 3.14a, b and c).

For true two-dimensional bodies, either two or three-dimensional pseudogravimetric transformation may be used. For bodies with limited extent, the three-dimensional pseudogravimetric transformation is necessary. In the presence of sources close to each other, the three-dimensional transformation may result in anomalies being affected by the neighbouring sources. It is important to recognise this problem as it may be difficult to isolate the effect of individual anomalies.

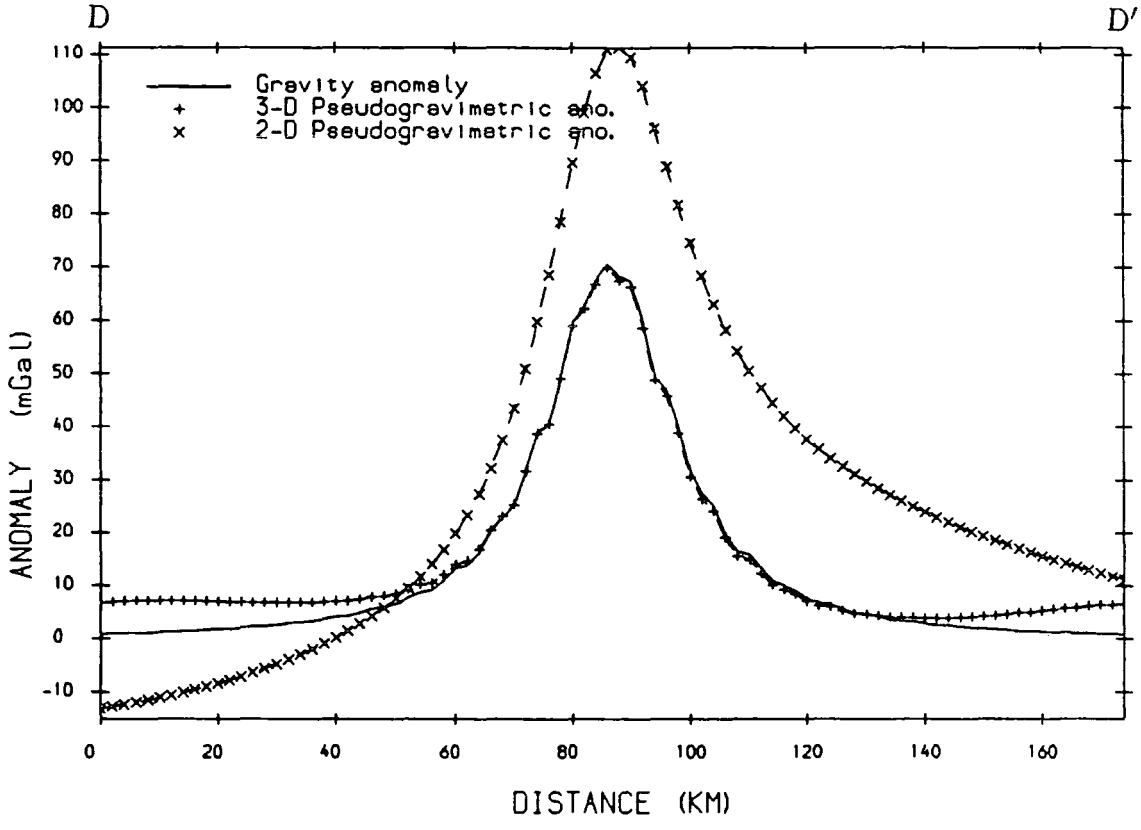

Figure 3.14a Comparison of the two (x) and three-dimensional (+) pseudogravimetric anomalies to the calculated gravity anomaly (line) along line DD′ figure 3.14c. The density (kg/m^2) to magnetization (A/m) ratio is 150:1.0.

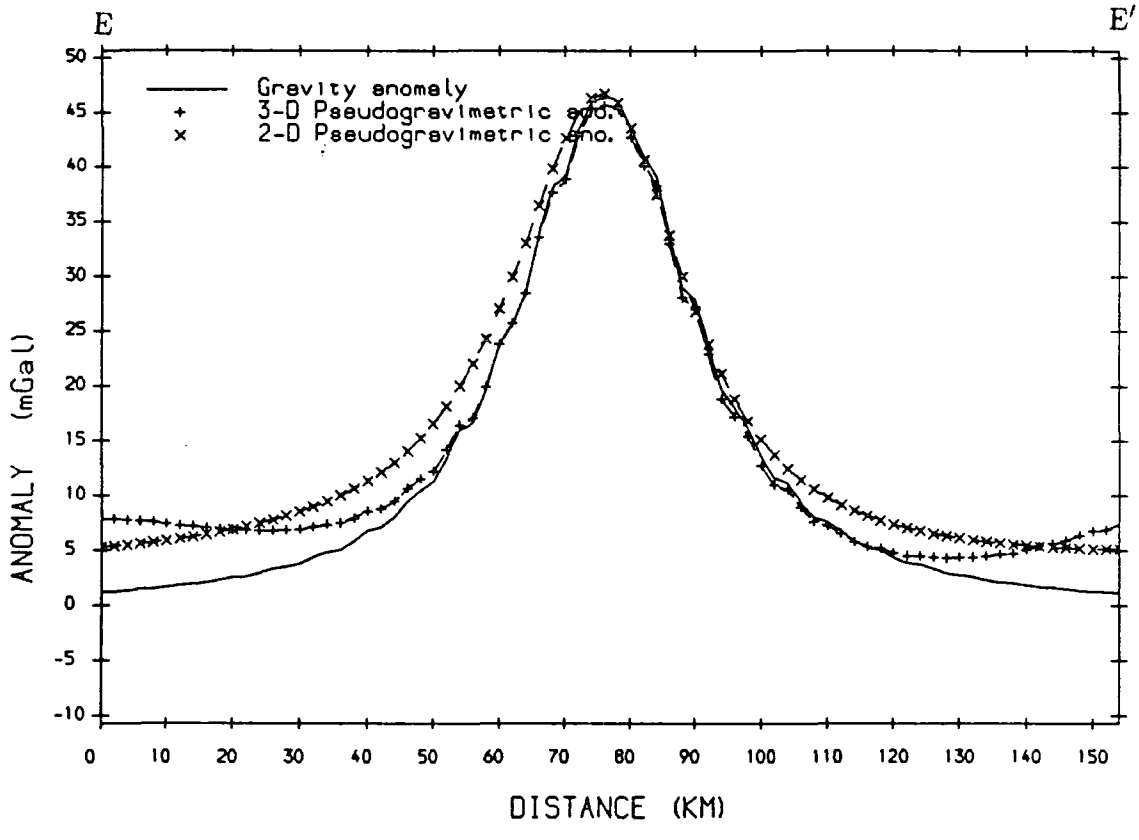

Figure 3.14b Comparison of the two (x) and three-dimensional (+) pseudogravimetric anomalies to the calculated gravity anomaly (line) along line EE′ figure 3.14c. The density (kg/m^2) to magnetization (A/m) ratio is 150:1.0.

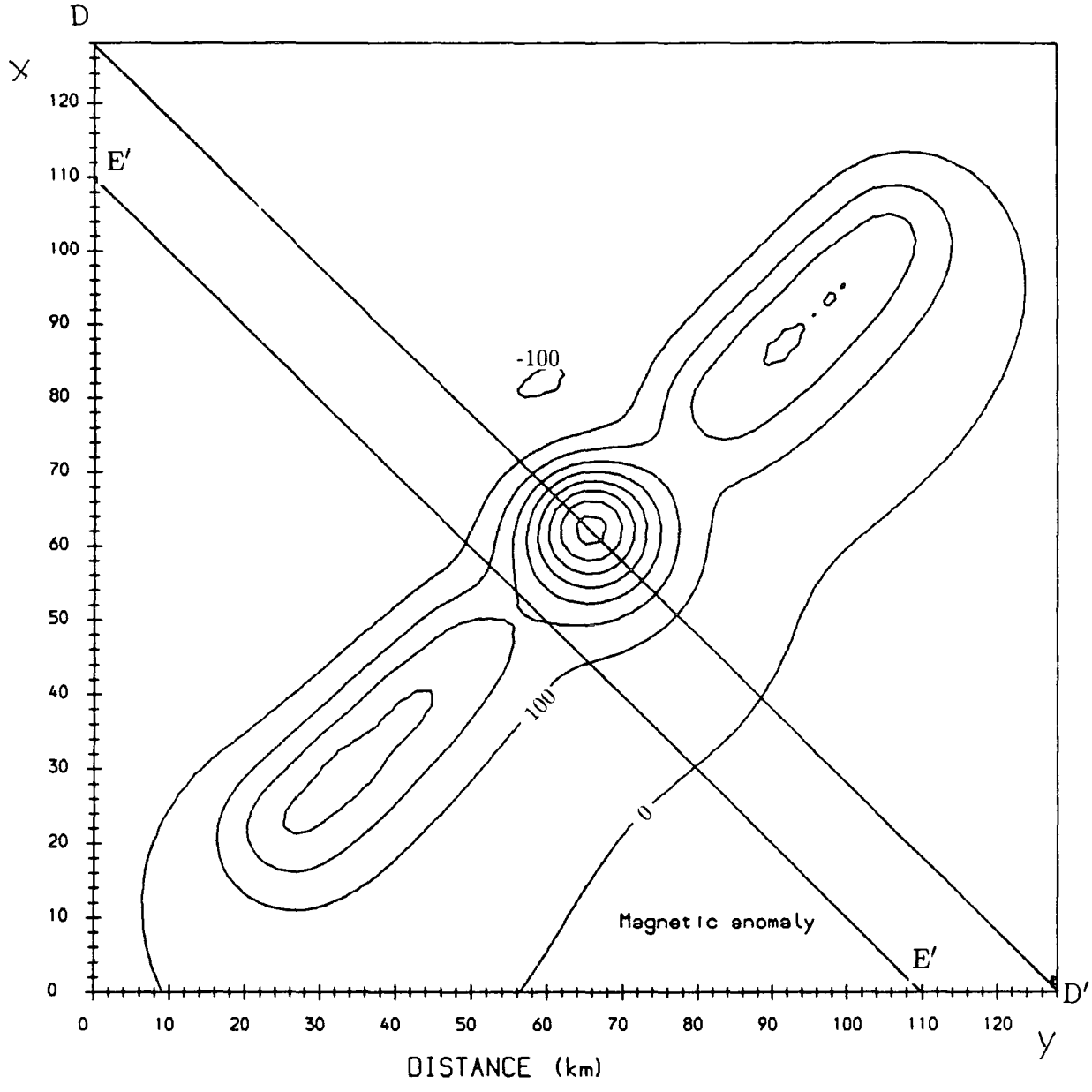

Figure 3.14c Magnetic anomaly of a non-linear feature Declination/Inclination are: earth's field -10.6/70.3°C and sources -10.6/70.3°. Magnetization of the source is 1.0 A/m. The contour interval is 100 nT. The spheres used as the sources have the centre of gravity, radii and (x,y) coordinates at : [15,10,(32,32)], [15,10,(48,48)], [15,15,(64,64)], [15,10,(80,80)], [5,10,(96,96)], [15,10,(24,24)], [15,10,(40,40)], [15,10,(88,88)] and (15,10,(104,104))

CHAPTER 4

Modelling the linear positive magnetic anomaly along the Great Glen fault

4.1 The anomaly

A prominent feature on the aeromagnetic map of northern Great Britain is a linear positive magnetic anomaly along the Great Glen fault (Great Glen anomaly, figure 4.1).The Great Glen anomaly is truncated at the southwest by the complicated magnetic high associated with the Mull Tertiary volcanic complex. To the northeast, it extends to the Moray Firth, where an echelon positive lies along the east coast of Sutherland. The Great Glen anomaly is thus essentially restricted to the mainland outcrop of the Great Glen fault. The anomaly has a roughly triangular cross section with the gradient steepening towards the sharp apex, which correlates closely with the line of the Great Glen fault (figure 4.2). The amplitude relative to the background is around 350 nT and the width at the half-peak value is about 40-50 km. The source of such a large amplitude, large width anomaly must be a major feature of the underlying crust. This chapter examines the source of the anomaly.

The Great Glen anomaly is disturbed by several regions of shorter wavelength anomaly which slightly obscure the linear trend. Some of these are situated over the known granitic masses, such as a triangular shaped anomalous region over Foyers granite (figure 4.1). An elongated magnetic high having two distinct peaks (north of Rannoch Moor) is associated with the Ben Nevis granite in the west and extends over the Corrieyairack granite to the east. On the northwestern side of the Great Glen fault superimposed short wavelength magnetic anomalies are conspicuous only over the Strontian granite. The shorter wavelength anomalies are thus mostly associated with the granitic intrusions and their aureoles.

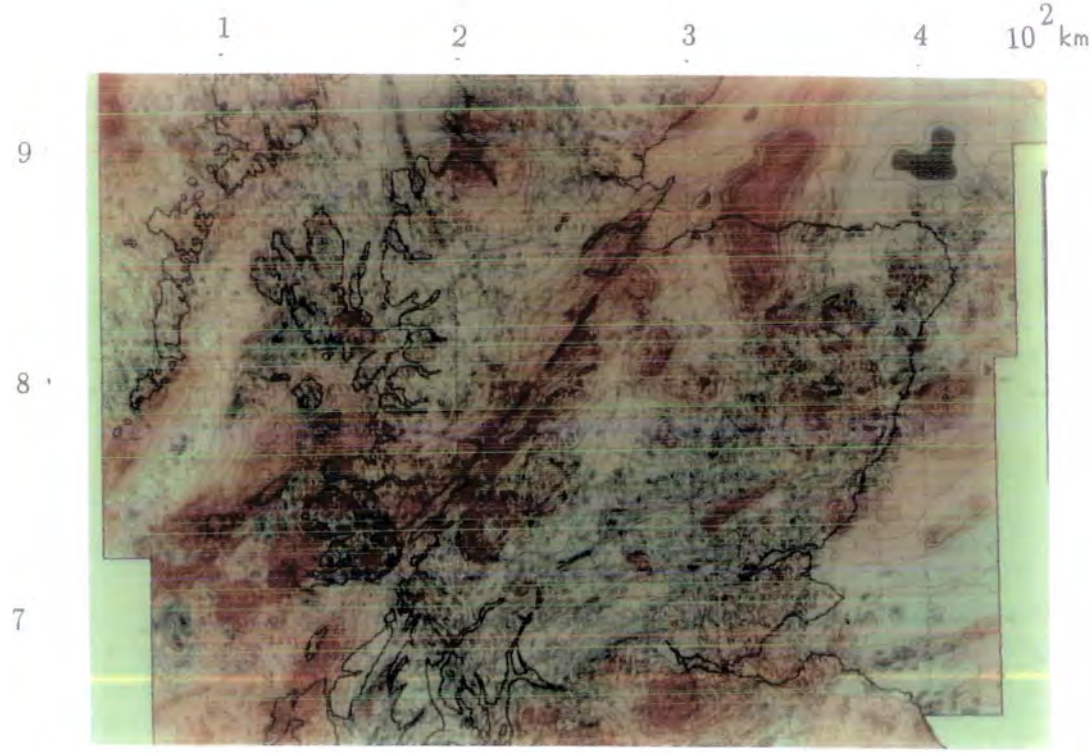

Figure 4.1a Aeromagnetic map of the Great Glen fault region from the aeromagnetic map of Great Britain, compiled by W. Bullerwell The scale is 1:625000. The contour interval is 10 nT. The colour code is: brown for positive anomalies and blue for negative anomalies.

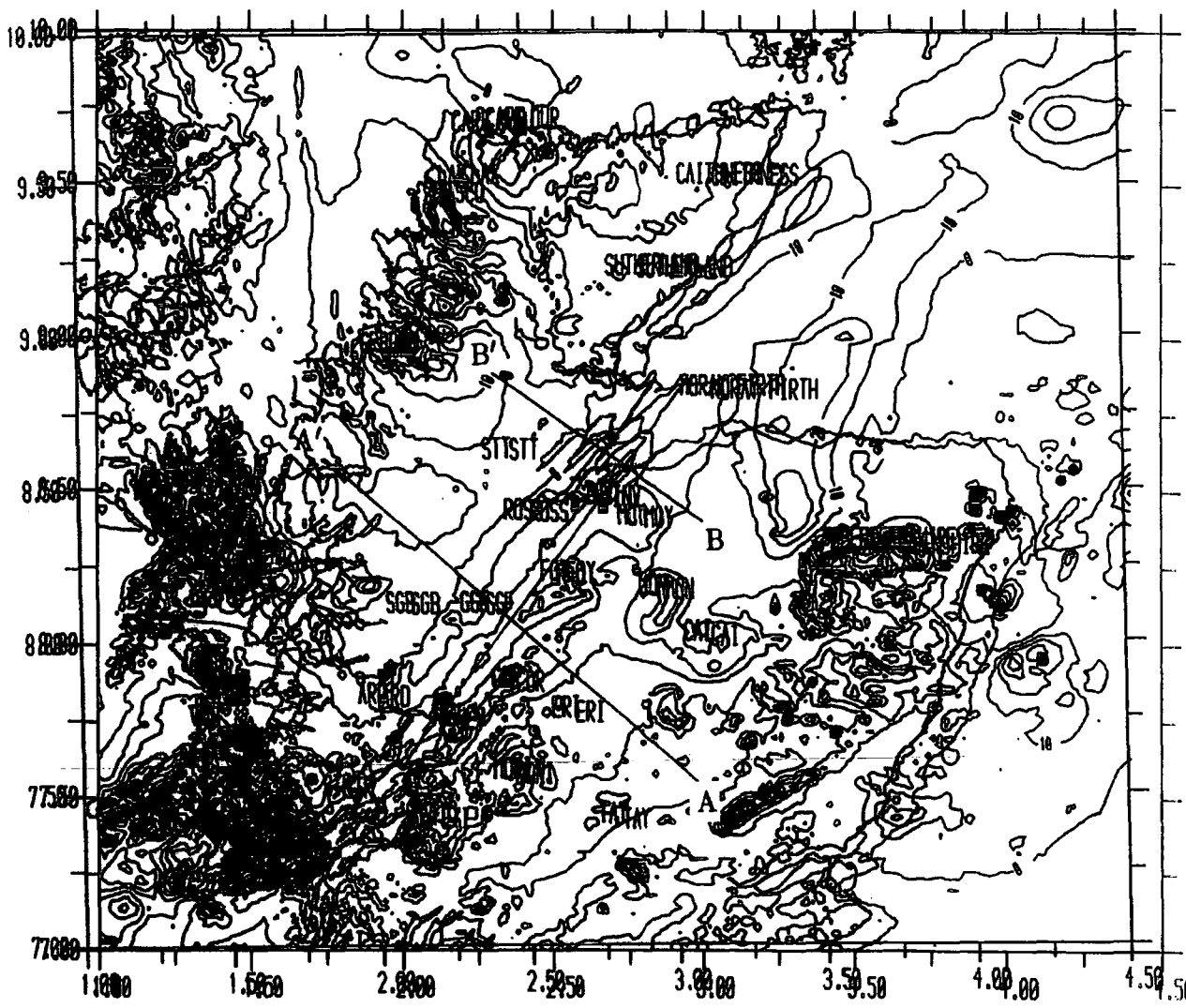

ARD-Ardgour, CAI-Cairngorm, CAPE-Cape Wrath, COLO-Colonsay, COR-Corrieyairack, DUR-Durness, ERI-Ericht fault, ETI-Etive granite, FOY-Foyers granite, GGF-Great Glen fault, GRB-Gruinard Bay, INV-Inverness, LAI-Laidon, LAX-Loch Laxford, MON-Monadhliath, MOR-Rannoch Moor, MOY-Moy granite, NEV-Nevis granite, ROSS-Central Ross, SCO-Scourie, SGB-Sgurr Beag, STR-Strontian, STT-Strathconon, TAY-Loch Tay.

Figure 4.1b Aeromagnetic map of northern Scotland. The axes are in British National Grid (BNG, x10^2 km). The Contour interval is 100 nT.

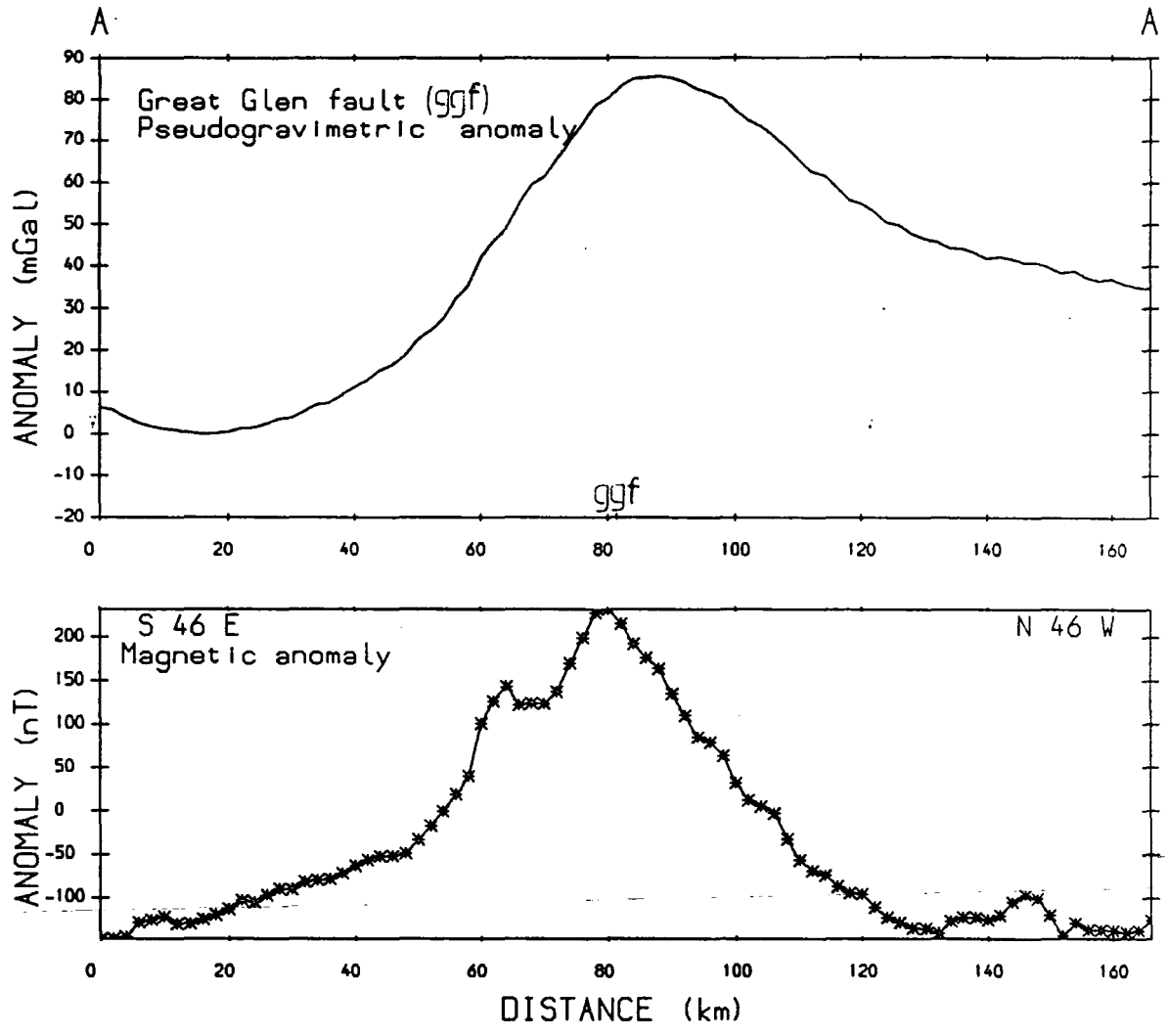

Figure 4.2 Pseudogravimetric (mGal, top) and magnetic anomalies (nT, bottom) along profile AA′ in figures 4.3 and 4.1b respectively.

The pseudogravimetric map (figure 4.3), transformed using density (kg/m3) to magnetization (A/m) ratio of 150:1.0, shows a prominent linear positive anomaly along the Great Glen fault from east of Mull northeastwards to Moray Firth and possibly extending to the east coast of Caithness. The peak of the pseudogravimetric anomaly lies slightly northwestwards of the line of the Great Glen fault (figure 4.2). The anomaly is asymmetrical with a steeper gradient to the southeast than to the northwest. The asymmetry probably indicates different crustal magnetization on the opposite sides of the fault and it may be disturbed by the magnetic anomaly from the Skye volcanic complex. The amplitude relative to the background is about 85 mGal. The anomaly is broader than the magnetic anomaly because of the relative amplification of the longer wavelengths. The width at half-peak value is about 60-65 km. On the southeastern side of the Great Glen fault, the linear trend is obscured by traces of the shorter wavelength anomalies caused by shallower and smaller structures. These appear as low amplitude features departing from the parallel contour lines along the Great Glen fault zone. The examples are the magnetic highs associated with the Foyers granite and the Moy granite. The gradient is less disturbed on the northwestern side. The linear trend here merges with the magnetic high over the Skye volcanic centres, a magnetic high near Gruinard Bay and a magnetic high near Cape Wrath.

4.2 Geological background

The geology of Scotland is described in Craig (1983) and this is the basic reference for this section. The Great Glen fault separates the main outcrop of Moine rocks of the Northern Highlands from the Moines of the Grampian Highlands (figure 4.4). The Moine rocks of the northwest Highlands are thrusted westwards onto the Lewisian basement (Archean) at the Moine Thrust. The Lewisian complex is made up of banded gneisses with composition ranging from ultramafic to acid which have been intensely modified so that their origin is often difficult to determine (Watson

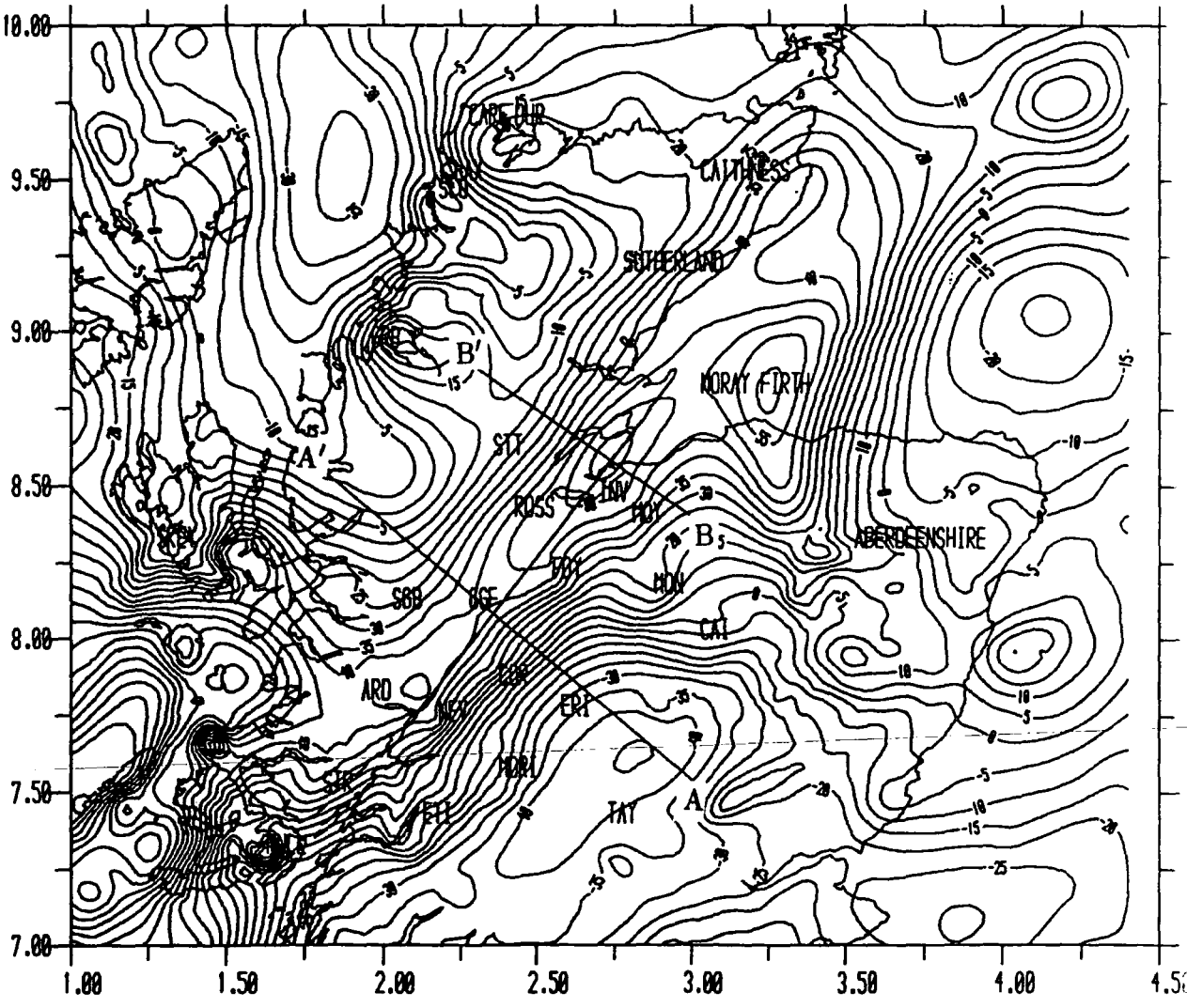

Figure 4.3 Pseudogravimetric map of northern Scotland transformed using density (km/m^3) to magnetization (A/m) ratio of 150:1. The inclination and declination of the earth's magnetic field and magnetization of the body used in the transformation are 70.3^o and -10.6^o respectively. The contour interval is 10 mGal. The locations and coordinates are as in figure 4.1.

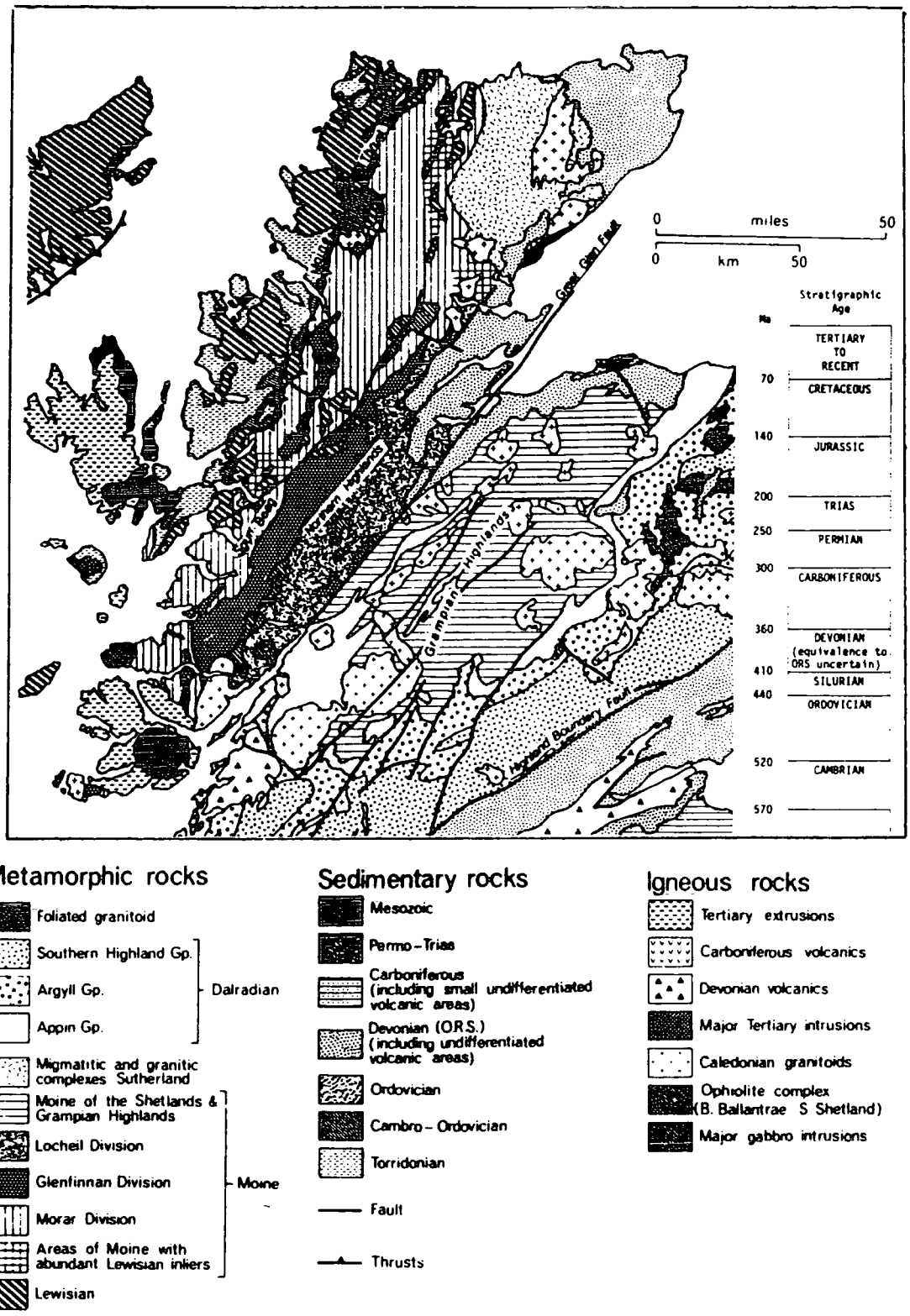

Figure 4.4 Simplified geology map of northern Scotland from Craig (1983).

1983). It can be classified into an older Scourian assemblage and a younger Laxfordian assemblage. Watson (1984) suggested that basement of Lewisian type underlies the Northern Highlands and probably much of the Grampian Highlands. To the south of the Great Glen fault the Grampian Moine rocks pass southwards into the Dalradian. In local areas along the Great Glen fault, Old Red Sandstone (Devonian) unconformably overlies the metamorphic Moines.

The Moines of the Northern Highlands north of the Great Glen fault are divided into three groups. The Locheil Division outcrops in the vicinity of the Great Glen fault and is underlain by the Glenfinnan Division (Harris 1983). The Glenfinnan Division is separated from the Morar Division by a slide contact (Johnson 1983a). To the south of the Great Glen fault, the Moines of the Grampian Highlands have been divided into the more northern Central Highland Division, and the Grampian Division further south, separated by a complex zone of sliding (Piaseki and van Breemen 1979). The Grampian Division may pass upwards into the Dalradian by a normal sedimentary transition (Johnson 1983a).

The start of the Moine deposition is not well defined. Brooks et al. (1977) suggested deposition between 1500 Ma and 1024 Ma for the Morar Division. The youngest Moine deposition has been placed at about 668 Ma (Johnson 1983a). The Moines may have been affected by a pre-Caledonian orogeny at 1000 Ma (Harris 1983). The Caledonian orogeny subsequently caused crustal shortening within the Moines through folding and thrusting (Harris 1983). The Sgurr Beag slide (460 Ma, Watson 1984) and the Moine thrust (430 Ma) formed at this time (Johnson 1983a). In central Scotland, the last major folding occurred at about 400 Ma (Mykura 1983). The Dalradian rocks are mostly metamorphosed marine sediments laid down from the end of Moine deposition until Lower Palaeozoic times (Johnson 1983b). The Old Red Sandstone was deposited during the Devonian (Harris 1983). It can be divided into Lower, Middle and Upper Old Red Sandstone. Only the Middle Old Red Sandstone strictly outcrops along the line of the Great Glen fault on the mainland although the

Upper Old Red Sandstone occurs to the northeast of Inverness.

The Moines on both sides of the Great Glen fault are intruded by a number of igneous masses with granite predominant. Classification and division of the granitoids are difficult (Brown et al. 1985) but they may be divided into the pre-and-syn, and late to post-tectonic plutons (Powell and Phillips 1985). Most of the granitoids in the region are late to post tectonic and correspond to the Newer granites (Ordovician-Devonian, Read 1961, Brown et al. 1985). Near the Great Glen fault the late-Ordovician to Silurian granites have diverse composition and petrology. Some of the plutons comprise multiple magmatic intrusion such as the Strontian and Foyers granites (Brown 1983). These intrusions are forcefully emplaced. The later post-tectonic plutons (late-Silurian to Devonian) are of the permitted intrusion type. Among them are those of Ben Nevis and Glen Etive which were accompanied by north-northeast trending dykes and veins. To the north of the Great Glen fault the dyke swarms are late to post-tectonic (Brown 1983). They are generally in an easterly direction. The last major igneous activity occurred during the early Tertiary. This formed a province along the west coast of Scotland (Emeleus 1983). The dyke swarms associated with this Tertiary igneous activity have a southeasterly trend.

4.3 Age, direction and magnitude of the Great Glen fault movement

Kennedy (1946) was the first to suggest that the Great Glen fault is a lateral-slip fault. This was based on a number of lines of evidence. The evidence includes: (1) the displacement of the assumed identical Strontian and Foyers granites on opposite sides of the Great Glen fault and of the regional injection belts, (2) the displacement of the metamorphic zones of the Grampians relative to the northern Highlands, and (3) relationship to the Strathconon, Ericht-Laidon and Loch Tay fault, which all have lateral displacement. The sinistral displacement of about 100 km was suggested to occur possibly during the post-Lower or post-Middle Old Red Sandstone. The

evidence from the Strontian and Foyers granites, however, is now suspect as these appear to differ structurally (Munro 1973) and in their trace elements (Pankhurst 1979).

Holgate (1969) suggested that the Palaeozoic sinistral displacement was followed by Tertiary dextral movement. He based this suggestion on dislocation of the Skye Tertiary dyke swarm at the line of the Great Glen fault. The sinistral displacement (about 130 km) occurred during the Lower to early Middle Old Red sandstone and the dextral movement (about 29 km) occurred after the Hebridean Tertiary vulcanicity.

Garson and Plant (1972), in contrast, suggested that the lateral movement along the Great Glen fault was wholly dextral, occurring during the Lower Old Red Sandstone and possibly Upper Cretaceous. The suggested displacement of 88-96 km was based on the metamorphic zones near the Foyers granite region which correlate with those of Caithness, and on the close correspondence of the areal distribution of migmatites and early intrusions (older granite, Read 1961) when the displaced sections are repositioned. The Newer granites also show similar displacement.

Winchester (1973) also argued from the metamorphic characteristics but inferred that the movement was sinistral. He observed the similarities of the metamorphic pattern and features of the Western Highland (Central Ross to Ardgour) and the Central Highlands (particularly of the Monadhliath complex). He calculated a displacement of about 160 km and also suggested that the Strontian and Foyers granites may have been intruded after 60 km of displacement had occurred. This gave the 100 km sinistral displacement originally proposed by Kennedy. The movement mainly postdates the Caledonian metamorphism of the Moines.

Palaeomagnetic studies also indicate transcurrent movement along the Great Glen fault (Storetvedt 1974,1975, Van der Voo and Scotese 1981, Table 4.1) with the

Reference	Direction	Magnitude km	Age
Storetvedt (1987)	dextral	300	Hercynian
	sinistral	600	M. Devonian
Storetvedt (1975)	sinistral	500	-
Storetvedt (1974)	sinistral	200-300	late Devonian
Holgate (1969)	dextral	29	Tertiary
	sinistral	130	Lower-Middle Old Red times
Garson and Plant (1972)	dextral	88-96	Lower Old Red times
Winchester (1973)	sinistral	160	post date Caledonian metamorphism
Mykura (1975)	dextral	-	-
Donovan et al. (1976)	dextral	30	post Devonian
Storetvedt and Torsvik (1983)	sinistral	-	late/post Devonian
Van der Voo and Scotese (1981)	sinistral	2000	Carboniferous
Kennedy (1946)	sinistral	100	post-Middle/lower Old Red times
Briden, et al. (1984)	-	small	-
Smith and Watson (1983)	sinistral	100-200	pre or early Devonian
Rogers et al. (1989)	dextral	25-29	post Old Red times
	sinistral	-	end by Emsian
Thirlwall (1989)	-	80	-

Table 4.1 The direction, magnitude and timing of the movement of the Great Glen fault.

inferred movement ranging up to 2000 km. For instance, Storetvedt (1987) inferred two main movements from the palaeomagnetic data. The earlier sinistral movement (600 km) occurred during the late Middle Devonian and a later dextral movement (300 km) occurred during the Hercynian.

The published evidence suggests that transcurrent movement has occurred along the Great Glen fault and this is supported by the remarkably straight outcrop across Scotland. Movement in both directions may have occurred as suggested by Holgate (1969) and Storetvedt (1987). The evidence mainly suggests significant sinistral displacement probably before the end of the Middle Old Red Sandstone, possibly followed by later smaller dextral movement. The early sinistral displacement appears to be at least 100 km and possibly much more.

4.4 Previous geophysical studies

The LISPB deep refraction profile (Bamford et al. 1977,1978) crosses the Great Glen fault near Inverness. This refraction profile yielded a three-layered crust with total thickness of nearly 30 km at the Great Glen fault. The upper crustal velocities (6.0-6.2 km/s) are associated with granites and Moine metasediments up to amphibolite facies. A mid-crustal layer velocity of about 6.4 km/s was earlier observed further north by Smith and Bott (1975) and was attributed to the granulite facies of the Lewisian basement rocks. At the Great Glen fault the top of this mid-crustal layer occurs at about 10 km in depth on the north side but its presence to the immediate south is unclear and possibly 3 km deeper. The deep lower crust along LISPB is interpreted as having a velocity greater than 7 km/s. Hall (1985) suggested that such velocities can be achieved by an increased proportion of mafic minerals appropriate to basic composition.

The WINCH (Western Isles North Channel, Brewer et al. 1983) seismic

reflection profile crosses the southwest extension of the Great Glen fault north of the Colonsay Basin. The total crustal thickness is nearly 30 km. Brewer et al. suggested that the fault may extend into the mantle but Hall (1986) indicated that the fault has no visible effect on the Moho. The is no obvious change in crustal reflection character across the fault line.

The Bouguer anomaly along the Great Glen fault is generally low (-10 mGal, Hussain and Hipkin 1981). A similar anomaly low extends over the Northern Highland, to the northwest of the Great Glen fault. A stronger low of up to -50 mGal dominates the Grampian Highlands. This region of anomaly low corresponds to the Moines outcrop and the Aberdeenshire granites. It is conspicuously lower over the granites, with the lowest value over the Cairngorm granite. There are two interpretations which have been suggested for the Bouguer anomaly lows. They may be associated with extensive granites at depth (Dimitropoulos 1981) or be due to a density contrast between the low density Moines and the Dalradian with a higher density by about 100 kg/m^3 (Hipkin and Hussain 1983). Over Moray Firth there is a deep gravity low caused by thick sediments. A local gravity high associated with the Mull Tertiary igneous centre occur to the southwest. There is no major gravity anomaly associated with the Great Glen fault itself on mainland Scotland.

The resistivity data and the magnetic induction data across the Great Glen fault zone indicate the presence of conductive near-surface rock which is connected along the Great Glen fault zone to a conductive zone in the deeper crust (Mbipom and Hutton 1983). This suggests that the near surface rocks along the Great Glen fault may have similar electrical properties to the deep crustal rocks.

Hall and Dagley (1970) modelled the Great Glen anomaly using a sloping step model between 8 and 15 km depth with 3.0 A/m magnetization. The sheet which lies south of the Great Glen fault has its sloping surface coinciding with the fault plane. The modelling, which was not presented, used smoothed aeromagnetic data

where shorter wavelength anomalies have been suppressed. Powell (1978a) modelled the origin of the smoothed linear magnetic high in terms of high magnetization (2.5 A/m) of varying thickness within the mid-crustal layer of LISPB to fit the above smoothed data. The seismic interface was assumed to separate more strongly magnetised pyroxene granulites below from the weakly magnetised amphibolised granulites above as it deepens southwards from the fault. Powell placed the base of the effective magnetization at an interface of varying depth between the mid and lower crust. The problem of both of the above models based on the smoothed anomalies is that the top of the magnetized body is much deeper then indicated by limiting depth criteria in the next section. Dimitropoulos (1981) modelled the gravity low along the LISPB line south of the Great Glen fault as due to granite body with the top at 7 km and bottom at 19 km. The smoothed aeromagnetic anomaly along the same line has two distinct peaks. The peak near the Great Glen fault has amplitude of about 250 nT and the peak near Monadhliath granite has amplitude of about 200 nT. Dimitropoulos calculated the magnetic anomaly of the granite body using a magnetization contrast of -1.5 A/m between the granites and the surrounding basement. The best fitting calculated anomaly to the smoothed magnetic anomaly was obtained in the presence of almost horizontal remanent magnetization.

4.5 Magnetization

The magnetizations of some of the different rock types in northern Scotland measured by previous workers are given in table 4.2. Most of the values were originally given in cgs units, either as intensities or susceptibilities. They are all converted to magnetization in the earth's magnetic field in the S.I system which is assumed to be entirely induced. The Lewisian rocks have magnetization mainly ranging from 0.1 to 3 A/m. The granulitic rocks generally have higher magnetization than others. The Moines which are of greenschist and amphibolite facies (Fettes et al. 1985) are weakly magnetised (Powell 1970). The Lewisian granites have magnetization of about

References	Area	Rock type	NS	magnetization in earth's field (A/m)
Powell (1970)	Gruinard Bay southwards	amphibolites and gneisses	70	0.1 A/m
	Gruinard Bay - Loch Laxford	Ultrabasics and pyroxene granulites (intermediate to basic)	90	(10 times above) 1 A/m
	Loch Laxford northwards	granites and pegmatites	50	0.4 A/m (several with 1 A/m)
	same region	magnetized amphibolites	3	5 A/m
	same region	gneisses and amphibolites	100	0.1 A/m
	east coast of south Uist	biotite gneiss basic gneiss	20 95	0.2 A/m 1.5 A/m
	near Moine Thrust	Moines		weakly magnetized
Powell (1978a)	Eastern Tiree	basic gneisses other associated rocks	95 167	1.5 A/m 3 A/m
Brown and Locke (1979)	Cairngorm Hill	Cairngorm granites		remanent (small) induced (.025 A/m)

Table 4.2 The measured magnetization values for some of the different rock types in North Scotland. NS is number of samples.

0.4 A/m, but the Cairngorm Newer granites have negligible remanence and a small induced magnetization of about 0.025 A/m.

Geophysical modelling applying suitable constraints may also gives some indication of the magnetisation. The magnetizations used to model some of the medium to long wavelength magnetic anomalies on the mainland and on the shelf north of Scotland are given in table 4.3. The anomalies in the Scourie to Durness area have been modelled as due to Scourian granulite basement having magnetization of 1.0-1.3 A/m below weakly magnetised Laxfordian gneisses (Bott et al. 1972). The smoothed magnetic anomaly along the LISPB line has been attributed to magnetization of 2.5 A/m within the 6.4 km/s middle crustal layer (Powell 1978a). To the north of Scotland, Watts (1971) associate large long wavelength magnetic anomalies west of Shetlands with Scourian granulite basement magnetization of 2.1 A/m. The magnetic basement in all of these areas has been suggested as having magnetic properties similar to those of pyroxene granulites.

The deepest limit of magnetic sources contributing to magnetic anomalies may be taken to be the Moho because the upper mantle (peridotite dominant) is probably weakly magnetic compared to the lower crust (mainly granulitic grade rock, Wasilewski et al. 1979). Furthermore, most rocks should lose their magnetization somewhat below 600°C. Measurements on amphibolites and granulites indicate that the Curie point temperature is about 550-575°C (Schlinger 1985). The Curie temperature of the Lewisian rocks given by Piper (1979) is somewhat lower (515-550°) which is probably reached at or near the Moho. The base of the magnetic crust below the Great Glen fault probably corresponds to the base of the lower crust at about 30 km depth, but may even be shallower.

The maximum bulk magnetization value may be taken to be about 3.0 A/m as the highest magnetisation of the crustal rocks exposed in the region from measurements and modelling, does not exceed 3.0 A/m (i.e. the Lewisian granulites). By

Reference	Rock type	Area	Magnetization
Powell (1978a)	assumed pyroxene granulites within mid-crustal layer of LISPB	model to explain the smoothed aeromagnetic anomaly along LISPB	2.5 A/m
Watts (1971)	magnetic basement (similar in magnetic properties to Scourian)	west of Shetlands	2.1 A/m
Bott et al. (1972)	magnetic basement (similar in magnetic properties to Scourian)	between Scourie and Durness	1.0-1.3 A/m
Hall and Dagley (1970)	sloping-step model	across the Great Glen Fault	1.0-3.0 A/m
Dimitropoulos and Donato (1981)	basement rocks	Moray Firth	2.0 A/m

Table 4.3 Magnetizations values used by previous workers to model some of the medium to long wavelength magnetic anomalies in Scotland.

analogy, the average magnetization of the source of the linear magnetic high is probably less than 3.0 A/m. The effective direction of magnetization has been assumed to be induced and along the present earth's magnetic field direction as discussed in section 3.1.7. The rocks of the upper crust in the Great Glen fault region are the Moine metamorphic rocks. The Moines and the Newer granites as exposed are probably too weakly magnetised (table 4.2) to give rise to any significant long wavelength magnetic anomaly along the Great Glen fault and thus the source of the anomaly probably underlies them.

4.6 Depth limits

The maximum possible depth to the top of a body causing an anomaly may be calculated using limiting depth methods. A number of methods have been published for gravity and/or magnetic anomalies (e.g. Bott and Smith 1958, Smith 1959a, Spector and Grant 1970). Simple methods include the half-width and gradient methods, and assume simple geometrical shapes. These may grossly overestimate the true depth to the body. The higher derivative methods often provide a more realistic limiting depth value compared to the simple methods, particularly where detailed profiles are available. Formulae to determine the limiting depth using second and third derivatives have been given by Smith (1959b) for both magnetic and gravity anomalies. The second derivative magnetic method of Smith has been applied here to the Great Glen fault magnetic anomaly.

According to Smith the maximum possible depth to the top surface of a body (having parallel magnetization) causing a magnetic anomaly F is given by

$$h^2 \leq \frac{6\pi(3l^2 + 2m^2 + 2n^2)^{\frac{1}{2}}}{15^{\frac{1}{2}}} \left(\frac{J_{max}}{|\frac{d^2F}{dz^2}|}\right)$$

where h is the maximum depth, J_{max} is the maximum magnetization within the body, $|\frac{d^2F}{dz^2}|$ is the maximum second derivative value of the observed magnetic anomaly (z

is positive downwards) and $s = (l, m, n)$ is a unit vector in the direction of the earth's field. The maximum second derivative of the anomaly along a profile at any particular sample point can be calculated using two first derivatives of the anomaly. The two first derivatives can be calculated by using the anomaly at the sample point and the anomaly at the point prior to it and, by using the anomaly at the sample point and the anomaly at the point beyond it. The second derivative is the rate of change of these two first derivatives. The limiting depth calculated using Smith's second derivative procedure is dependent on the maximum second derivative and the magnetization contrast. The maximum second derivative obtained from anomaly sampled at discrete points may only be an estimate of the true value and a large magnetization contrast gives deeper maximum depth to the top of the body. The Great Glen anomaly has the maximum observed change of gradient about 20 km northeast of Inverness. The maximum observed second derivative here is estimated to be 65 nT/km^2. Assuming that the magnetization of the Great Glen anomaly is 3.0 A/m as discussed in the earlier section, the maximum depth to the top of the source is less than 7 km. If the average magnetization of the source is lower, then the maximum depth is less.

Geophysical modelling may give a more accurate estimate of the depth to the top of the body causing a magnetic anomaly. This is discussed later in the modelling section. It will be shown that modelling indicates the source is actually shallower than obtained from the second derivative method. The calculated limiting depth of about 7 km obtained from the second derivative method may thus be a substantial overestimate of the actual depth. Nevertheless it indicates that the top of the source causing the linear positive magnetic anomaly along the Great Glen fault lies in the upper crust.

4.7 Modelling of the source of the Great Glen anomaly

4.7.1 Procedure

The Great Glen magnetic and pseudogravimetric anomalies include superimposed shorter wavelength anomalies and they may also be affected by anomalies from neighbouring sources. These effects must be avoided as far as possible in order to obtain anomaly profiles perpendicular to the fault which represent the linear source. Based on both the pseudogravimetric (figure 4.3) and the aeromagnetic map (figure 4.1), a profile AA′ (figure 4.2) perpendicular to the fault which is relatively free of the shallower effects and neighbouring anomalies was selected for the main interpretation. The pseudogravimetric map shows that the profile southeast of the anomaly is perpendicular to the contours. The effects of the neighbouring and shallower anomalies on the pseudogravimetric anomaly profile are probably minimal here. However, the pseudogravimetric profile northwest of the peak cuts obliquely across the contour trend. It may therefore, include some contribution from the source situated west of the profile in the Skye region, partly causing asymmetry of the profile. This profile is probably as good as can be obtained and has been used to model the source of the linear magnetisation along the Great Glen fault. The magnetic profile is disturbed by an obvious shorter wavelength anomaly to the southeast of the anomaly peak. The short wavelength components need to be suppressed. This is already effected in the pseudogravimetric anomaly. A second profile BB′ which crosses the Great Glen anomaly northeast of Inverness where the apex is sharpest has also been used for the interpretation.

The standard modelling routine (GRAV, Bott 1986) and the non-linear optimisation routine (MINUIT, James and Roos 1969 and OPTIGRAV, Westbrook 1973) have been used in the pseudogravimetric modelling. An initial model was first assumed by applying suitable constraints. The gravity anomaly was calculated using GRAV.

The calculated anomaly was then compared with the pseudogravimetric profile. The model parameters were changed within the limits of the constraints to obtain a satisfactory fit between the calculated and the observed anomalies. This model was then used as a starting model for non-linear optimisation. A model which gives an accurate fit may then be obtained easily. Alternatively, the initial model may be used to start the non-linear optimisation. The subroutine SEEK gives an approximate solution. The subroutine SIMPLEX then obtains a more accurate result. Non-linear optimisation is dependent on the starting model. The resulting model may represent a local minimum and may not be geologically feasible. The use of GRAV enables more tightly constrained parameters to be initially applied so that more satisfactory models can be obtained. In the direct magnetic modelling using MINUIT and OPTIMAG (Westbrook 1973), a similar procedure has been be used.

In the pseudogravimetric modelling, the magnetic anomaly of the final model can be re-calculated using MAG (Bott 1988) and compared to the aeromagnetic data along the profile used. This comparison is a useful test. If the calculated magnetic anomaly and the observed aeromagnetic anomaly differ greatly, then remodelling needs to be carried out until satisfactory fit of the calculated gravity anomaly to the pseudogravimetric anomaly, and the calculated magnetic anomaly to the observed magnetic anomaly, are obtained. The model then fits both the pseudogravimetric anomaly and the magnetic anomaly. Both the aeromagnetic and pseudogravimetric maps show that the width of the anomaly to be modelled is smaller than its strike length. Therefore two-dimensional modelling methods may be used without serious error.

Modelling was first carried out to investigate the type of cross-sectional shape that can validly be the source of the Great Glen magnetic and pseudogravimetric anomalies. This was followed by an estimation of the maximum possible depth to the top of the source, and of the minimum possible magnetization. Some models showing the range of possible structures are given in the later part of the section.

4.7.2 Geometry of the source

The two extreme types of cross-sectional shape which need to be investigated are (1) a strongly magnetized triangular region with horizontal base and outward dipping sides with a sharp apex near the fault, and (2) a strongly magnetized basinal feature with horizontal shallow top and inward dipping sides. Tests have been carried out on the inward and outward dipping models using a high average magnetization of 2.5 A/m with the top at relatively shallow depth. Pseudogravimetric modelling was first carried out. The magnetic anomalies of both the models were then calculated and compared to the observed magnetic anomaly and a best fit to both pseudogravimetric and magnetic anomaly was obtained by trial and error. The calculated pseudogravimetric anomalies of the outward and inward dipping models both give quite a good fit to the observed pseudogravimetric anomaly (figures 4.5a and 4.6a respectively). The pseudogravimetric modelling, therefore, cannot be used to distinguish between the inward and outward dipping features. The calculated magnetic anomalies from both of these models, however, indicate that the magnetic anomaly of the outward dipping model with the peak at shallow depth (3 km) simulates the sharp apex of the observed magnetic anomaly (figure 4.5b), but that of the inward dipping model does not (figure 4.6b). The problem with the inward dipping model is that the features at the base of the model are too deep to satisfy the sharp apex of the magnetic anomaly.

Direct magnetic modelling has also been used to test the validity of the inward dipping feature. This is to test whether magnetic modelling can explain the apex of the observed magnetic anomaly. Both the profiles, the main profile AA′ and profile BB′ which cuts across the region of maximum gradients of the Great Glen anomaly, have been used. As in the pseudogravimetric modelling, the models have their top at the surface and a magnetization of 2.5 A/m. The calculated magnetic anomalies of the model along AA′ (figure 4.7) cannot quite simulate the observed sharpness at the apex as closely as that of the outward dipping model with the top at shallow depth (figure 4.5b). This is even more clearly shown along the profile BB′ (figure

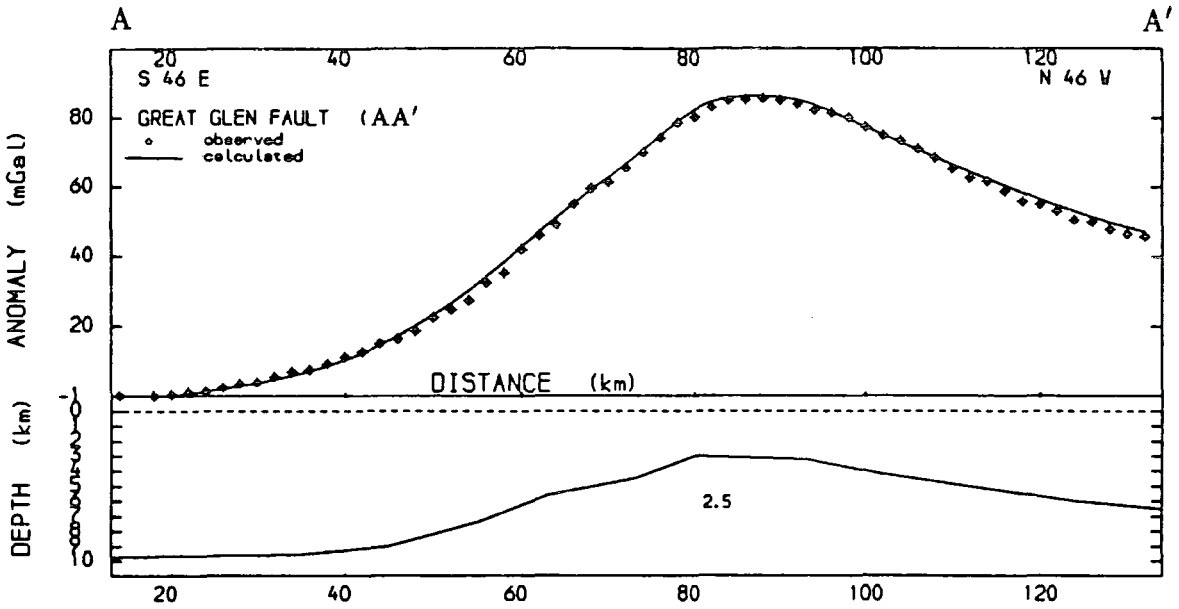

Figure 4.5a The calculated pseudogravimetric anomaly of an outward dipping model along AA′ compared to the observed pseudogravimetric anomaly. The top of the model is at about 3 km and the magnetization is 2.5 A/m. The density (kg/m^3) to magnetization (A/m) ratio is 150:1.0.

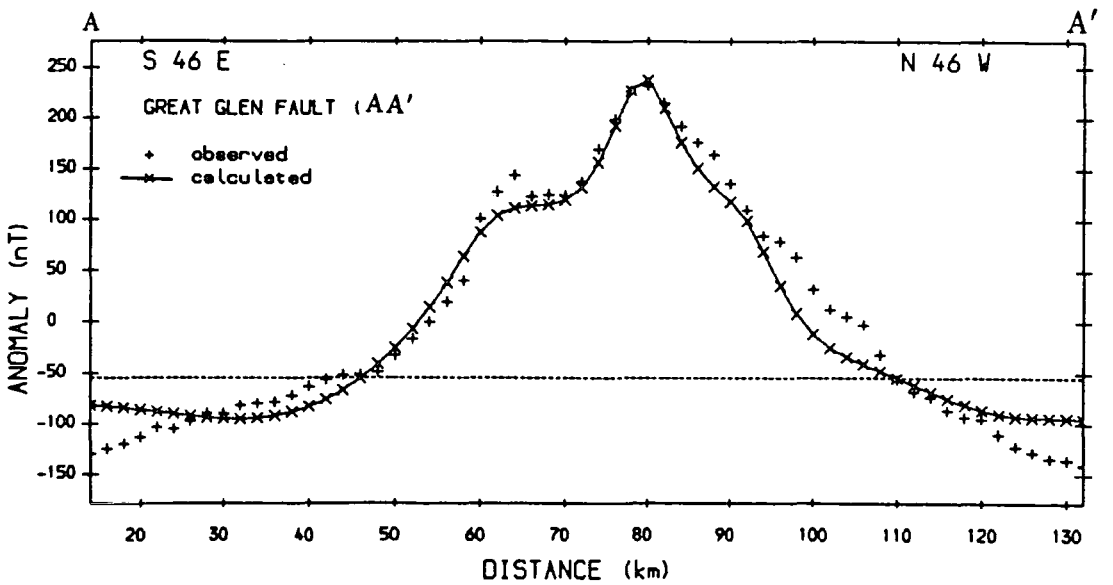

Figure 4.5b The calculated magnetic anomaly of the outward dipping model in figure 4.5a compared to the observed magnetic anomaly. Magnetization and inclination along the profile are 2.5 A/m and 74 ^{o} northwestward espectively.

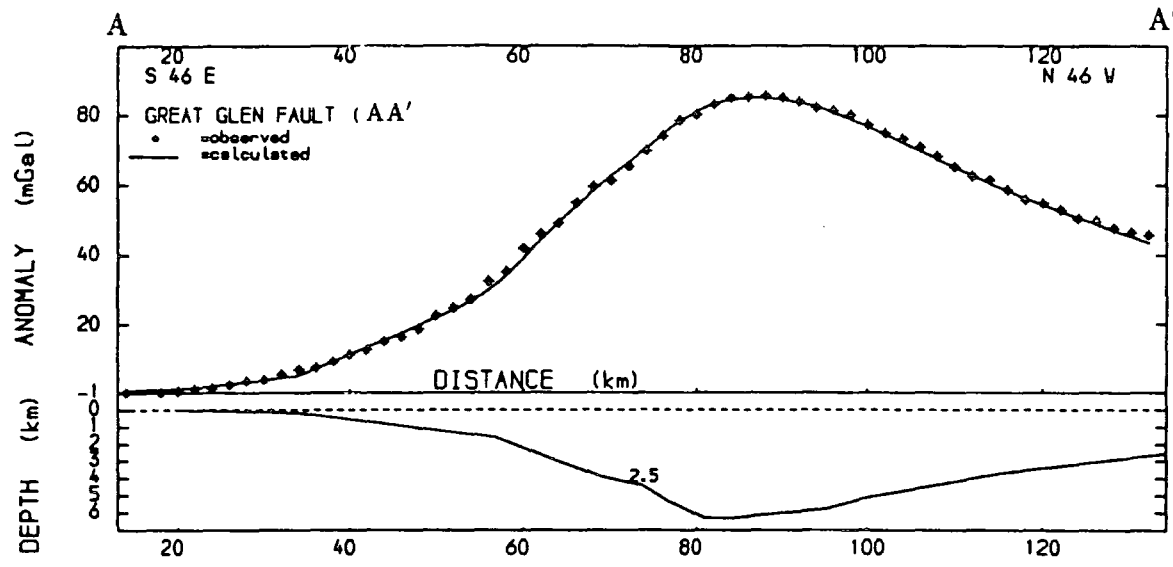

Figure 4.6a The calculated pseudogravimetric anomaly of an inward dipping model along AA′ compared to the observed pseudogravimetric anomaly. The top of the model is at the surface and the magnetization is 2.5 A/m. The density (kg/m^3) to magnetization (A/m) ratio is 150:1.0.

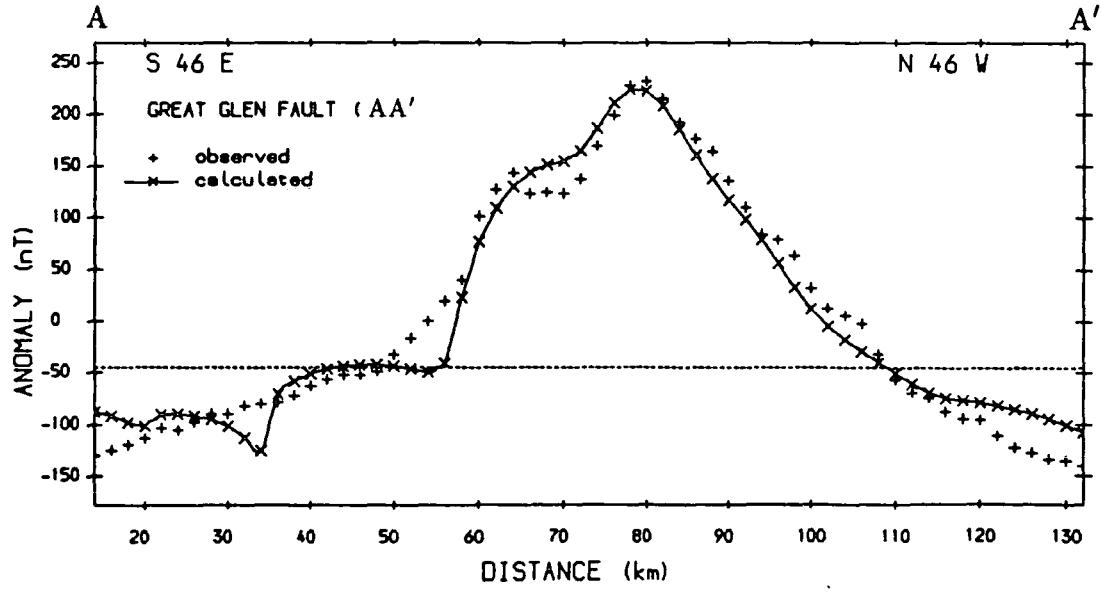

Figure 4.6b The calculated magnetic anomaly of the inward dipping model in figure 4.6a compared to the observed magnetic anomaly. Magnetization and inclination along the profile are 2.5 A/m and 74° northwestwards respectively.

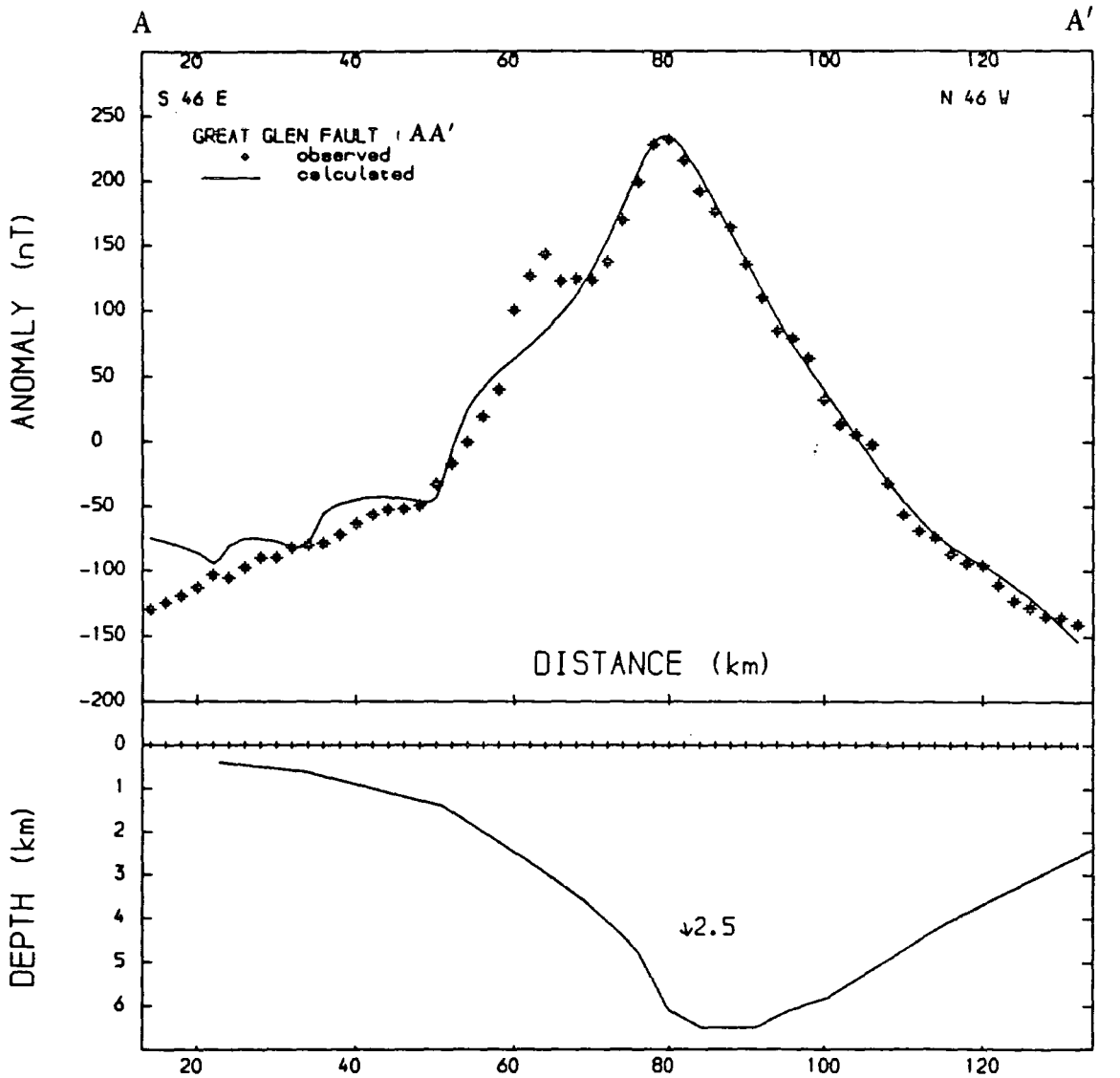

Figure 4.7 Magnetic modelling along the profile AA′ using the inward dipping feature. Magnetization and inclination along the profile are 2.5 A/m and 74° northeastwards respectively.

4.8) where the very high second and higher derivatives cannot be reproduced by the model. This suggests that the outward dipping feature is a more consistent source of the linear magnetic high along the Great Glen fault. Furthermore, rocks having high magnetization at or near the surface with a lateral extent indicated by the inward dipping model have not been reported along the linear magnetic high region. The outcropping rocks are mainly the weakly magnetized Moines. It is concluded that the outward dipping model is the more realistic representation of the source.

4.7.3 Estimation of the depth to the top of the body

A test on an outward dipping model along AA′ with the apex at 7 km depth indicates that the calculated pseudogravimetric anomaly gives a relatively good fit to the observed pseudogravimetric anomaly (figure 4.9a). The calculated magnetic anomaly of the model, however, cannot simulate the sharp apex of the observed magnetic anomaly (figure 4.9b). This demonstrates that a deep source cannot explain the magnetic anomaly. The relatively good fit of the calculated with the observed pseudogravimetric anomalies is because the sharp apex observed in the magnetic anomaly has been suppressed in the pseudogravimetric transformation.

Magnetic modelling was next used to estimate the depth to the top. This specifically aimed at getting a best fit at the apex of the observed magnetic anomaly. This is because the second and higher derivatives at the apex place a limit on the maximum depth to the top of the outward dipping feature for any specified magnetization. Higher values indicate a shallower source. Magnetic modelling was used instead of pseudogravimetric modelling because the sharp apex is suppressed in the pseudogravimetric anomaly. Both the profiles, the main profile AA′ and the profile BB′ were used. The only constraint applied on the modelling was the magnetization. Magnetization values of 1.0 A/m (about the minimum magnetization limit of the outward dipping feature as discussed later) and 2.5 A/m (probably about the maximum

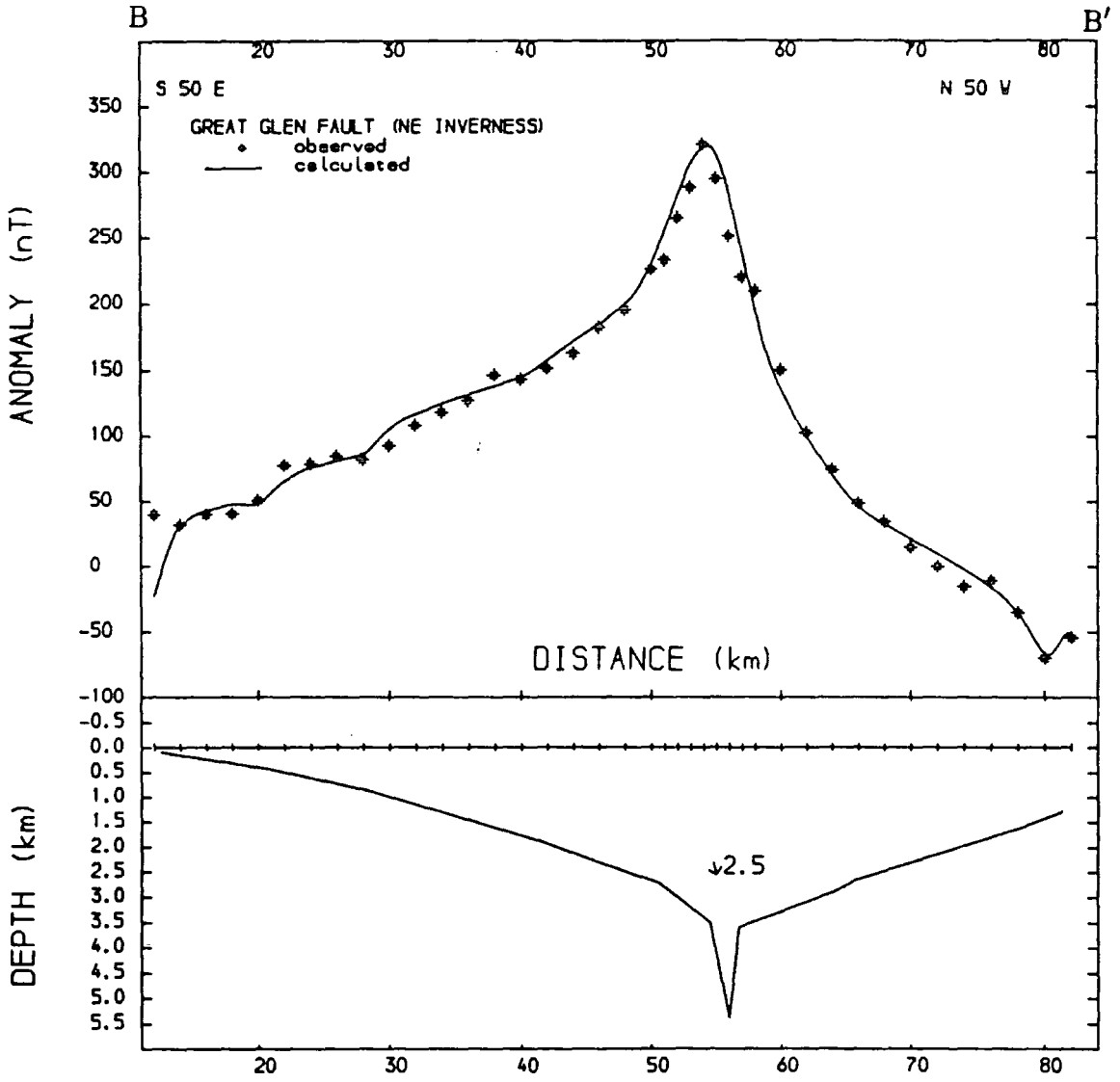

Figure 4.8 Magnetic modelling along the profile BB′ using the inward dipping feature. Magnetization and inclination along the profile are 2.5 A/m and 74° northeastwards respectively.

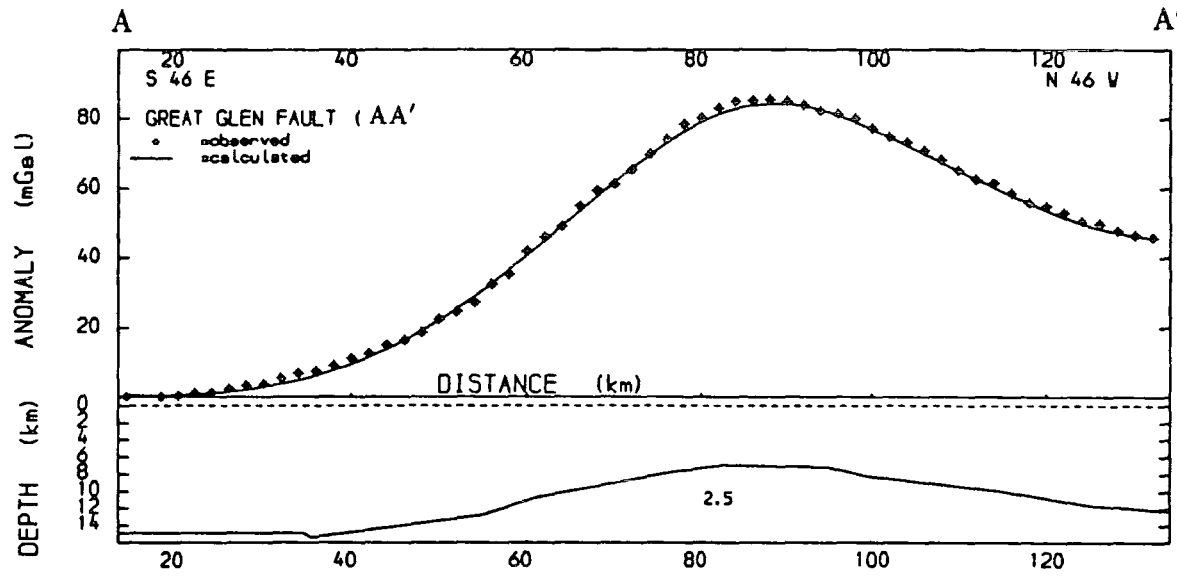

Figure 4.9a The calculated pseudogravimetric anomaly of an outward dipping model along AA′ compared to the observed pseudogravimetric anomaly. The top of the model is at about 7 km and the magnetization is 2.5 A/m. The density (kg/m^3) to magnetization (A/m) ratio is 150:1.0.

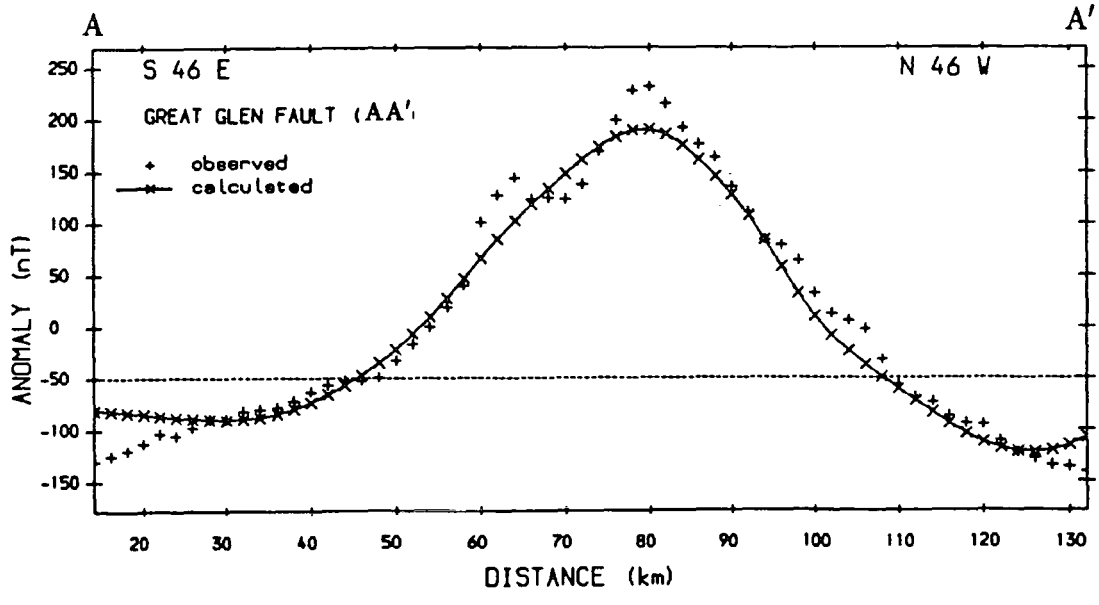

Figure 4.9b The calculated magnetic anomaly of the outward dipping model in figure 4.9a compared to the observed magnetic anomaly. Magnetization and inclination along the profile are 2.5 A/m and 74° northwestwards respectively.

magnetization) were used. Modelling the magnetic profile along AA′ yielded depth to the peak of the outward dipping feature of about 2.5 km (figure 4.10) and 5.5 km (figure 4.11) below the observation level, for magnetization of 1.0 and 2.5 A/m respectively. The magnetic anomaly along profile BB′ yielded a shallower depth of about 1.0 km (figure 4.12) and less than 2.5 km (figure 4.13) for magnetization values of 1.0 and 2.5 A/m respectively. Where the top was at greater depth the misfit at the apex became more pronounced in all these cases. These results indicate that the source of the magnetic anomaly along the Great Glen fault is probably less than 6 km deep and is probably much shallower in some places. The source clearly lies at least partly within the upper crust and partly above the 10 km deep 6.4 km/s seismic interface.

4.7.4 Estimation of a lower limit on the magnetization of the body

A lower limit on the magnetization may be obtained by modelling the Great Glen feature with its peak near the earth's surface and its base at the greatest realistic depth. As mentioned earlier, the base is probably above the Moho (about 30 km depth). Pseudogravimetric modelling along profile AA′ assuming the base at the Moho yields the least feasible value of average magnetization of about 0.8 A/m (figure 4.14). This is about the smallest magnetization recorded for Lewisian granulitic rocks of northern Scotland (tables 4.2 and 4.3).

4.7.5 A range of realistic models

This section explores a range of possible models to explain the Great Glen anomaly obtained by pseudogravimetric modelling using the profile AA′. Pseudogravimetric modelling has been used to emphasized the broad features and to suppress the local variation. The pseudogravimetric profile has a gentler slope northwest of the fault and the background anomaly is of a higher magnitude here than to the southeast. This

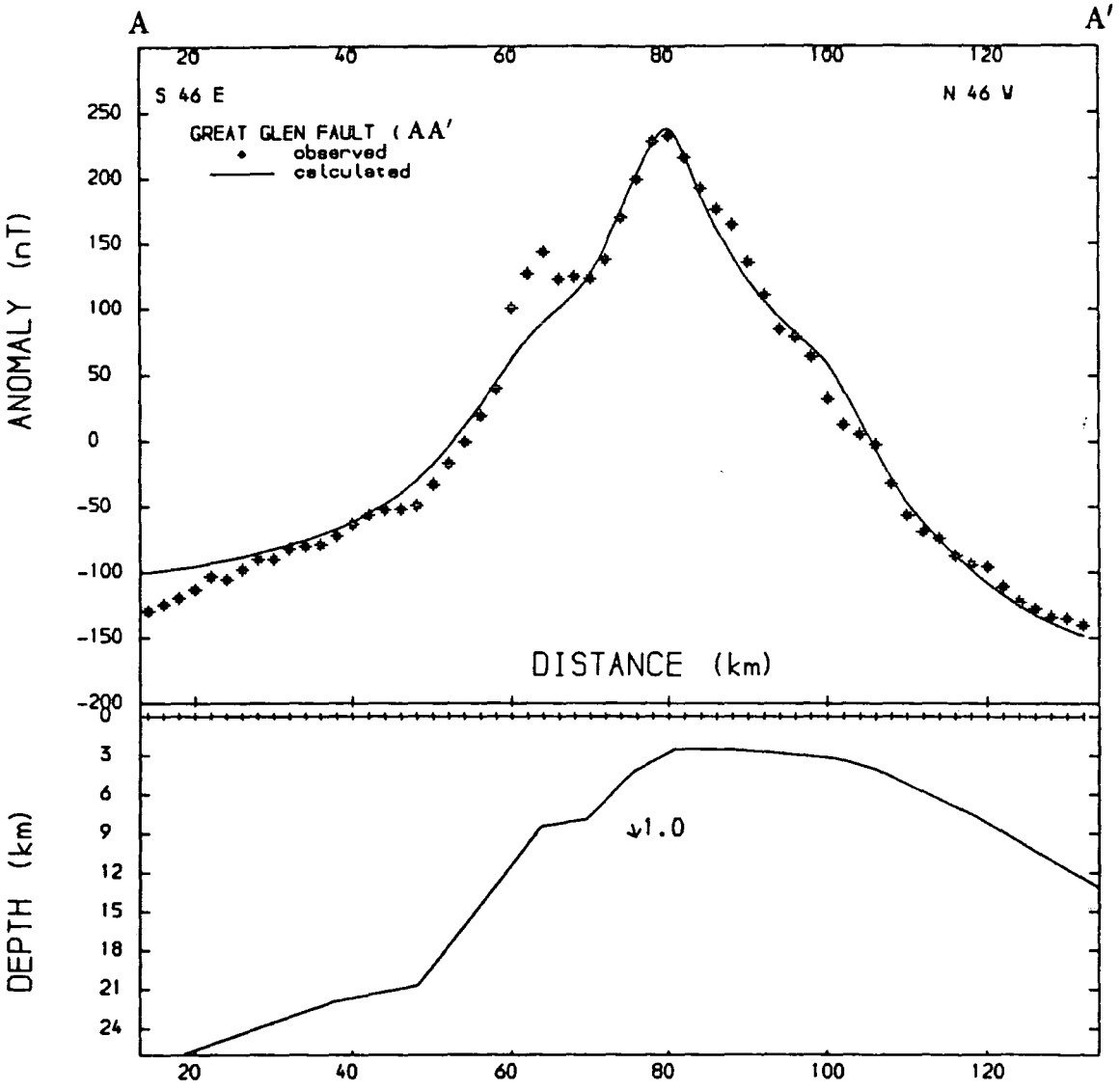

Figure 4.10 Depth modelling using the magnetic anomaly along AA′ using the outward dipping feature by obtaining a best fit at the apex of the magnetic anomaly. The magnetization used is 1.0 A/m and the inclination along the profile is 74^o northwestwards.

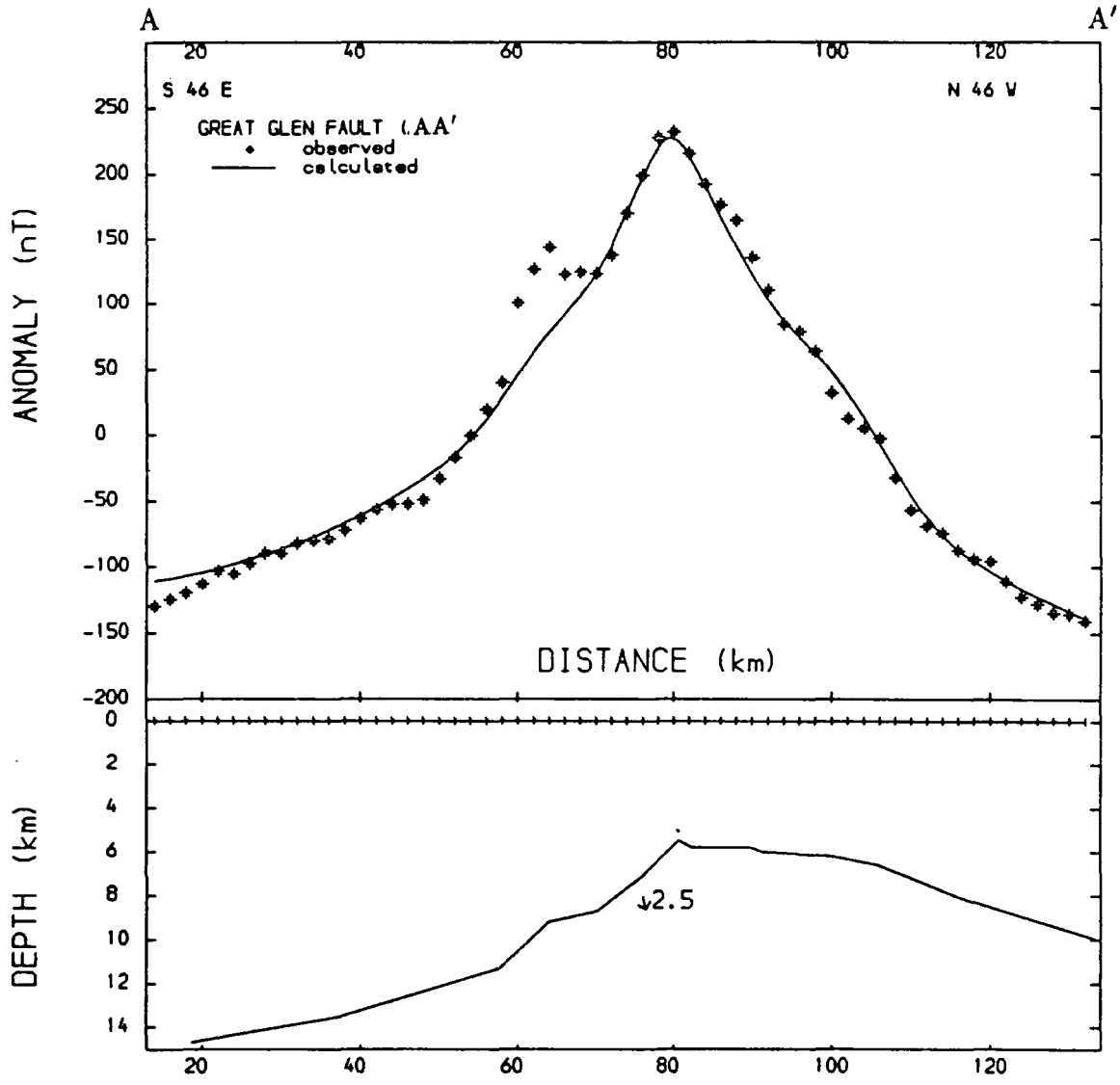

Figure 4.11 Depth modelling using the magnetic anomaly along AA′ using the outward dipping feature by obtaining a best fit at the apex of the magnetic anomaly. The magnetization used is 2.5 A/m and the inclination along the profile is 74° northwestwards.

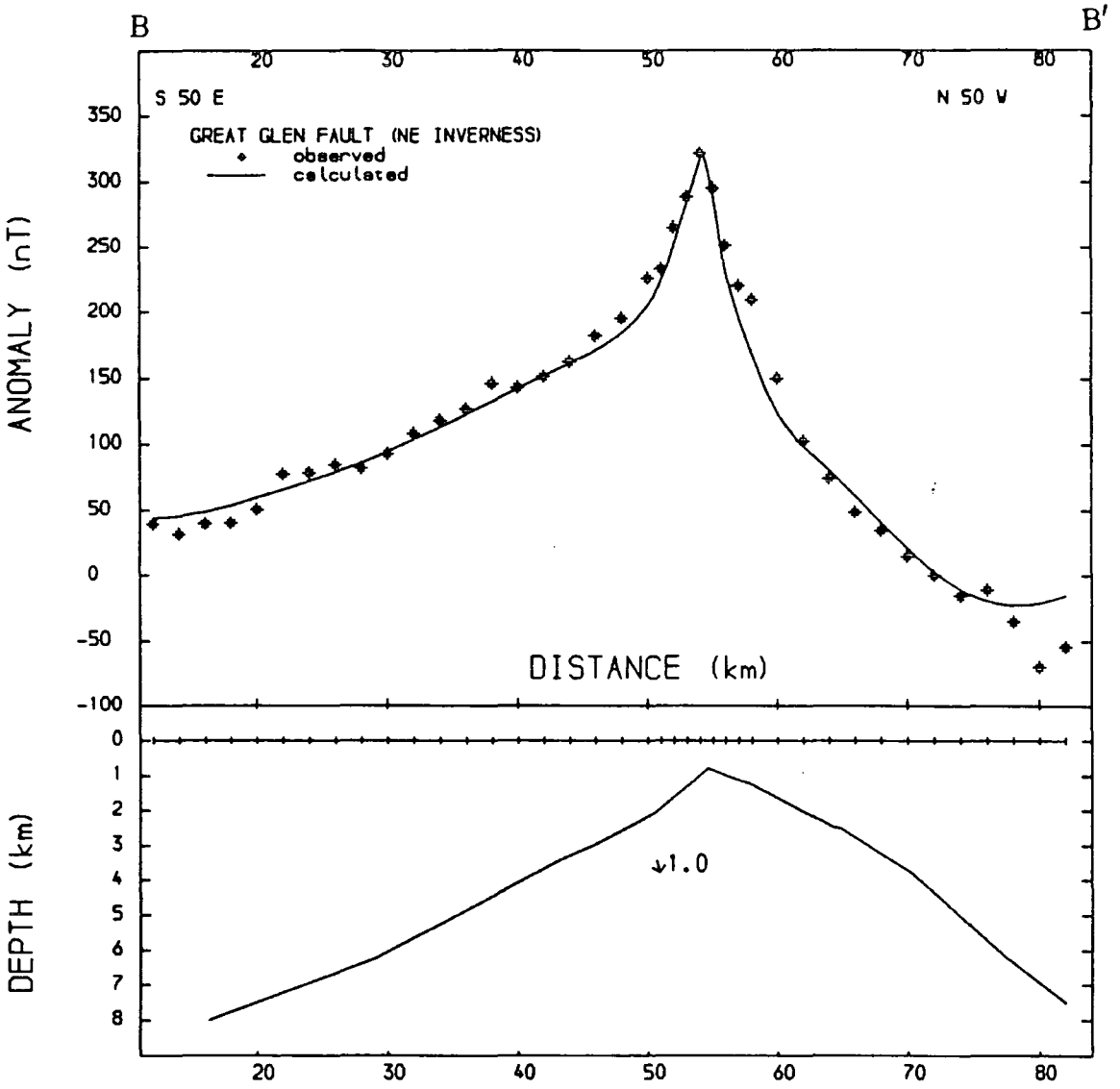

Figure 4.12 Depth modelling using the magnetic anomaly along BB′ using the outward dipping feature by obtaining a best fit at the apex of the magnetic anomaly. The magnetization used is 1.0 A/m and the inclination along the profile is 74^{o} northwestwards.

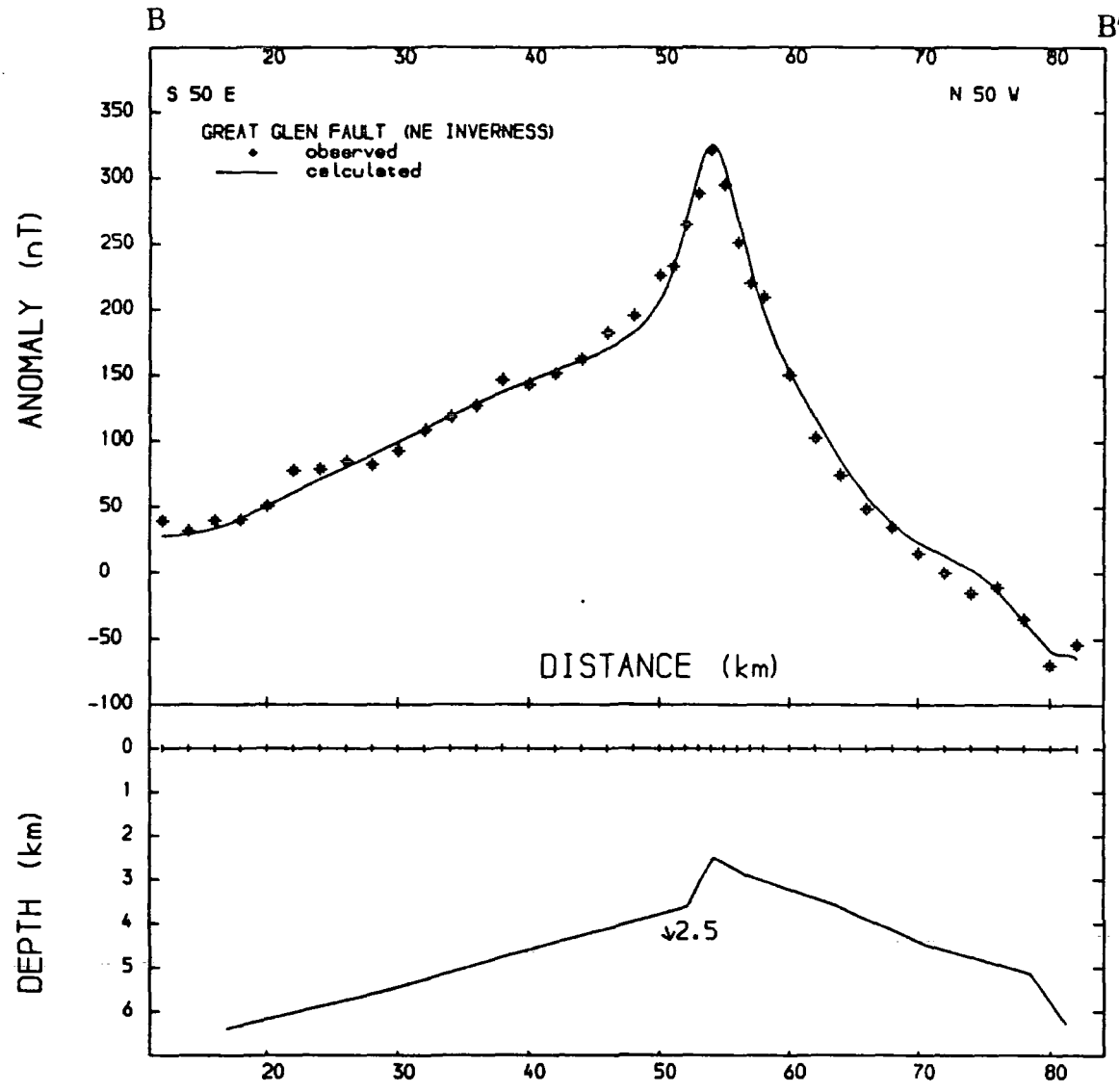

Figure 4.13 Depth modelling using the magnetic anomaly along the profile BB′ using the outward dipping feature by obtaining a best fit at the apex of the magnetic anomaly. The magnetization used is 2.5 A/m and the inclination along the profile is 74° northwestwards.

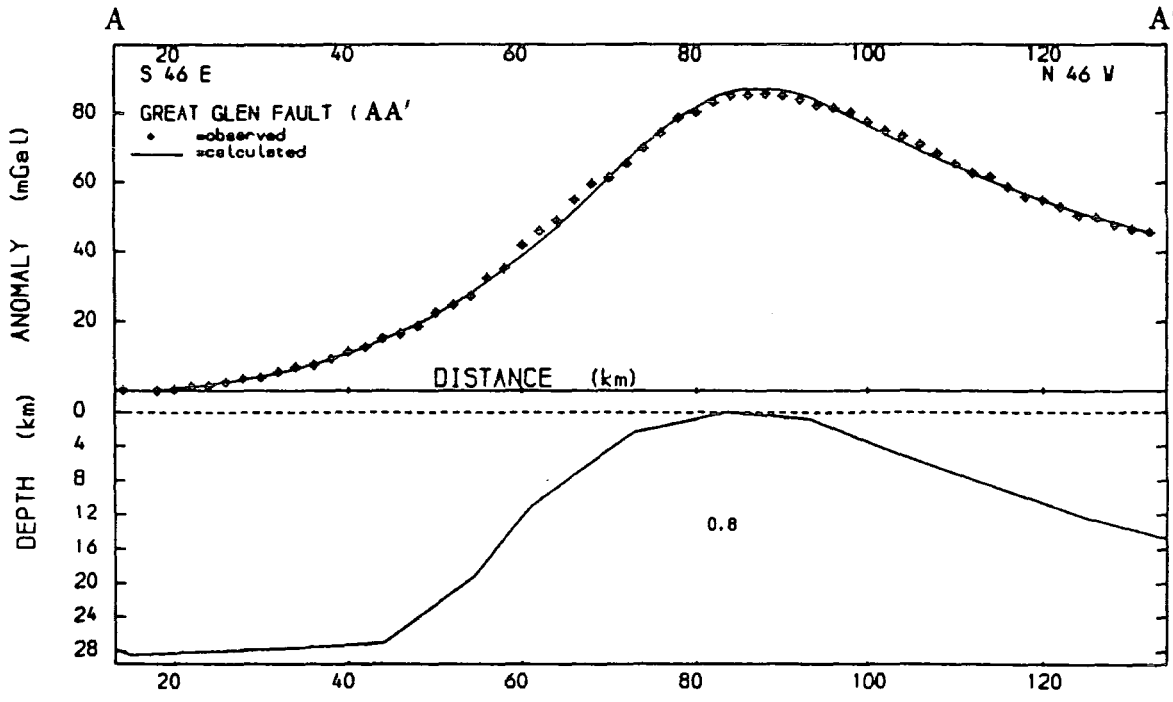

Figure 4.14 Pseudogravimetric modelling along profile AA′ with the top of the outward dipping model at the surface and the base at the Moho (30 km). The magnetization obtained is 0.8 A/m. The density (kg/m^3) to magnetization (A/m) ratio is 150:1.0.

can be modelled as due to an outward dipping feature of homogenous magnetization (single-body model) which passes into a semi-infinite slab at the northwestern end (figure 4.15). It is unrealistic to suppose that the local anomaly associated with the fault extends indefinitely on one side in this way. A more likely model (two-body model) explains the anomaly in terms of a local nearly symmetrical region of high magnetization superimposed on a contrast in magnetization between the crustal blocks on opposite sides of the fault. This idea is now developed.

The local Great Glen pseudogravimetric anomaly is attributed to an outward dipping nearly symmetrical feature of limited extent on both sides of the fault (the Great Glen feature). The base is assumed to be horizontal in most models. A slab of crust north-west of the Great Glen fault is assumed to have significantly higher magnetization than southeast of it. This slab explains the regional difference in the anomaly level across the fault. Modelling has been carried out using the optimization routine with the following constraints:

(a) The local Great Glen feature is initially set up with its top near the fault constrained to a specified depth. The base is at any arbitrary depth but is kept horizontal. The magnetization is specified.

(b) The magnetic slab is assumed to have its upper and lower surface at the same depth as the top and base of the local Great Glen fault feature respectively, thus overlying the northeastern part of the Great Glen feature with common interface. The magnetization of the slab is determined as an unknown.

A range of different values of depth to the top and magnetization (table 4.4) have been used, to show the range of possible models of this type. The magnetization is within the range 1.0-2.5 A/m and the depth to the top varies between 1 and 5 km. The models obtained are shown in figures as indicated in table 4.4.

In all of the two-body models, the Great Glen feature defining the source of the linear magnetic anomaly has an apex which is slightly north of the fault trace but is

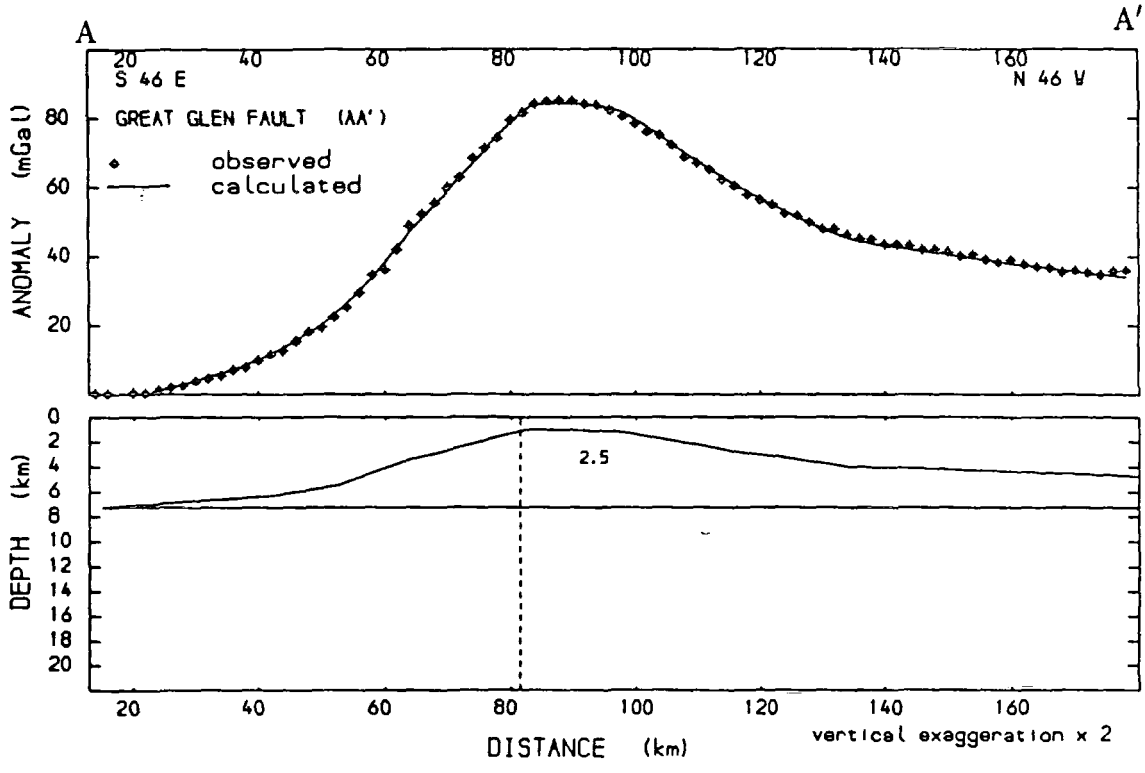

Figure 4.15 Pseudogravimetric modelling along profile AA′ using a single-body model with the top of the outward dipping model at 1 km depth and magnetization of 2.5 A/m. The density (kg/m^3) to magnetization (A/m) ratio is 150:1.0.

Depth to the top (km)	Magnetizations (A/m)	Models given in figures
1.0	2.5	4.16a
	2.0	4.16b
	1.5	4.16c
	1.0	4.16d
3.0	2.0	4.17a
	1.5	4.17b
	1.0	4.17c
5.0	2.5	4.18a
	2.0	4.18b

Table 4.4 The sets of depth to the top of the Great Glen feature and the magnetization values, and the relevent the two-body model shown.

almost symmetrical about the apex. This differs from the single-body model where the anomalous body is less symmetrical (compare figure 4.15 and 4.16a). The base of these models obtained using the same magnetization and depth to top are at about the same depth.

The magnetization of the slab in the two-body models is generally about half the value of that of the Great Glen feature. The Great Glen feature has a width of about 80-90 km at the base. The modelled thickness is dependent on the assumed depth to the top and magnetization. For any specified depth to the top, the thickness increases with decreasing magnetization. This can be seen in the set of models shown in figures 4.16(a,b,c and d), 4.17(a,b and c) and 4.18(a and b). For a specific magnetization, the thickness of the body only increases slightly when the depth to the top changes from 1.0 to 5.0 km (compare figures 4.16a, 4.17a and 4.18a). The smallest thickness of about 7 km is obtained from the model having depth to the top of 1 km and magnetization of 2.5 A/m (figure 4.16a). The greatest modelled thickness is less than 20 km (figure 4.16d).

The source of the Great Glen feature need not necessarily have a horizontal base. A lensoid body can also explain the observed anomaly. A model obtained using a magnetization contrast of 2.5 A/m and depth to the top of about 3 km is shown in figure 4.19. The body is thicker northwest of the fault then to the southwest. The shape of the lower surface of such a model, however, cannot be easily constrained.

The semi-infinite magnetic slab used in the modelling of the two-body model may in reality have its upper surface shallower or deeper than the top of the Great Glen feature. Similarly the lower surface may not coincide with the base of the Great Glen feature. Models of this type have been obtained assuming the slab extends from 1 km to a depth of 20 km on the northeastern side of the fault. The models with the top of the Great Glen feature at 1 km and magnetizations of 2.5 and 1.0 A/m are given in figures 4.20a and 4.20b respectively, with top at 3 km and magnetization

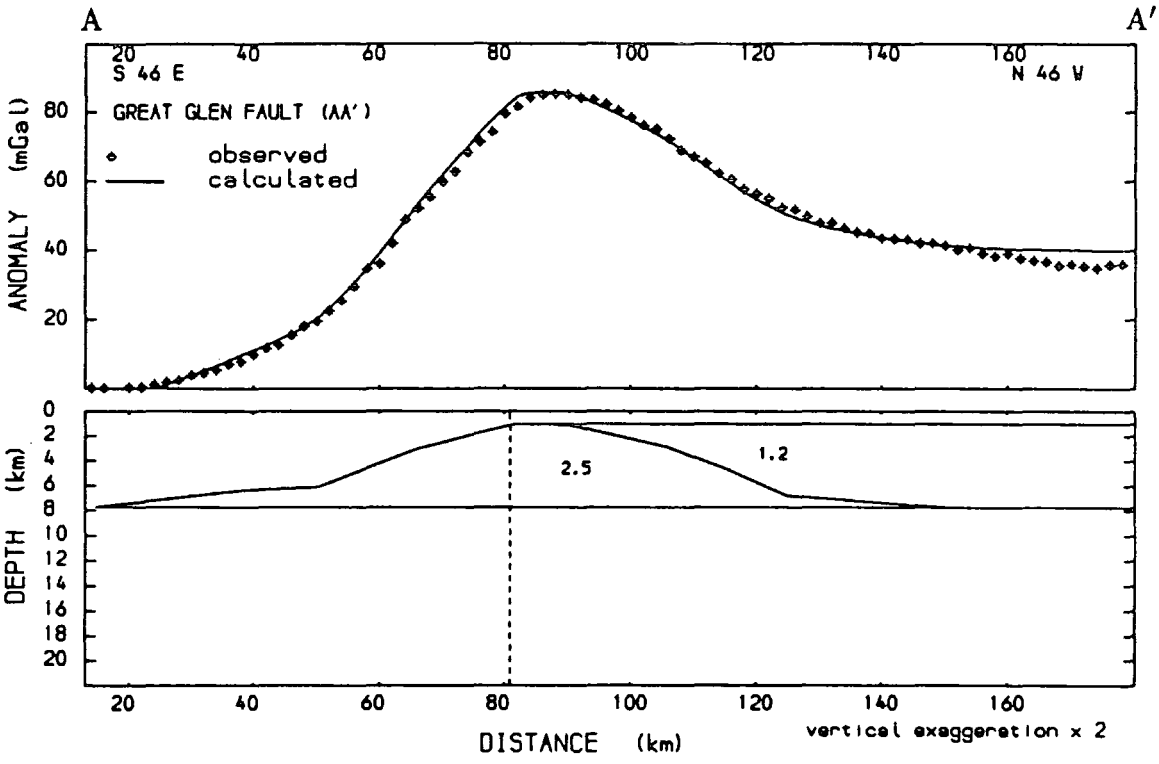

Figure 4.16a Pseudogravimetric modelling along profile AA′ using the two-body model with the top of the Great Glen feature at 1 km and magnetization of 2.5 A/m. The density (kg/m^3) to magnetization (A/m) ratio is 150:1.0.

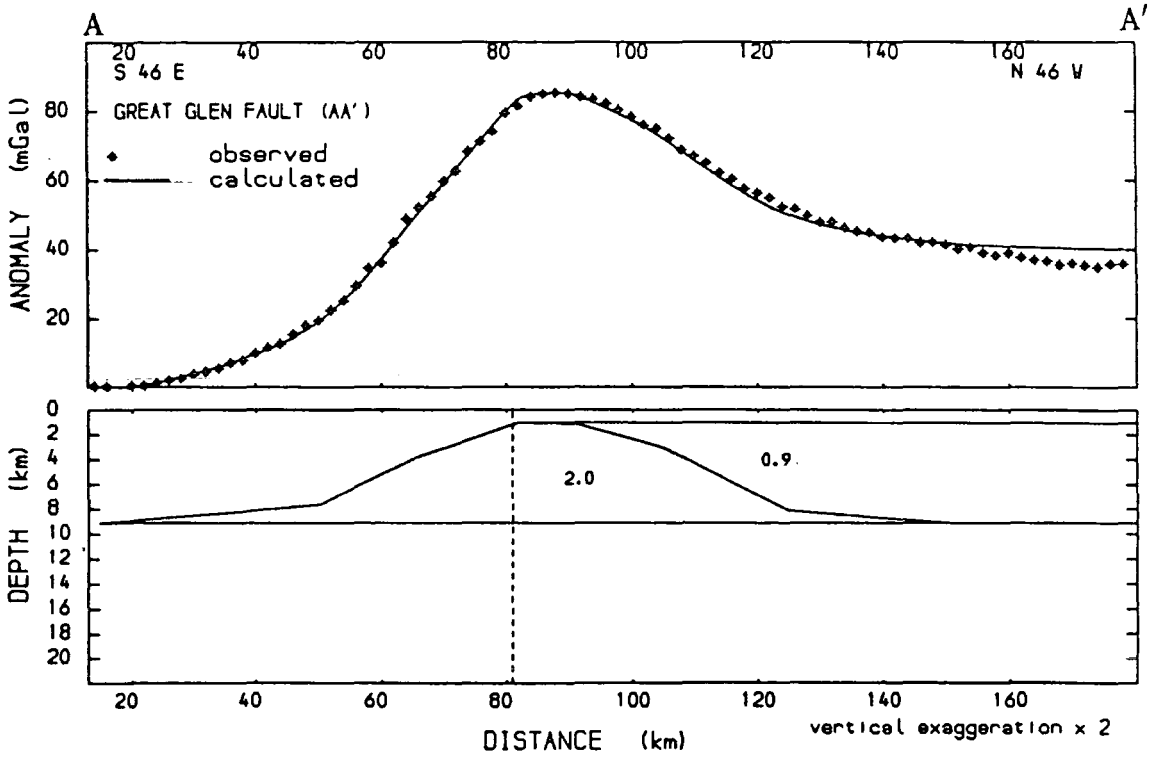

Figure 4.16b Pseudogravimetric modelling along profile AA′ using the two-body model with the top of the Great Glen feature at 1 km and magnetization of 2.0 A/m. The density (kg/m^3) to magnetization (A/m) ratio is 150:1.0.

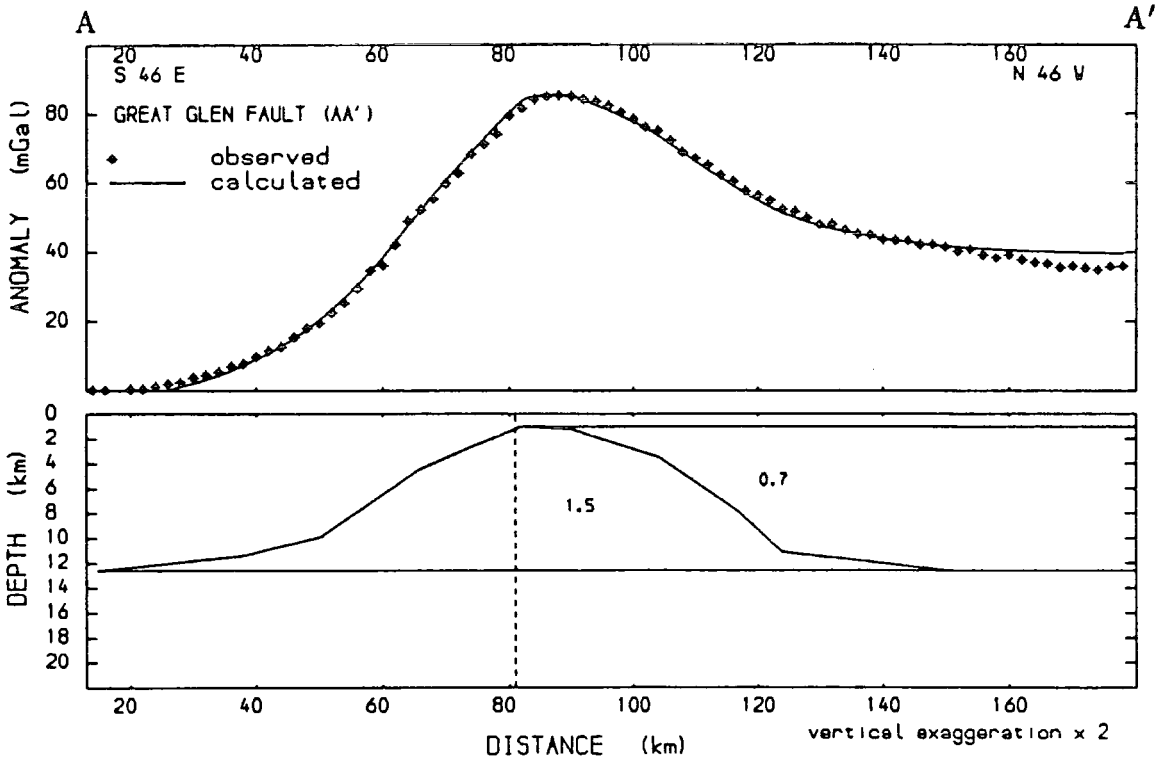

Figure 4.16c Pseudogravimetric modelling along profile AA′ using the two-body model with the top of the Great Glen feature at 1 km and magnetization of 1.5 A/m. The density (kg/m^3) to magnetization (A/m) ratio is 150:1.0.

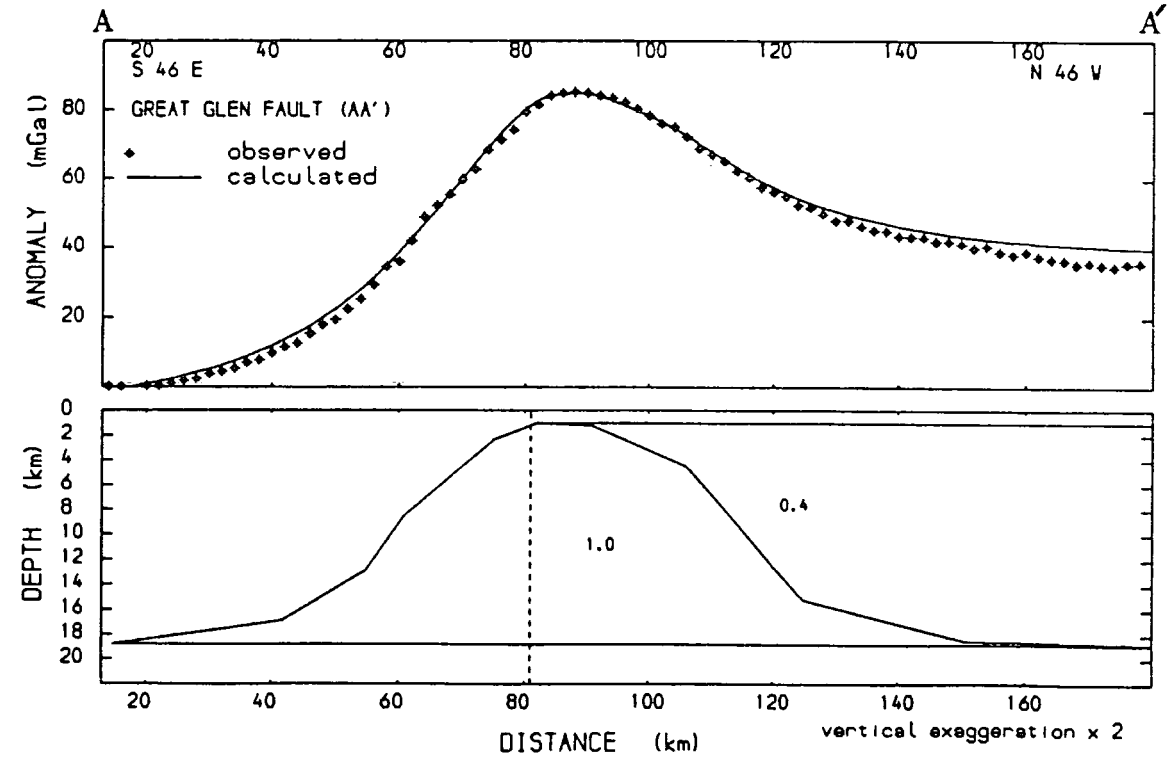

Figure 4.16d Pseudogravimetric modelling along profile AA′ using the two-body model with the top of the Great Glen feature at 1 km and magnetization of 1.0 A/m. The density (kg/m^3) to magnetization (A/m) ratio is 150:1.0.

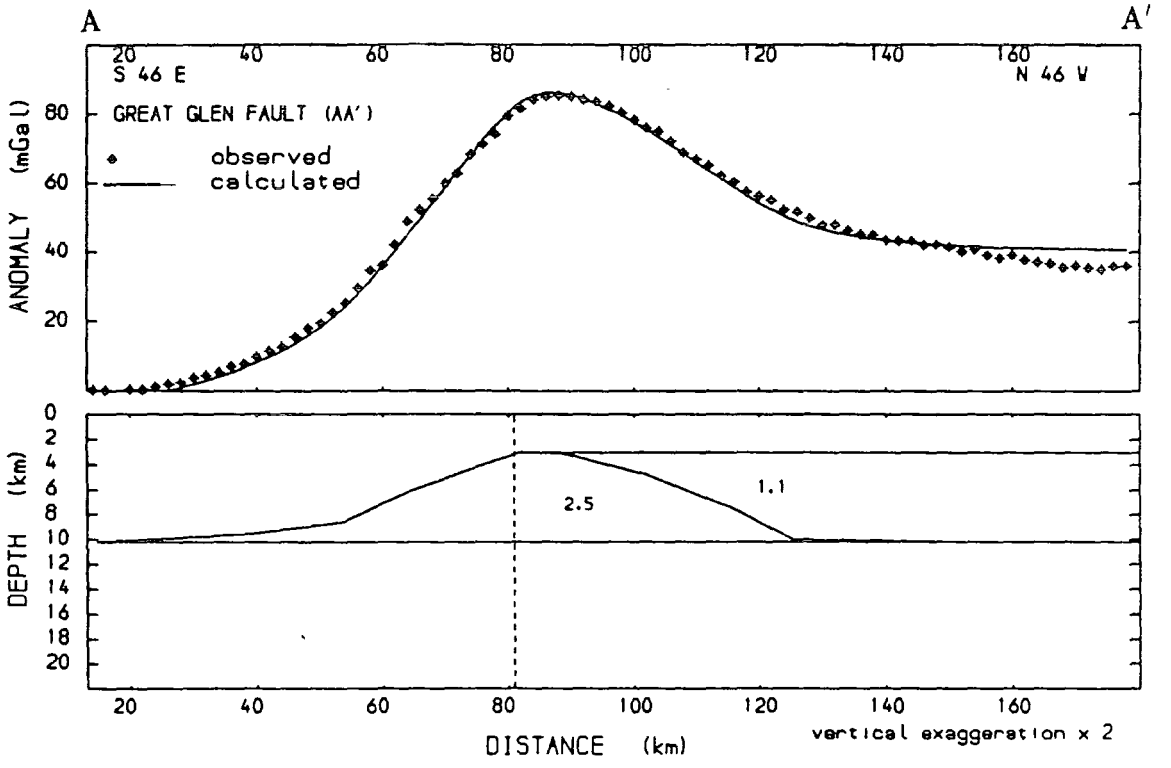

Figure 4.17a Pseudogravimetric modelling along profile AA′ using the two-body model with the top of the Great Glen feature at 3 km and magnetization of 2.5 A/m. The density (kg/m^3) to magnetization (A/m) ratio is 150:1.0.

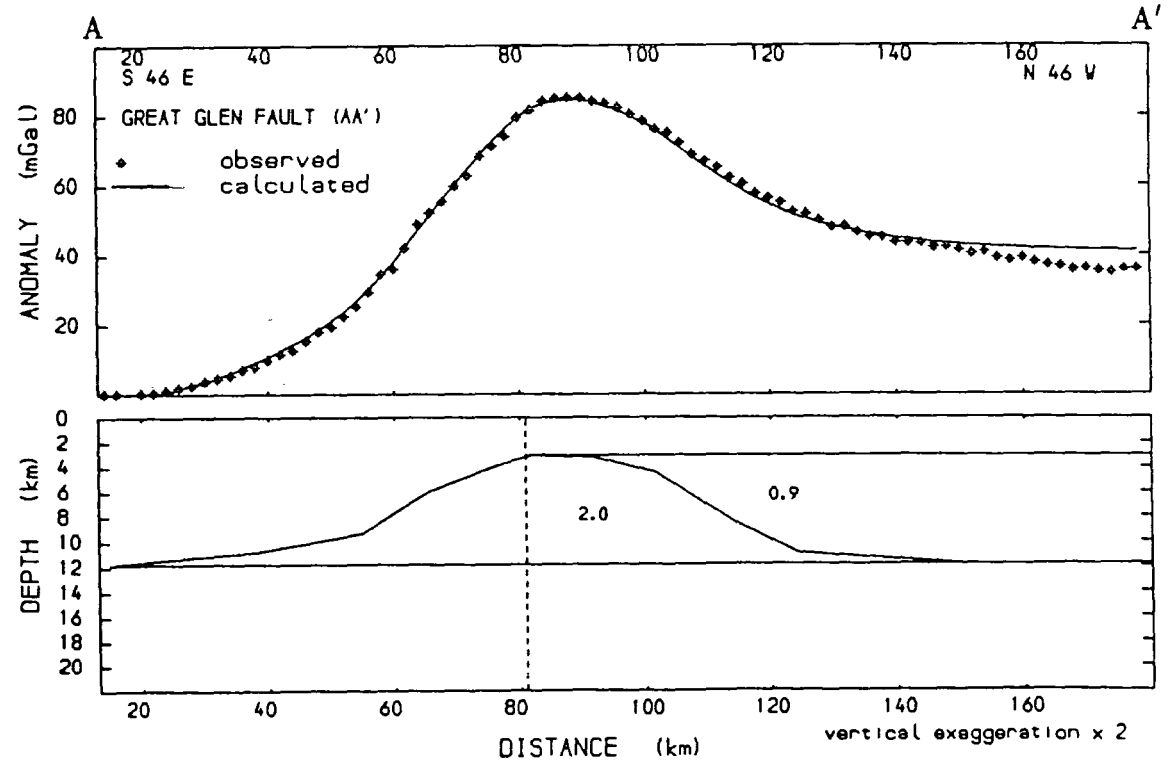

Figure 4.17b Pseudogravimetric modelling along profile AA′ using the two-body model with the top of the Great Glen feature at 3 km and magnetization of 2.0 A/m. The density (kg/m^3) to magnetization (A/m) ratio is 150:1.0.

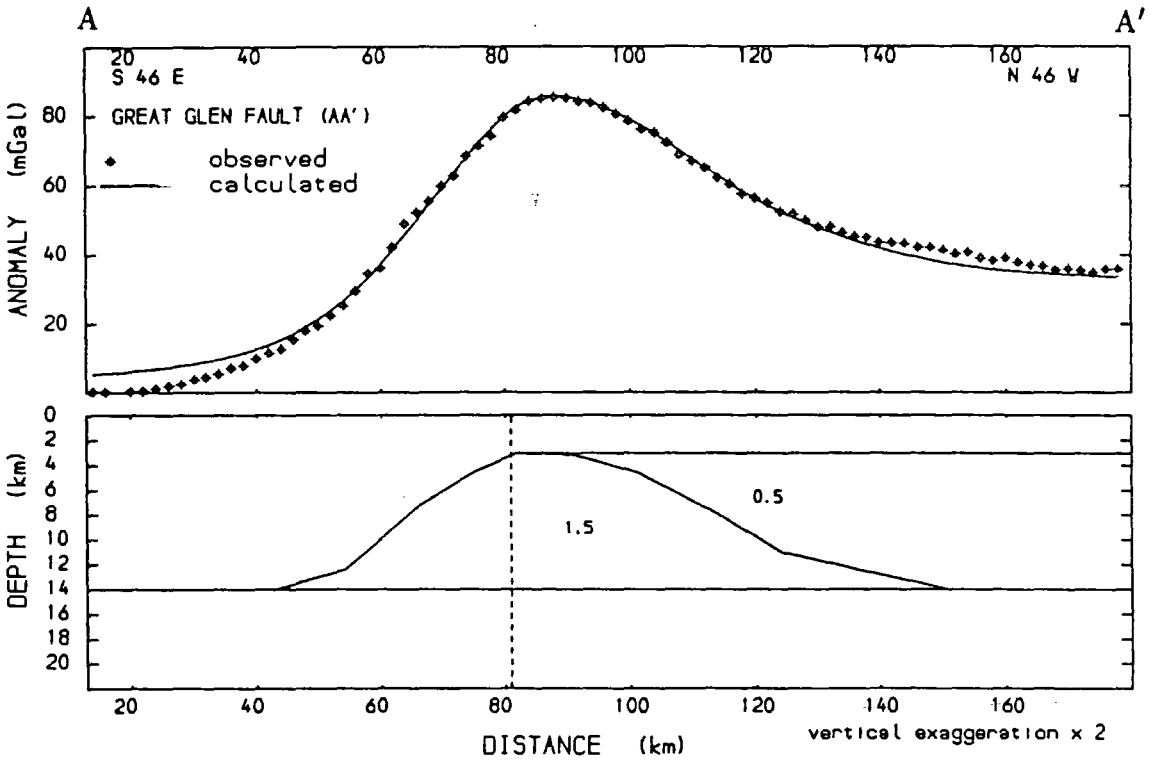

Figure 4.17c Pseudogravimetric modelling along profile AA′ using the two-body model with the top of the Great Glen feature at 3 km and magnetization of 1.5 A/m. The density (kg/m^3) to magnetization (A/m) ratio is 150:1.0.

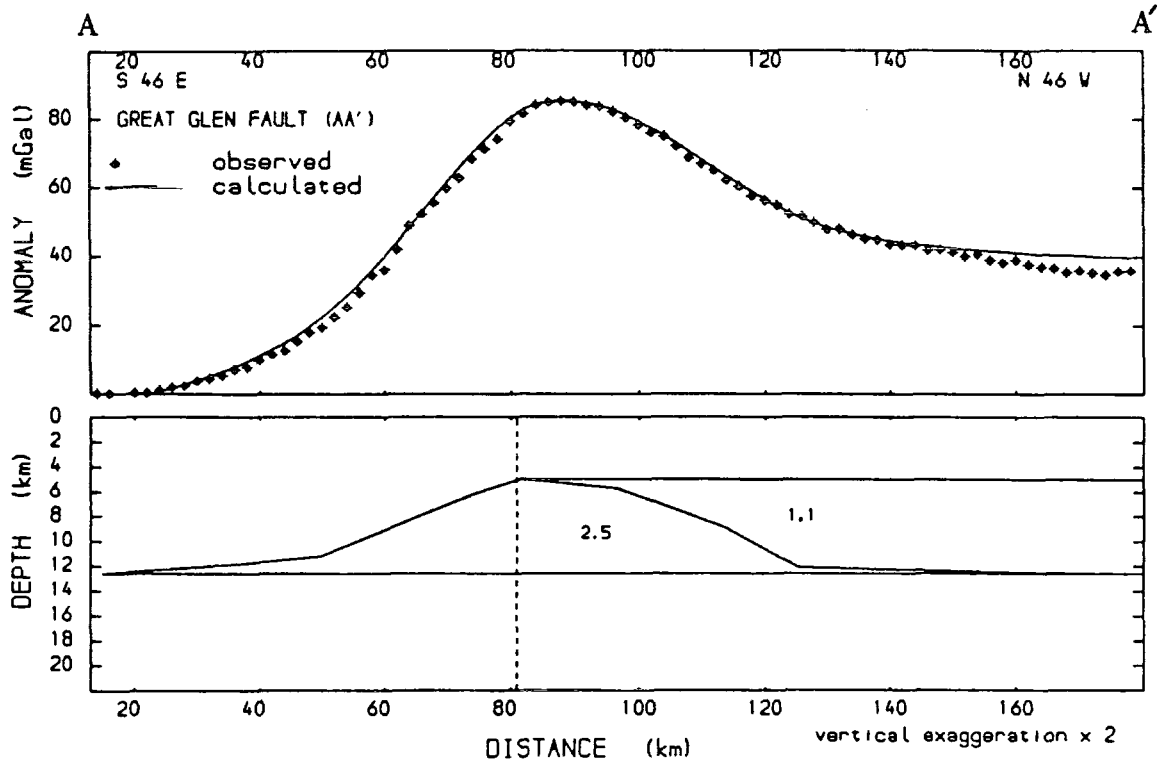

Figure 4.18a Pseudogravimetric modelling along profile AA′ using the two-body model with the top of the outward dipping feature at 5 km and magnetization of 2.5 A/m. The density to magnetization ratio is 150 kg/m^3 : 1 A/m.

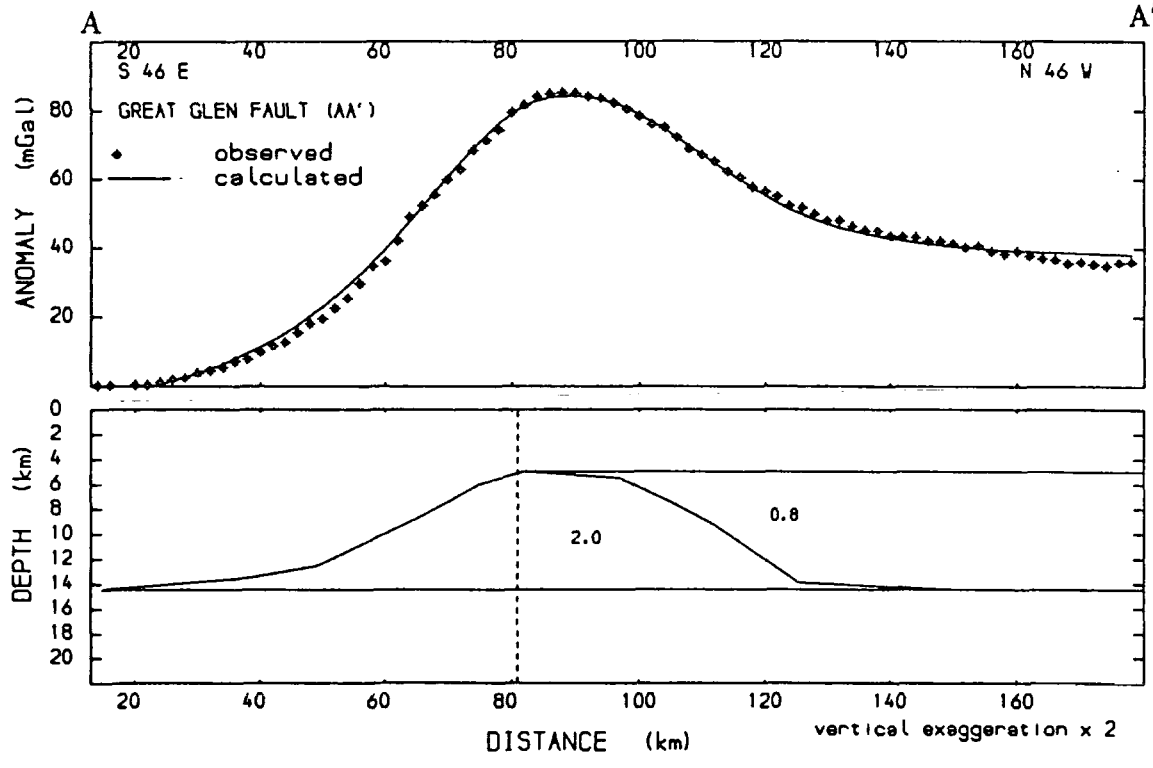

Figure 4.18b Pseudogravimetric modelling along profile AA′ using the two-body model with the top of the Great Glen feature at 5 km and magnetization of 2.0 A/m. The density (kg/m^3) to magnetization (A/m) ratio is 150:1.0.

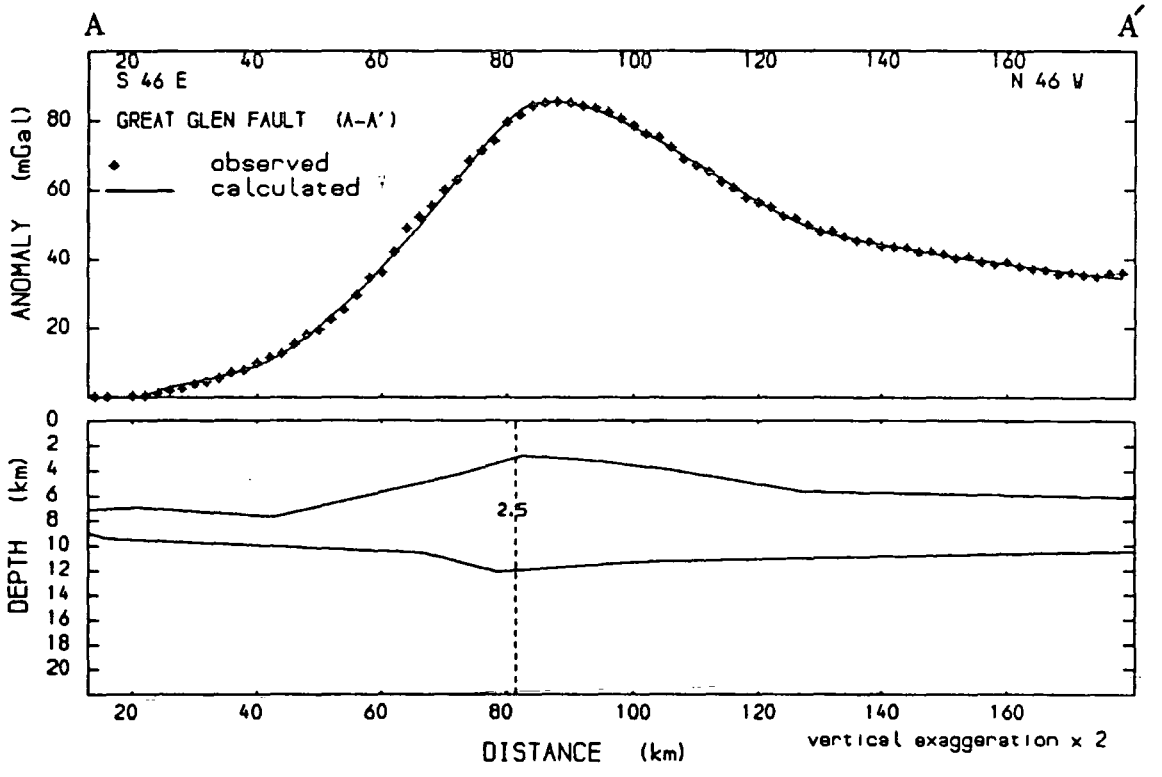

Figure 4.19 Pseudogravimetric modelling along profile AA′ using a lensoid shaped body with the top about 3 km and magnetization of 2.5 A/m. The density (kg/m^3) to magnetization (A/m) ratio is 150:1.0.

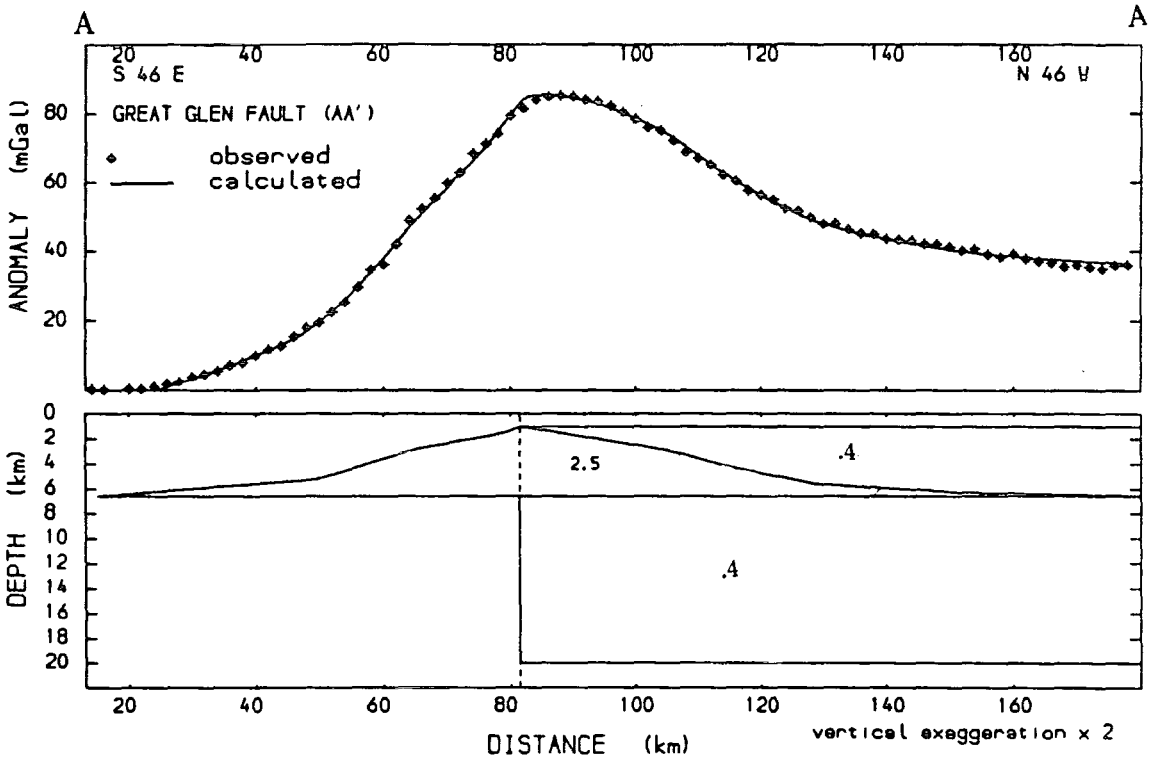

Figure 4.20a Pseudogravimetric modelling along profile AA′ using the two-body model with the top of the Great Glen feature at 1 km and magnetization of 2.5 A/m. The density (kg/m^3) to magnetization (A/m) ratio is 150:1.0.

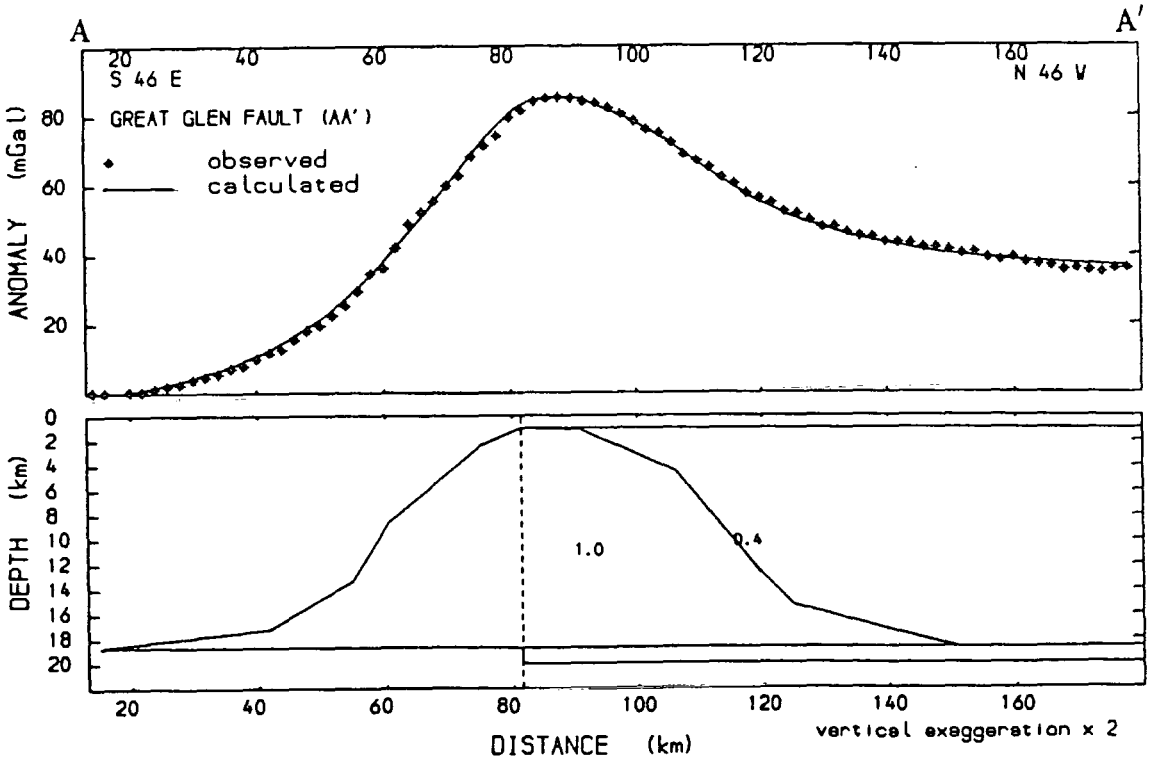

Figure 4.20b Pseudogravimetric modelling along profile AA′ using the two-body model with the top of the Great Glen feature at 1 km and magnetization of 1.0 A/m. The density (kg/m^3) to magnetization (A/m) ratio is 150:1.0.

of 2.5 A/m in figure 4.21 and with top at 5 km and magnetizations of 2.5 and 2.0 A/m in figures 4.22a and 4.22b respectively. The Great Glen feature thus obtained is almost symmetrical and is rather thinner than in the models shown in figures 4.16a and d, 4.17a and 4.18a and b. Some of the models have the symmetry about both the Great Glen fault and the apex (figures 4.21 and 4.22). In figures 4.20, 4.21 and 4.22 the magnetization of the slab remains almost constant irrespective of the depth and magnetization of the Great Glen feature. The 19 km thickness used in the above modelling results in a slab magnetization of about 0.4 A/m.

A more complex model with the magnetization of the Great Glen feature north of the fault superimposed on that of the magnetic slab can also explain the observed anomaly. The models with the top of the Great Glen feature at 1 km and magnetization of the feature southeast of the fault of 2.5 and 1.0 A/m are given in figures 4.23a and 4.23b respectively. The model with the top of the Great Glen feature at 5 km and magnetization of 2.5 A/m is given in figure 2.24. The magnetic slab is assumed to extent from 1 to 20 km depth. As in figures 4.21 and 4.22 the Great Glen feature is also almost symmetrical about both the apex and the fault (figure 4.23). The thickness is only slightly less than that of the two-body model. The magnetization of the magnetic slab is again about 0.4 A/m irrespective of the values of the assumed parameters.

Direct magnetic modelling has also been carried out on the two-body model and the complex model. Examples of the two-body modelling using a Great Glen feature with magnetization of 2.5 A/m, top at 5 and 1 km, and slab thickness of 19 km (from 1 to 20 km depth) are given in figures 4.25 and 4.26. Examples of the Great Glen feature with magnetization of 2.5 A/m and depth to the top of 5 and 1 km superimposed on the slab northwest of the fault extending from 1 km to 20 km are given in figures 4.27 and 4.28. The apex has a slight shift northwestwards relative to the fault. The models with top at 5 km are slightly asymmetrical about the apex (figures 4.25 and 4.27). They are comparatively thicker than those obtained from the

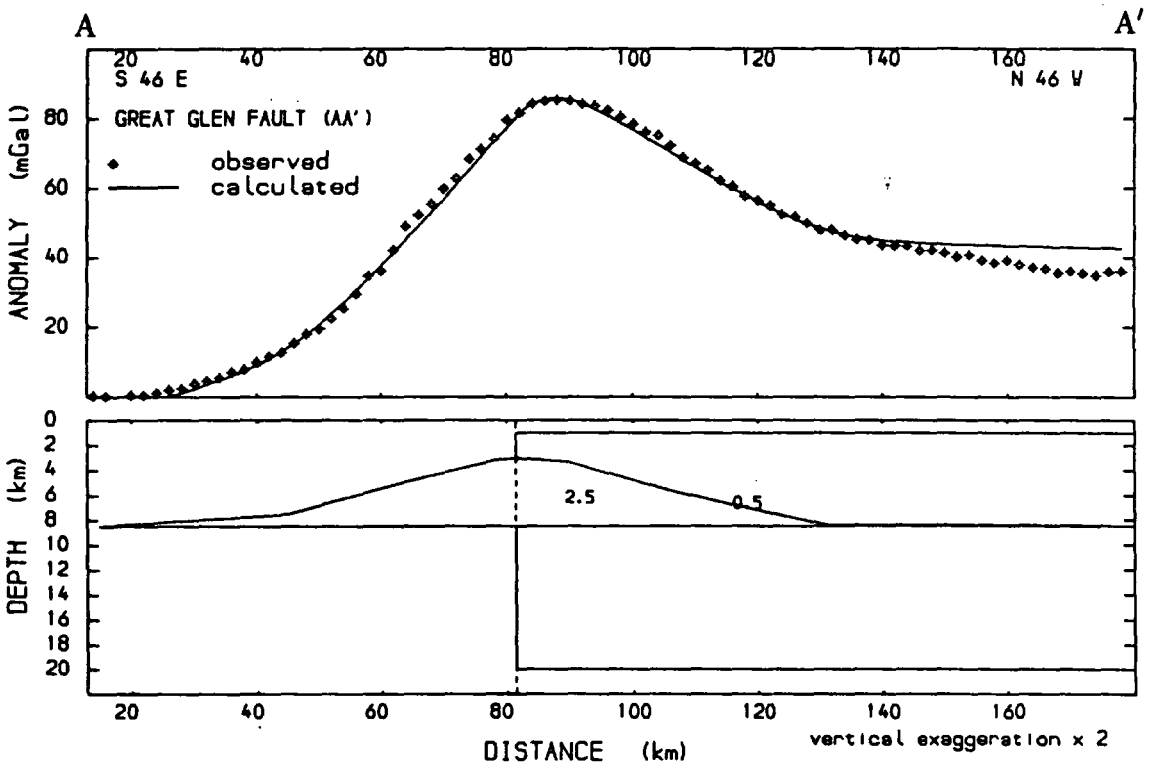

Figure 4.21 Pseudogravimetric modelling along profile AA′ using the two-body model with the top of the Great Glen feature at 3 km and magnetization of 2.5 A/m. The density (kg/m^3) to magnetization (A/m) ratio is 150:1.0.

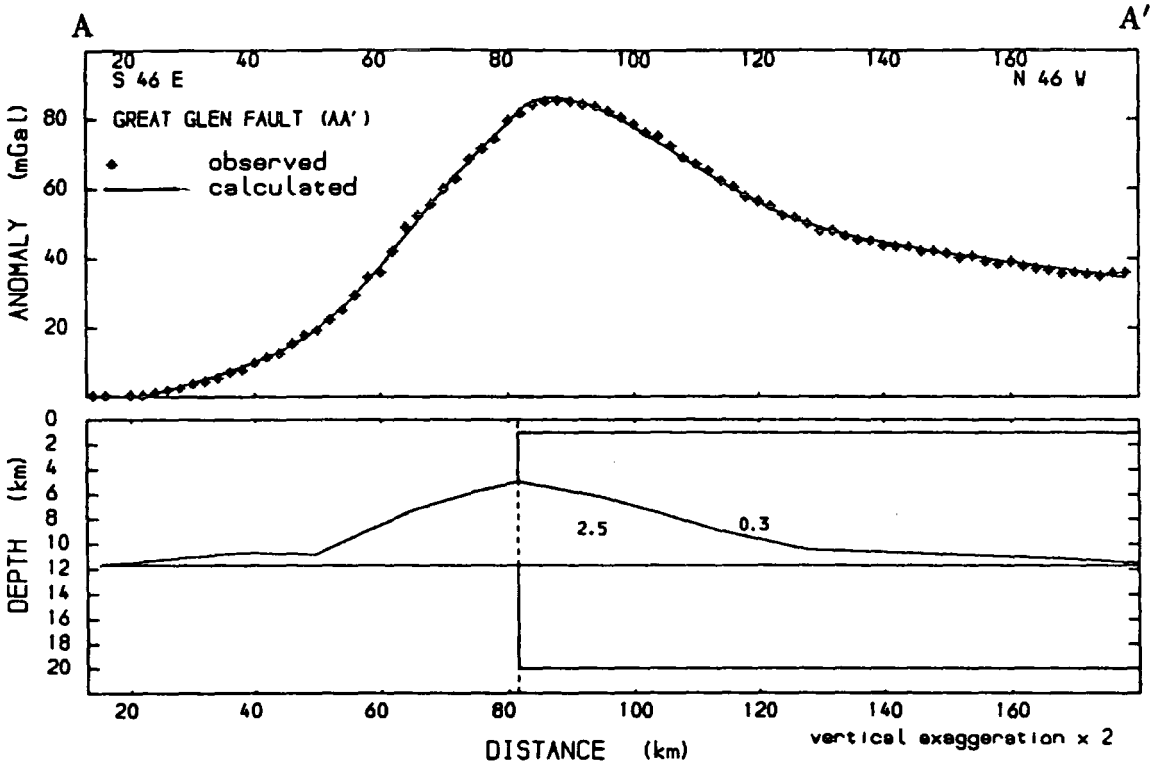

Figure 4.22a Pseudogravimetric modelling along profile AA′ using the two-body model with the top of the Great Glen feature at 5 km and magnetization of 2.5 A/m The density (kg/m^3) to magnetization (A/m) ratio is 150:1.0.

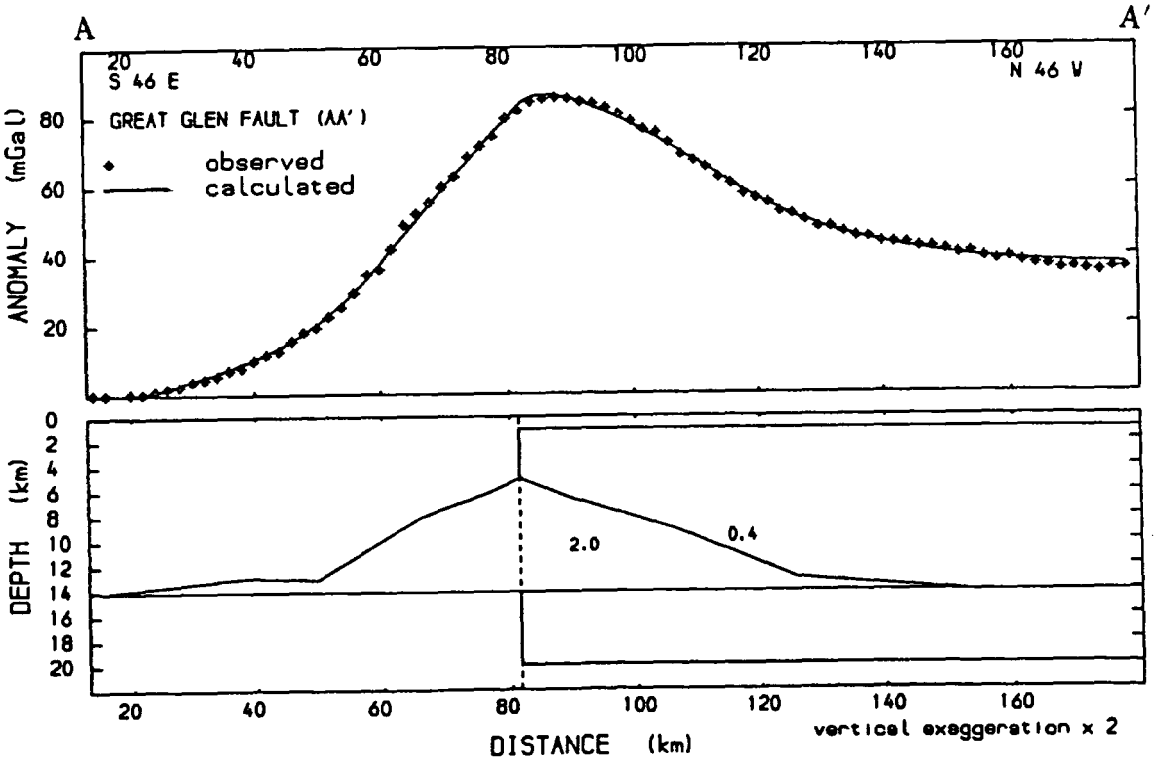

Figure 4.22b Pseudogravimetric modelling along profile AA′ using the two-body model with the top of the Great Glen feature at 5 km and magnetization of 2.0 A/m. The density (kg/m^3) to magnetization (A/m) ratio is 150:1.0.

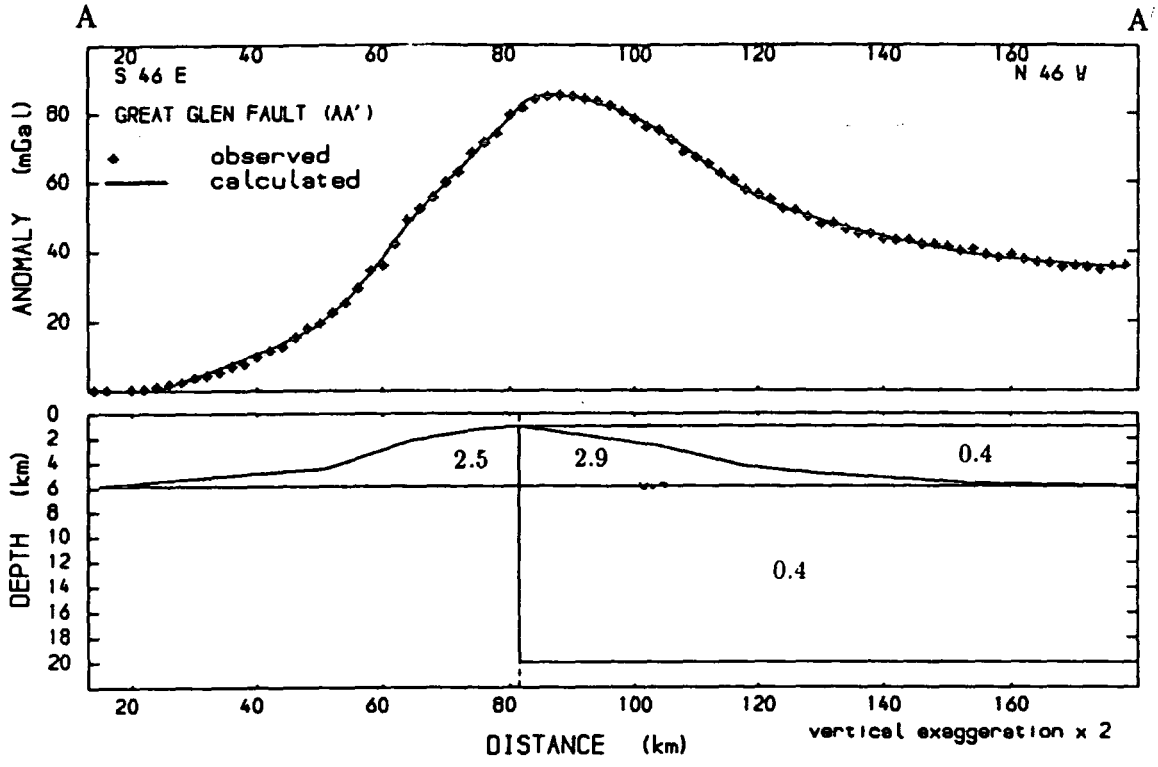

Figure 4.23a Pseudogravimetric modelling along profile AA′ using the three-body model with the top of the Great Glen feature at 1 km and magnetization of 2.5 A/m. The density (kg/m^3) to magnetization (A/m) ratio is 150:1.0.

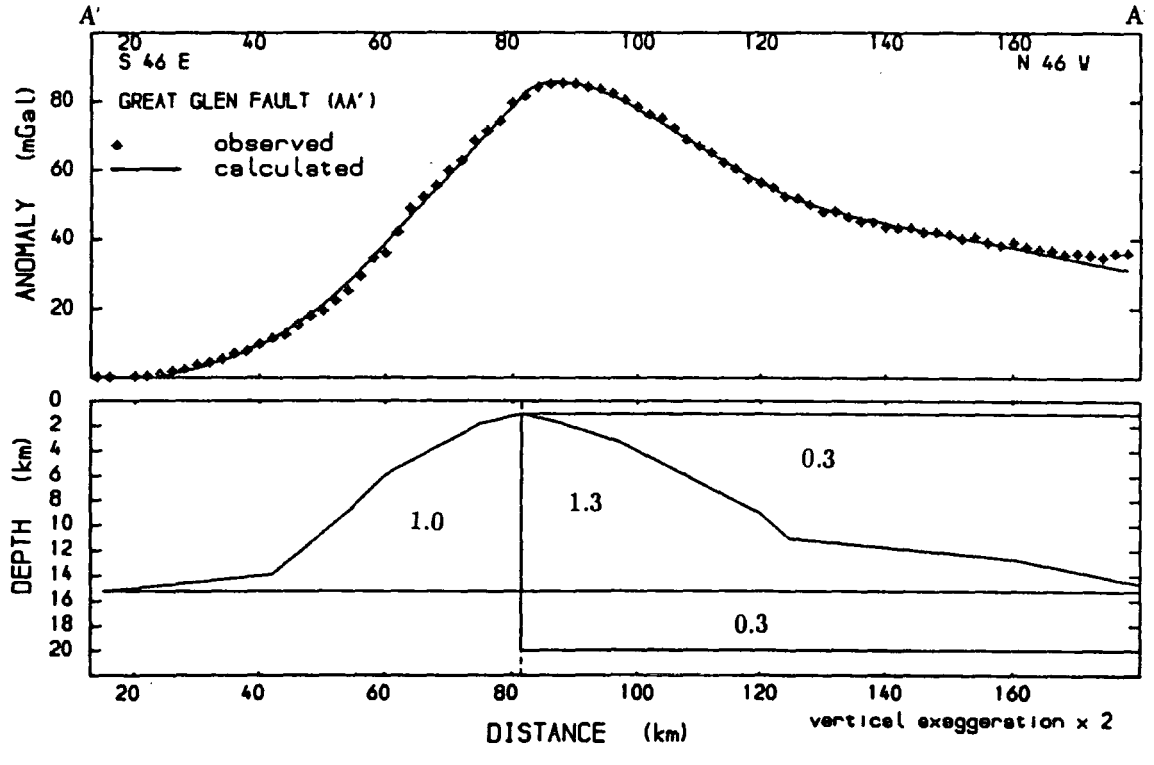

Figure 4.23b Pseudogravimetric modelling along profile AA′ using the three-body model with the top of the Great Glen feature at 1 km and magnetization of 1.0 A/m. The density (kg/m^3) to magnetization (A/m) ratio is 150:1.0.

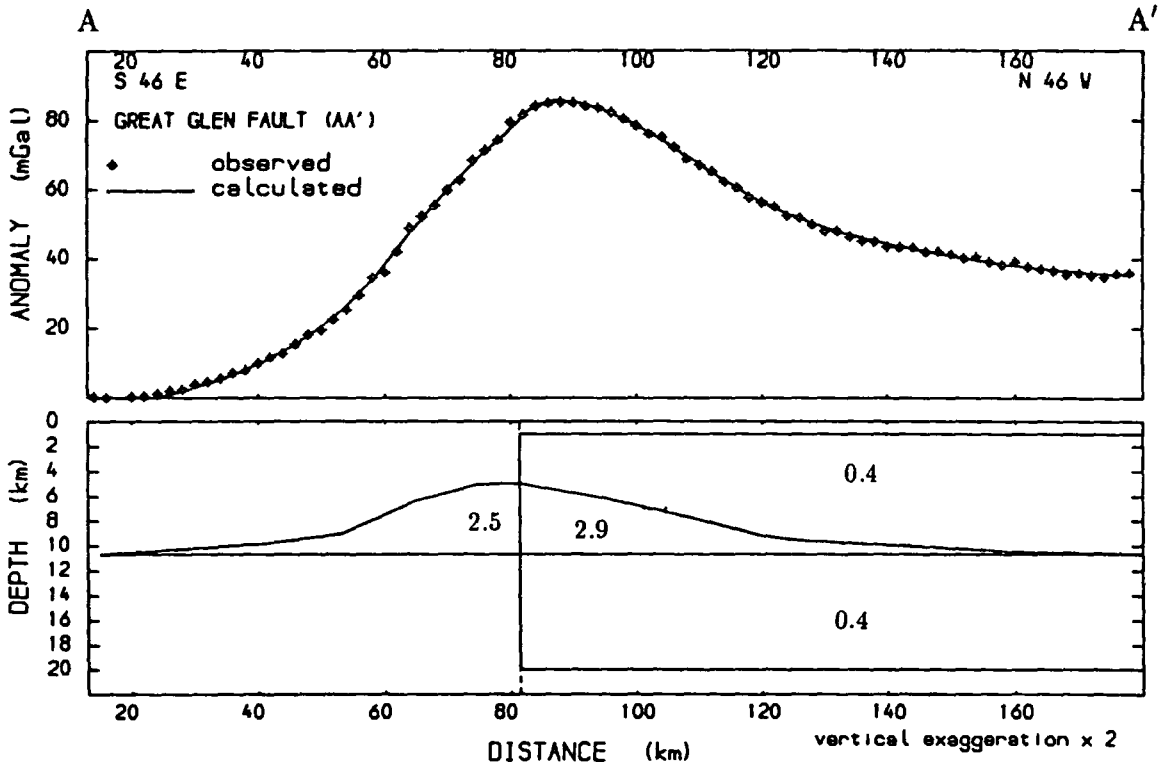

Figure 4.24 Pseudogravimetric modelling along profile AA′ using the three-body model with the top of the Great Glen feature at 5 km and magnetization of 2.5 A/m. The density (kg/m^3) to magnetization (A/m) ratio is 150:1.0.

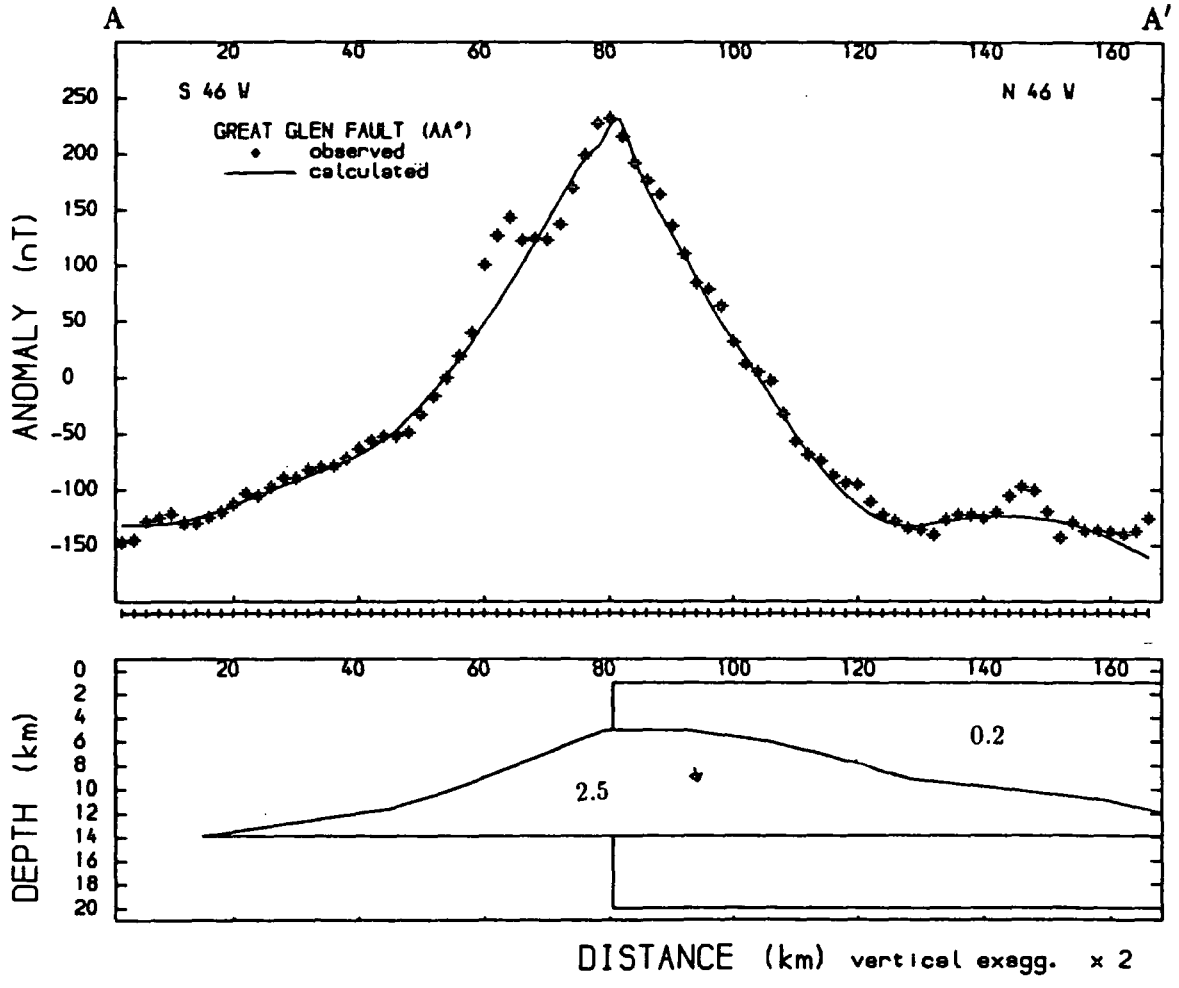

Figure 4.25 Magnetic modelling along AA′ using a two-body model, a local Great Glen feature, and a magnetized slab with a thickness of 19 km (1 to 20 km depth). The magnetization of the Great Glen feature is 2.5 A/m and the top is at 5 km depth. The inclination along the profile is 74° northwestwards.

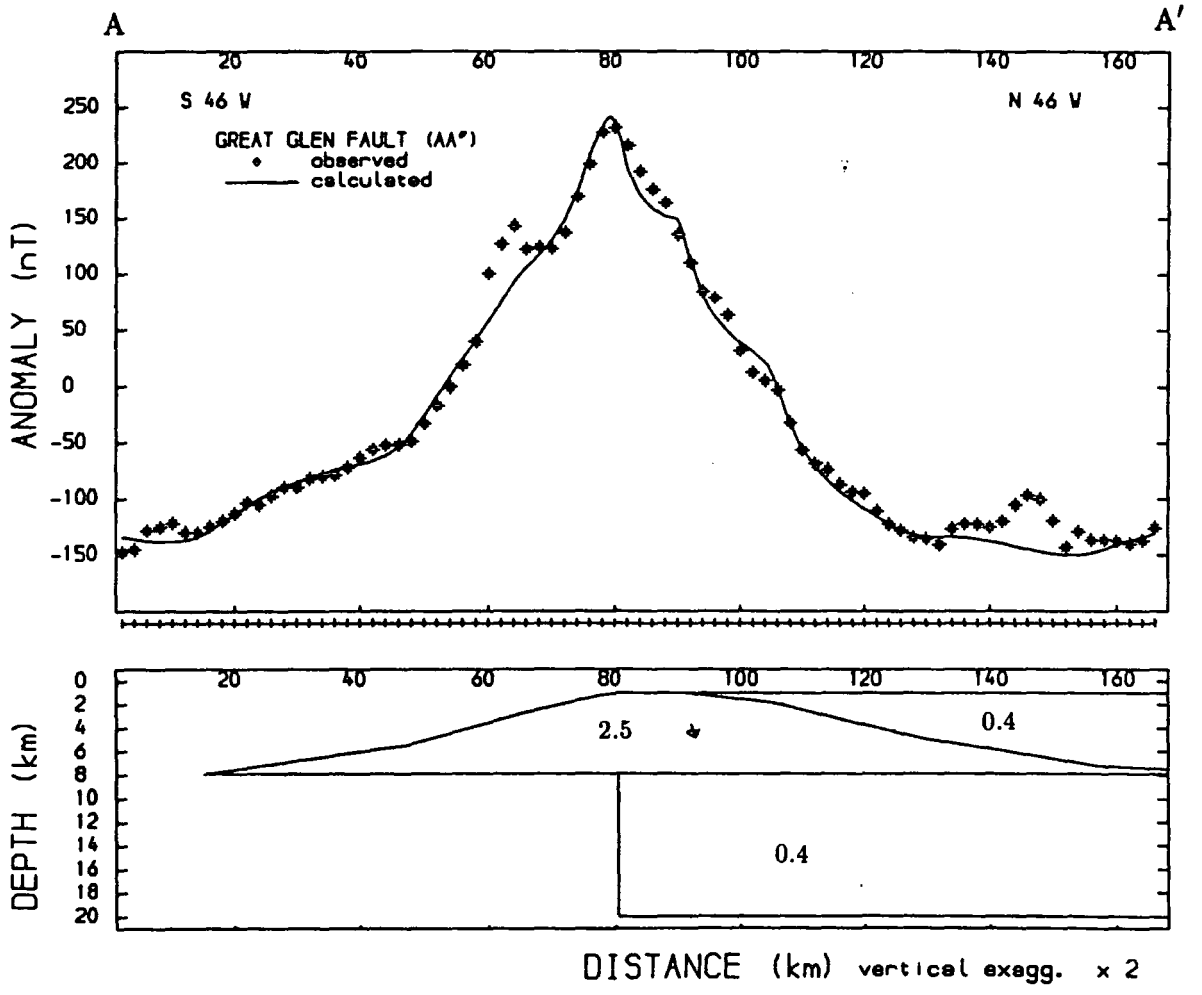

Figure 4.26 Magnetic modelling along AA′ using a two-body model, a local Great Glen feature, and a magnetized slab with a thickness of 19 km (1 to 20 km depth). The magnetization of the Great Glen feature is 2.5 A/m and the top is at 1 km. The inclination along the profile is 74° northwestwards.

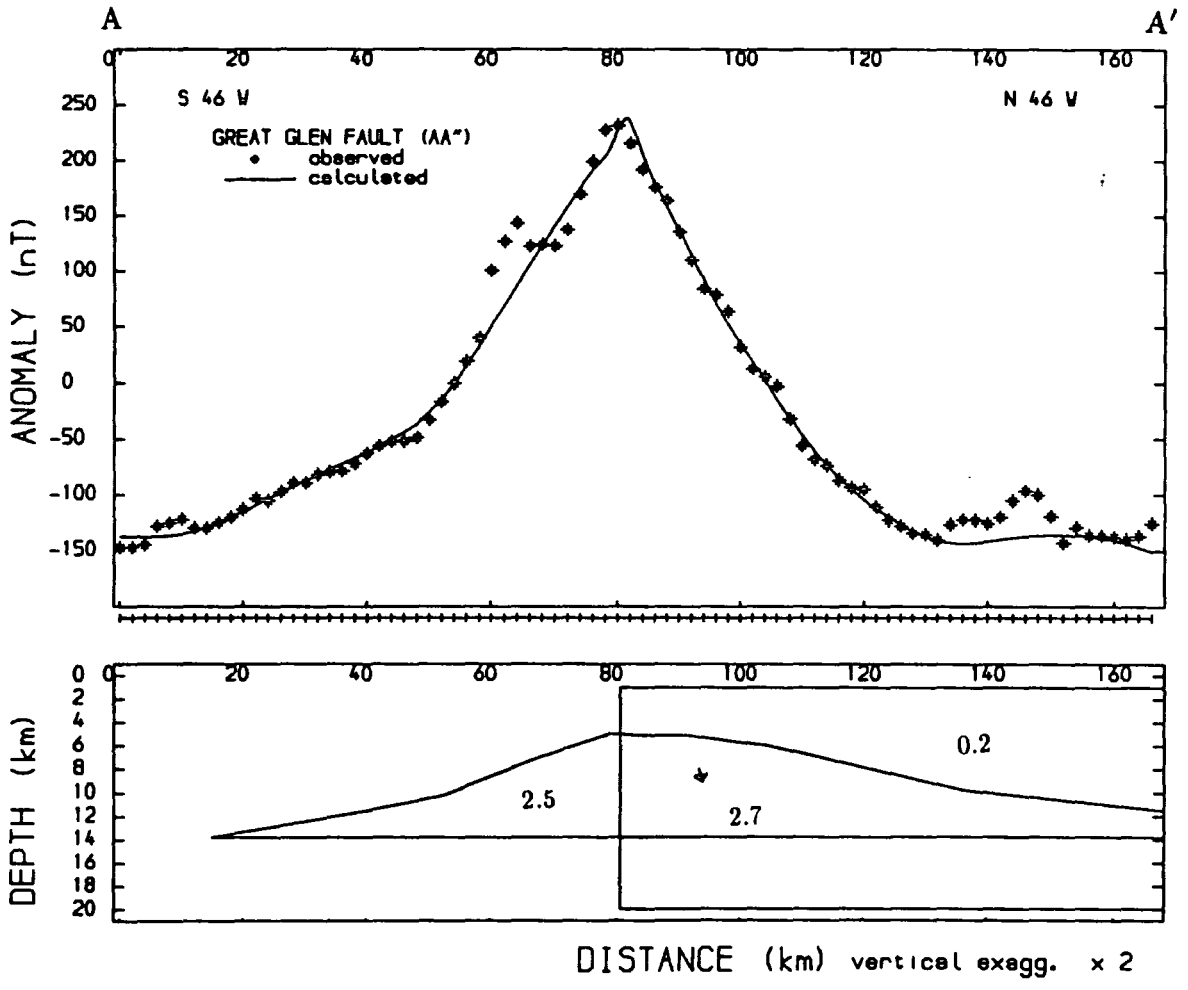

Figure 4.27 Magnetic modelling along AA′ using a three-body model, a Great Glen feature with a magnetization of 2.5 A/m and the top at 5 km, a magnetized slab having a thickness of 19 km (1 to 20 km depth) and the magnetization of the Great Glen feature northwest of the fault superimposed on the magnetization of the magnetized crustal slab. The inclination along the profile is 74^{o} northwestwards.

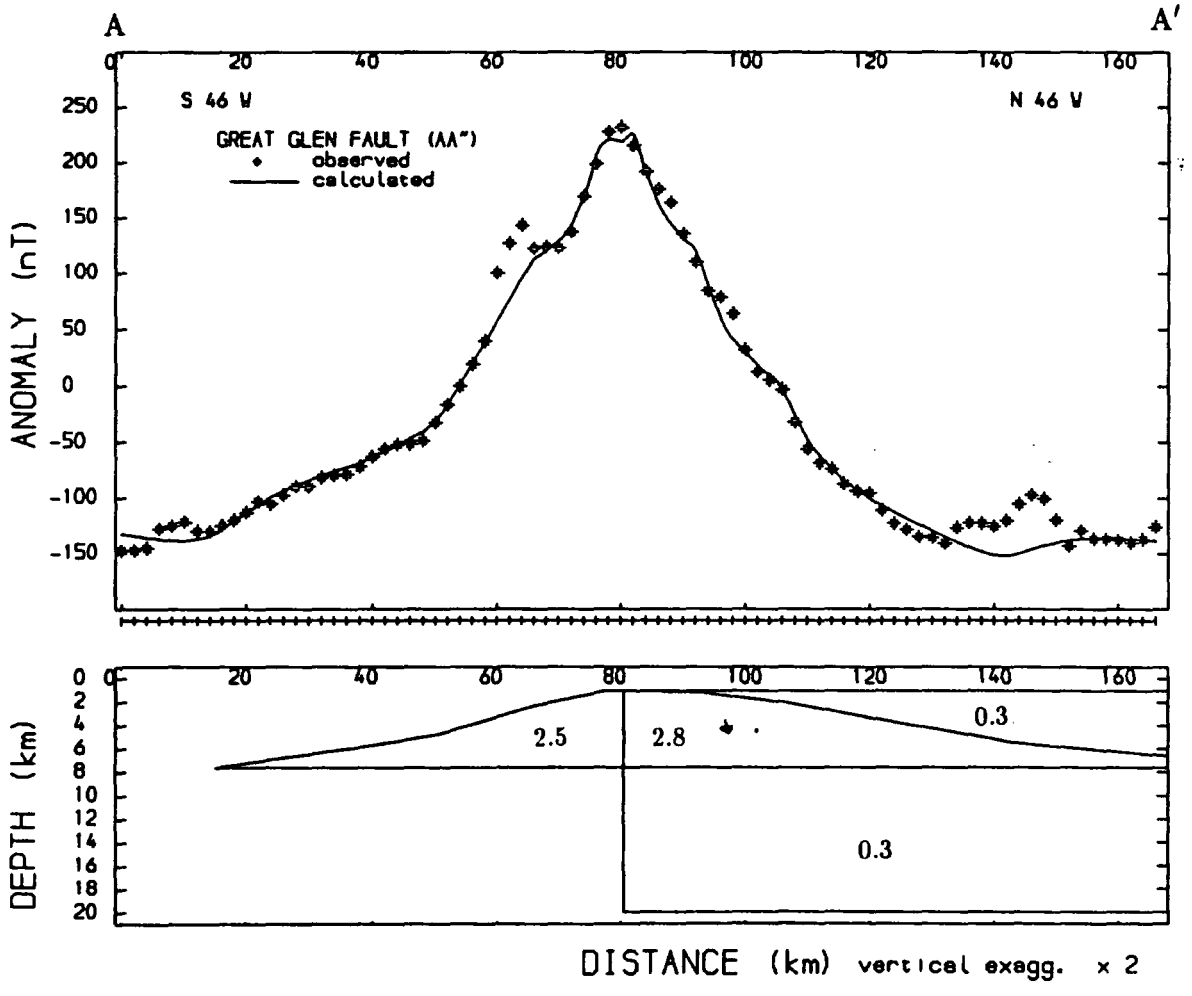

Figure 4.28 Magnetic modelling along AA′ using a three-body model, a Great Glen feature with a magnetization of 2.5 A/m and the top at 1 km, a magnetized slab having a thickness of 19 km (1 to 20 km depth) and the magnetization of the Great Glen feature northwest of the fault superimposed on the magnetization of the magnetized crustal slab. The inclination along the profile is 74^o northwestwards.

pseudogravimetric modelling (figures 4.22a and 4.24). The models obtained with top at 1 km is almost symmetrical about the apex (figures 4.26 and 4.28). The thickness is only slightly greater than obtained from pseudogravimetric modelling (figures 4.20a and 4.23a). The magnetization of the slab ranges between 0.2 to 0.4 A/m.

This section has shown a range of models which can account for the major features of the Great Glen anomaly. The most realistic models include a nearly symmetrical outward dipping feature with high magnetization and apex near the fault and a magnetized slab northwest of the fault.

4.8 Geological interpretation of the Great Glen fault magnetic anomaly

The Great Glen magnetic anomaly traversing mainland Scotland has an apex which correlates closely with the line of the Great Glen fault. The pseudogravimetric transformation which emphasizes the longer wavelength anomaly components results in an anomaly which shows similar close correlation but with an apex lying slightly northwestwards of the line of the Great Glen fault. The close association suggests that the anomaly and the fault are related to each other. The magnetic profile along AA′ (figure 4.2) which is relatively free of the effect of the neighbouring and shorter wavelength anomalies is almost symmetrical about the fault. The pseudogravimetric profile along the same line has a slight asymmetry about the apex with a steeper slope to the southeast than the northwest. It shows the background value is of a higher magnitude northwest of the fault. This high amplitude (about 350 nT) and large width (half-width of 60-65 km) magnetic anomaly must be essentially due to a major feature within the crust beneath the Great Glen fault and extending on both side of it.

A single-body outward dipping feature of strong magnetization within the crust can be used to explain the Great Glen anomaly. The model which has an apex slightly

northwest of the fault and passes into a semi-infinite slab (figure 4.15) is probably not the most realistic model to explain the Great Glen anomaly with its local high over the fault and higher background value northwest of the fault. A more realistic model is as follows. The local anomaly high is caused by a strongly magnetized outward dipping feature (the Great Glen feature) approximately symmetrical about the apex and about the fault (figures 4.21, 4.22 and 4.23). This is superimposed on the higher background level to the northwest which is best interpreted in terms of a magnetized crustal slab to the northwest of the fault. The Great Glen feature has a higher magnetization (1.0 to 2.5 A/m) than the slab (about 0.4 A/m). The base of the feature is modelled as mainly horizontal for simplicity. A slab feature which gives a magnetization contrast across the Great Glen fault has been earlier used by Bott and Browitt (1975) to interprete the difference in the magnetic anomaly value across the Great Glen fault between Orkney and Shetland Islands. The two-body model, comprising of the magnetized Great Glen feature and the slab can thus explain the local anomaly high and the higher background value northwest of the fault more realistically. The Great Glen anomaly, therefore, cannot be attributed to a sloping step feature as modelled by Hall and Dagley (1970). The presence of the magnetic slab northwest of the fault is probably a result of the transcurrent movements of the Great Glen fault bringing alongside rocks of different magnetic properties. The origin of the Great Glen feature is described below.

The estimation of the maximum depth to the top of the Great Glen feature initially used Smith's (1959b) second derivative method on the magnetic anomaly. Magnetic modelling to determine the depth to the top, specifically at the sharp apex of the magnetic anomaly using the single-body model has also been carried out. The Smith method gives a maximum depth of less than 7 km along BB$'$ and the modelling gives a depth of less than 5.5 km along AA$'$. This differs from the interpretation of Powell (1978a). Powell modelled the Great Glen feature as within the mid-crustal layer of the LISPB profile with its top at least at 10 km depth beneath the Great Glen fault. The actual top has been shown to lie at least partly within the upper crust. The Great

Glen feature, however, cannot be directly associated with the outcropping granitic intrusions and their aureoles even though some of the short to medium wavelength magnetic anomalies along the Great Glen fault are closely associated with some of these intrusives. This is because the igneous intrusions and their associated contact metamorphic rocks occur as isolated masses and do not resemble the modelled shape. Furthermore, the observed magnetization of the granites is much less than the minimum possible magnetization (0.8 A/m) determined from the modelling.

The estimated magnetization of the Great Glen feature of greater than about 0.8 A/m is within the measured magnetization of the pyroxene granulites of the Lewisian (tables 4.2). To the northwest of the Great Glen fault, along the northwestern coast of mainland Scotland, some of the longer wavelength magnetic anomalies have been associated with those of the high density and strongly magnetized Scourian assemblage of the Lewisian (Bott et al. 1972). The similarity of the magnetization here suggests that similar rocks might possibly make up the Great Glen feature that underlies the outcropping weakly magnetized Moines. The Moines and the granulitic rocks are, however, of different densities. According to Hipkin and Hussain (1983), the Moines have a measured density of about 2738 kg/m^3 while the pyroxene granulites have densities of about 2879 kg/m^3. If the Great Glen feature is caused by the shallowing of Lewisian pyroxene granulites underlying the weakly magnetized and less dense Moines, then the density contrast would produce a linear positive gravity anomaly of at least +40 mGal amplitude. But such an anomaly is not observed on the gravity map (Hussain and Hipkin 1981). This indicates that simple shallowing of the Lewisian granulites along the fault line is unlikely to be the cause of the Great Glen feature.

One of the ways in which magnetic minerals can form is by breakdown of some of the metamorphic minerals in amphibolite and greenschist facies rocks on progressive heating (Turner 1968, Murrell 1985). A linear heat source along the line of the fault would be required to produce a symmetrical linear magnetized region. Movements

along transcurrent faults such as the Great Glen fault may produce frictional heating as discussed below.

As mentioned earlier, a close correlation of the apex of the models with the line of the Great Glen fault across mainland Scotland is clear. This suggests that the formation was probably closely related to the activity of the fault. The transcurrent movement may have generated the required frictional heat energy. Such heat energy would be conducted outwards on both sides of the fault to form a symmetrical heated region with outward dipping sides. Breakdown of the metamorphic minerals to form the magnetite may have occurred in this region. This magnetized enriched region would be defined by the temperature isotherm at which breakdown occurs. The possible conditions where magnetite can be formed due to progressive heating are described below. Alternatively the magnetic minerals may have been produced the ductile shear zone or by fluid flow associated with the fault but these ideas are difficult to test.

The greenschist facies, although weakly magnetised, has Fe^{3+} ions which are tied up in the chlorites. In the amphibolite facies, magnetite is common but the potentially magnetic Fe^{3+} and Ti may be mainly tied up in the hornblende, biotite and garnet (Mayhew et al. 1985, Ramberg 1948). The metamorphic biotites and chlorites such as those in the Moines and Lewisian may thus break down to produce magnetite when progressively heated. With suitable partial pressure of oxygen, the break down of these metamorphic biotites to magnetite may occur at temperatures greater than 500°C (Turner 1968), and the decomposition of chlorites may be initiated at a temperature of 520°C (Murrell 1985). Further heating may cause granulitization of amphibolites which can results in the release of Fe as discrete oxide grains. Engles and Engles (1962) indicated that the transition from amphibolites to granulites occurs over a temperature range of 600 – 625°C whereas Buddington and Lindsley (1964) gave a temperature range of 560 – 625°C. Others have indicated a transition temperature of about 700°C (Frost and Frost 1987). The Great Glen feature may thus be related to the formation of magnetite due to the progressive heating and

granulitization, probably of the Moines, if the transcurrent movement of the Great Glen fault produced sufficient frictional heat.

The summary of the suggested mode of formation of the Great Glen feature is as follows. The temperature and pressure conditions in normal continental crust and the relation to type of deformation and style of metamorphism can be generalised as was done by Sibson (1983, figure 4.29). Under normal conditions the greenschist facies occur at a depth of about 14-15 km at a temperature of about 350°C. At deeper levels (greater than 20 km) the amphibolites develop. Assuming such normal conditions under the Great Glen fault at the start of the heat generating movement, a temperature increase of about 200°C is necessary to attain the break down temperature (about 520°C) of chlorites and biotites present in the greenschist and amphibolite zone. The heat generated along the Great Glen fault was conducted away from the fault and the progressive heating would produce the strongly magnetized outward dipping region. This is approximately defined by the 520°C temperature isotherm. During the transcurrent movements blocks of different magnetizations were moved alongside and are now adjacent to each other. This results in the present magnetization contrast across the fault. Calculation of the temperature rise in the crust due to the fault movement is discussed in the following section.

4.9 Thermal modelling

4.9.1 Heat generation along transcurrent fault

Sibson (1983) indicated that the displacement of a transcurrent fault zone occurs by brittle fracturing at shallow depth passing downwards into a quasi-plastic shear zone (ductile zone, figure 4.29). The transcurrent movements result in mechanical work done on the rock during deformation (Wintsch 1985) causing the generation of heat (Scholz et al. 1979, Pavlis 1986). The heat may be produced by frictional

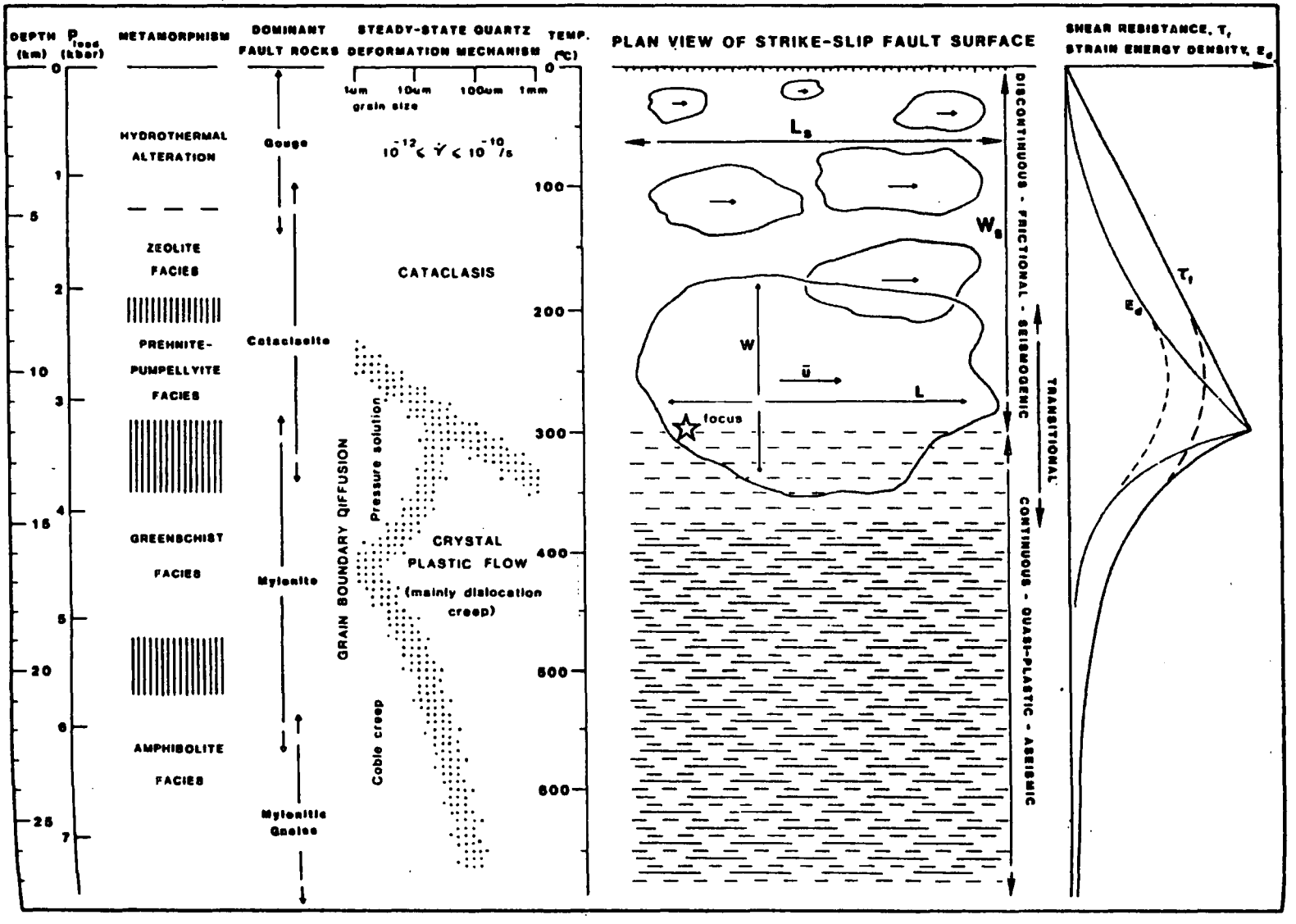

Figure 4.29 The generalized variation with depth of the different parameters such as temperature, pressure, deformation and metamorphism in the crust (Sibson 1983)

heating at a shallow level (Scholz et al. 1979) or by plastic deformation in the ductile shear zone (Nicolas et al. 1977). In narrow fault zones where the strain rate and displacement are large, the temperature rise may be large (as much as 1000^o C) and frictional melting may occur (McKenzie and Brune 1972, Cardwell et al. 1978, Passchier 1982). In the ductile zone, the temperature rise may be smaller (Wintsch 1985). The temperature increases may be buffered by partial melting of the rocks in the axial zone. The generation of heat results in anomalous temperature in the fault zone and this causes the heat to be carried away by conduction on both sides of the fault. Metamorphic isograds on each side of the fault should correspond to the maximum temperature attained by the heat generated (Nicolas et al. 1977). Similarly the temperature isograd where the biotite or chlorite may break down to produce magnetite or granulites to occur may be a function of the heat conducted away from the fault.

The heat Q'' generated per unit area per unit time on the fault is

$$Q'' = \nu\tau \qquad 4.1a$$

where ν is the relative velocity across the fault surface and τ is the shear stress on the fault. The shear stress is affected by the different deformational behaviour of the crustal rocks. In the upper crust, the deformation involves cataclasis and frictional sliding (Sibson 1983). The magnitude of the shear stress in the upper crust is affected by the coefficient of friction f and the normal stress σ_n on the fault ($\tau = f\sigma_n$). The source of the normal stress is mainly lithostatic pressure ($\rho_c g z$, where ρ_c is the crustal density, g is the gravitational attraction and z is the depth). However, pore fluid pressure can reduce the effective normal stress. Where the pores are not connected, pore fluid pressure may be large, but in dry condition or in the presence of fracturing normally associated with major faulting the pore fluid pressure is small (Turcotte et al. 1980). The effect of tectonic pressure is generally small. The shear stress at any depth z during faulting is given by

$$\tau_z = f_e \rho_c g z \qquad 4.1b$$

where f_e is the effective coefficient of friction. A linear relationship between shear stress and depth thus probably exist within the brittle upper crust on the fault plane.

In the ductile or plastic zone the movement is by creep and is temperature dependent. The magnitude of shear stress on the fault plane can be assumed to take the form (Turcotte et al. 1980)

$$\tau_z = \tau_m e^{(1-(z/D_b)^n)} \qquad 4.1c$$

where D_b is the thickness of the brittle zone, τ_m is the value of shear stress given by equation 4.1b when $z = D_b$ and n is the value which determines the rate of decrease of T_m with depth. The depth D_b of the brittle/ductile transition zone is determined by the response of quartz to stress with increase in temperature. The plasticity becomes dominant at a temperature of about 300-350^{o}C (figure 4.29) corresponding to the start of the greenschist facies metamorphic condition (Sibson 1983). In the mantle, viscous flow predominates and the shear stress can be assumed to be small. Knowledge of the shear stress and the relative rate of movement across the fault enable calculation of the heat generation along the fault. The subsequent temperature rise and the distribution away from the fault can then be determined. The finite difference method used for these purposes is discussed below.

4.9.2 Finite difference procedure

In the presence of heat generation along a transcurrent fault, the temperature T satisfies (Lachenbruch 1980)

$$\frac{1}{\alpha}\frac{\partial T}{\partial t} = \nabla^2 T + \frac{Q'''}{K} - E_u \qquad 4.2$$

where t is the time, α is the thermal diffusivity of the solid where $\alpha = K/\rho c$ (K is thermal conductivity, ρ is the density and c is the specific heat) and Q''' is heat generated per unit volume per unit time. The terms in equation 4.2 represents the rate of heat increase, the heat conduction, heat generation and heat convection (E_u). The con-

vective effect is negligible even for a temperature rise to about 1000°C (Lachenbruch 1980), so equation 4.2 reduces to the heat conduction equation with $E_u = 0$.

The analysis of the multi-dimensional time-dependent heat conduction problem using analytical methods is difficult, particularly with complicated boundary conditions. The finite difference procedure is one of the numerical methods which can be used to deal with such a problem more easily. The basis of the method is first discussed and this is followed by its application to the present problem.

Assume a section xz (figure 4.30, the fault is in the y plane at x=0) with heat generation at the fault plane. The two-dimensional time-dependent heat conduction equation is

$$\frac{1}{\alpha}\frac{\partial T}{\partial t} = \frac{\partial^2 T}{\partial x^2} + \frac{\partial^2 T}{\partial z^2} + \frac{Q'''}{K} \qquad 4.3$$

The problem is to determine the temperature at the fault plane and the corresponding temperature distribution away from the fault plane for any time $t > 0$ for a given initial and boundary condition.

One method of evaluating the differential equation 4.3 is by approximation of the derivatives using Taylor series. The Taylor series expansion of the functions $f(x+h)$ and $f(x-h)$ are

$$f(x+h) = f(x) + hf'(x) + \frac{h^2}{2!}f''(x) + \frac{h^3}{3!}f'''(x) + ..$$

and

$$f(x-h) = f(x) - hf'(x) + \frac{h^2}{2!}f''(x) - \frac{h^3}{3!}f'''(x) + ..$$

From these relations the first derivatives of the function $f(x)$ can be approximated by

$$f'(x) = \frac{f(x+h) - f(x)}{h} \qquad \text{forward difference,}$$

$$f'(x) = \frac{f(x) - f(x+h)}{h} \qquad \text{backward difference,}$$

or

$$f'(x) = \frac{f(x+h) - f(x-h)}{2h} \qquad \text{central difference.}$$

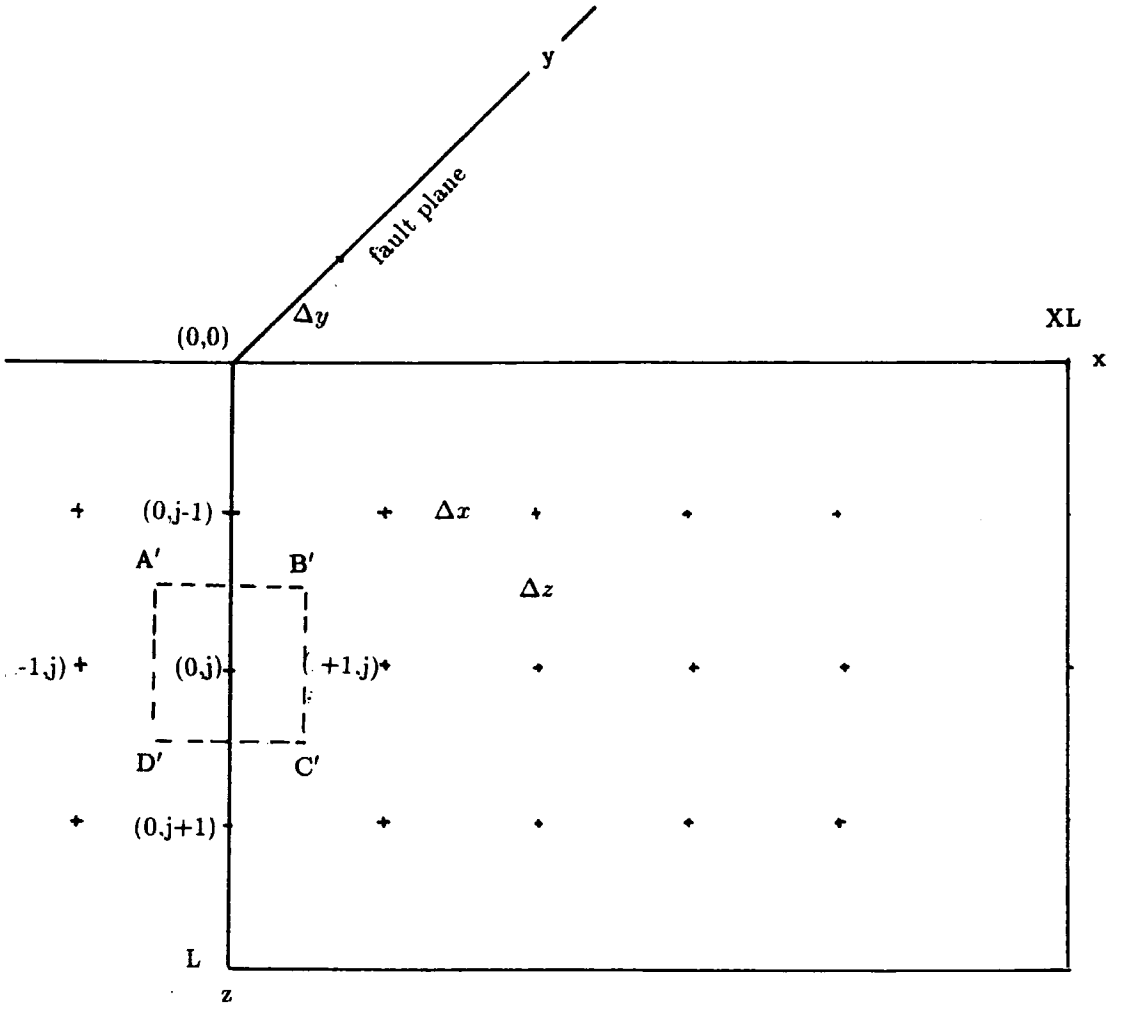

Figure 4.30 Depth section and grid points used in the finite difference procedure.

The second derivative can also be written in the different forms, but only the central difference form is shown here as

$$f''(x) = \frac{f(x-h) - f(x) - f(x) + f(x+h)}{h^2}$$

In a two dimensional system with temperatures known at the grid points (figure 4.30) the second derivatives in the x and z directions can be written as

$$\frac{\partial^2 T(i,j)}{\partial x^2} = \frac{T(i-1,j) - T(i,j) - T(i,j) + T(i+1,j)}{(\Delta x)^2} \qquad 4.4a$$

$$\frac{\partial^2 T(i,j)}{\partial z^2} = \frac{T(i,j-1) - T(i,j) - T(i,j) + T(i,j+1)}{(\Delta z)^2} \qquad 4.4b$$

where Δx and Δz are the sample spacing. The forward difference time derivative can be written as

$$\frac{\partial T(i,j)}{\partial t} = \frac{T(i,j)^{k+1} - T(i,j)^k}{\Delta t} \qquad 4.5$$

where Δt is the time increment, $T(i,j)^k$ and $T(i,j)^{k+1}$ are the temperatures at time t and $t + \Delta t$ respectively.

The derivatives can be evaluated separately and substituted in the differential equation 4.3. The calculations can be started at time $t = 0$ when the initial conditions are known. The calculations give the temperatures $T(i,j)^{k+1}$ at time $t + \Delta t$ from the values $T(i,j)^k$ at time t. These then can be used as the initial temperature to determine the temperature at the next time increment.

There are a number of finite difference procedures for solving the time-dependent differential relation in equation 4.3. The explicit method is direct and simple. The time difference Δt, however, must be small else instability will be introduced. The implicit method removes this restriction but requires more calculation. Modification can be made to both methods to improve the stability and the truncation of errors. Modified methods based on implicit and implicit-explicit procedures may give better results. However, they generally involve solving simultaneous equations which restrict the efficiency of the method when dealing with time function multi-dimensional

problems. The explicit method is prefered due to its simplicity. The simplest explicit representation obtained by substituting equation 4.4 and 4.5 into equation 4.3 is

$$\frac{T(i,j)^{k+1} - T(i,j)^k}{\alpha \Delta t} = \frac{T(i+1,j)^k - T(i,j)^k - T(i,j)^k + T(i-1,j)^k}{(\Delta x)^2}$$

$$+\frac{T(i,j+1)^k - T(i,j)^k - T(i,j)^k + T(i,j-1)^k}{(\Delta z)^2} + \frac{Q'''}{K.} \qquad 4.6$$

Barakat and Clark's (1966) modified procedure, based only on the explicit procedure, improves the solution. It is unconditionally stable and is reported to have better or comparable accuracy to the implicit method and has the directness of the fully explicit method. This procedure has been used. The method assumes two multilevel finite-difference representations for equation 4.3

$$\frac{u(i,j)^{k+1} - u(i,j)^k}{\alpha \Delta t} = \frac{u(i+1,j)^k - u(i,j)^k - u(i,j)^{k+1} + u(i-1,j)^{k+1}}{(\Delta x)^2}$$

$$+\frac{u(i,j+1)^k - u(i,j)^k - u(i,j)^{k+1} + u(i,j-1)^{k+1}}{(\Delta z)^2} + \frac{Q'''}{K} \qquad 4.7a$$

and

$$\frac{v(i,j)^{k+1} - v(i,j)^k}{\alpha \Delta t} = \frac{v(i+1,j)^{k+1} - v(i,j)^{k+1} - v(i,j)^k + v(i-1,j)^k}{(\Delta x)^2}$$

$$+\frac{v(i,j+1)^{k+1} - v(i,j)^{k+1} - v(i,j)^k + v(i,j-1)^k}{(\Delta z)^2} + \frac{Q'''}{K} \qquad 4.7b$$

where u and v are temperatures at the specified grid points and time, then $u(i,j)^{k+1}$ and $v(i,j)^{k+1}$ can be obtained by solving these equations. The temperature estimate at any time level (k+1) may given by

$$T(i,j)^{(k+1)} = \frac{u(i,j)^{(k+1)} + v(i,j)^{(k+1)}}{2}.$$

The calculation of equations 4.7a and 4.7b are carried out explicitly with the former starting from x=0 and z=0 and the latter from a specified x=XL and z=L values (figure 4.30). XL and L are the distances where the temperature $T(i,j)^{k+1}$ is not expected to affect the boundary conditions.

The simple explicit equation (equation 4.6) has been used to determine the temperature rise at the fault. For $\Delta x = \Delta z$ the simple explicit equation can be rewritten as

$$T(i,j)^{k+1} = \lambda\Big(T(i-1,j)^k + T(i+1,j)^k + T(i,j-1)^k + T(i,j+1)^k\Big) +$$

$$(1-4\lambda)T(i,j)^k + \frac{Q'''}{K}(\Delta x)^2 \qquad 4.8$$

where $\lambda = \alpha\Delta t/(\Delta x)^2$. To calculate the temperature at any point after time $t + \Delta t$ from an initial temperature distribution, the local rate of heat generation per unit volume Q''' must be known. In the present problem the rate of heat generation per unit area Q'' occurs along the fault plane (0,j), while at other points there is no heat generation. Q''' can be determined from Q''. For calculations involving points $(0,j)$ (shown in figure 4.30), the temperatures $T(0,j)$ is the average temperature of A'B'C'D' (Gebhart 1971). The total heat produced for an area of $\Delta z\Delta y$ per unit time is $\Delta z\Delta y Q''$. The heat is contained in the volume $\Delta x\Delta z\Delta y$. The heat produced per unit volume per unit time in A'B'C'D' is thus

$$Q''' = \frac{Q''}{\Delta x.}$$

The temperature $T(i,j)^{k+1}$ along the fault plane after time $t + \Delta t$ in term of Q'' is (Gebhart 1971)

$$T(i,j)^{k+1} = \lambda\Big(T(i-1,j)^k + T(i+1,j)^k + T(i,j-1)^k + T(i,j+1)^k\Big) +$$

$$(1-4\lambda)T(i,j)^k + \frac{Q''}{K}\Delta x. \qquad 4.9$$

Having obtained the temperature at time $(t + \Delta t)$, Barakat's modified procedure can then be used to determine the temperatures at grid points away from the fault. The heat generation at these points (other than the points along the fault plane) is zero.

The implementation in the programme (FDHEAT, Appendix 4.1) written to calculate the temperature along the fault and the subsequent temperature distribution is as follows:

(1) An initial crustal temperature distribution at time $t = 0$ is calculated. The calculation procedure is discussed in the next section.

(2) The temperatures at grid points along the fault plane due to the addition of heat generated by the fault movement at time $t + \Delta t$ is then calculated. This is done using equation 4.9.

(3) The temperature distribution at time $t + \Delta t$ can then be calculated using Barakat's procedure. This gives a new temperature distribution.

(4) The temperatures at time $t + \Delta t$ is set to temperatures at time t. This temperature distribution is used as the new initial temperature distribution.

(5) The temperatures at the fault is again calculated as in step 2 and the iteration can be continued until the required time or until a steady state condition is achieved.

The time-dependent finite difference procedure described above has been tested against an analytical steady state solution. The steady state solution with heat generation along fault plane has been given by Scholz et al. (1979). Using a set of boundary conditions the two-dimensional steady state solution can be calculated. Similar boundary conditions can be applied in the finite difference procedure. The iterations are carried out until the temperature reaches a steady state. Comparison of the results from the two procedures indicates that the time-dependent finite difference procedure approximates the steady state analytical solution within the 5 percent error reported by Scholz et al. A typical comparison is shown in figure 4.31.

4.9.3 Temperature distribution in the crust

In normal continental crust the temperature distribution is mainly caused by a combination of the heat generated by radioactive elements (uranium, thorium and potassium) and the heat flowing upwards from below the radiogenic layer. The temperature distribution can generally be regarded as steady state but may be disturbed by local generation of heat such as due to fault movement.

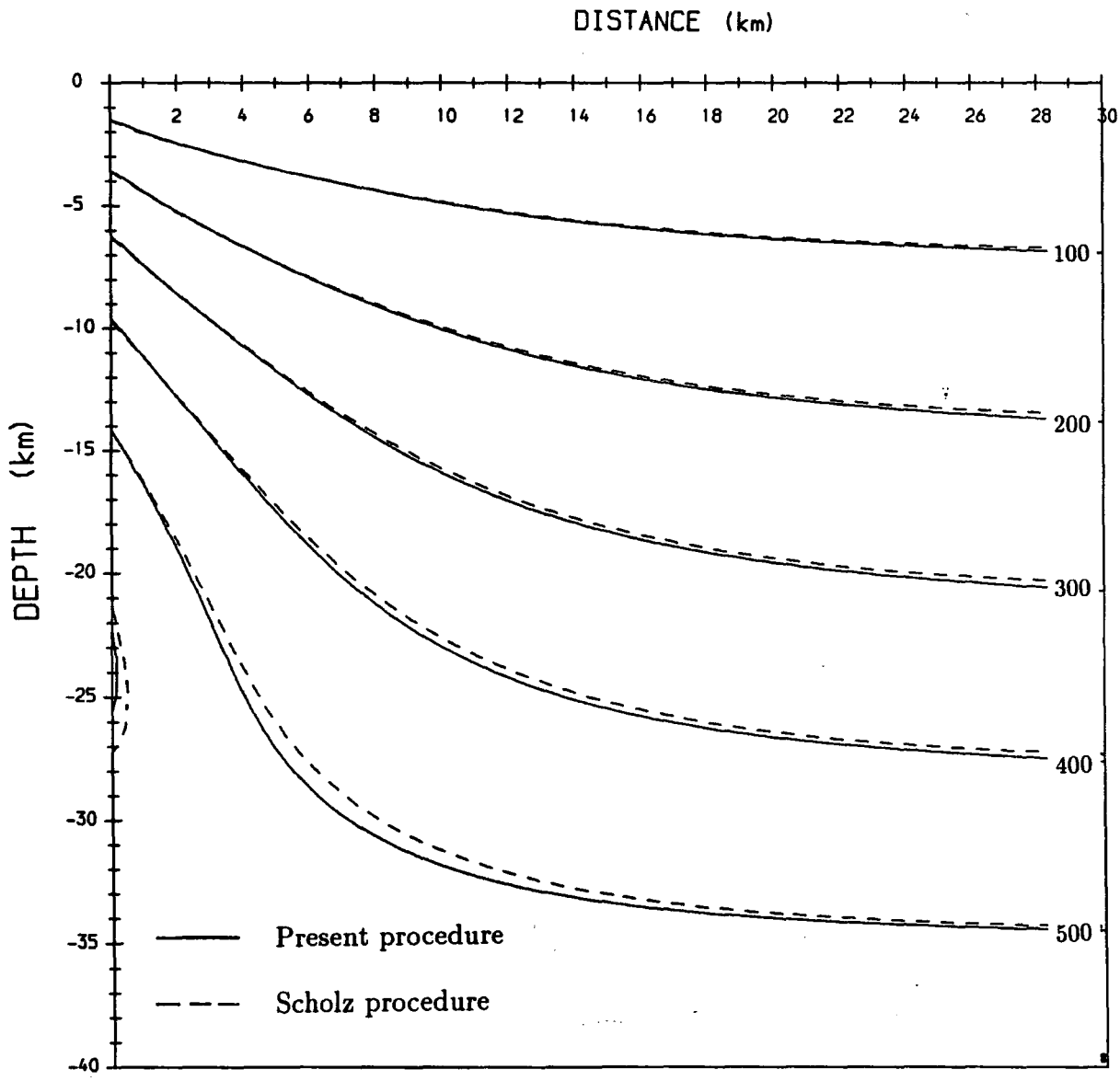

D=10 km (characteristic depth), QS=2.5 mW/m^3 (surface radioactive heat generation), qs=60 mW/m^2 (surface heat flow), RHO=2800 kg/m^3 (density), SH=1.17 kJ/kg K (specific heat capacity), K=1.5 W/m K (thermal conductivity), STMAX=100 MPa (maximum shear stress), RM=0.03 m/year (rate of fault movement)

Figure 4.31 Comparison of the crustal temperature distribution obtained using Scholz et al. (1979) steady state equation and the finite difference procedure.

There are three different models for the vertical distribution of radiogenic heat sources in continental crust and metamorphic terrain. These are (1) uniform distribution with depth, (2) linear decrease with depth and (3) an exponential distribution

$$Q_z''' = Q_s''' e^{-z/D}$$

(Morgan et al. 1987) where z is the depth, Q_z''' and Q_s''' are the rate of radiogenic heat generation at depth z and the surface respectively and D is the characteristic depth or the decrement factor and has a dimension of distance. There is no obvious preference amongst the models but recent work seems to favour the exponential model. Kremenetsky et al. (1989) described the exponential model as consistent with the general setting that the upper and lower crust are made up of felsic and mafic rocks respectively and it remains valid even after differential erosion (Cermak and Rybach 1989).

Using the exponential model, the temperature distribution T_z in the crust as a function of depth z can be calculated from Turcotte and Schubert (1982)

$$T_z = T_0 + \frac{q_d z}{K} + \frac{\rho H_s D^2 (1 - e^{-z/D})}{K} \qquad 4.10$$

where T_0 is the temperature at the surface, $\rho H_s = Q_s'''$, H_s is heat generation per unit mass, ρ is the density and q_d is the heat flow contribution from below the radiogenic zone. The surface radiogenic heat generation has an approximately linear relationship with surface heat flow q_s given by (Roy et al. 1968)

$$q_s = q_d + DQ_s'''. \qquad 4.11$$

In assuming the linear relationship between the radiogenic heat generation and the surface heat flow, q_d can be replaced by $q_s - \rho H_s D$. The crustal temperature distribution can be determined provided that the radiogenic heat generation by the surface rock, the characteristic depth and the surface heat flow are known.

4.9.4 Assumptions for the thermal modelling

The various parameters used in the thermal modelling carried out later are discussed in this section.

(1) Thermal conductivity, density, specific heat and diffusivity.

The thermal conductivities of some of the rock types in the United Kingdom have been compiled from published data and British Geological survey reports by Wheildon and Rollin (1986). The mudstones and siltstones generally have thermal conductivity of less than 2.0 W/m K, the sandstones a value of about 3.0 W/m K, and that of the the granites mainly lies within 3.0-3.5 W/m K. The mean thermal conductivity of the Moines measured by Richardson and Powell (1976) is about 3.4 W/m K. This value is relatively high when compared to values generally attributed to metamorphic rocks used in thermal modelling such as reported in a series of papers on heat production in continental lithosphere in Geophysical Research Letters (1987, pages 248-322). The values mainly range between 2.0 to 3.0 W/m K. Thermal conductivity decreases slightly with temperature and, therefore with depth. Richardson and Powell using the Schatz and Simmons (1972) conductivity-temperature relation estimated that the thermal conductivity value of Moine of about 3.4 W/m K decreases to about 2.1 W/m K at a temperature of 500°C. Richardson and Powell assumed this value for the Moines above 750 K. The actual crustal rocks during the heat generating movement of the Great Glen fault were probably the metamorphic Moines and a deeper granitic rocks. Taking into account the increase of temperature with depth, a value of 2.75 W/m K has been assumed for these quartz rich crustal rocks in the present modelling.

The density of the Moines and Lewisian as measured by Hipkin and Hussain (1983) are 2738 and 2879 kg/m^3 respectively. A density of 2800 kg/m^3 has been assumed to represent the density of the crust underlying the Great Glen fault as used and this is unlikely to be in serious error. The specific heat capacity of the crustal rocks has

been taken as 1.17 kJ/kg K (e.g. Bott 1982). The thermal diffusivity ($\alpha = K/\rho c$) obtained using the above values is $0.84 \text{x} 10^{-6} \text{m}^2/\text{s}$

(2) Heat flow, surface radioactive heat generation and characteristic depth D.
The geothermal map of the United Kingdom (Downing and Gray 1986) shows that the surface heat flow in Eastern Highlands of Scotland southeast of the Great Glen fault reaches over 70 mW/m^2. Along part of the Great Glen fault the heat flow reaches up to about 60 mW/m^2. In the absence of knowledge of the palaeoheat flow, a value of 60 mW/m^2 has been taken to represent the heat flow along the Great Glen fault region during the fault movements.

An estimated value of the characteristic depth D in Eastern Highlands granites is about 6 km (Webb et al. 1987). D values for a number of metamorphic provinces in different regions compiled by Fountain et al. (1987) range from 4.5 to 14.5 km. A value of 10 km has been adopted here as a realistic compromise.

The present surface heat production in the batholith of the Eastern Highland is about 7 $\mu\text{W/m}^3$ (Webb et al. 1987) and the value for the Moines as measured by Richardson and Powell (1976) is 1.7 ± 0.6 $\mu\text{W/m}^3$. A value of 2.5 $\mu\text{W/m}^3$ has been used to allow for possible granite at the depth. This value is near the upper limit of the mean measured value for the Moines (2.3 $\mu\text{W/m}^3$), therefore it is not seriously in error if granite is absent.

The parameters above have been used to estimate the temperature distribution with depth using equation 4.10. This temperature distribution has been used in the modelling. The plot of temperature against depth using the parameters above is shown in figure 4.32. Plots for linear geothermal gradients of 20 K/km and 25 K/km are also shown for comparison. As the geothermal gradient decreases with depth, a linear temperature gradient will overestimate the temperature at depth.

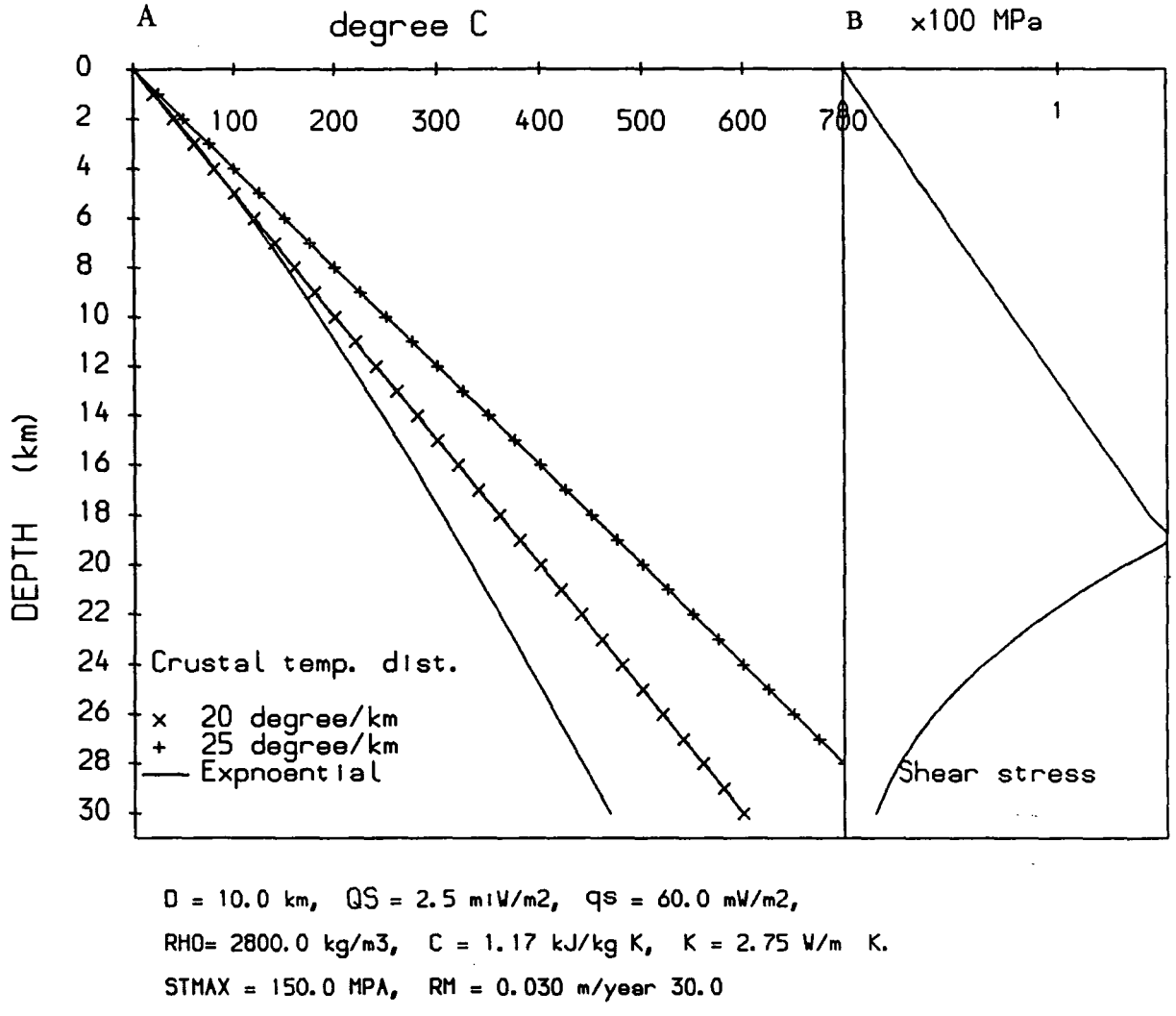

D - characteristic depth, QS - surface radioactive heat generation, qs - surface heat flow, RHO - density, C - specific heat capacity, K - thermal conductivity, STMAX - maximum shear stress, RM - rate of movement

Figure 4.32 (A) Plot of temperature as a function of depth for linear temperature gradient of 20 and 25 °C/km, and an exponential temperature increase calculated using the equation of Turcotte and Schubert (1982). (B) A plot of shear stress as a function of depth with a linear increase at the brittle zone and exponential decrease at the ductile zone (Turcotte et al. 1980). The maximum shear stress is taken to be at the brittle/ductile transition zone.

(3) Shear stress along transcurrent faults

The shear stress related to deformation along a transcurrent fault is not well defined. Shear stress of up to 200 MPa has been reported for the Moine thrust (Ord and Christie 1984). Lower values have been generally associated with transcurrent faults with an upper limit of about 100-150 MPa (Sibson 1986, Scholz et al. 1979). Values within this range have been used in the thermal modelling here. In the brittle zone, the shear stress rises linearly with depth up to the limiting shear stress at the brittle/ductile transition. The shear stress then decreases rapidly as approximated by equation 4.1c. It is assumed that below the Moho the shear stress is small. A typical plot of shear stress with depth is shown in figure 4.32. The peak shear stress is assumed to be at the 325^{o}C temperature level corresponding to the brittle-ductile transition zone (figure 4.29).

(4) Rate of movement of the Great Glen fault.

The Great Glen fault horizontal displacement of about 100-200 km inferred from the geological evidence (e.g. Smith and Watson 1983) has been taken to be the minimum value. Larger displacement suggested by palaeomagnetic evidence (600 km, Storetvedt 1987) has been taken to be the maximum displacement. The geological and the palaeomagnetic evidence indicate that the Great Glen fault movement took place mainly from the Devonian to Carboniferous (table 4.1). The movement which occurred by the end of the Middle Old Red Sandstone times was essentially sinistral (section 4.3). The post-Lower Devonian sinistral movement is probably small (Rogers et al. 1989) and thus the heat generating movement may be assumed to be mainly Lower Devonian. Based on displacement of faults active during granite emplacement and the relationship of dyke swarms associated with the granites, Plant et al. (1983) suggested that the transcurrent movements in the region were accompanied by uplift. The uplift period occurred during the cooling period of the Caledonian metamorphism which ended at about 400 Ma (Smith and Watson 1983). The main transcurrent movement is assumed to have occurred within the late orogenic uplift period and

before the end of the Lower Devonian (probably over about 20 to 30 million years). A displacement of 600 km is assumed to occur within this period giving a rate of movement of about 20 to 30 mm/year to be used in the modelling. The heat generated on the fault based on a rate of movement of 20 mm/year and a maximum shear stress of 150 MPa is 97.4 mW/m^2

(5) Procedural constraint

In applying the explicit finite difference procedure to time-dependent conduction problem, the time interval used must be sufficiently small. This is necessary to ensure that the finite difference relation approximates the original differential equation closely to avoid instability and to obtain an accurate result. In using the simple explicit equation (equation 4.8), stability can be achieved if all the terms are positive (Gebhart 1971), hence $(1 - 4\lambda)T(i,j)^k \geq 0$ (for $\Delta x = \Delta z$). As $\lambda = \alpha\Delta t/(\Delta x)^2$, $\Delta t \leq (\Delta x)^2/4\alpha$. In the calculation, for any finite sampling interval the time increment must satisfy the above limitation. For a sampling interval of 1 km, thermal conductivity of 2.75 W $m^{-1}K^{-1}$, density of 2800 kg m^{-1} and specific heat capacity of 1.17 kJ kg^{-1} K^{-1}, the increment must be less than 9700 thousand years.

(6) The magnetized region.

The magnetized outward dipping region defining the Great Glen feature is assumed to form at temperature isograd of 520°C and greater where breakdown of the metamorphic biotite or chlorite and granulitization may occur.

4.9.5 Results of the thermal modelling

The factors affecting the thermal model are (1) the heat generation on the fault plane and conduction away from the fault, and (2) the temperature distribution in the crust (due to radioactivity and deeper sources) at the onset of the heat generation period.

The temperature distribution in the crust used in the following modelling is as shown in figure 4.32. This has been calculated using a surface heat flow of 60 mW/m^2, a characteristic depth of 10 km, surface heat generation of 2.5 $\mu W/m^3$, specific heat capacity of 1.17 kJ/kg K, density of 2800 kg/m^3 and thermal conductivity of 2.75 W/m K. The thermal diffusivity is then 0.84 x 10^{-6} m^2/s. The heat conduction and generation calculations used the above parameters, a maximum shear stress of 150 MPa with a vertical distribution as shown in figure 4.32 and a relative rate of movement of 30 mm/year, except where stated otherwise.

Modelling was initially carried out to determine the depth z and the distance x from the fault where the temperature increase due to the heat generated (Q''_f) on the fault plane does not affect the boundary conditions over the relevant time period. The initial and boundary conditions were set to zero values. A 1 x 1 km^2 sampling grid and a time increment of 9000 years were used. The test was done by carrying out the iteration of the finite difference procedure until a steady state temperature distribution was attained with x and z values sufficiently large for the temperature to remain undisturbed at the base and edges. Such a temperature distribution was obtained after about 70-75 million years provided that the depth of the base is about 90 km and the half-width is 90 km. A square area of 90 by 90 km^2 sampled on a 1 x 1 km^2 grid has been used for the modelling and for presentation of the results. The computation of the 7777 iterations needed to approach steady state took about 500 seconds cpu time on the Durham Amdahl 5860 Computer.

Two different procedures can be used to obtain the final temperature distribution. The first procedure (procedure 1) carries out the finite difference calculations using the pre-existing crustal temperature distribution as the initial and boundary conditions and includes the radioactive heat generation. The calculations using equation 4.7 can be carried out for any specified time duration of fault movement. This gives directly the crustal temperature distribution at that time. The results show a progressive increase in temperature with time as indicated by the shallowing of the temperature

isotherms, the highest value being on the fault. This increase is most rapid for the first 30 million years and does not change very much beyond this time. The temperature increase for 30 million years extends laterally about 50 km from the fault (figure 4.33).

In the second procedure (procedure 2), equation 4.7 is also used, but with the omission of the pre-existing temperature field. The initial and boundary conditions are set to zero. This results in a temperature distribution purely due to the heat generation on the fault (fault temperature distribution). Figures 4.34a, b and c show the fault temperature distribution at 30, 65 and 70 million years respectively. A progressive outward temperature increase with time can be clearly observed. The increase is most rapid before 30 million years and does not change significantly beyond 65 million years (compare figures 4.34b and c). The crustal temperature distribution can be obtained by adding the temperature distribution due to faulting at any given time to the pre-existing steady temperature distribution. Tests have been carried out to determine the accuracy of this procedure. A comparative plot of the crustal temperature distributions obtained by procedure 1 and procedure 2 for 30 million years are given in figure 4.35. The tests for less than 10 million years indicate that the results from both procedures give a fairly good fit. There is a slight difference between the two results with progressive increase in time (figure 4.35) where the change in temperature from the initial condition is large. This difference decreases with increasing distance from the fault.

If the fault temperature distribution caused by a specific Q''_f value is known, procedure 2 can easily be used to obtain the crustal temperature distribution due to other Q''_f values. This can be done since the temperature increase is linearly dependent on the heat generation. Any change in the Q''_f value causes a proportional change in the temperature increase provided that the pattern of shear stress versus depth is unchanged. The temperature distribution produced by the fault movement has been calculated for up to 75 million years at 5 million year interval using the parameters given earlier and archived on tape. The initial temperature distribution was also

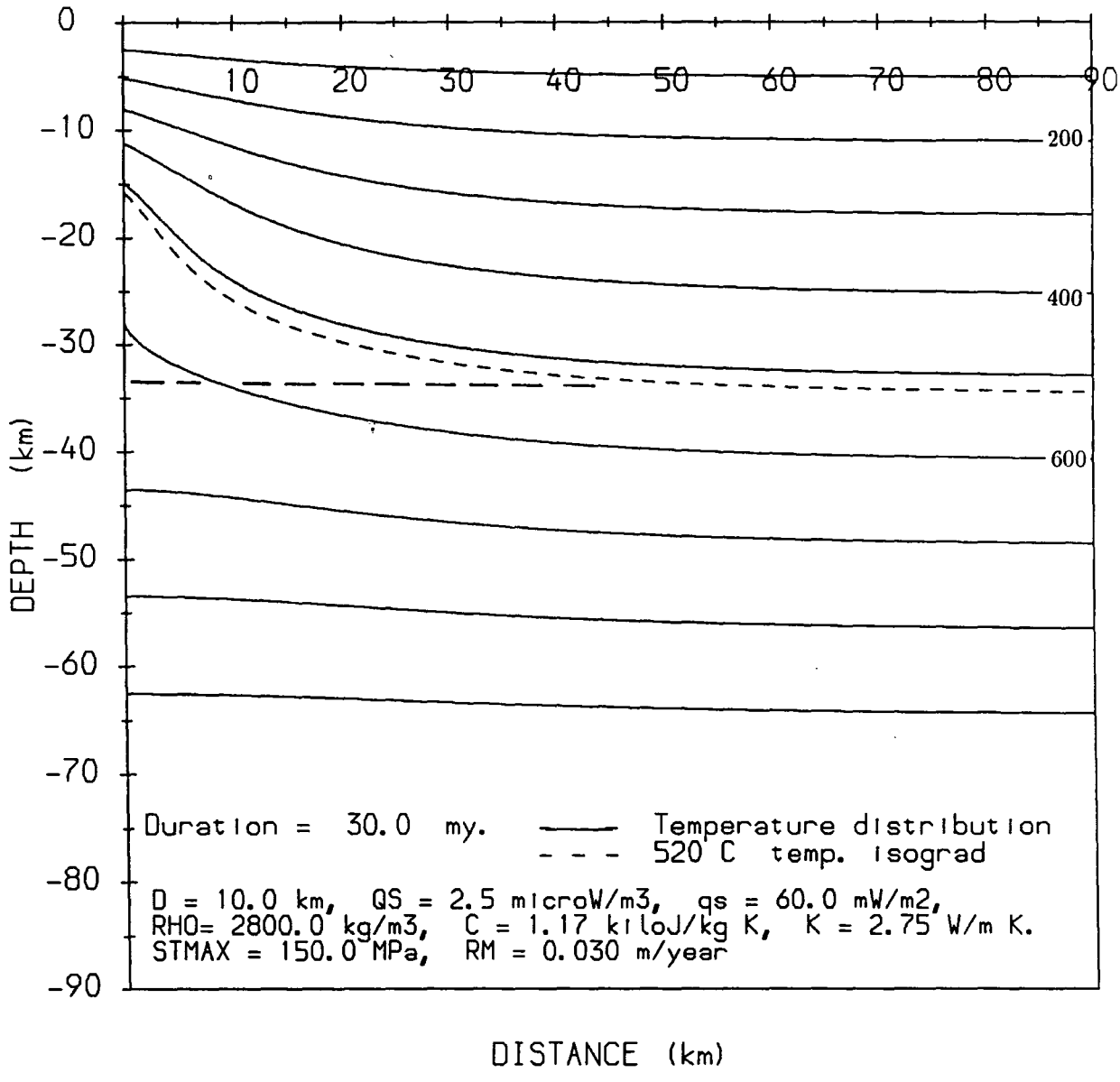

Figure 4.33 The temperature distribution (°C) in the crust for 30 million years calculated using the parameters given above and the pre-existing crustal temperature distribution as the initial and boundary conditions (procedure 1). The thermal model with its top defined by the 520°C isotherm is also shown. The explaination of the abbreviation used in this and subsequent figures are as in figure 4.32

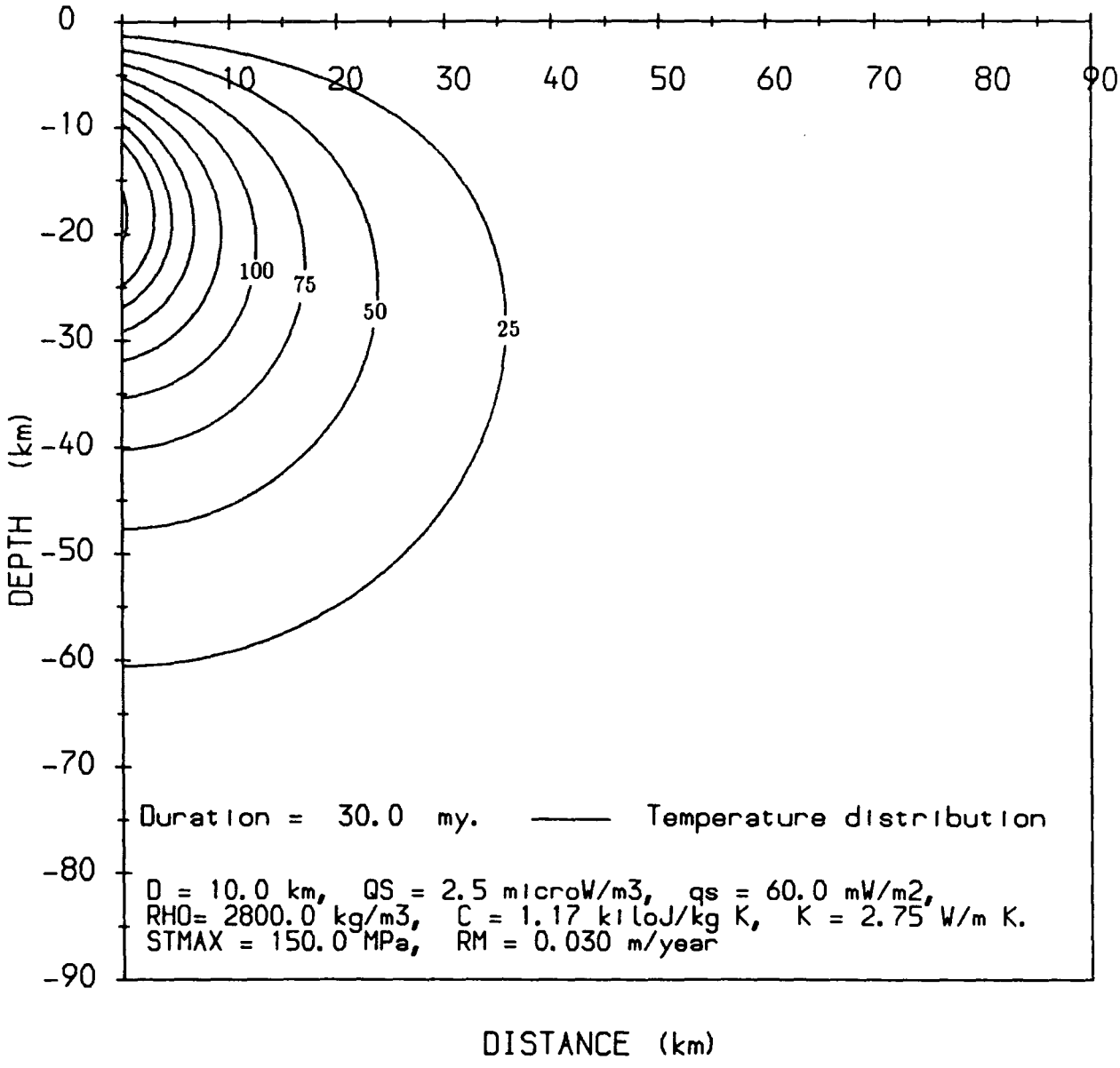

Figure 4.34a Temperature distribution (°C) due to heat generated on the fault for 30 million years calculated using the parameters above, and initial and boundary conditions set to zero.

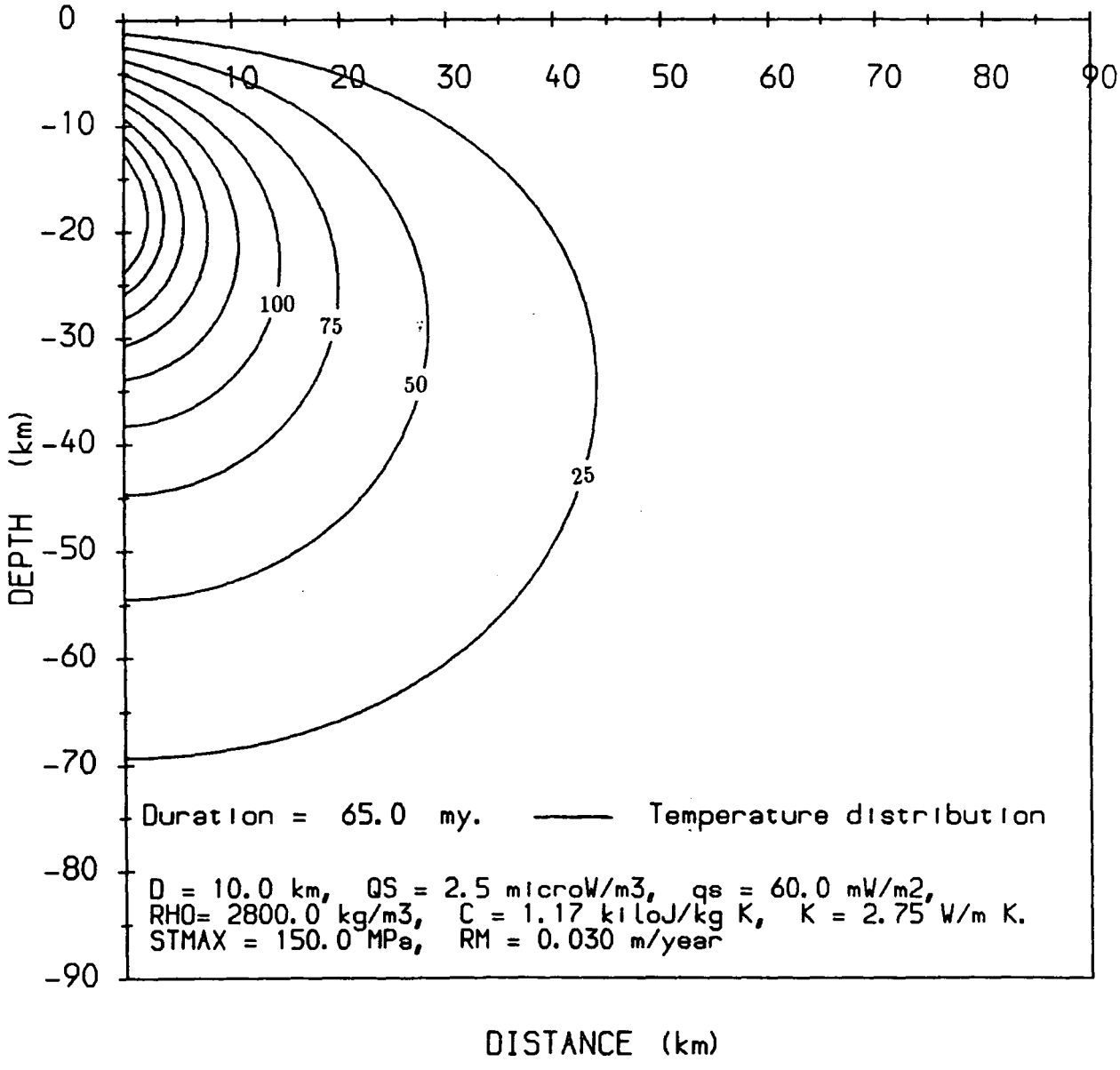

Figure 4.34b Temperature distribution (°C) due to heat generated on the fault for 65 million years calculated using the parameters above, and initial and boundary conditions set to zero. There is no significant increase in temperature after the 60 million years period. (compare with the result in figure 4.34c for 70 million years)

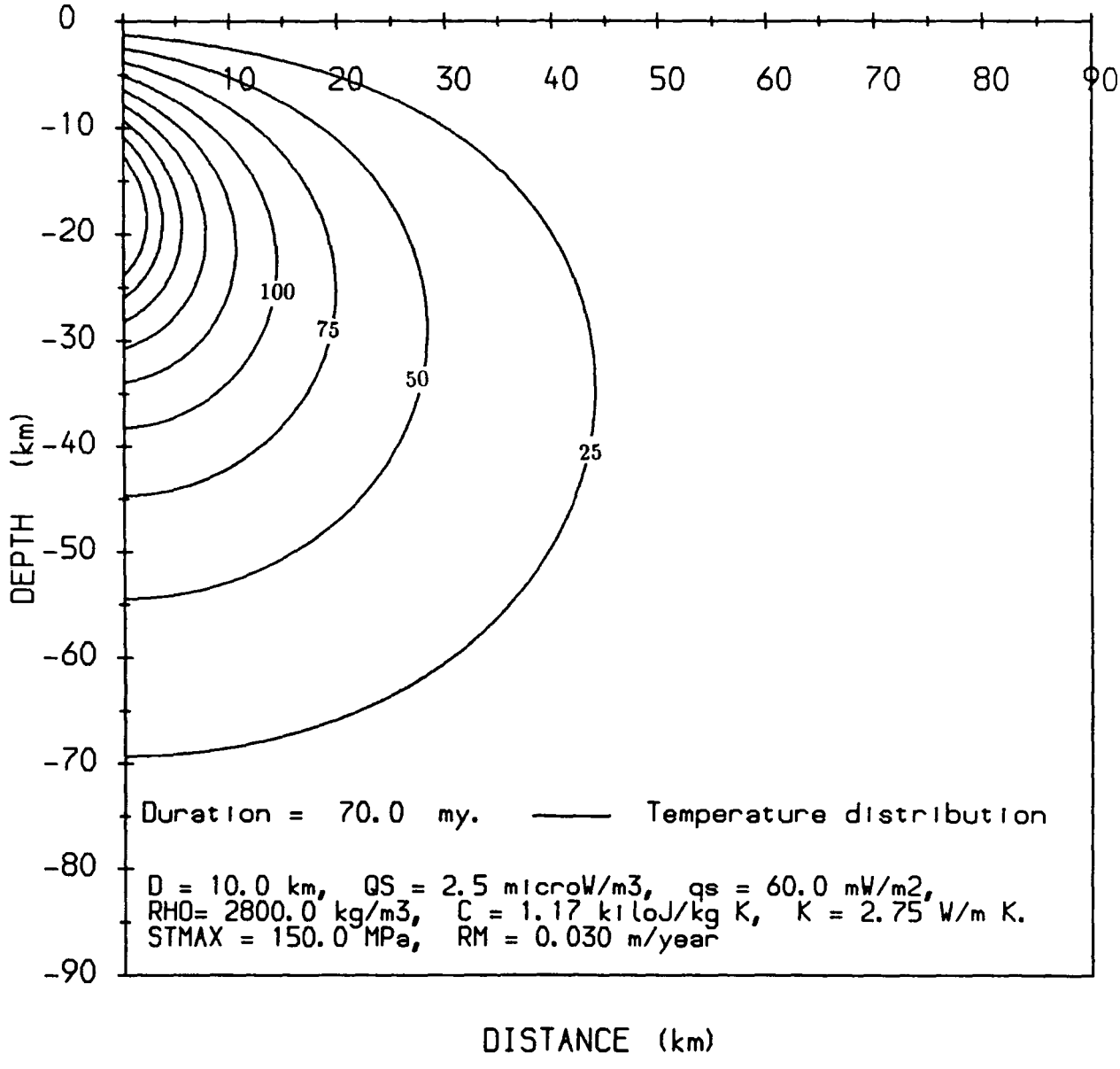

Figure 4.34c Temperature distribution (°C) due to heat generated on the fault for 70 million years calculated using the parameters above, and initial and boundary conditions set to zero.

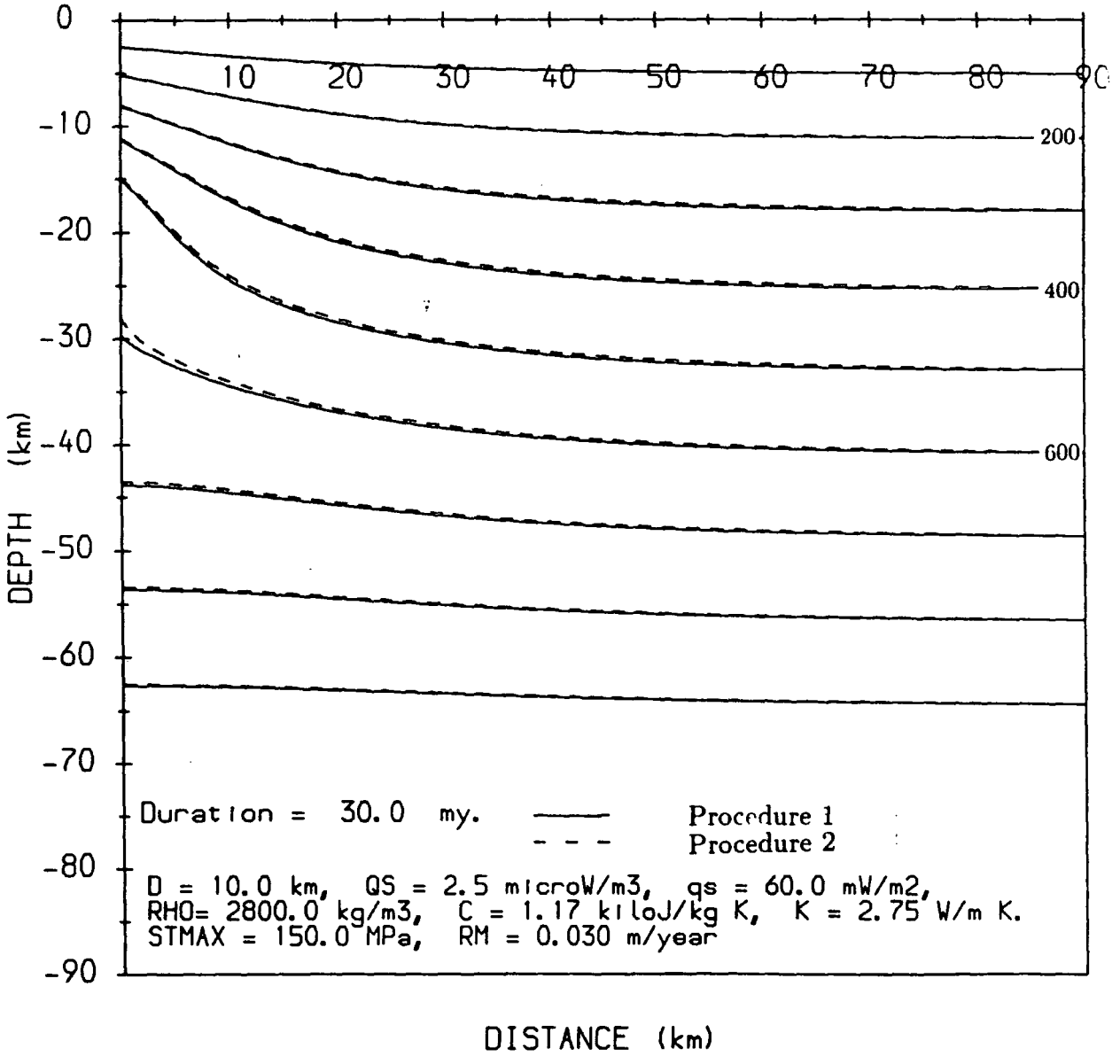

Figure 4.35 Comparison of the temperature distribution (°C) for 30 million years calculated using procedure 1 with the distribution calculated using procedure 2.

calculated and archived. The crustal temperature distribution for various assumptions can then be easily calculated using these archived results.

The top of the magnetized region which causes the Great Glen anomaly is assumed to be defined by the 520°C isotherm. Since the heat generating movement along the Great Glen fault probably occurred over about 20 to 30 million years (section 4.9.4), the crustal temperature distributions calculated over the period of fault movement from 10 to 40 million years are emphasized.

The crustal temperature distributions calculated using the parameters given earlier for 20 and 30 million years are shown in figures 4.36 and 4.33 respectively. The temperature isotherms are plotted at 100°C interval and the 520°C isotherm is also shown. The half-width of the thermal models is about 30-35 km for 10 million years and 40-50 km for the 20, 30 and 40 million years. The half-width of the feature causing the Great Glen fault magnetic anomaly calculated earlier using the pseudogravimetric method is about 40-45 km (at the southeastern side of the Great Glen fault). This suggests that the the duration of movement of the fault at 30 mm/year needs to be at least 20 million years. The vertical extent of the thermal model is slightly greater than most of the models calculated using the pseudogravimetric method. This is due to the high heat generation at the fault. A smaller heat generation would produce a smaller vertical extent. This suggests a smaller rate of movement may apply.

The thermal models obtained using a smaller rate of heat generation have been calculated at 10, 20, 30 and 40 million years. The model for the 20 million years is shown in figure 4.37. A maximum shear stress of 100 MPa has been assumed but the other parameters used are the same as in the earlier models. This could be produced by a rate of movement of 20 mm/year at a maximum shear stress value of 150 MPa. The half-width of the thermal model is about the same as those calculated using a rate of movement of 30 mm/year and maximum shear stress of 150 MPa. The depth extent of about 8-12 km for 20-40 million years movement is comparable with that obtained

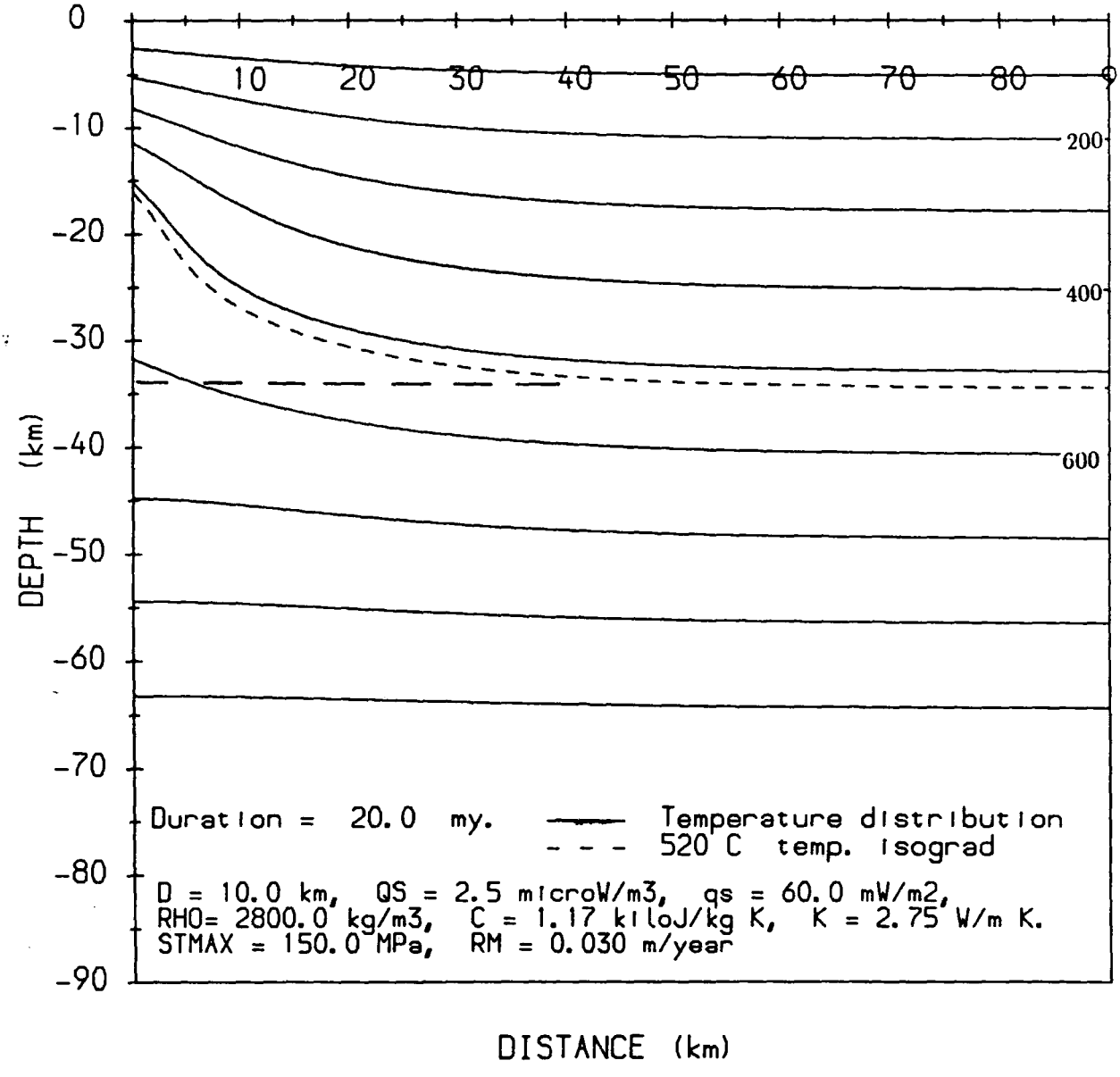

Figure 4.36 The temperature distribution (°C) in the crust for 20 million years calculated using the parameters given above. The thermal model with its top defined by the 520°C isotherm is also given.

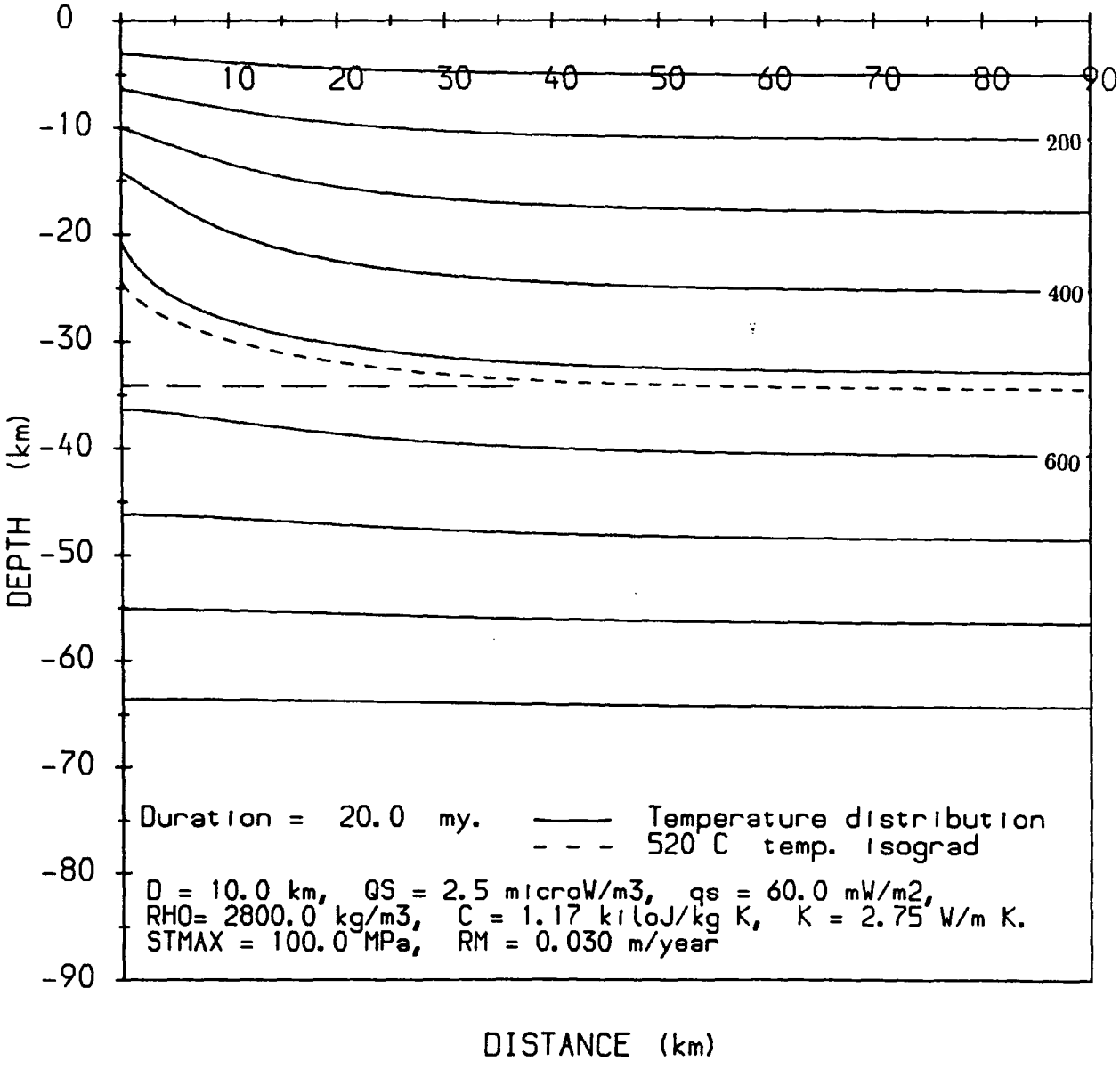

Figure 4.37 The temperature distribution (°C) in the crust for 20 million years calculated using the parameters given above. The maximum shear stress is 100 MPa. The thermal model with its top defined by the 520°C isotherm is also given.

from the pseudogravimetric modelling (about 7-18 km).

From the modelling, it has been shown that the movement of the Great Glen fault can possibly produce sufficient heat to raise significantly the isotherm appropriate to the breakdown of the metamorphic chlorite and biotite to form magnetite. Heat generation of at least about 97.4 mW/m^2 (maximum shear stress of 150 MPa and a rate of movement of 20 mm/year), and a duration of movement of at least 20 million years are required as modelled. A marked difference between the results of the pseudogravimetric and thermal modelling is that the thermal model is at a relatively greater depth than the pseudogravimetric model. This could be accounted for by uplift during or after the fault movement.

A higher surface heat flow or a smaller thermal conductivity can produce a thermal model at a shallower depth as shown in figures 4.38 and 4.39. Figure 4.38 shows the temperature distribution at 30 million years calculated using a higher surface heat flow of 70 mW/m^2 while the other parameters remain the same as given earlier. The base of the thermal model is at about 24 km depth, the thickness at the fault is about 12 km and the half-width about 40-50 km. Figure 4.39 shows the temperature distribution at 30 million years calculated using a thermal conductivity of 2.5 W/m K while the other parameters remain the same as given earlier. The base of the thermal model is at about 30 km depth, the thickness is about 16 km and the half-width is about 40-50 km.

4.10 Discussion

The Great Glen magnetic anomaly is almost symmetrical and has its apex near the line of the Great Glen fault. This suggests that source must be closely associated with the fault rather than with the other metamorphic geology of the region. The source has been modelled as a strongly magnetized outward dipping feature with its apex

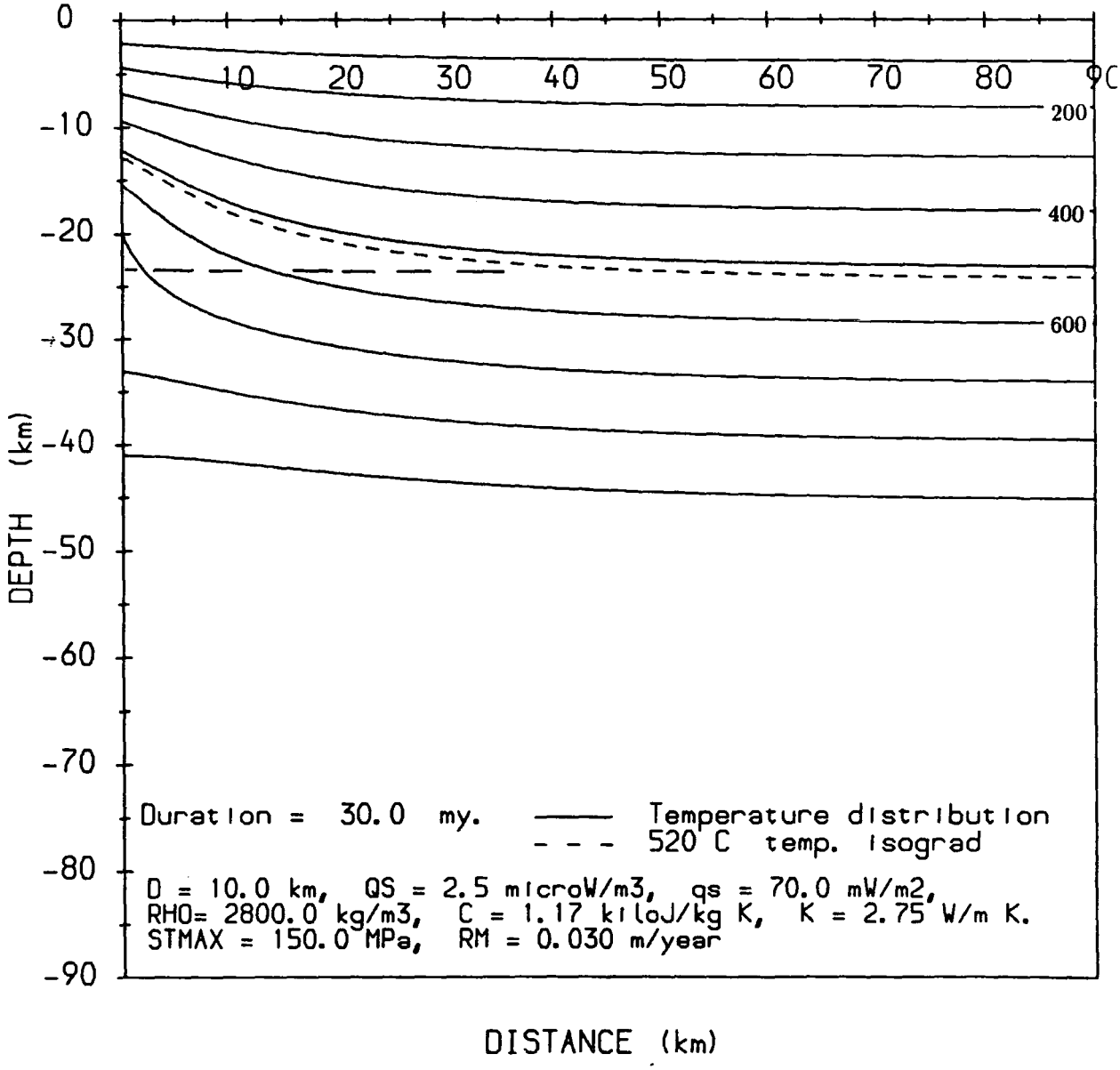

Figure 4.38 The temperature distribution ^{o}C in the crust for 30 million years calculated using the parameters given above. The surface heat flow used is 70 mW/m^2. The thermal model with its top defined by the 520^{o}C isotherm is also given.

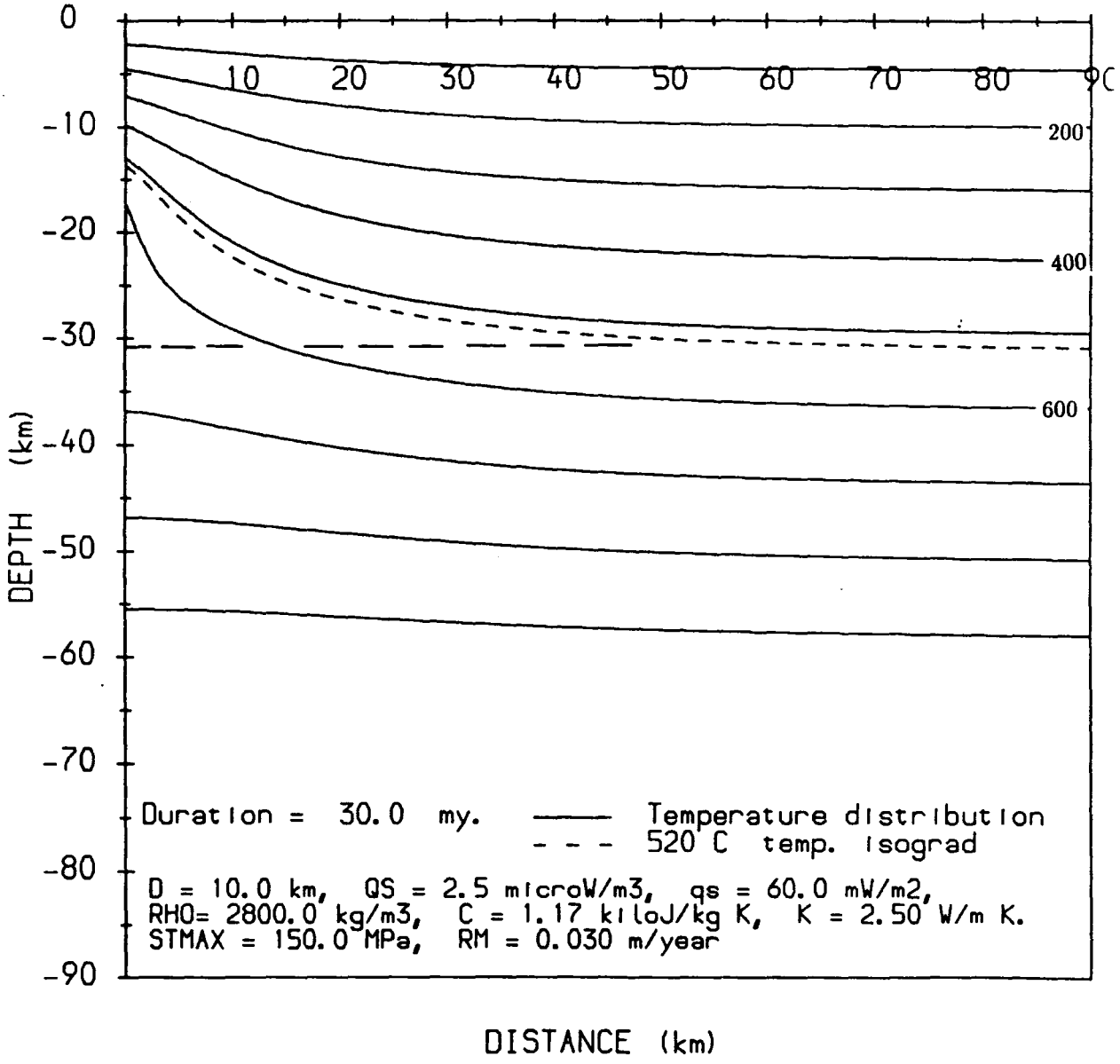

Figure 4.39 The temperature distribution °C in the crust for 30 million years calculated using the parameters given above. The thermal conductivity used is 2.5 W/m K. The thermal model with its top defined by the 520°C isotherm is also given.

near or on the fault plane. Its origin has been interpreted as due to frictional heating on the fault plane caused by transcurrent movement (frictional heating hypothesis). The heat generated resulted in a temperature rise which was conducted from the fault to form an outward dipping crustal temperature distribution symmetrical about the fault. The strongly magnetized region was possibly formed as a result of magnetite being formed at temperatures greater than 520°C by breakdown of metamorphic biotites or chlorites. There are, however, problems associated with this frictional heating hypothesis. These problems will be examined here, and alternative possible sources of origin proposed and described.

The first problem with the frictional heating hypothesis is the magnitude of the transcurrent movement required to generate the necessary heat. From the thermal modelling the Great Glen fault needs to have moved at a rate of 20 mm/year for about 20 million years to give a total displacement of at least 400 km. This amount of displacement is near the upper limit of the likely movement of the Great Glen fault. The sinistral and dextral displacement inferred from the palaeomagnetic evidence is about 600 and 300 km respectively (Storetvedt 1987) while geological evidence suggests the movement is only about 100-200 km (e.g. Smith and Watson 1983). Furthermore, the displacement of 400 km is greater than the lateral extent of the Great Glen magnetic anomaly and its causative body (about 200-250 km).

A second problem is the occurrence of the Great Glen anomaly only across mainland Scotland. This might suggest that it was formed after the transcurrent movements. It is also possible that the anomaly does extend on one or both sides, but is masked by other anomalies such as the Mull anomalies and the basin in the Moray Firth.

A third problem concerns the magnitude of the coefficient of friction required. The magnitude of the shear stress on an active transcurrent fault plane is still controversial. Laboratory studies of the coefficient of friction of crustal rocks under normal continental condition suggests that the peak shear stress can exceed 100 MPa (Tur-

cotte et al. 1980). However, based on the low value of the surface heat flow in the vicinity of the San Andreas fault, shear stress on an active transform fault is expected not to exceed 10 MPa (Lachenbruch and Sass 1980). This low shear stress value has been explained by Lachenbruch (1980) as due to fluid pressure close to the normal stress acting on the fault plane. This occurs when confined water is heated and hydrostatic pressure increases causing a reduction of the effective normal stress. Turcotte et al. (1980) suggested that fracturing within a major fault zone should produce sufficient porosity to prevent increase in pore fluid pressure. O'Neil and Hanks (1980) suggested that the lack of raised heat flow in regions of active transcurrent faulting is due to heat produced being removed by hydrothermal convection. Turcotte et al. (1980) also suggested that circulation at large depth can redistribute the heat flow but will not change the mean surface heat flow value. Williams and Narasimhan (1989) proposed three possible models to explain the coincidence of both high shear and absence of anomalous heat flow along the San Andreas fault: (1) permanent weakness model. This model explains the absence of anomalous heat flow by the presence of a low ambient stress on the fault within the high ambient stress crust, or a low resisting stress on the fault due to the presence of fault gouge and near-lithostatic pore pressure. (2) Transient fault weakness fault model. The presence of a temporary temperature increase due to the fault movement causing increase in pore fluid pressure thus lowering the shear stress and heat generation, and (3) hydrothermal circulation model. The heat generated at the fault plane is carried away by hydrothermal circulation as described by O'Neil and Hanks (1980) and Turcotte et al. (1980). Williams and Narasimhan (1989) carried out modelling based on the convective effect which includes the presence of gravity induced fluid flow from the fault. The modelling is able to explain the presence of high stress faulting and low heat flow anomaly along the transcurrent fault.

Attempts have been carried out using hydrofracturing stress measurements in shallow wells near San Andreas fault to resolve this conflict between shear stress magnitude deduced from surface heat flow measurements on an active transform fault and that

inferred from the laboratory measurements. While measurements in some wells appeared to support the heat flow data, others support the laboratory results (Zoback et al. 1980, McGarr et al. 1982). Extrapolation of the stress data to a greater depth (14 km) using a simple elastic model, suggests that the shear stress value is greater than that deduced from the surface heat flow measurements (McGarr et al. 1982). Hydrofracturing measurements in deeper wells (up to about 0.9 km) are still unable to resolve this problem because of the complexity of the data (Hickman et al. 1988, Stock and Healy 1988). The shear stress value along an active transcurrent fault as predicted by the laboratory data has been used in the present thermal modelling. A heat generating fault model with high shear stress of up to 150 MPa seems to be successful in explaining other geological features such as the bi-symmetry of metamorphism near the Alpine fault of New Zealand (Scholz et al., 1979), in Lauvaux-Angers and Montague Noire shear zone of France, and Maydan shear zone of Afghanistan (Nicolas et al., 1977). The thermal modelling of Scholz et al. (1979) is further supported by argon depletion data for the New Zealand Alpine fracture.

It is assumed that the heat generation is along a plane but the fault may be a broad zone. This reduces the average heat generation (Lee and Delaney 1987). The broadening of a transcurrent fault zone probably occurs at the ductile zone but the brittle fault zone where most of the heat is generated probably remains relatively thin (e.g. Sibson 1983).

Because of doubts as to the effectiveness of shear heating we need to explore other possible sources of heat for metamorphism related to the Great Glen fault. Another possibility which might cause a substantial temperature rise along a fault zone is fluid flow within the crust. The fluid flow hypothesis is described here as an alternative to the frictional heating hypothesis. Evidence for large scale fluid flow within the crust has been reviewed by Torgersen (1990). Fluid flow is often channelled along a shear zone when present (Etheridge et al. 1983, ODP 1987). Fluid circulated through the deep crust should be relatively hot.

Beach (1976) indicated that fluid flow can cause temperature increase in a shear zone in the following ways: (1) Exothermic heat may be released when reactions occur below the equilibrium pressure and temperature. The magnitude is, however, difficult to assess. (2) Radioactive heat might arise from enrichment of radioactive elements brought in by the fluid. Kerrich (1986) showed that fluid movement into the Abitibi Greenstone Belt shear zone in United States carried radiogenic materials. The presence of anomalous radioactive elements has also been demonstrated by Gates and Gundersen (1989) for shear zones in eastern United States. Modelling of temperature rise due to the radioactive heating by Beach indicates that a temperature rise of about 20 to 30°C at 15-20 km depth can occur for fluid flow duration of 10 to 100 million years. (3) Convective heat transfer is the most important thermal effect caused by fluid flow (Beach 1976) and is most likely to have been effective when the Great Glen fault is active. Such hot fluid convectively raising up a fault zone would raise the temperature in the vicinity of the fault. This might result in an outward dipping temperature distribution symmetrical about the fault where magnetite can be formed as described previously.

Studies of oxygen isotopic composition of minerals within shear zones have enabled Kerrich et al. (1984) to determine the temperature conditions of the fluid moving through shear zones. They reported temperatures of up to 500-540°C and 580-640°C for the shear zones in Lagoa Real, Brazil and Coniston, Ontario respectively. In Lagoa Real the depth at which the temperature equilibration has taken place was estimated to be at about 15 km. Fluid inclusion studies have also been used by Parry and Bruhn (1986) to determine fluid temperature for the Wasatch fault Utah, United States. A minimum fluid temperature of 223-253°C was reported. As the fluid may cool as it rises, even higher temperatures may occur at deeper crustal levels.

The main factors affecting the magnitude of the temperature increase on a fault due to fluid flow are as follows:

(1) Source of the fluid: The hot fluids can be derived from the mantle, or lower crust

(Beach 1976) as a result of magmatic or metamorphic activity (Kerrich et al. 1984) or from deep circulation of meteoric water. Fluids are released in the deeper crust by prograde metamorphism (dehydration process, Murrell 1986). Fluids released during prograde metamorphism may be trapped and heated in the deeper crust. Similarly meteoric water circulating at depth may also be heated. The meteoric fluid may be derived by dewatering of sedimentary rocks (Kerrich et al. 1984) or meteoric reservoirs as a result of thrust faulting (McCaig 1988). Nesbitt and Muehlenbachs (1989) indicated that in regions of transcurrent faulting the fluids to a depth of about 15 km are mainly convected meteoric water.

(2) Initial temperature of the fluid: The maximum temperature the metamorphic fluid can attain is similar to the temperature of the peak metamorphism. Within the Great Glen fault region, the peak metamorphism temperature in the middle amphibolite facies of Moines was about 640^{o}C (Fettes et al. 1985) but higher temperature may have occurred deeper in the crust. Fluids from the mantle would be at a higher temperature than the crustal temperature. The temperature attained by the meteoric water depends on the temperature of the rocks through which the fluid flows. The fluids passing through the Lagoa Real shear zone mentioned earlier have been shown to be meteoric with a temperature of 500-540^{o}C in the shear zone (Kerrich et al. 1984).

(3) Mechanism of fluid transport: Besides the two factors above, an efficient fluid transport mechanism is necessary. Fluid movement in the crustal rocks at depths greater than 10 km can occur in two ways, (a) fluid flow along fracture systems and (b) pervasive flow along grain boundaries (Ferry 1986). In the pervasive process the fluid flow can be continuous. In the fracture system, fluid flow may cause chemical reactions which produce secondary minerals filling up the voids. This can stop the fluid flow. Torgersen (1990) described the time dependent cyclic process (suggested by Nur and Walder, in press) between high hydrostatic pore pressure and lithostatic pore pressure which enables the continuity of flow. Such a process has been suggested by Williams and Narasimha (1989) to reconcile the presence of low surface heat flow and high shear stress along San Andreas fault. The fluid flow within the Great Glen fault may have occurred by this process. Away from the fault zone, fluid flow may

have occurred by pervasive flow and convection due to geothermal gradient.

A sketch of hot fluid flow in the crust channelled into a transcurrent fault zone is shown in figure 4.40. Sibson (1983) suggested that transcurrent fault may form shear zone below the brittle/ductile transition zone. This shear zone may be a region of low fluid pressure causing fluid in the adjacent areas to flow into the region. The hot fluid rising up the fault may form the symmetrically heated zone about the fault as shown in the diagram.

Another possible origin for the source of the Great Glen feature is crustal CO_2 streaming associated with Great Glen fault which might produce magnetite-bearing granulite. Lamb and Valley (1984) suggested that granulite may be formed by CO_2 streaming. The widened shear zone below the brittle-ductile transition zone beneath a transcurrent fault may form the upward passage for CO_2 from the mantle or the deeper crust. The CO_2 may induce magnetite forming reactions (Frost and Chacko 1989) within the shear zone and the adjacent regions bordering the shear zone. The possible sources of the CO_2 associated with granulite metamorphism are listed by Crawford and Hollister (1986): (1) oxidation of graphite, (2) reaction of silicate and carbonate minerals to form calc-silicates and CO_2, and (3) exolution from mantle-derived melt or mantle-derived fluid (Etheridge et al. 1983). The first source would be closely associated with graphite bearing granulites and the second with carbonates. Mafic igneous activities may also be accompanied by CO_2 production (Frost and Frost 1987).

The frictional heating and fluid flow hypotheses can both explain the close relationship between the Great Glen anomaly and the Great Glen fault by temperature increase with formation of magnetite under appropriate conditions. The viability of both hypotheses depends on a sufficient temperature rise being attained. In the frictional heating hypothesis, the temperature increase depends on high shear stress and high rate of slip movement. In the fluid flow hypothesis, the temperature increase depends

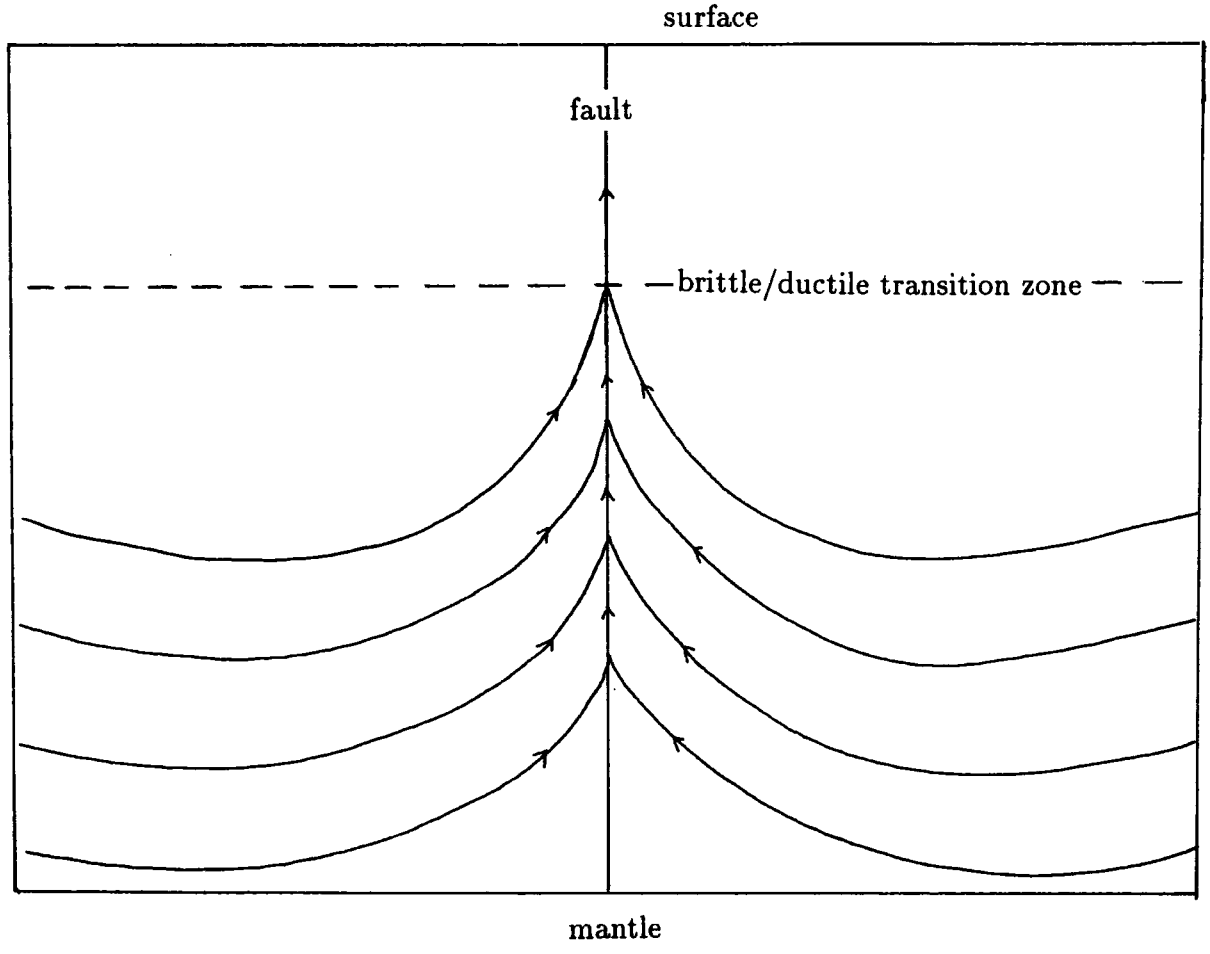

Figure 4.40 A sketch showing fluid flow in the crust in the presence of a vertical fault zone. The source of the fluid may be metamorphic, fluid from the mantle or meteoric.

on the temperature of the source fluids and effective fluid transport. Assuming that the necessary temperature rise is attained, the large displacement required by the frictional heating hypothesis may be explained if both sinistral and dextral movement have occurred. The 100-200 km displacement inferred from the geological evidence is only a net displacement. The fluid flow hypothesis has the advantage of being independent of the magnitude of the transcurrent movement and may have occurred after the main movements. It is difficult to model as has been done for the frictional heating hypothesis.

CHAPTER 5

Pseudogravimetric modelling in the Midland Valley of Scotland

5.1 The magnetic map

The Midland Valley is bordered along its southeastern side, from Ballantrae to Leadburn, by a series of small elongated magnetic anomalies (figure 5.1, the locations are given in figure 5.1b). These anomalies are closely associated with the Southern Upland fault, and are probably related to features such as the Ballantrae complex which causes the elongated magnetic anomaly in the Ballantrae area. The amplitude of these anomalies reaches over 400 nT. To the north, the Midland Valley is bordered by the Highland Boundary fault where an obvious 40 km long elongated anomaly occurs along strike towards the northeast of the fault outcrop. This anomaly is due to the Highland Boundary complex and has an amplitude reaching over 500 nT. To the southwest of this elongated anomaly, along the Highland Boundary fault, there are a series of very short wavelength, low amplitude positive magnetic anomalies which are just visible on the aeromagnetic map. The continuation of the magnetic anomalies along the two faults into Ireland can be seen on the magnetic map of Ireland by Morris (1989).

An obvious feature on the aeromagnetic map of the Midland Valley is the prominent belt of positive magnetic anomalies traversing the region from Arran to the Firth of Forth. A continuation of the belt into Ireland can be observed on the map of Morris (1989). A slightly elongated magnetic high occurs over Arran. This is closely associated with the known Tertiary igneous centre. This anomaly, which encloses the Northern granite and extends over the Central igneous complex of Arran, has an amplitude of over 400 nT. To the east of Arran, prominent short wavelength anomalies occur over Renfrewshire, Dunbartonshire and Stirlingshire. These are as-

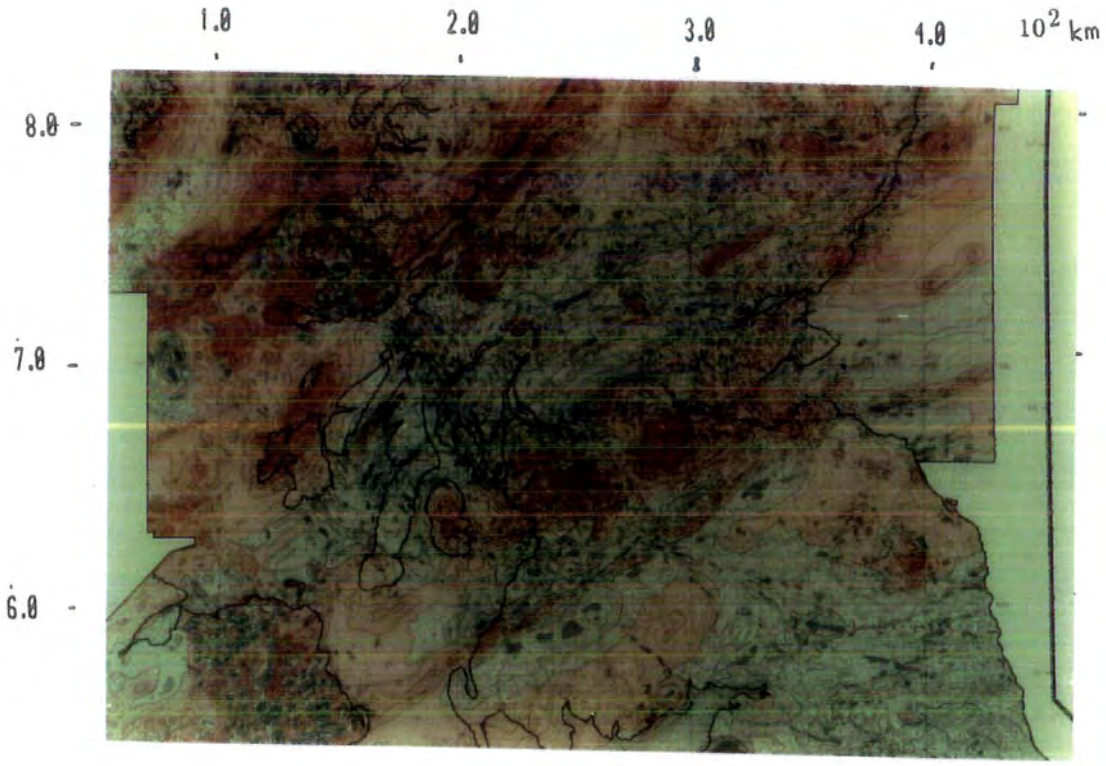

Figure 5.1a Aeromagnetic map of the Midland Valley from the British Geological Survey aeromagnetic map of Great Britain, compiled by W Bullerwell. The scale is 1:625000.

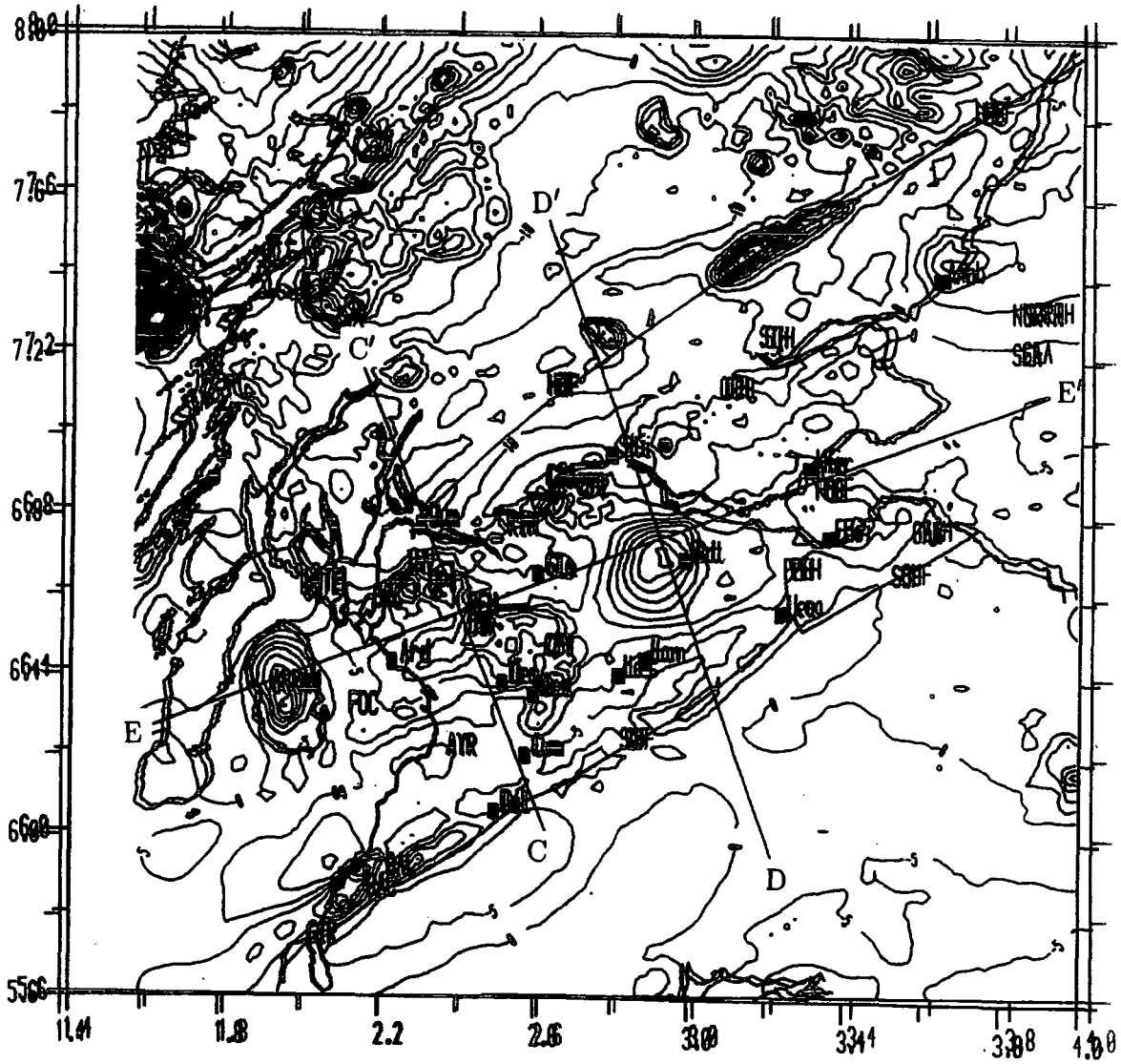

Arb-Arbroath, Ard-Ardrossan, AYR-Ayrshire, Bath-Bathgate, BAC-Ballantrae Complex, BAL-Ballantrae, Cum-Cumnock, CP1-Clyde Plateau lavas and Clyde Plateau area, CP2-Clyde Plateau lavas, Dal-Dalmellington, Dea-Deaconhill, Dis-Distinkhorn, Dum-Dumbarton (Dunbartonshire), DWF-Dusk Water fault, Edi-Edinburgh, FOC-Firth of Clyde, FOF-Firth of Forth, Gla-Glasgow, GAH-Garleton Hills, GIR-Girvan, GRC-Great Cumbrae, HBC-Highland Boundary Complex, HBF-Highland Boundary fault, INV-Inverclyde District, Kir-Kirkcaldy, KIH-Kilpatrick Hills, Lan-Lanark (Lanarkshire), Lea-Leadburn, Les-Lesmahago, OCH-Ochil Hills, PEH-Pentland Hills, REH-Renfrewshire, Sti-Stirling (Stirlingshire), CAA-Campsie area, SIH-Sidlaw Hills, SUF-Southern Upland fault.

Figure 5.1b Aeromagnetic map of the Midland Valley. The coordinates are in British National Grid (x10^2 km). The contour interval is 50 nT. The Southern Upland and Highland Boundarys fault are shown. The profiles CC′ and DD′ used in the modelling are also given.

sociated with the Carboniferous lavas. The anomalies in these areas are quite distinct and will be discussed later. Further east, an almost circular anomaly occurs over the Bathgate region but has no obvious surface representation. Its amplitude reaches over 400 nT. To the east of this circular anomaly, short wavelength anomalies dominate the region including Edinburgh, part of Firth of Forth and the Garleton Hills. These may be associated with the Carboniferous lavas which outcrop in the Garleton Hills region. To the northeast of the Midland Valley, a slightly elongated anomaly occurs over Arbroath with amplitude reaching about 350 nT. This anomaly lies at the southwestern end of a northeast-southwest trending positive anomaly occurring over the North Sea. No obvious strongly magnetized outcrops can be associated with this anomaly. While the Carboniferous lavas and Tertiary igneous rocks show prominent magnetic signatures, the late Silurian to Lower Devonian lavas do not. In some of the areas where these lavas outcrop (Ochil, Sidlaw and Pentland Hills), the aeromagnetic anomalies show only slight magnetic highs. They are of much lower amplitude than those over the Carboniferous lavas. This indicates that the late Silurian to Lower Devonian lavas are weakly magnetized compared to the Carboniferous lavas and the Tertiary igneous complex.

The aeromagnetic anomalies associated with the Carboniferous lavas can be classified into two groups:

(1) The anomalies over the Renfrewshire region (CP1). These are marked by mainly short wavelength positive anomalies with some amplitudes greater than 250 nT. They superimpose to form longer wavelength anomalies. The anomalies over Garleton Hills are included in this group although their amplitudes are lower.

(2) The anomalies over the Dunbartonshire (Kilpatrick Hills) and Stirlingshire (Campsie area, CP2). These anomalies exhibit both positive and negative peaks with amplitudes between about +250 nT to -400 nT and are generally of shorter wavelength than those of the CP1 lavas.

5.2 The pseudogravimetric map

The pseudogravimetric map (figure 5.2) uses a density to magnetization ratio of 150 kg/m^3: 1 A/m. The pseudogravimetric transformation, which suppresses the shorter wavelength anomalies, markedly affects the magnetic anomalies related to the Carboniferous lavas (figure 5.2). The magnetic highs over Renfrewshire (CP1) are smoothed into an elongated feature. The peak (about 45 mGal above a regional value) of the elongated pseudogravimetric anomaly high lies over the main outcrop of the Clyde Plateau lavas to the southwest of Glasgow but does not extend over the lava outcrops in the Deaconhill region. This may be due to the thinner sub-surface extension of the CP1 type lava here. The pseudogravimetric anomaly associated with the Carboniferous lavas north of Glasgow (CP2), however, is less well developed than those to the southwest of Glasgow. This may be caused by the different types of igneous associations as described later. The geological section (Paterson and Hall 1986) for the Stirling District indicates that the lavas are only slightly thinner than those in the Inverclyde District. The magnetic anomalies from east of Bathgate to the Garleton Hills region formed low amplitude pseudogravimetric anomalies, and those due to the late Silurian to Lower Devonian lavas are totally suppressed.

The effect of the transformation on the other magnetic highs such as those over Arbroath, the Ballantrae and Highland Boundary complexes is to smooth them out considerably. The Arbroath anomaly has a peak of about 30 mGal above the regional value, and the Ballantrae and Highland Boundary complexes have peaks at about 15-20 mGal. The elongated magnetic highs which mark the Southern Upland fault in the aeromagnetic map are not clearly resolved in the pseudogravimetric map. However, the medium wavelength anomalies over Arran and Bathgate are prominent on the pseudogravimetric map, with amplitudes of about 40 and 65 mGal above a regional value respectively.

A prominent feature on the pseudogravimetric map is a long wavelength elon-

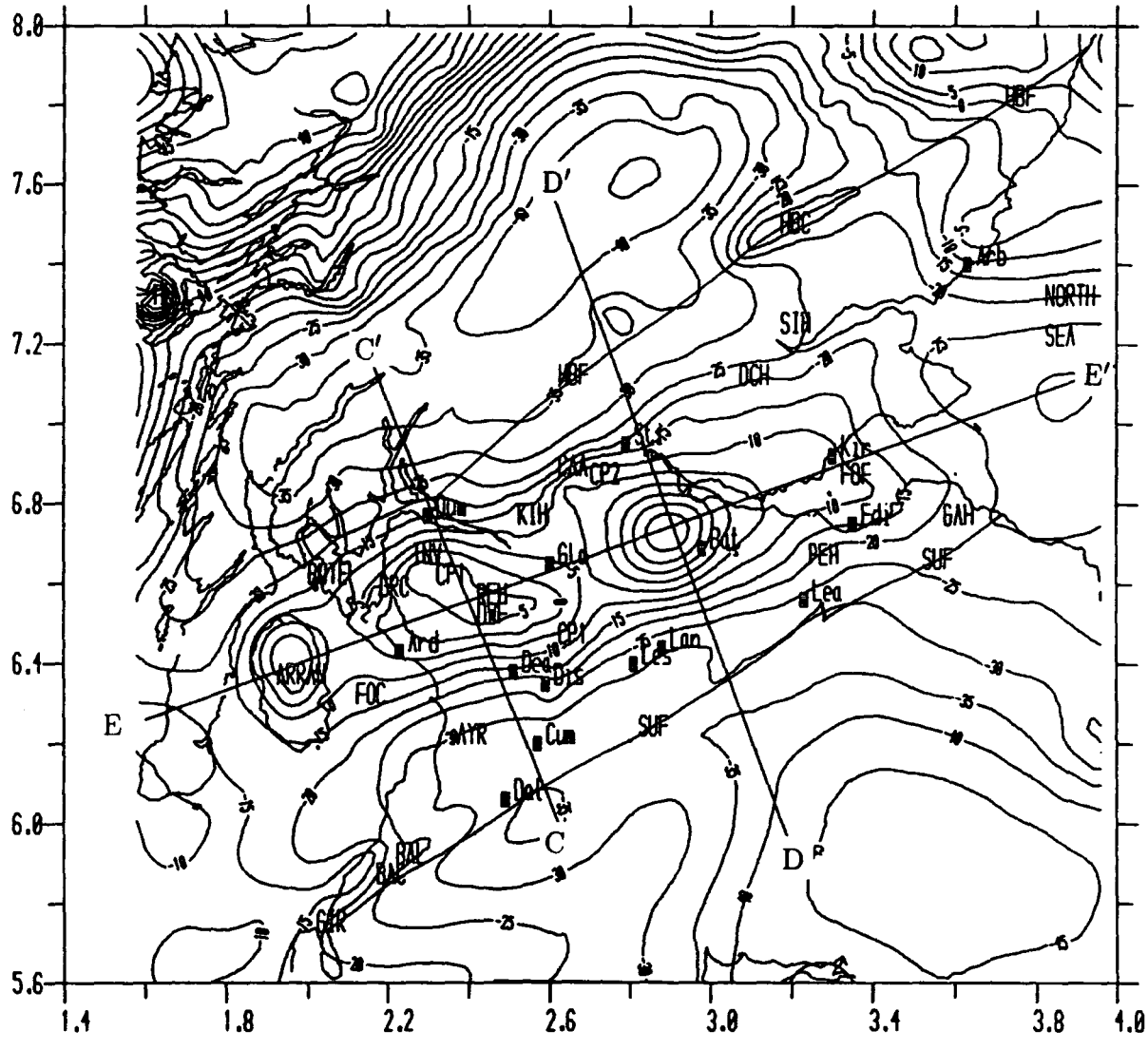

Figure 5.2 Pseudogravimetric map of the Midland Valley, transformed using density (kg/m^3) to magnetization (A/m) ratio of 150:1. The inclination and declination of the earth' field and magnetization are 70.3 and -10.6^o respectively. The cContour interval is 5 mGal. The locations and coordinates are as in figure 5.1b The. Southern Upland and Highland Boundary fault are shown. The profiles CC′ and DD′ used in the modelling are also given.

gated region of pseudogravimetric high covering almost the whole of the Midland Valley. This anomaly is not so obvious on the aeromagnetic map. Upward continuation of the aeromagnetic anomaly, however, clearly reveals this elongated feature (figure 5.3). The trend of the feature is oblique to the Southern Upland and Highland Boundary faults.

This elongated pseudogravimetric anomaly is bordered by almost parallel contours on both the northern and southern flanks and encloses the Arran, Bathgate and Clyde Plateau lava highs. The Arbroath anomaly is separated from this region, probably indicating differing genesis.

The separation of the superimposed anomalies of different wavelengths is problematical. However, if the sources of the shallow anomalies can be inferred, the separation of the deeper component may be carried out. This chapter discuss the modelling of the Clyde Plateau lavas anomaly, the separation of the different anomaly components and the modelling of the local Bathgate anomaly.

5.3 Geology

The Midland Valley is a graben-like feature with the almost parallel Highland Boundary and Southern Upland faults forming the northern and southern boundaries respectively. Figure 5.4 shows the geological map by Craig (1983). The present discussion of the geology is taken mainly from Craig (1983) and Cameron and Stephenson (1985).

There are no basement rocks exposed in the Midland Valley. However, crustal xenoliths found within the volcanic vents may be used to indicate the presence of a basement complex similar to the Lewisian granulites underlying the region (Graham and Upton 1978, Upton et al. 1983).

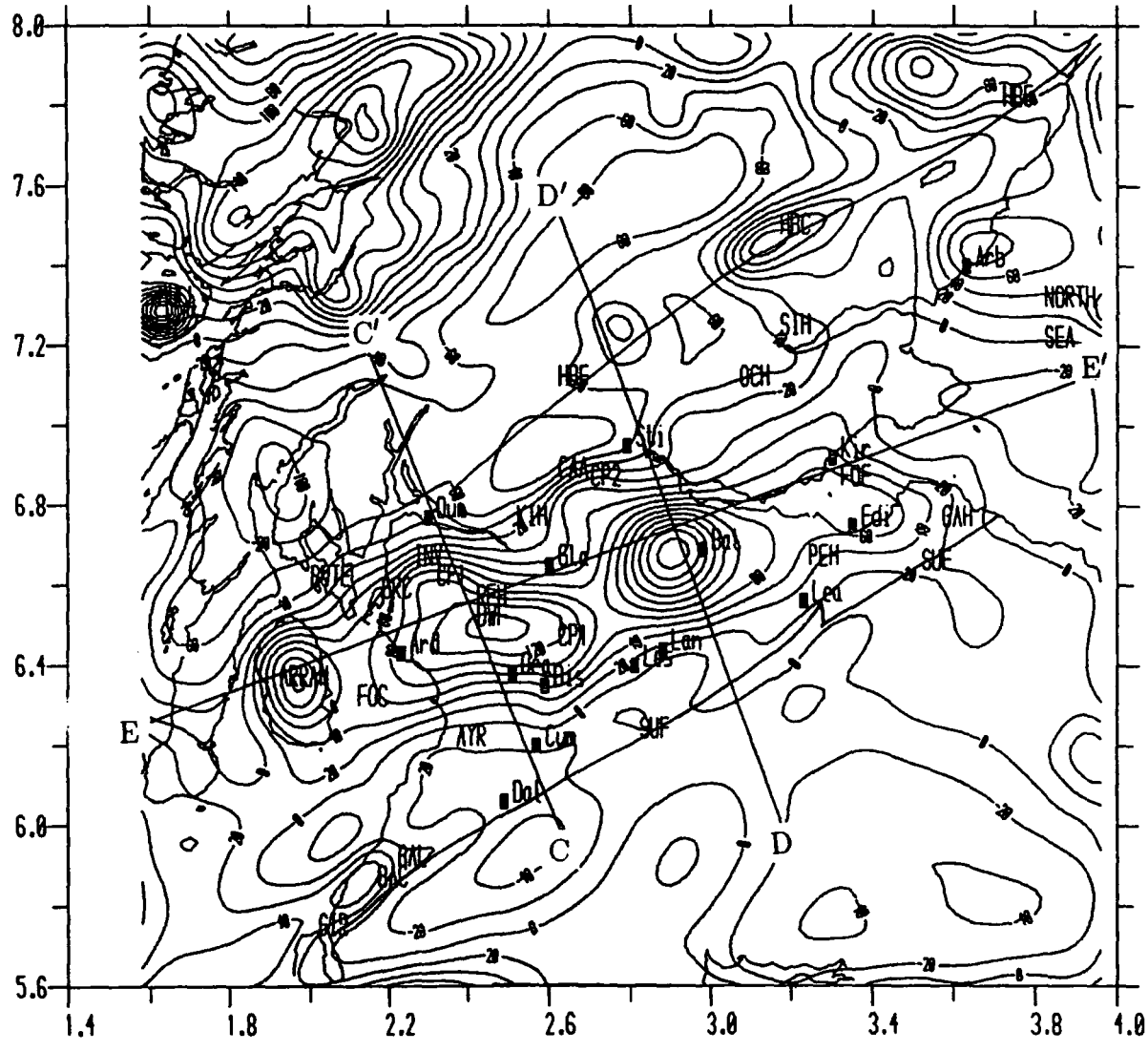

Figure 5.3 Aeromagnetic map of Midland Valley upward continued by 5 km. The contour interval is 20 nT. The locations and coordinates are as in figure 5.1b. The Southern Upland and Highland Boundary fault are shown. The profiles CC′ and DD′ used in the modelling are also given.

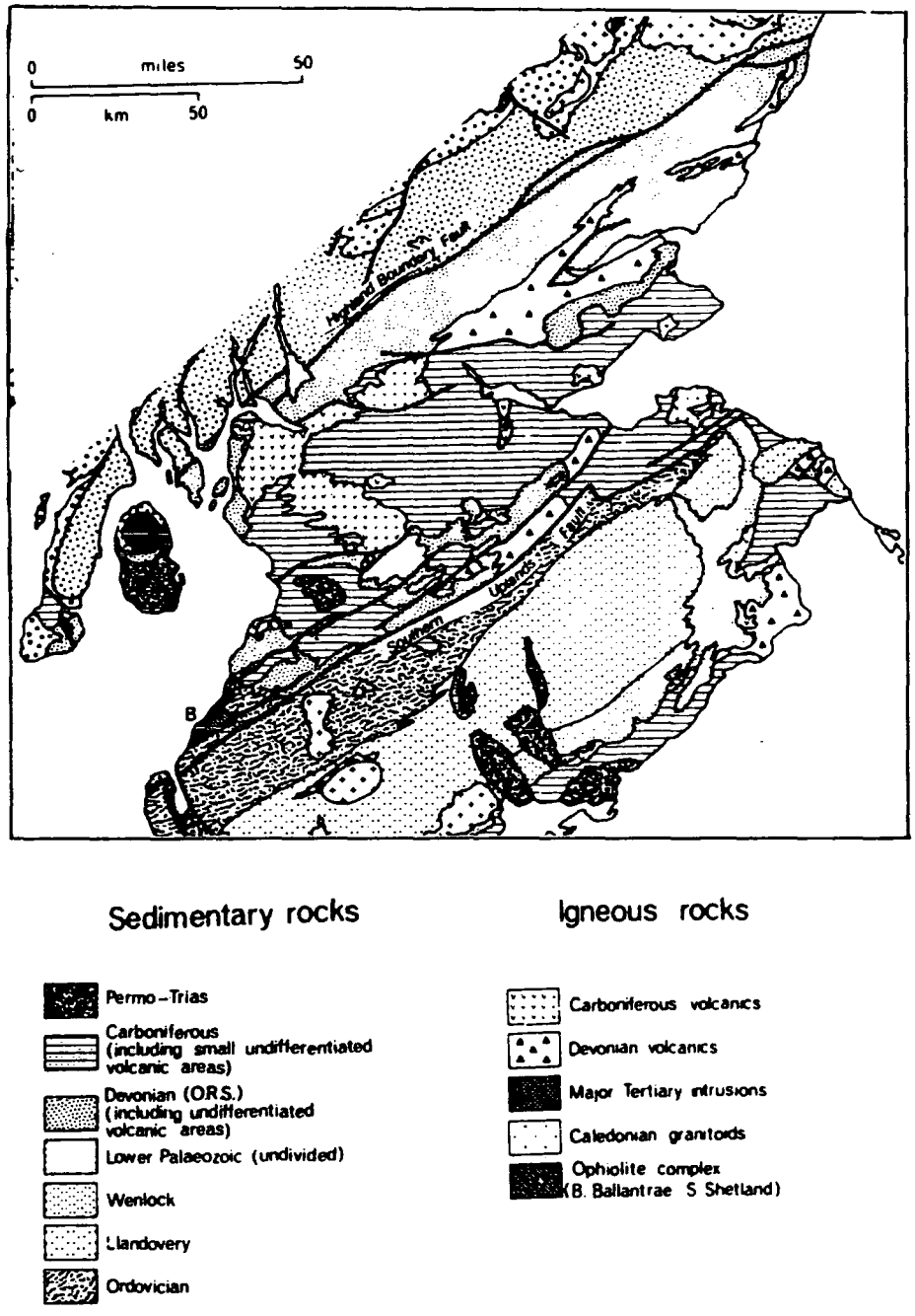

Figure 5.4 Simplified geological map of Midland Valley from Craig (1983).

The Ordovician and the Silurian are the oldest exposed rocks in the Midland Valley and consists mainly of strongly folded conglomerates, sandstones and mudstones. They occur as inliers, essentially in the Girvan-Ballantrae district (mainly Ordovician) and in the Lesmahago and Pentland Hills regions (Silurian). The Lesmahago inlier displays a thickness of about 2.5 km but the exposed sequences in other inliers are relatively thin (about 1 km). The Lower Palaeozoic Girvan-Ballantrae complex is a typical ophiolitic assemblage which includes serpentinites, pillow lavas and cherts (Watson 1983). The Highland Boundary Complex (Ordovician), also ophiolitic in character, consists of black shales, carbonates and pillow lavas (Dempster and Bluck 1989).

The Devonian Old Red Sandstone and the associated volcanic rocks cover a substantial area along the Highland Boundary fault. They also outcrop in the Pentland Hills, Lanarkshire and southwest Ayrshire. Only the Lower and Upper Old Red Sandstone occur in the Midland Valley and the Middle Old Red Sandstone (Middle Devonian) is missing. The Lower Devonian rocks include conglomerates, sandstones and lavas, while those of the Upper Devonian consist of sandstones and siltstones. Southeast of the Highland Boundary fault, the Lower Devonian rocks have an aggregate thickness of about 4-7 km while to the northwest of the Southern Upland fault, the Lower Devonian rocks are thinner. The thickest Upper Devonian rocks (about 3 km) are in the Firth of Clyde region. Carboniferous sediments and lavas cover a major part of the Midland Valley. The Carboniferous sediments are divided into the Calciferous Sandstone Measures, the Millstone Grit series and the Coal Measures. The thickness of each group varies and can reach up to 2 km. The Permian sandstones which occur in the central Ayrshire are the youngest sedimentary rocks within the Midland valley and have a thickness of up to 450 metres.

Early igneous activity is evident by the presence of igneous clasts in the Ordovician and Silurian inliers (Cameron and Stephenson 1985). The late Silurian to Lower Devonian volcanic activity displays a calc-alkaline suite of basalts, andesites,

dacites, rhyolites and pyroclastic rocks (Brown 1983). The rocks are largely exposed in the northwestern part of the Midland Valley, in the Ochil and Sidlaw Hills (thickness of up to 2 km). They also outcrop in the south in the Pentland Hills region (thickness of up to 1.8 km). In the Sidlaw Hills, the volcanic rocks are olivine basalts, basaltic andesites and dacite interbedded with the Old Red Sandstone sediments (Brown 1983). In the Ochil Hills, the rock types are similar, but include felsic intrusions and pyroclastics (Francis 1983). In the Pentland Hills, tuffs and Old Red Sandstone sediments are intercalated with olivine basalts, pyroxene and hornblende andesites and rhyolites (Brown 1983). A number of igneous intrusions also occurred during this period but are of small size. The largest is the Distinkhorn complex (Cameron and Stephenson 1985).

The next phase of igneous activity started during the Lower Carboniferous with widespread formation of alkali olivine-basalt and related lavas. Localised events occurred up to the Lower Permian. The most notable volcanic sequence is the Clyde Plateau lavas (Lower Carboniferous). Most of the lavas are basic (Cameron and Stephenson 1985). MacDonald (1975) classified the lavas into three associations. The first association consists of macroporphyritic lavas (the compositions range from ankaramite to trachyte) which includes those of the Renfrewshire area and Garleton Hills. The second consists of the microporphyritic lavas which includes the lavas of the Kilpatrick Hills and Campsie area. The compositions are mainly feldspar-phyric hawaiites and mugearites. The third association is of ankaramites and olivine or olivine-pyroxene microporphyritic basalt occurring in most Namurian and younger lavas. The lavas have varying thickness, probably ranging up to 1.0-2.5 km in the Clyde Plateau. The rocks in the region are cut by quartz-dolerite dykes and sills (late Carboniferous) towards the end of the vulcanicity. The dyke swarm has a general eastwards trend cutting rocks from Lower Devonian to Middle Coal Measures.

Igneous activity during the Tertiary period was dominated by the Tertiary volcanic centres and their associated dyke swarms and sills. Some of the dykes are

related to the dyke swarm originating from Mull (Cameron and Stephenson 1985). The general trend is northwest-southeast. On the Isle of Arran, Tertiary igneous activity formed the Northern Granite, Central Igneous complex and the Tighvein complex (Emeleus 1983).

The graben-like feature of the Midland Valley shows that the region has been downfaulted along the boundary faults. In the northeastern part of the Midland Valley, the Highland Boundary fault has been estimated to be downthrown by about 2.5-3.0 km, with the main displacement probably occurring before the deposition of the Upper Devonian rocks (Cameron and Stephenson 1985). On the Southern Upland fault, the main displacement was probably during the Lower and Middle Devonian with a pre-Carboniferous throw of about 0.9 km with some accompanying lateral movements (Cameron and Stephenson 1985). The recent view is that the lateral movements were large and the boundary faults are essentially transcurrent faults. Ordovician lateral movements have been suggested and inferred by many workers (Anderson and Oliver 1986, Elders 1987, Hutton 1987, Dempster and Bluck 1989, Thirlwall 1989).

A number of evolutionary models for the Lower Palaeozoic have been presented by various workers. One evolutionary model is that the Midland Valley was a fore-arc basin during the Ordovician and Silurian separating an accretionary prism to the south from a basement-arc terrain to the north (e.g. Dewey 1971, Lambert and McKerrow 1976, Leggett et al. 1983). Another evolutionary model is that the Midland Valley originated from an inter-arc region bounded by a back-arc basin to the north and a fore-arc basin to the south (Longman et al. 1979, Bluck 1983,1985, Williams and Harper 1988). Hutton (1987) interpreted the Midland Valley as a detachment from the Laurentian foreland. The ophiolites were obducted onto the Midland Valley during the Lower Ordovician. This detached Midland Valley moved alongside the Laurentian continent and reached the present position by a large-scale lateral movement. Dempster and Bluck (1989) suggested that none of the Scottish

basement including the Midland Valley were in situ relative to the Laurentian continent. They also suggested that the Highland Boundary complex is a part of the Midland Valley and was not in contact with the Dalradian to its north during the Ordovician. During the Silurian, the Midland Valley was still a basin (eg. Williams and Harper 1988). The present position of the Midland Valley was reached by the Devonian (Hutton 1987, Thirlwall 1989). The Lower Devonian rocks were deposited in the newly subsiding graben unconformably over the older rocks. The Middle Devonian was a period of uplift, folding, faulting and erosion. The Upper Devonian rocks thus lie unconformably over the Lower Devonian rocks. They pass upwards into the Carboniferous sediments. Deposition of the terrestrial Permian rocks occurred in restricted localities. The present landscape is mainly due to erosion during the Tertiary and glaciation during the Quaternary.

5.4 Previous geophysical work

Early gravity work (McLean and Qureshi 1966) in the western part of the Midland Valley indicated a positive regional gravity anomaly over the Midland Valley. This was explained as due to the relatively thinner crust relative to the Grampian Highlands (north of the Highland Boundary fault) and the Southern Uplands (south of the Southern Upland fault). The regional gravity map of Hussain and Hipkin (1981), shows a relatively strong gradient along the Highland Boundary fault. Hipkin and Hussain (1983) suggested that the crustal changes which explain the gravity anomaly along the Southern Upland fault occur within the lower crust beneath the Southern Uplands. In the Midland Valley, local gravity highs generally occur where high positive magnetic anomalies are present. The gravity high over Arran has been modelled by McLean and Wren (1978) as an elongated basic mass with the top at a depth of at least 1.3 km.

Seismic studies reveal that the structure beneath the Midland Valley is made

up of three to four main crustal velocity layers (Table 5.1). The LISPB deep crustal profile (Bamford et al. 1977) which crosses the Midland Valley in an almost north-south direction near Edinburgh defines a three-layered crustal structure. The top two layers were attributed to Palaeozoic rocks and the third deeper layer, the upper boundary of which lies at 7-8 km depth, was interpreted as crystalline basement. P-wave studies from LOWNET (Crampin et al. 1970) yielded a three-layered upper crustal structure similar to Bamford et al. (1977). Based on refraction studies traversing the region, Davidson et al. (1984) obtained a three-layered upper crustal structure. The top layer has been assigned to Carboniferous and Upper Old Red Sandstone rocks, the middle layer to Lower Old Red Sandstone and Lower Palaeozoic rocks, and the third layer is top crystalline basement. Both the Upper Palaeozoic and Lower Palaeozoic sequences correspond to layer one of Bamford et al. (1977) and Crampin et al. (1970). According to Davidson et al. (1984) the crystalline basement starts at a shallow depth of about 3-4 km. The deeper crystalline basement was not defined. Conway et al. (1987) presented seismic profiles running almost east-west along the Midland Valley, which yielded a crustal structure similar to Davidson et al. (1984) as well as a deeper basement (the top is at 7-9 km depth) which may be of the amphibolite-granulite facies. Hall (1974) interpreted a seismic reflection survey of the Clyde Plateau lavas between Glasgow and Ardrossan as indicating a lava thickness of at least 900 metres.

Previous magnetic studies have mainly dealt with localised anomalies. Park (1961) carried out a vertical field magnetic survey over some localised anomalies in the vicinity of the Dusk Water fault. McLean and Walker (1978) studied some of the magnetic anomalies in the Firth of Clyde and Bute, some of which are related to the Clyde Plateau lavas. A number of studies have also been carried out on the Bathgate magnetic anomaly. Powell (1970) modelled the source as due to a spherical body 16 km in diameter with the top 4.8 km deep but later (Powell 1978a) attributed it to either inhomogeneity within the basement (ultrabasic rocks) or a disk-shaped basic intrusion having similar magnetic properties to the Carboniferous lavas. Hossain

L	Crampin et al. 1970	Bamford et al. 1977	L	Davidson et al. 1984	Conway et al. 1987	Freeman et al. 1988
1	v=3.0 b<3-4 UP	v=4.5-5.0 b<3-4 UP	1	v=3.0-3.7 b<3 C,UORS	v=2.7-5.0 b<1.5-3.5 C,UORS	
			2	v=4.0-5.5 b=3-7 LORS,LP	v=5.2-5.7 b=3-7 LORS,LP	
2	v=5.67 b=7-8 LP	v=5.8-6.0 b=7-8 LP	3	v=6.0-6.1 b=7-8 TCB	v=5.9-6.1 b=7-9 TCB	b=5sTWTT
3	v> 6.4 LCB	v> 6.4 LCB	4		v> 6.4 LCB	b=10.5sTWTT

C - Carboniferous, UORS - Upper Old Red Sandstones, LORS - Lower Old Red Sandstones, UP - Upper Palaeozoic, LP - Lower Palaeozoic, TCB - Top crystalline basement, LCB - Lower crystalline basement, v - velocity (km/s), b - base of layer (km), L - layer, sTWTT - sec. two way travel time.

Table 5.1 Crustal structure from previous seismic studies.

(1976) suggested thickening of a near surface lava extending to a depth of about 5 km or a deep intra-basement igneous intrusion with its top at a depth of 10 km. Davidson et al. (1984) proposed that the source of the Bathgate magnetic anomaly originates within the top crystalline basement. Conway et al. (1987) suggested that the source is a thick pile of weathered or vesicular lava within the Palaeozoic rocks but no modelling was carried out.

5.5 Susceptibility and magnetization values

The bulk susceptibility and magnetization values of some of the rock types in the Midland Valley and the adjacent regions have been reported in the literature. The susceptibility values in c.g.s. units have been converted to magnetization values in the earth's magnetic field in SI units (table 5.2).

The Carboniferous lavas have varied magnetization with values up to 5.5 A/m (Cotton 1968). The high and varied magnetization causes the prominent short wavelength magnetic anomalies. The major part of the Devonian lavas is probably much less magnetic since the magnetic anomalies where these lavas outcrop are hardly visible on the aeromagnetic map. Powell (1970) reported that the Devonian Old Red Sandstone lavas with a magnetization value of 1.5 A/m may partly cause the elongated magnetic anomaly northeast of Dalmellington (table 5.2).

Some of the Tertiary sills have high susceptibility values (McLean and Wren 1978) but the anomalies are inconspicuous on the aeromagnetic map. The serpentinites also have high susceptibility values and occur mainly within the Ballantrae complex and the Highland Boundary complex.

Reference	Location	Rock types	age	Mag. in earth field (A/m)
Cotton 1968	Clyde Plateau	lavas	Ord.	.95-5.50
Powell 1978b	Girvan-Ballantrae	serpentinite	Ord.	3.00
	Girvan-Ballantrae	volcanic and sedimentary	Ord.	1.25
	Girvan-Ballantrae	basic rocks and gabbros	Pre-Ord.	0.25
Powell 1978a	-	vent rock	-	3.0
McLean and Wren 1978	western MV	sill	Ter	0.002-1.10
	Millstone	lavas(olivin-basalt)	Carb.	0.85-1.15
	Clyde Plateau	lavas(olivin-basalt)	Carb	1.40-3.60
	Argyll	dyke	Ter.	1.25-1.75
Kelling 1961	Barrhill	greywackes	Ord.	0.29-0.65
	Barrhill-Newton Steward	greywackes	Ord.	0.42
Floyd and Trench 1988	Scaur Water	greywackes	Ord.	< .55
Powell 1970	Dalmellington	Spilite/greywackes	Ord.	1.5
	NE Dalmellington and New Cumnock	Spilite/greywackes and ORSL (along SUF)	Ord. Dev.	1.5
	Central Highland	Dalradians	Pal	weak
Trench et al. 1988	Ballentrae	ophiolites	Ord.	0.001-5.0

Pal-Palaeozoic, Ord.-Ordovician. Dev.-Devonian, Ter.-Tertiary, Carb.-Carboniferous, ORSL-Old Red Sandstone lavas, MV-Midland Valley, SUF-Southern Upland fault

Table 5.2 Measured magnetization of the different rock types in the Midland Valley and the adjacent areas.

5.6 Modelling procedure

The elongated long wavelength magnetic and pseudogravimetric anomalies over the Midland Valley are bordered on the northwestern and southeastern sides by anomaly lows. Modelling of the source and those of the local anomalies is best carried out across this elongation. A line parallel to this elongation was first estimated. The line EE′ (figure 5.2) can be drawn to pass near the apex of the Arran and Bathgate pseudogravimetric anomalies and over the Clyde Plateau lavas anomaly. Profiles perpendicular to this line have been used for modelling. The profile CC′ for modelling the Clyde Plateau lavas anomaly passes at about the middle of the Clyde Plateau lava anomaly elongation. The profile DD′ used for modelling the Bathgate anomaly passes near the apex of the local Bathgate pseudogravimetric anomaly.

The limited strike extent of the source of the local anomalies such as the Bathgate anomaly means that standard two-dimensional modelling which assumes large strike extent may not give an accurate result. True three-dimensional modelling as discussed in the previous chapter is unnecessarily complicated and thus the two-dimensional modelling with an end correction factor has been used where required.

Magnetic modelling was initially carried out to obtain the magnetic anomaly of the Clyde Plateau lavas. This is possible because the depth extent and the magnetization of the Clyde Plateau lavas are quite well defined as described in the literature. The modelling has been used to indicate the validity of using magnetization along the earth's magnetic field and to determine the presence of a regional component. The pseudogravimetric modelling was also used to show the presence of a deeper source. The final modelling of the sources used both the magnetic and pseudogravimetric methods. Pseudogravimetric modelling was first carried out to give an estimate of the model. The magnetic anomaly of the model was then calculated and compared to the observed magnetic anomaly. The model was modified to obtain a reasonable fit. Only a general fit to the observed magnetic anomaly was obtained at this stage.

The gravity anomaly of this modified model was then recalculated and compared to the observed pseudogravimetric anomaly, and readjustment to obtain a better fit was again carried out. These steps were carried out until a model which gives a satisfactory best fit to both the observed pseudogravimetric and magnetic anomalies was obtained. The magnetic optimization routine was also used for modelling.

5.7 The Clyde Plateau lavas

5.7.1 The magnetic and the pseudogravimetric profiles, and the geology

The profile CC′ (figures 5.1 and 5.2) chosen to model the Clyde Plateau lavas passes near Dunbarton and Deaconhill. The depth to the base of the lavas in these areas has been reported in the literature and the surface outcrop is clearly shown on geological maps. The magnetic profile (figure 5.5) has an amplitude of about 350 nT above a regional value. It has a number of distinct short wavelength components. The pseudogravimetric transformation suppresses these short wavelength anomalies to give a broad positive feature across the Midland Valley (figure 5.5). The resulting pseudogravimetric anomaly has an amplitude of about 45 mGal assuming density to magnetization ratio of 150 kg/m^3 : 1 A/m. Correlation of the pseudogravimetric and the aeromagnetic anomalies with the geology along profile CC′ is discussed below.

The Highland Boundary fault zone corresponds to a local magnetic high, and it can also be identified in the pseudogravimetric profile by a local change of gradient (figure 5.5). This local magnetic high occurs over the Old Red Sandstone and is probably due to the Old Red Sandstone lavas and the Highland Boundary complex rocks along the fault. Further south along the profile, the boundary between the Clyde Plateau lavas and the Old Red Sandstone is marked by a local magnetic low. This forms the northern limit of the Clyde Plateau lavas outcrop. This boundary,

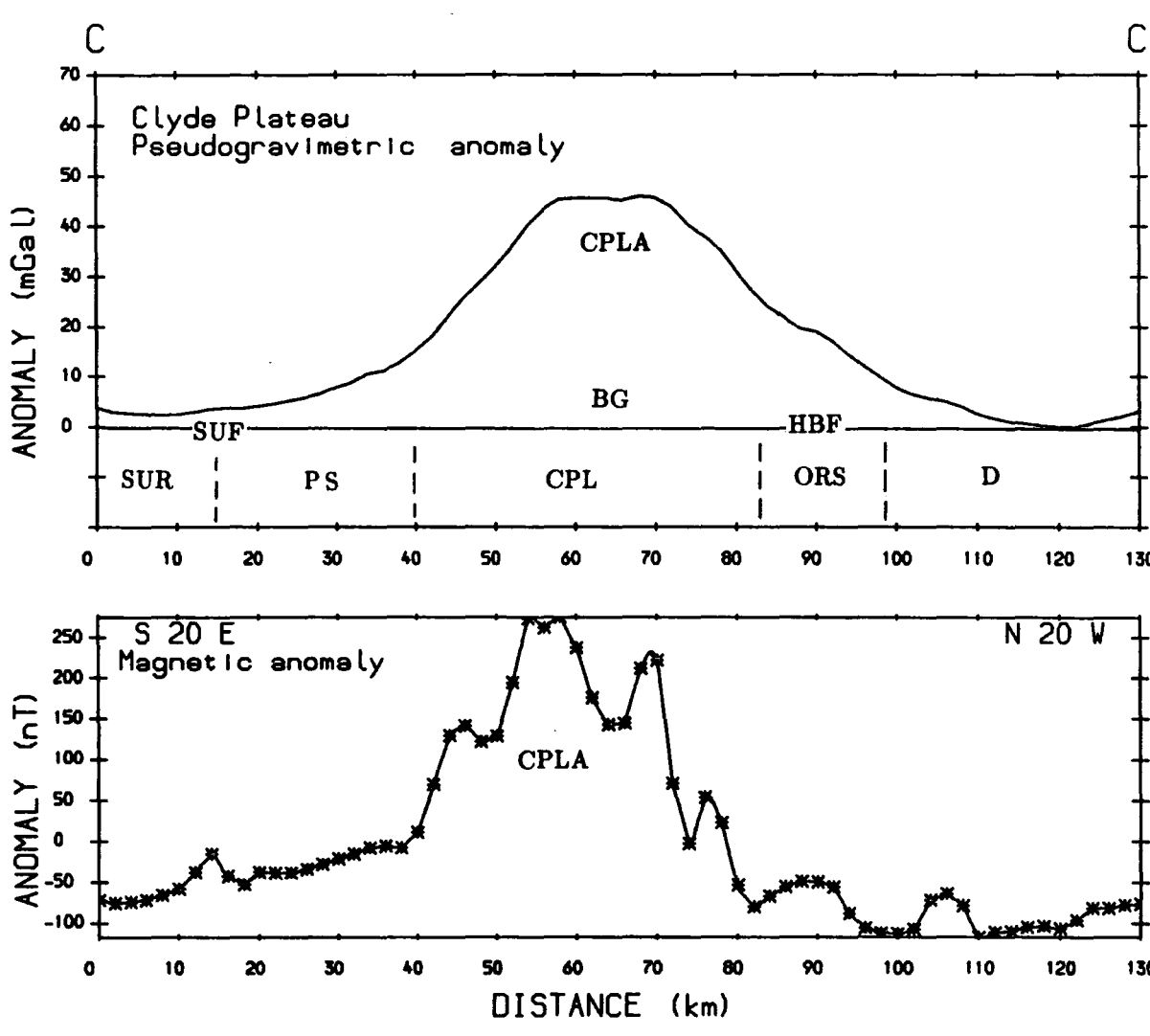

SUR - Southern Upland rocks, PS - Palaeozoic sedimentary rocks, CPL - Clyde Plateau lava, ORS - Old Red sandstone, D - Dalradians , SUF - Southern Upland fault, HBF - Highland Boundary fault, BG - background anomaly, CPLA - Clyde Plateau lavas anomaly

Figure 5.5 Pseudogravimetric and magnetic anomalies (profile CC′ figures 5.2 and 5.1 respectively), and the surface geology along the same profile.

is not obvious on the pseudogravimetric profile. The Clyde Plateau lavas do not occur north of the Highland Boundary fault. In the southern part of the profile, the lavas are bordered by the Old Red Sandstones. The boundary is indicated in the magnetic profile by a marked change of gradient. In the pseudogravimetric profile the boundary is marked only by a slight change of gradient. The Palaeozoic sedimentary rocks here are probably weakly magnetized. The Southern Upland fault zone is marked by a local magnetic high and is not obvious on the pseudogravimetric profile. Within the Clyde Plateau lavas the magnetic profile shows a number of short wavelength features. These may be related to lavas of locally different magnetization, to local vents or dykes, or to faulting.

The magnetic profile clearly defines the boundary between the highly magnetized Clyde Plateau lavas and the less magnetic surrounding rocks. This is not obvious on the pseudogravimetric profile. Comparison of the magnetic and pseudogravimetric anomalies with the geology suggests that the Clyde Plateau lavas anomaly (CPLA) is superimposed on a background anomaly (BG).

5.7.2 Thickness and magnetization of the Clyde Plateau lavas

Stratigraphic sections (Paterson and Hall 1986) along the northern Midland Valley (northern Arran, South Bute, Great Cumbrae, Inverclyde District, Dumbarton District and Stirling District) indicate that the Clyde Plateau lavas are thickest in the Inverclyde District reaching a measured thickness of 1 km. Along the Dusk Water fault, the thickness of the lava has been reported to be at least 300 m (Park 1961). A seismic reflection survey of the Clyde Plateau lavas north of Ayrshire and Renfrewshire indicated that the lava thickens southwestward from Glasgow area (Hall 1974). A thickness of 900 m was reported. A seismic refraction profile within the Midland Valley (Conway et al. 1987) which crosses the Clyde Plateau gives a velocity of up to 5 km/s which may be associated with the lavas. The 5 km/s velocity layer

reaches a depth of about 2.5 km.

The bulk susceptibility values of the Clyde Plateau lavas measured by Cotton (1968) yields a mean magnetization in the earth's magnetic field, of about 2.5 A/m. The measurements of McLean and Wren (1978) gave magnetization values ranging from 1.4 to 3.6 A/m. The Lower Palaeozoic rocks (except the ophiolitic complexes) generally have low magnetization values. The late Silurian to Lower Devonian lavas along the profile do not contribute significantly to the long wavelength anomaly.

5.7.3 Modelling

Magnetic modelling was first carried out assuming that the observed anomaly along the profile CC′ (figure 5.5) is caused only by the lavas. The constraints applied to the model are, (1) the thickness of the lavas is 1-2.5 km and (2) the surface extent of the lavas is restricted by the outcrop and the topography of the lavas. The width of the base of the lavas is taken to be smaller than the surface outcrop. A base wider than the surface outcrop is geologically unrealistic because the lavas would then underlie the older rocks. The first model (model 1) assumes a body magnetized along the earth's magnetic field direction. The anomaly calculated from this model is given in figure 5.6. A second model (model 2) assumes remanent magnetization is present in the lavas. The mean inclination and declination of the remanent magnetization for the Lower Carboniferous lavas are about 209^o and 30^o respectively (Tosvik et al. 1989). Figure 5.7 shows the calculated magnetic anomaly obtained by using the constraints mentioned earlier and the remanent magnetization direction given above.

The calculated magnetic anomaly for model 1 gives a good general correlation to the observed anomaly and clearly displays a positive magnetic high over the outcrop of the lavas. This is flanked by negative values on both sides with lower values on the northern side. The observed magnetic anomaly is also flanked by negative values

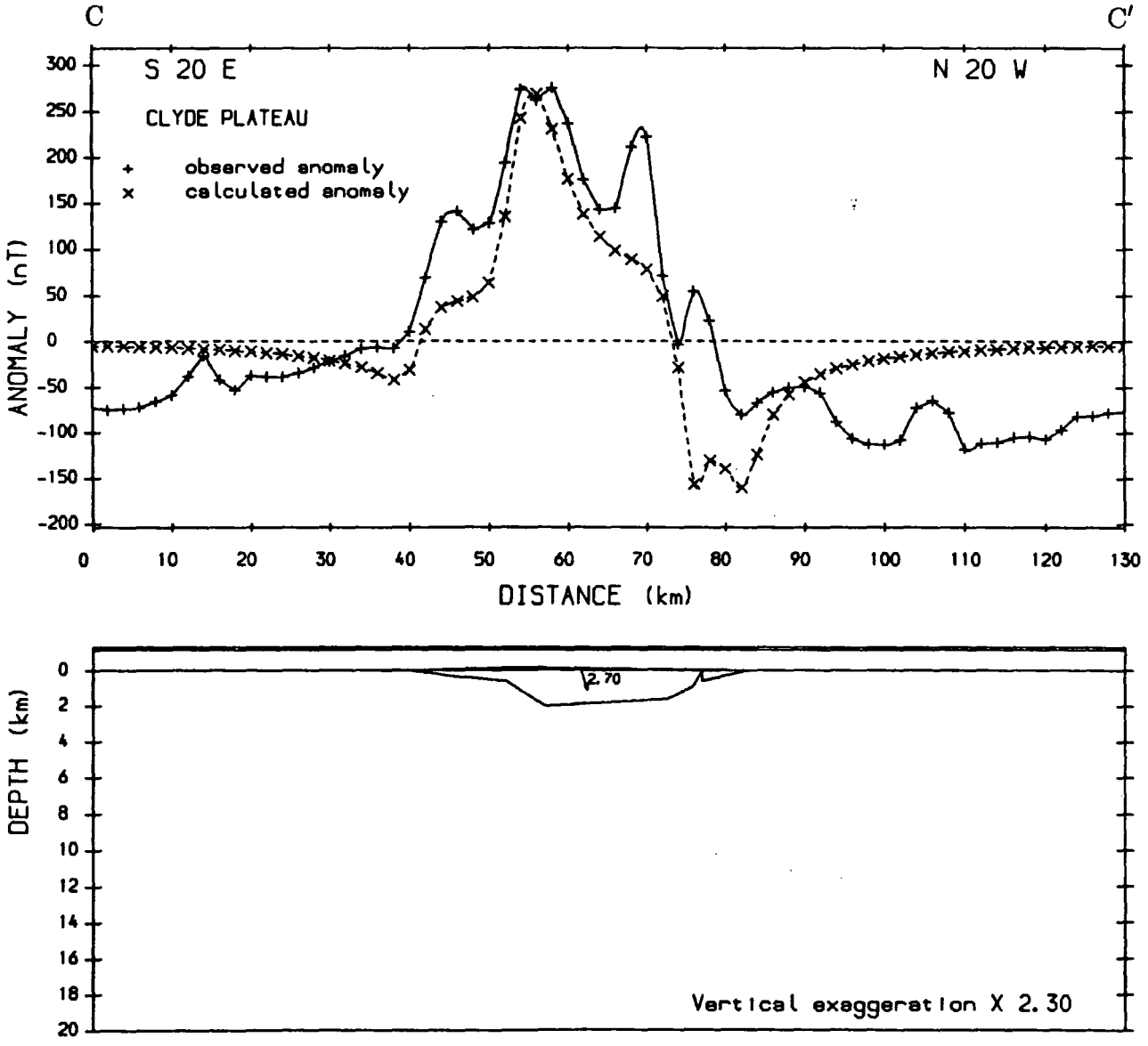

Figure 5.6 Model of the Clyde Plateau lavas having magnetization along the earth's magnetic field direction (the inclination is 70.3° and declination is -10.4°). The calculated anomaly has a lower negative value north of the lavas. This is similar to the observed anomaly. The magnetization is 2.7 A/m.

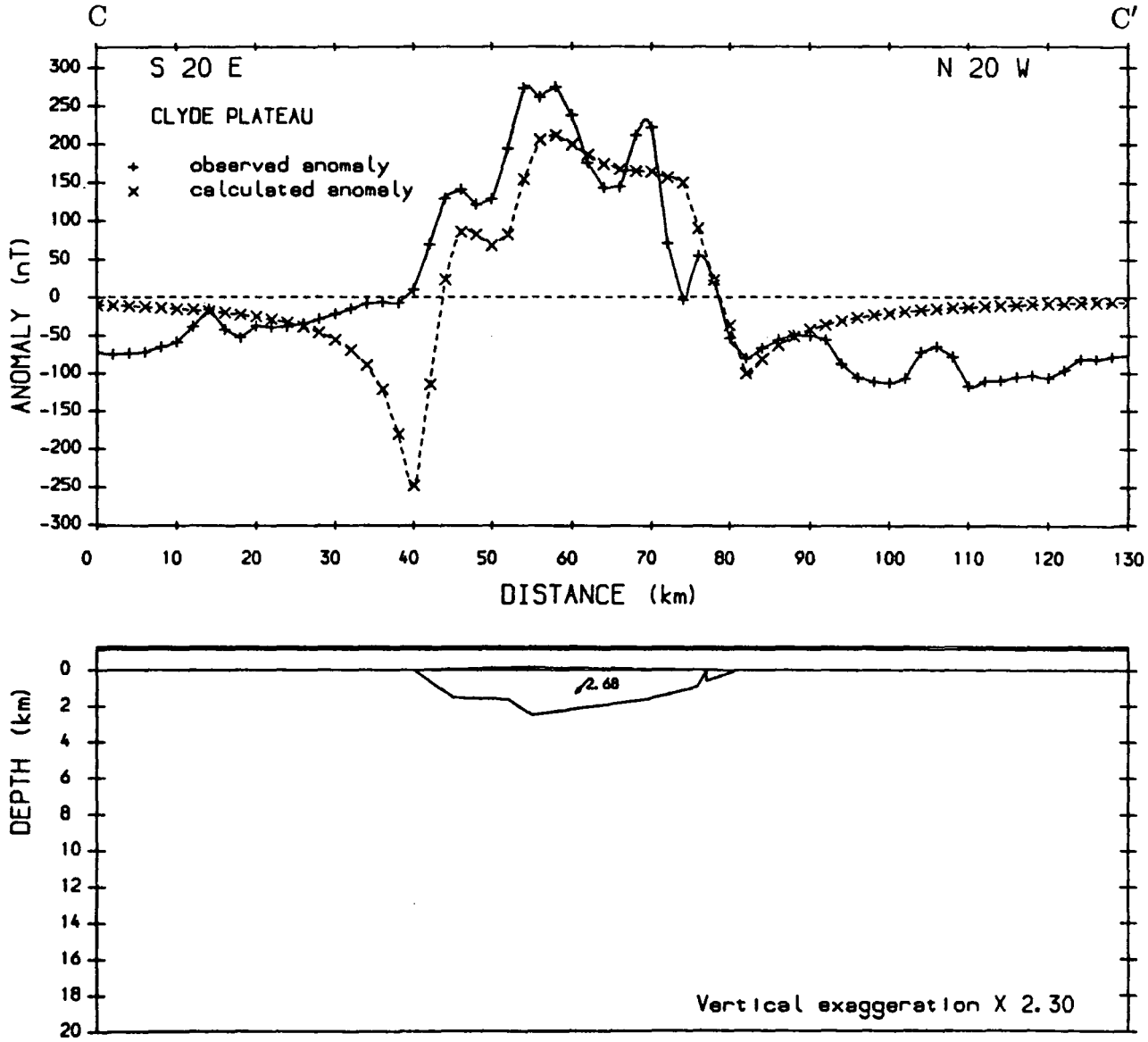

Figure 5.7 Model of the Clyde Plateau lavas having remanent magnetization in the palaeofield direction (the inclination is 30° and declination is 209°). The direction of the earth's magnetic field is as in figure 5.6. The calculated anomaly has a lower negative value south of the lavas body. The magnetization is 2.68 A/m.

with lower values on the northern side. Model 2 which has a remanent magnetization can also produce a positive magnetic high with negative values on both sides. The negative values are lower on the southern side. This conflicts with the observed magnetic anomaly which has more negative values on the northern side.

The modelling carried out above suggests that the anomaly calculated using a model with its magnetization along the earth's magnetic field can simulate the observed anomaly more closely within the accuracy of the modelling. This model is probably more appropriate than the model with a strong remanent magnetization in the Carboniferous field direction. The reason why the remanent magnetization does not contribute substantially to the total magnetization has been discussed in chapter 4. Among the causes which may reduce the contribution of the remanent magnetization in the lavas as mentioned by Torsvik et al. (1989) are, (1) the presence of both normal and reverse polarity in individual lava layers with some layers having dual polarity, (2) grain growth and oxidation, and (3) viscous behaviour. Subsequent modelling and discussion will be based on the assumption that the magnetization is induced along the present earth's magnetic field.

The calculated anomaly along profile CC′ for model 1, shows a general similarity with the expected lavas anomaly but does not explain the observed anomaly fully. The calculated anomaly away from the lavas is at a higher level than the observed magnetic anomaly on both sides. The differences in the longer wavelength component suggest that the anomaly of the Clyde Plateau lavas is probably being superimposed on an anomaly from deeper sources. This has been tested using pseudogravimetric modelling. The sources were initially assumed to be caused only by the lavas. The lava body (figure 5.8) which can by itself produce an anomaly that fits the observed pseudogravimetric anomaly has to extend across the Highland Boundary fault. As the lavas terminate well south of the Highland Boundary fault, such a model does not explain the pseudogravimetric profile. Besides the lavas, other sources must contribute to the anomaly. The outcropping Dalradian rocks north of the Highland

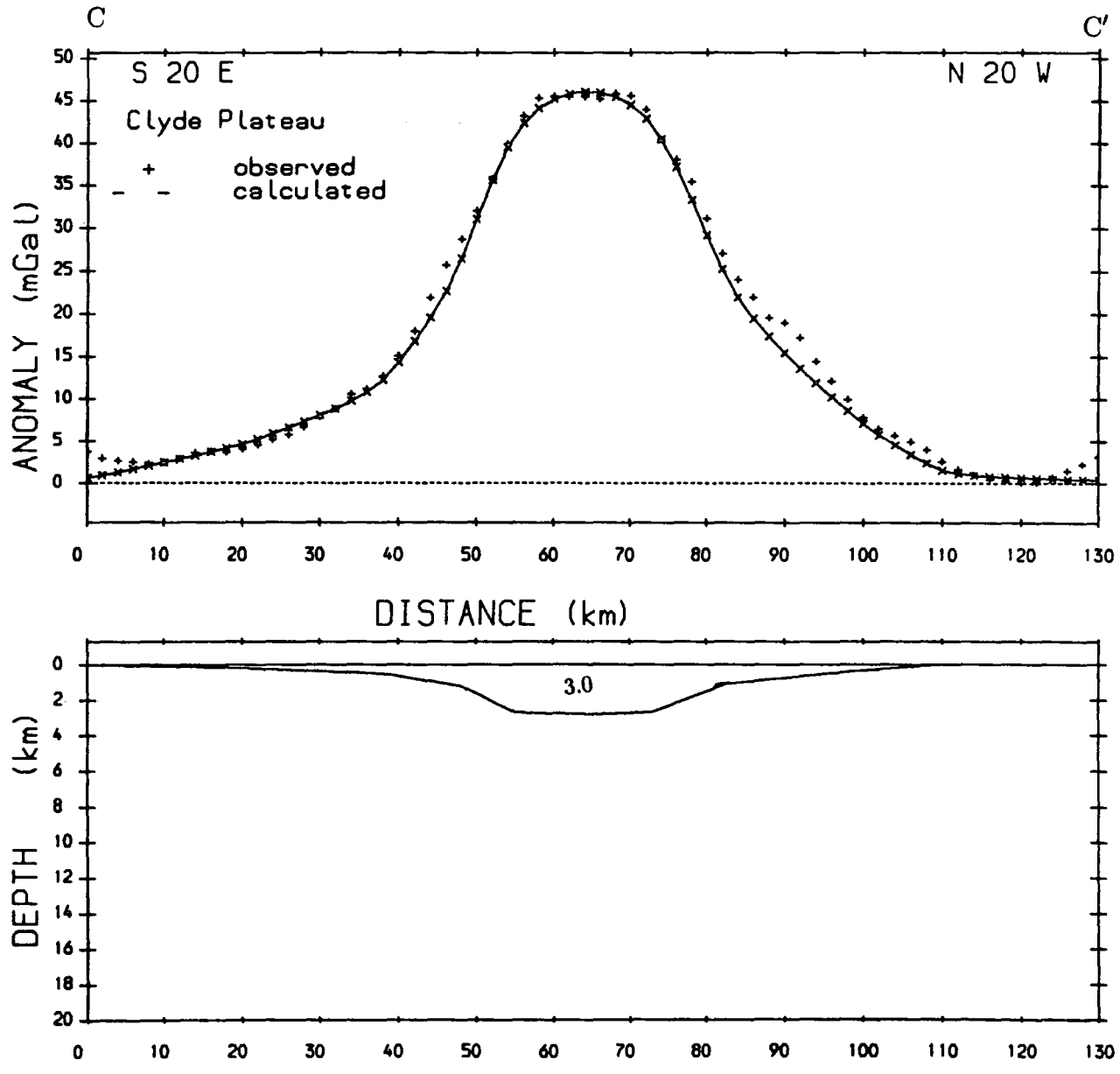

Figure 5.8 Pseudogravimetric modelling assuming that observed pseudogravimetric profile is caused only by the Clyde Plateau lavas. The magnetization used is 3.0 A/m. The density (kg/m^3) to magnetization (A/m) ratio is 150:1.0.

the Highland Boundary fault are weakly magnetized (Powell 1970). Therefore, they probably do not contribute much to the pseudogravimetric profile. A contribution from a deeper source seems essential. Similarly along the southern part of the profile, the lavas would need to extend over the outcropping Old Red Sandstones to completely explain the anomaly. This is not possible. The weakly magnetized Palaeozoic sedimentary rocks are unlikely to contribute significantly to the pseudogravimetric profile. The pseudogravimetric modelling thus confirms that the Clyde Plateau lavas cannot be the only source of the anomaly along the profile CC′. Furthermore, the Clyde Plateau lavas anomaly calculated from model 1 (figure 5.6) can only explain the central positive part of the observed pseudogravimetric (figure 5.9).

From the modelling done, it can be concluded that the magnetic anomaly along profile CC′ is partly caused by the Clyde Plateau lavas and partly caused by another deeper source. The deep source produce a broad positive anomaly upon which the Clyde Plateau lavas anomaly is superimposed.

The separation of the different anomaly components is problematical. However, since the Clyde Plateau lavas are quite well constrained, the contributions from the deeper source can be estimated. This is assumed to be a single body. This body is taken to lie within the deeper crystalline basement and thus the top of the body is deeper than 7 km. An average magnetization value of 1.5 A/m was used in the modelling. The geometry of the deep source was first estimated by modelling the inferred regional component of the pseudogravimetric profile (figure 5.10). The anomalies due to the Clyde Plateau lavas (figure 5.6) and the deep body were then combined and the resulting anomaly was compared with the observed pseudogravimetric anomaly. The geometries of the lavas and the deep source were changed until a reasonable fit of the calculated anomaly to the observed pseudogravimetric anomaly was obtained. The magnetic anomaly of the composite body was then calculated and compared with the observed magnetic anomaly. The geometries of the source bodies were again modified until a reasonable fit between the calculated and the observed magnetic anomaly

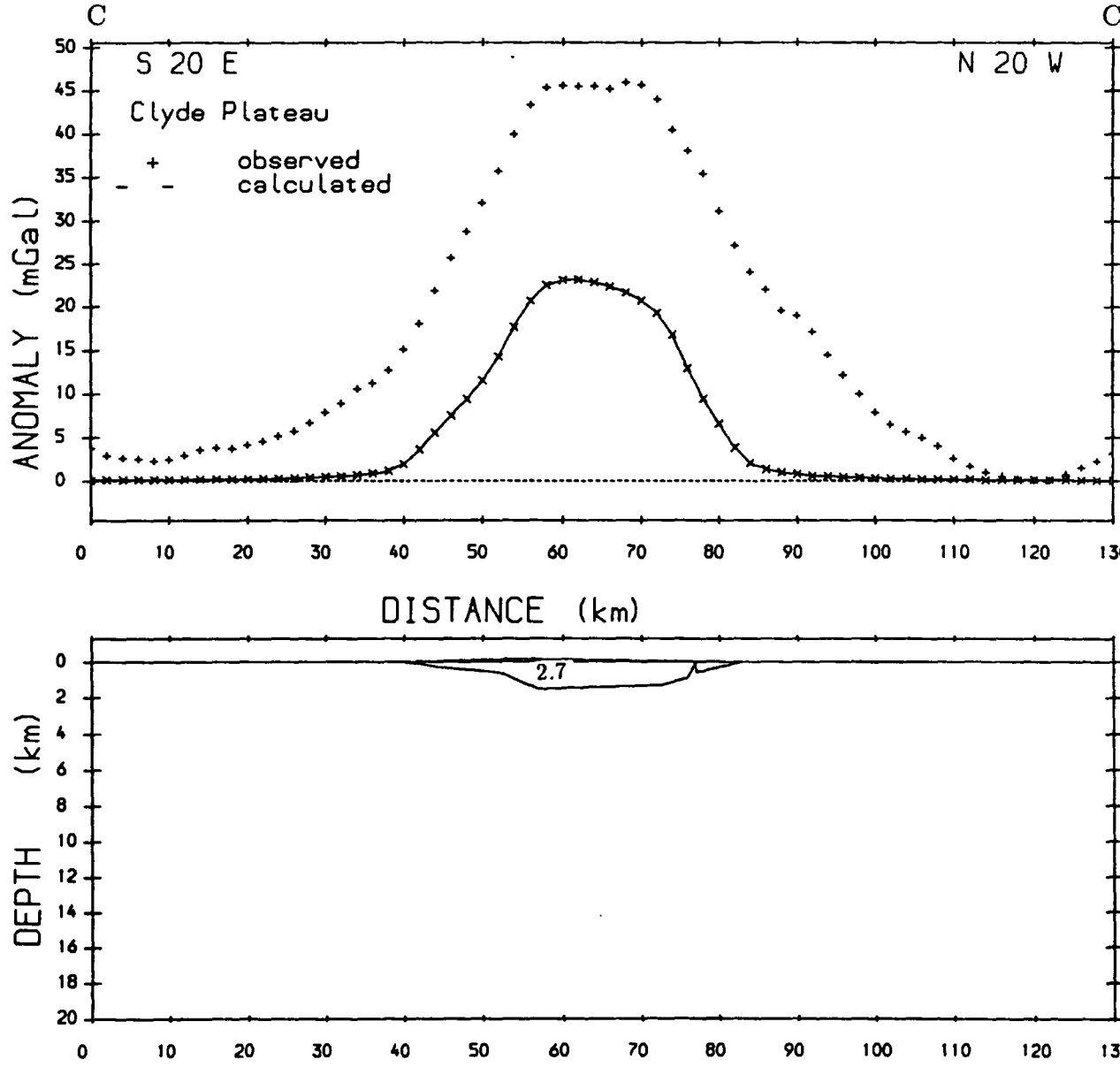

Figure 5.9 The expected gravity anomaly of the Clyde Plateau lavas calculated using the model in figure 5.6. The magnetization used is 2.7 A/m. The density (kg/m^3) to magnetization (A/m) ratio is 150 : 1.0. The anomaly can only explain the central part of the observed pseudogravimetric anomaly.

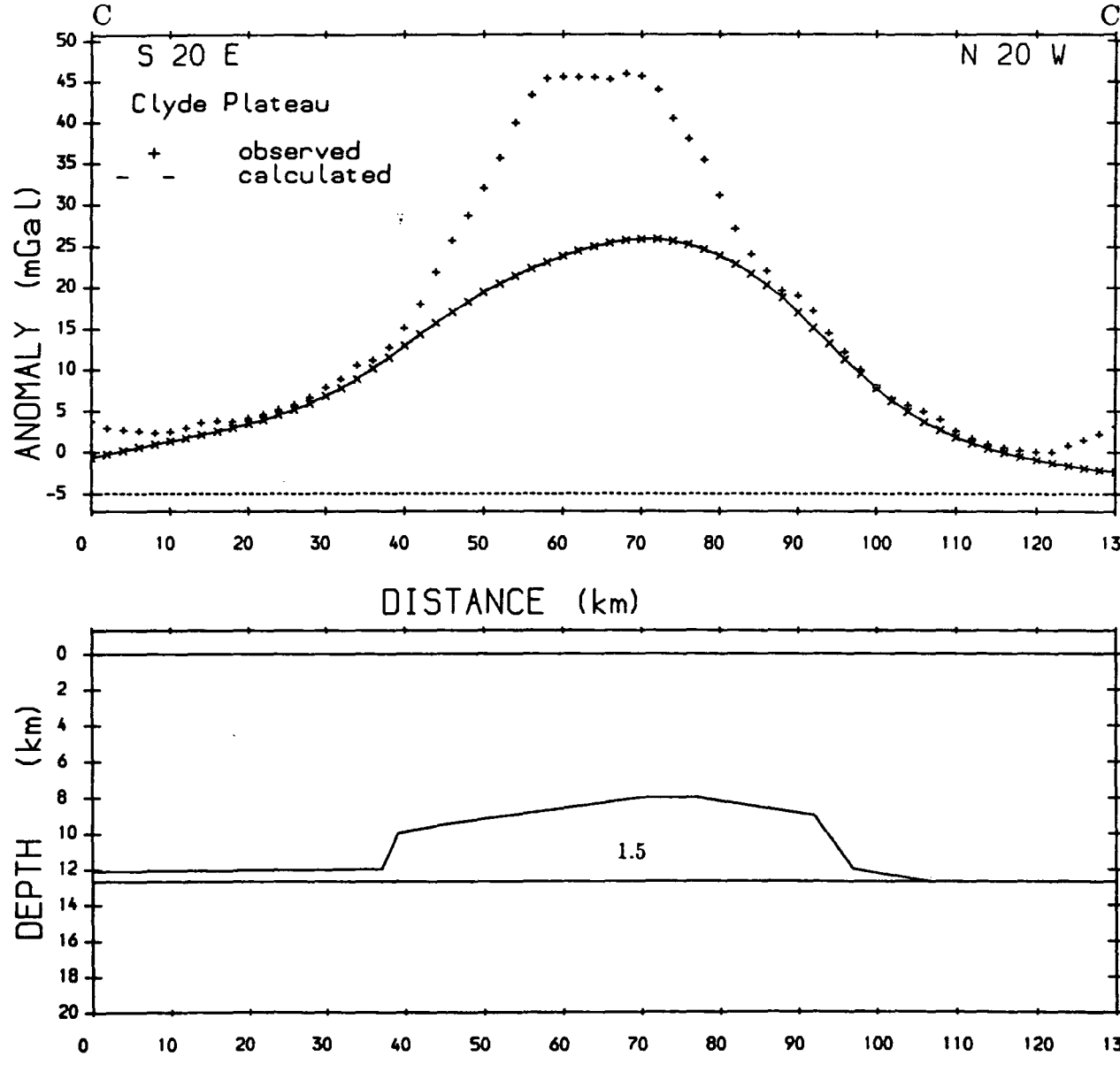

Figure 5.10 The estimated geometry of the deep source explaining the inferred regional component of the observed pseudogravimetric anomaly. The magnetization of the body is 1.5 A/m. The density (kg/m^3) to magnetization (A/m) ratio is 150:1.0.

was obtained. The above procedure was repeated until the resulting model produced an approximately satisfactory fit to the observed pseudogravimetric and magnetic anomalies.

Modelling was carried out for the deep source at different depths. Figures 5.11 and 5.12 show the results obtained from the modelling with the top of the deep source at about 7.5 km and 13 km depth respectively. The results show that the magnetic anomaly along CC′ can be modelled using reasonably well constrained outcropping Clyde Plateau lavas together with a deep seated body. The depth at which the deep source is located cannot be satisfactorily constrained.

The composite model obtained above was used as a starting geometry for the magnetic optimization routine. This rapidly gives a model which can simulate the short wavelength components. Additional body points were used to define the base of the Clyde Plateau lavas. The magnetization values of both the lavas and the deep source were set as variables. The base of the deep source was kept horizontal and fixed. The result using a deep source with the top at about 13 km depth indicates that the Clyde Plateau lava magnetic anomaly along profile CC′ can be caused by lavas with irregular base and a deep source with high magnetization (figure 5.13). The deep source could be of lower magnetization and larger depth extent.

5.8 Bathgate anomaly

The obvious difficulty in modelling the Bathgate anomaly is the lack of any surface indication of its source. In addition, the local Bathgate anomaly is superimposed on a long wavelength anomaly. The source of this long wavelength anomaly has been assumed to be the same as for profile CC′.

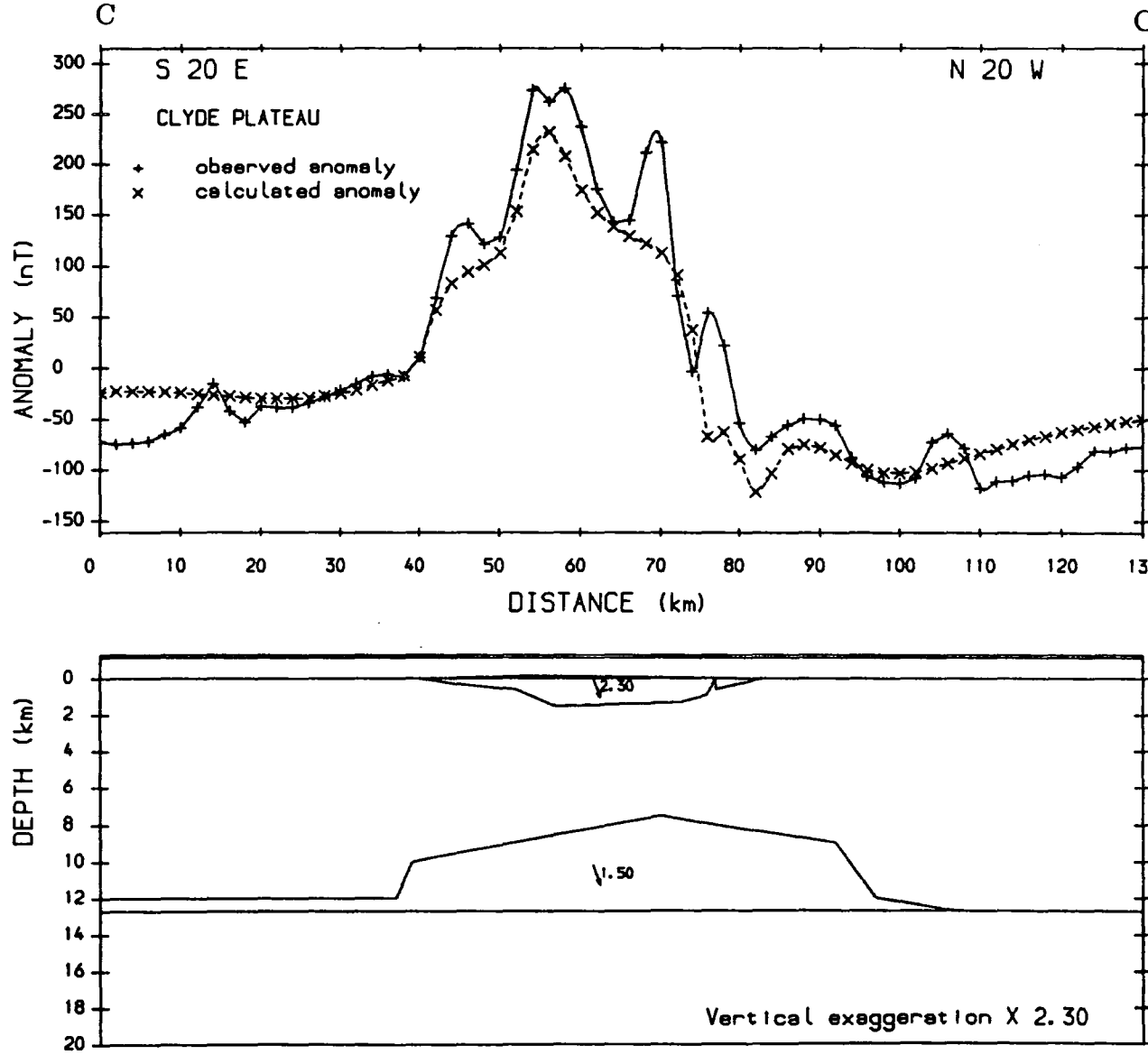

Figure 5.11a Magnetic modelling using a composite source. The top of the deeper source is at about 7.5 km depth. The magnetization of the deep source is 1.5 A/m and that of the Clyde Plateau lavas is 2.3 A/m. The inclination and declination are as in figure 5.6.

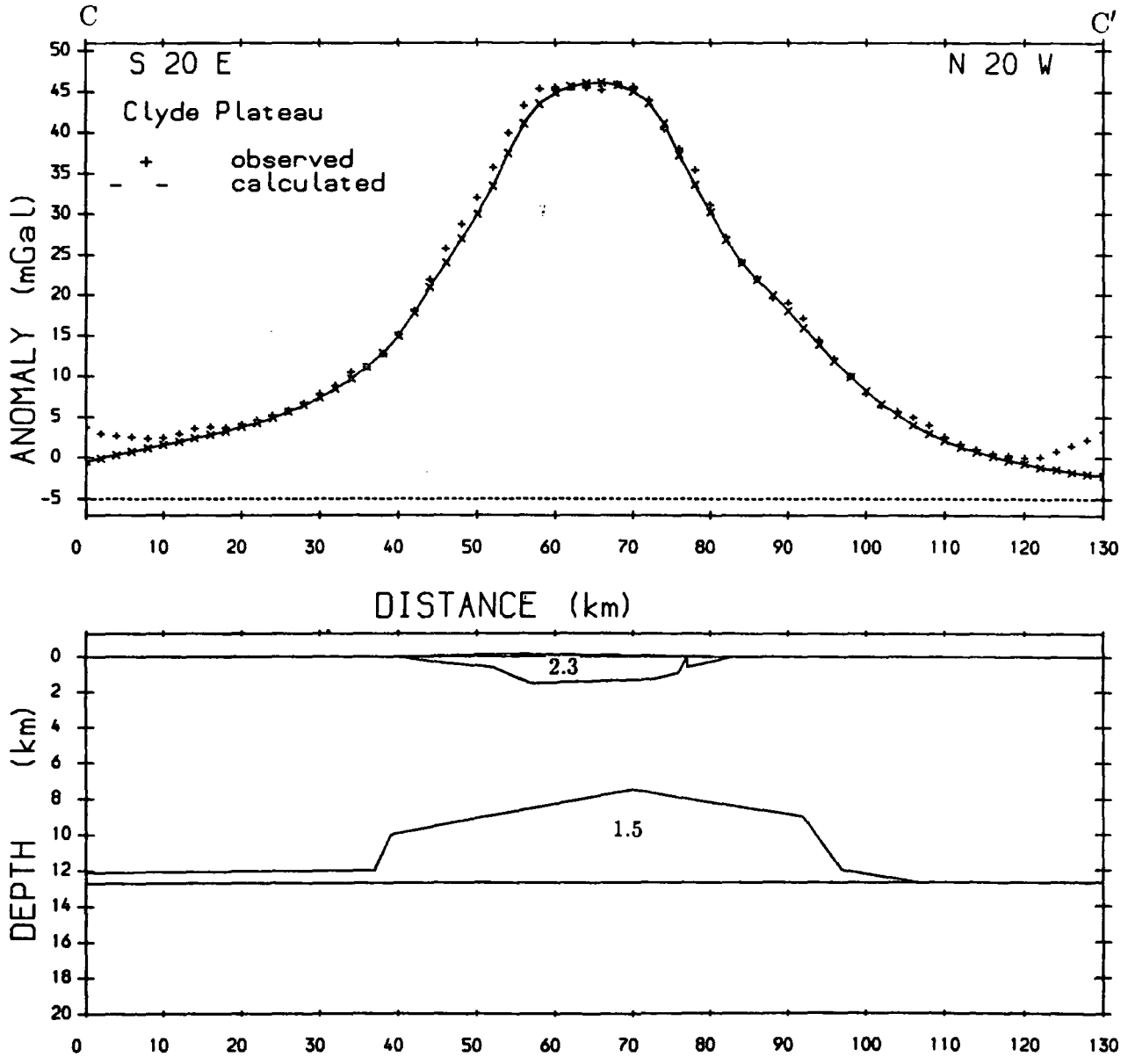

Figure 5.11b Pseudogravimetric modelling using the same source as in figure 5.11a. The density (kg/m^3) to magnetization (A/m) ratio is 150:1.0.

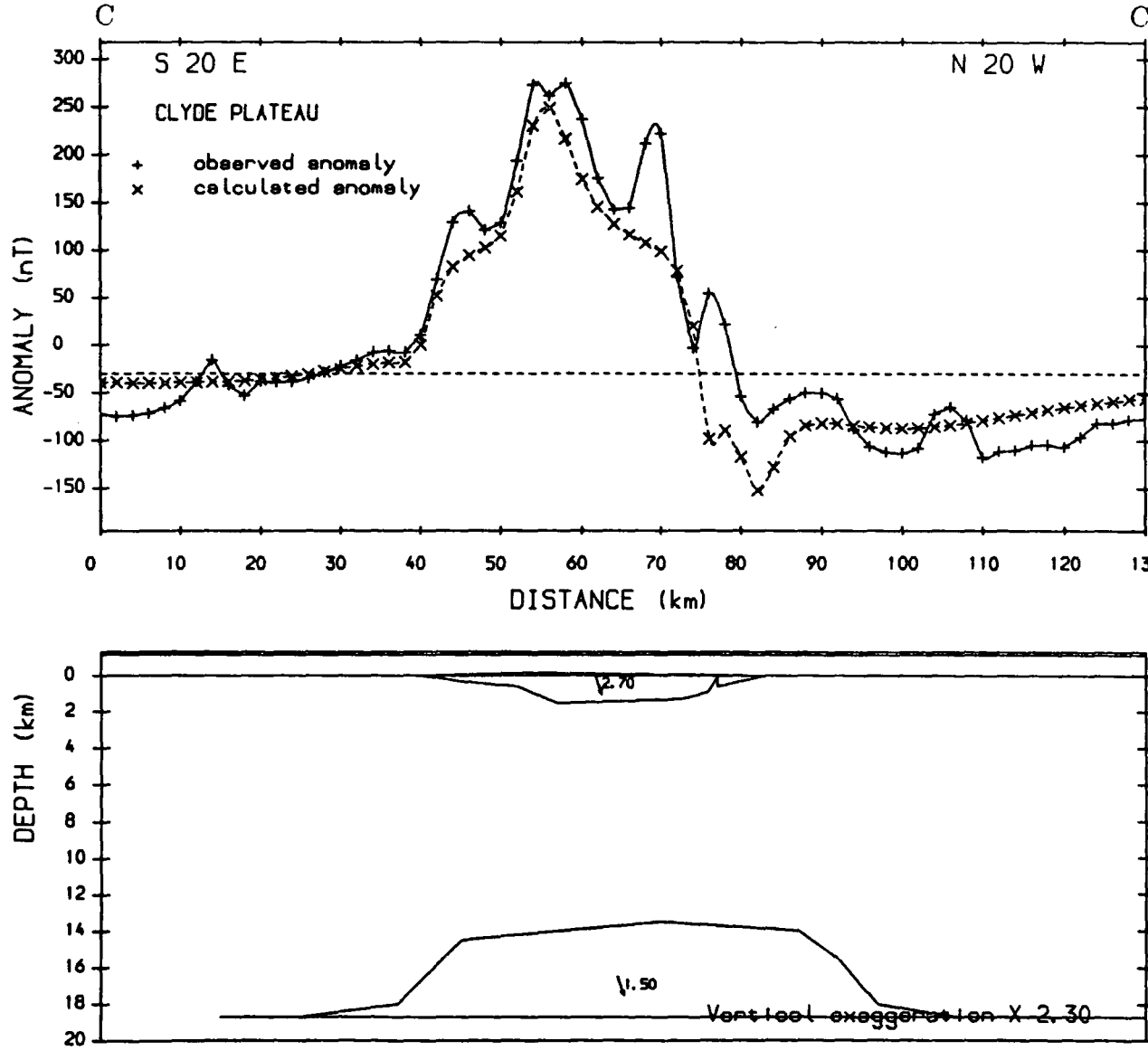

Figure 5.12a Magnetic modelling using a composite source. The top of the deeper source is at about 14 km depth. The magnetization of the deep source is 1.5 A/m and that of the Clyde Plateau lavas is 2.7 A/m. The inclination and declination are as in figure 5.6.

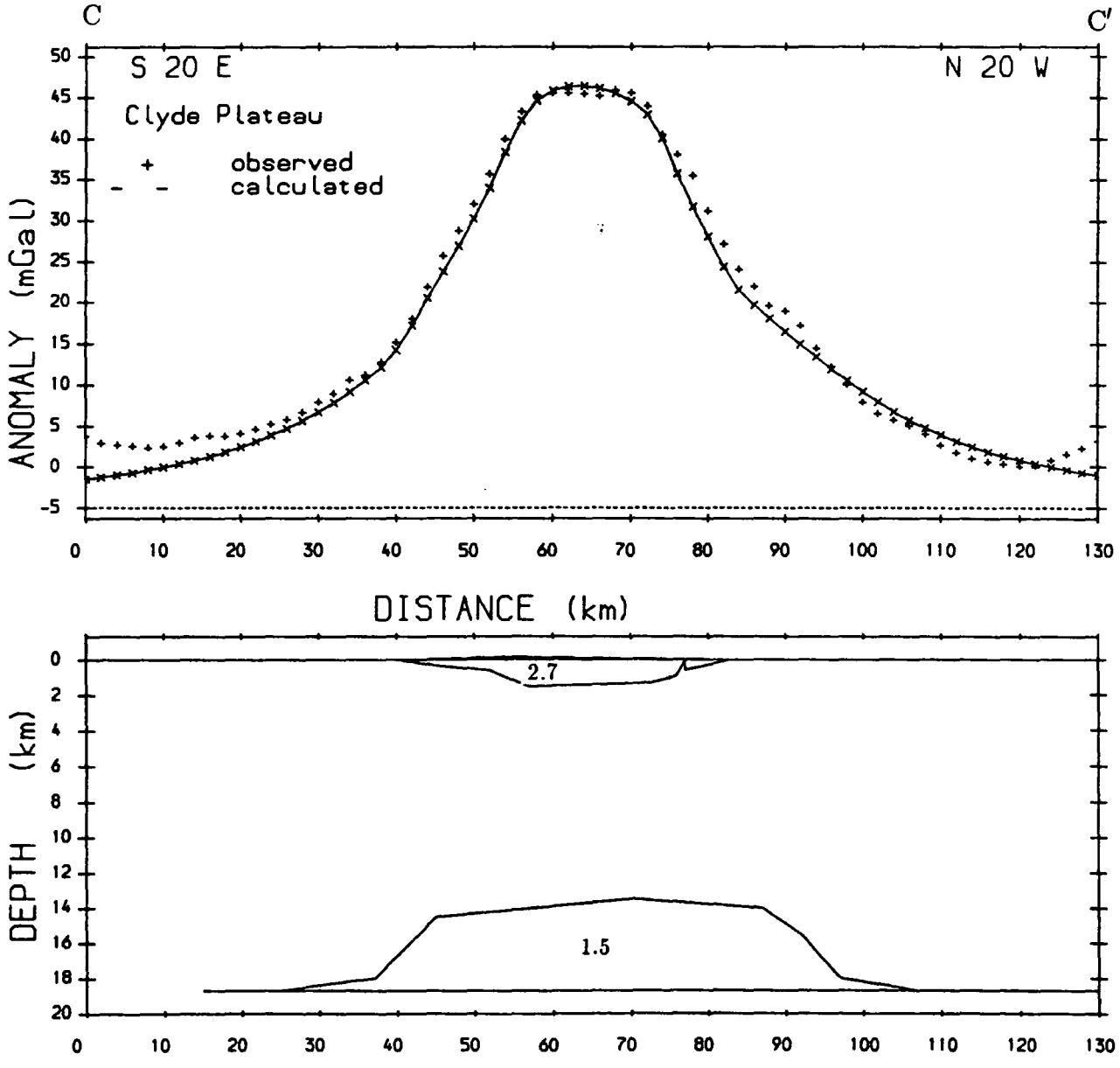

Figure 5.12b Pseudogravimetric modelling using the same source as in figure 5.12a. The density (kg/m^3) to magnetization (A/m) ratio is 150:1.0.

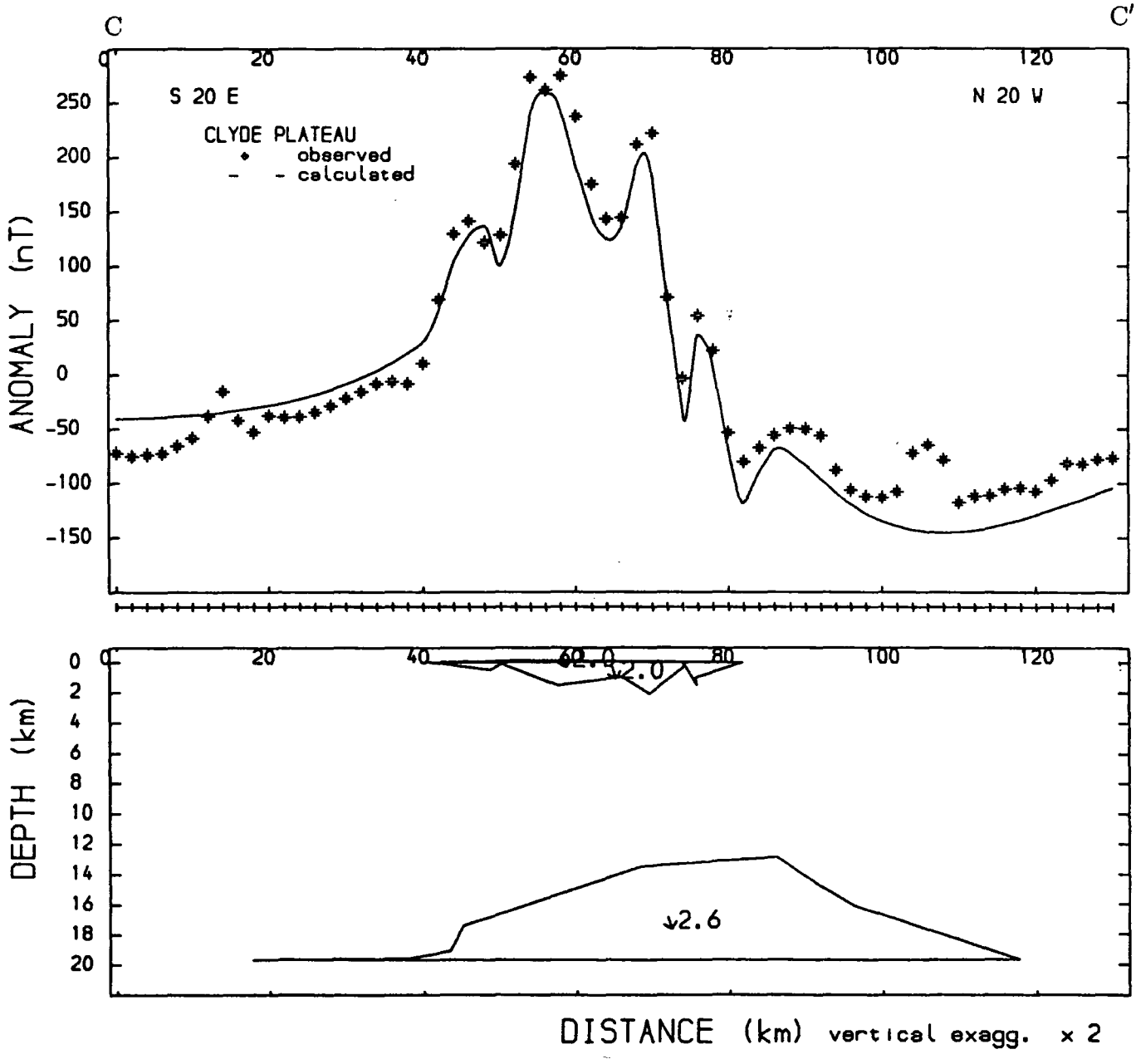

Figure 5.13 Modelling using the magnetic optimization routine.

5.8.1 The magnetic and pseudogravimetric profiles, and the geology

The magnetic and pseudogravimetric profiles (DD′) across the Bathgate anomaly are shown in figure 5.14. The magnetic profile indicates that the local Bathgate anomaly (BA) is a prominent positive high with an amplitude of about 450 nT. This positive high lies mainly over the Carboniferous rocks. The northern part of this anomaly is bordered by a low amplitude local magnetic high occurring within weakly magnetized Devonian lavas. The Highland Boundary fault which lies north of this local anomaly is marked by a local magnetic high. To the north of the Highland Boundary fault, a magnetic high occurs within granitic rocks which intrude the weakly magnetized Dalradian rocks. The southern part of the local Bathgate anomaly is bordered by a magnetic low lying within the Lower Old Red Sandstones and the Devonian lavas. The Southern Upland fault is marked by a local magnetic high which is probably due to the ophiolitic rocks along the fault. The magnetic anomaly south of the Southern Upland fault is featureless confirming that the rocks of the Southern Uplands are effectively non-magnetic. The short wavelength features, marked by the break in the slope of the local Bathgate anomaly, are probably due to some of the highly magnetized sills and dykes traversing the region.

The pseudogravimetric transformation reveals the presence of a medium wavelength anomaly (local Bathgate anomaly, BA figure 5.14) superimposed on a long wavelength anomaly (BG). The long wavelength anomaly is less conspicuous on the magnetic profile. The composite pseudogravimetric anomaly reaches a maximum of about 60 mGal (the density to magnetization ratio is 150 kg/m^3 : 1 A/m). As in the Clyde Plateau region, the different wavelength components may originate from different sources. The two anomaly components are marked by distinct changes in gradient on the pseudogravimetric profile. The local Bathgate pseudogravimetric anomaly is distinguished by its steep slope bordered by a gentle slope. The local magnetic anomaly marking the Highland Boundary fault is almost totally suppressed by the pseudogravimetric transformation. A local change in gradient marks the Southern

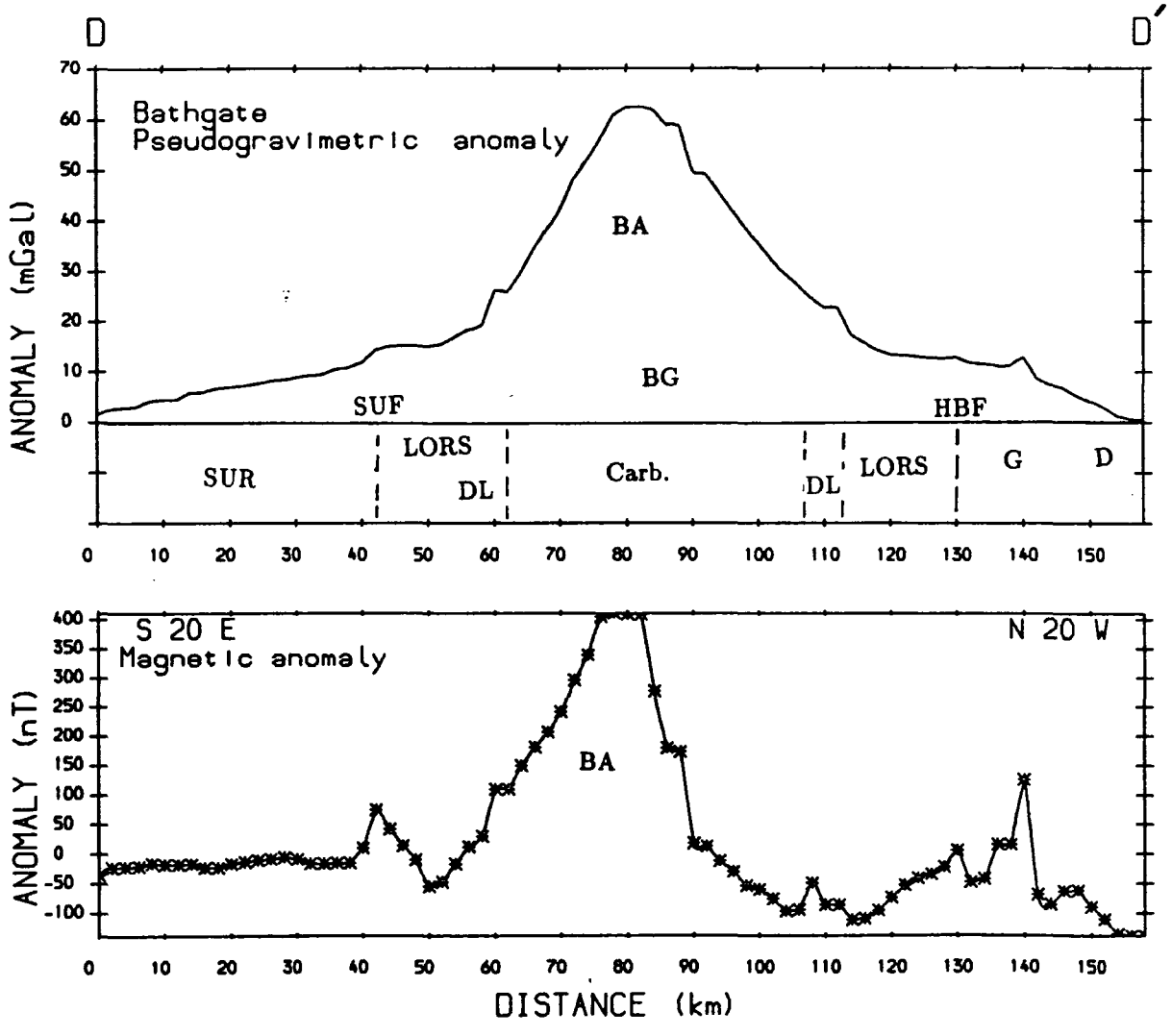

SUR - Southern Upland rocks, DL - Devonian lavas, LORS - Lower Old Red Sandstones, Carb. - Carboniferous rocks, G - Granite, D - Dalradians, SUF - Southern Upland fault, HBF - Highland Boundary fault, BA - local Bathgate anomaly. BG - Background anomaly

Figure 5.14 The magnetic and pseudogravimetric anomalies along profile DD′ and the geology along the same profile.

Upland fault.

5.8.2 Constraints and development of the model

The depth range and magnetization values used to explain the long wavelength anomaly along profile CC′ have similarly been used in the modelling of the Bathgate anomaly. The source of the local Bathgate anomaly do not have any surface representation. Two models are developed here for the local Bathgate anomaly and they are discussed below.

The Bathgate magnetic anomaly lies mainly over the outcrop of the Carboniferous rocks and is partly within the Central Coalfield syncline. The high amplitude of the local magnetic anomaly suggests that the source is strongly magnetized. The strongly magnetized rocks in the region are the Carboniferous lavas, and the Ordovician ophiolitic complexes which occur only along the Southern Upland and the Highland Boundary faults. The Devonian lavas do not contribute significantly to the magnetic anomaly and are assumed to be largely weakly magnetized. The Carboniferous lavas occur mainly within the Calciferous Sandstone Measures (figure 5.15). The inferred structure contour map of the top of the Sandstone Measures over the Bathgate region by Holliday (1986) shows that the deepest contour is 750 metres while the deepest contour for the base of the Sandstone Measures in the same region is 2000 metres. The deep borehole data from the British Geological survey confirms the presence of lavas underlying the Carboniferous sediments. The Rashiehill Farm borehole (BNG: 283860 673010) indicates that the lavas are present from about 807 metres to the base of the borehole at 1170 metres. The lavas are commonly of fine-grained vesicular type and some are weathered. The Salsburgh no. 1A borehole (BNG: 281670 664870) shows that ash, volcanic and basalt are present at a depth of about 1200 metres to the base of the borehole at 1300 metres. The locations of both the boreholes are near the apex (about BNG: 290000 673000) of the circular pseudogravimetric anomaly.

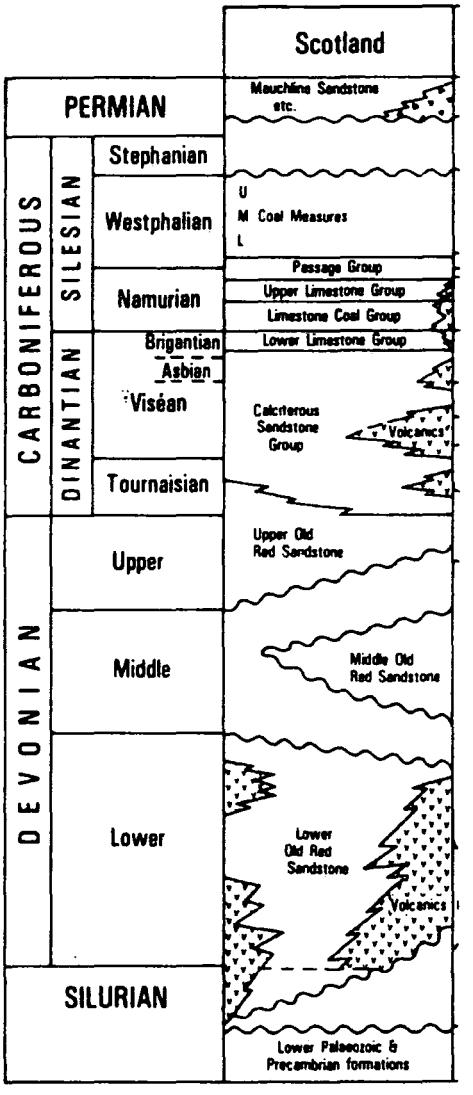

Figure 5.15 A generalised succession of Devonian and Carboniferous rocks in Scotland (Holliday 1986).

The first model for the source of the local Bathgate anomaly assumes it is caused by Carboniferous lavas.

The Bathgate anomaly has an obvious near-circular shape and no prominent short wavelength components. The rather smooth contours defining the anomaly are similar to those over Arran which has been inferred and modelled as a concealed basic body of shallow depth (McLean and Wren 1978). A second model proposed for the local Bathgate anomaly is similarly based on a circular intrusive body. No definite depth control can be applied. The magnetization value of granulitic fragments of about 3.0 A/m (Powell 1978a) has been assumed to be the minimum value. Powell (1978a) and Hossain (1976) used a value of 5 A/m for an intra-basement source.

The local Bathgate magnetic anomaly along DD′ has a more negative value on the northern side of the main positive anomaly. This is similar to the Clyde Plateau lavas magnetic profile CC′. The bulk magnetization of the Clyde Plateau lavas has been shown to be effectively along the present earth's magnetic field. The magnetization of a large body in the deep crust (magnetic basement) can be assumed to be essentially along the earth's magnetic field (section 3.7.1). The magnetization used in the modelling along profile DD′ has been assumed to be along the present earth's magnetic field.

5.8.3 Modelling

A magnetization of 1.5 A/m similar to the value used to model along profile CC′ has been used for the magnetic basement. The top of the magnetic basement is placed at about 14 km. The source of the local Bathgate anomaly has been placed above the magnetic basement. The two-dimensional gravity modelling with end correction procedure has been used on the local Bathgate anomaly because of its limited width. As has been done earlier for the Clyde Plateau, the pseudogravimetric profile

was first used to determine the geometry of the basement and the magnetic profile used to determine the geometry of the local Bathgate anomaly. These were combined and the geometries modified until a reasonable fit to the observed magnetic and pseudogravimetric anomalies were obtained.

The modelling was first carried out based on the assumption that the local Bathgate anomaly is caused by the lavas. The top of the lavas is assumed to be at about 800 m and the base at about 2100 m. The geometry of the lavas is assumed to be similar to the model obtained for the Clyde Plateau lavas, a body with a wide top and a narrower base. The magnetization is set as a variable and was changed to obtained a satisfactory fit with the observed anomalies. The result is shown in figures 5.16a and b. The magnetization required by lava body constrained between the above depths is about 6.7 A/m.

A lava model with the top at about 800 metres and a magnetization value of 2.7 A/m similar to the magnetization value obtained for the Clyde Plateau lavas and basement feature as described earlier results in a thicker lava body (figure 5.17a and b). The lavas reached a depth of about 5.5 km.

The second model used to explain the local Bathgate anomaly assumes the geometry of the source to be a circular intrusive body with a wide base and a narrower top. Two possible models are presented here: (a) a body with its top at about the upper surface of the top crystalline basement (about 4 km) and (b) a body with its top at the upper surface of the deep crystalline (7.5 km, table 5.1). A magnetization of 3.0 A/m has been used for the model with the top at about 4 km. The base of this body extends to 9.4 km (figures 5.18a and b). A similar body has been used to model the feature with the top at about 7.5 km depth. It requires a higher magnetization of about 4.0 A/m (figures 5.19a and b). The actual parameters defining the composite source may not be easily constrained from the modelling.

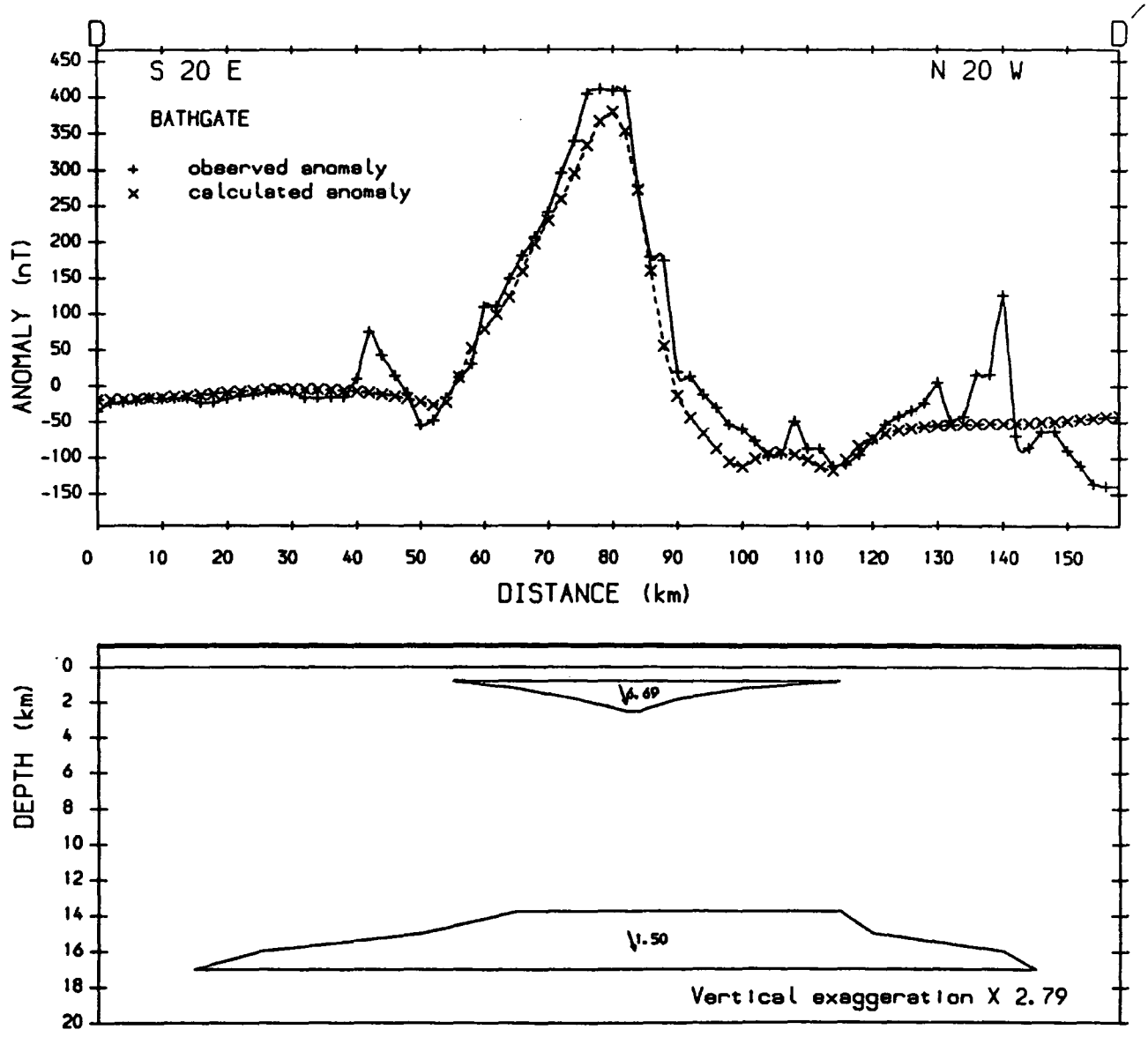

Figure 5.16a Modelling along profile DD′ using a deep source and a shallow lava body constrained between 800 m and 2100 m. The magnetization of the deep source is 1.5 A/m. The magnetization required to obtain a good fit is 6.7 A/m. The inclination and declination of the body and the earth's magnetic field are 70.3°C and -10.4°C.

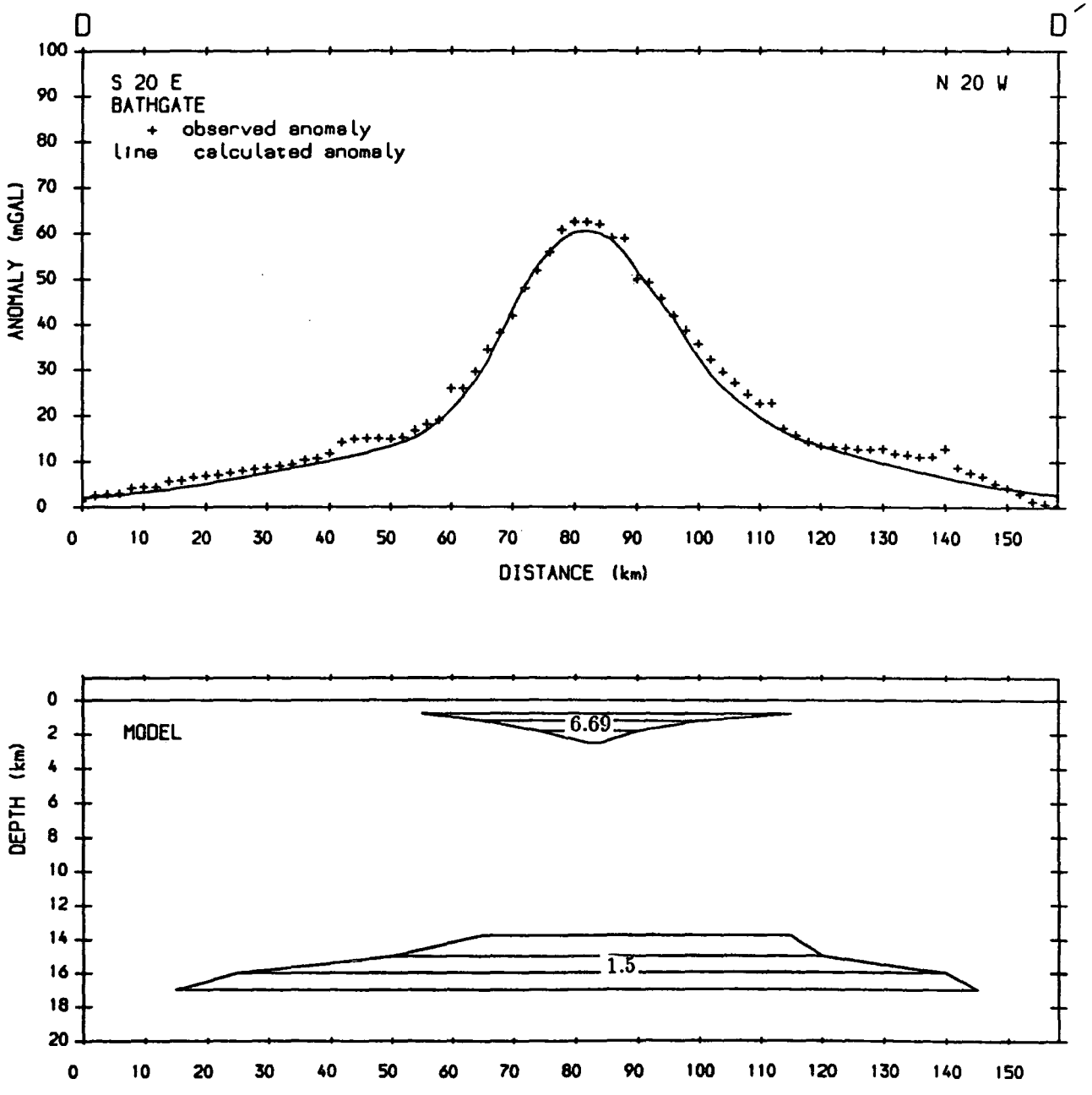

Figure 5.16b Pseudogravimetric modelling along profile DD′ using the same sources as in figure 5.16a. The density (kg/m^3) to magnetization (A/m) ratio is 150:1.0.

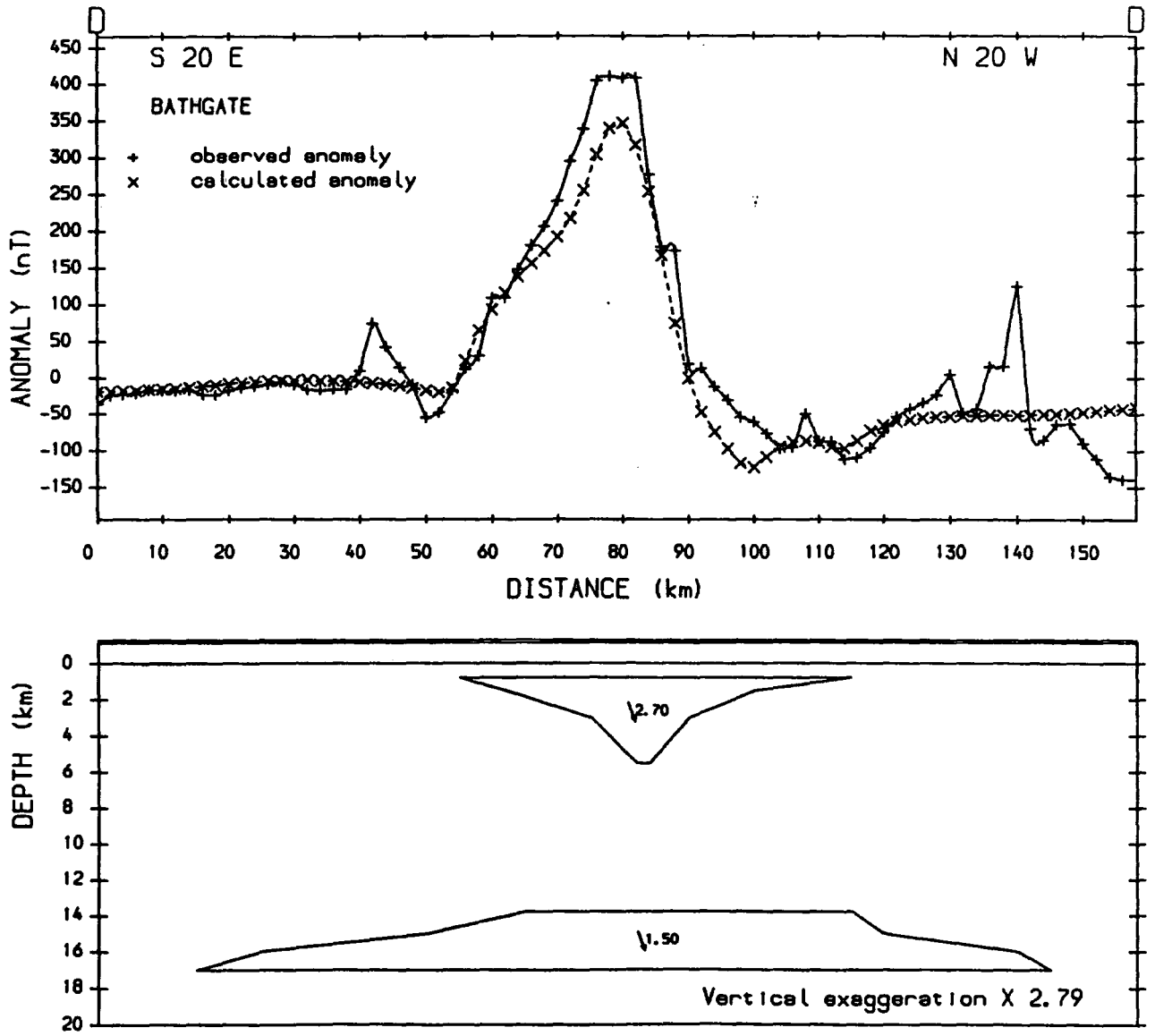

Figure 5.17a Modelling along profile DD′ using a deep source and a shallow lava body with the top at 800 m and a magnetization value of 2.7 A/m. The magnetization of the deep source is 1.5 A/m. The base of the lava body reaches to about 5.5 km depth. The inclination and declination of the body and the earth's magnetic field are 70.3°C and -10.4°C.

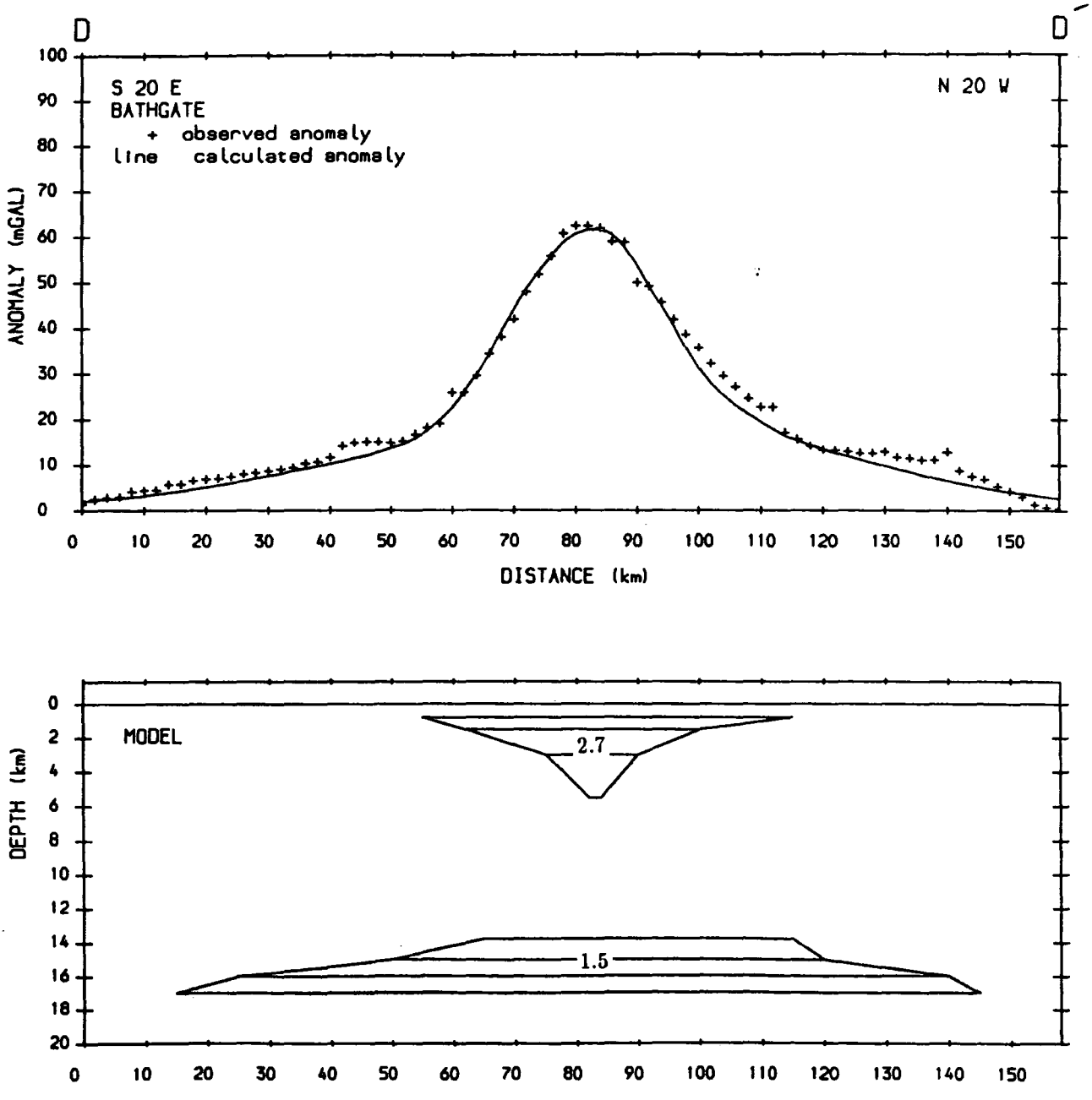

Figure 5.17b Pseudogravimetric modelling along profile DD′ using the same sources as in figure 5.17a. The density (kg/m^3) to magnetization (A/m) ratio is 150:1.0.

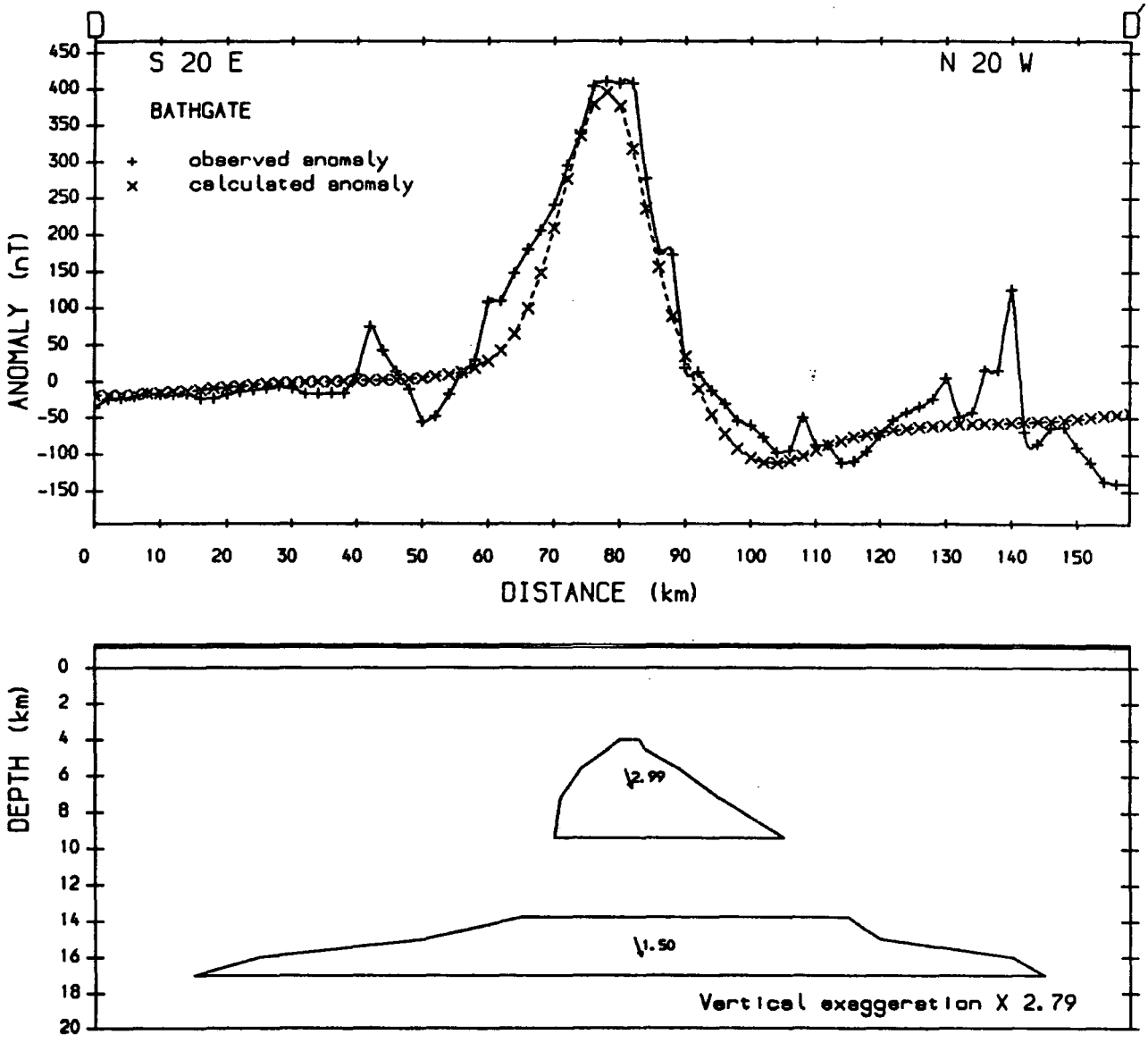

Figure 5.18a Modelling along profile DD′ using a deep source and an unexposed circular body with the top at 4 km depth, and a magnetization value of 3 A/m. The base reaches to 9.4 km. The magnetization of the deep source is 1.5 A/m. The inclination and declination of the body and the earth's magnetic field are 70.3°C and -10.4°C.

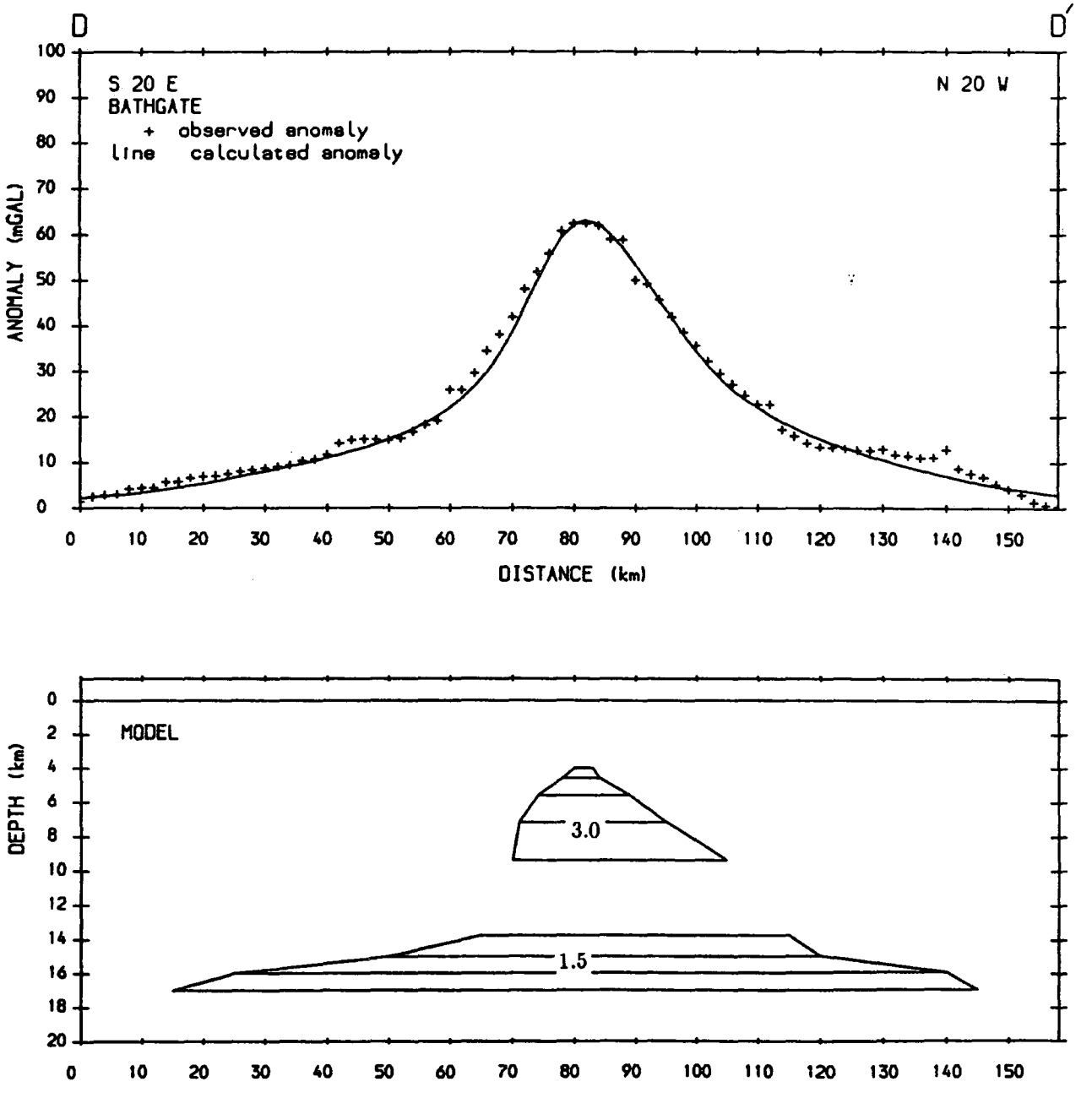

Figure 5.18b Pseudogravimetric modelling along profile DD′ using the same sources as in figure 5.18a. The density (kg/m^3) to magnetization (A/m) ratio is 150:1.0.

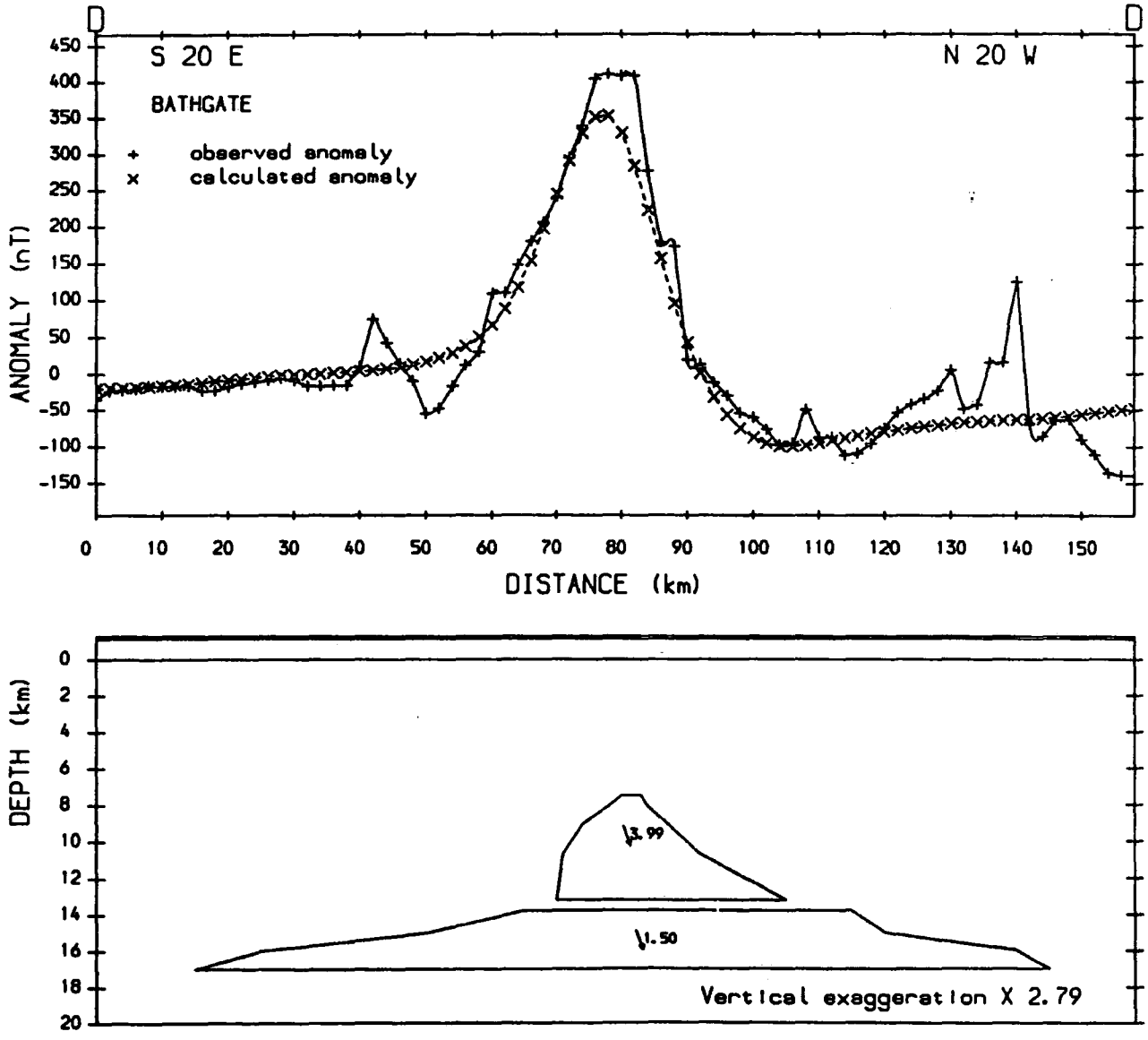

Figure 5.19a Modelling along profile DD′ using a deep source and an unexposed circular body similar to figure 5.18 with the top at 7.5 km depth. The magnetization value required is 4 A/m. The magnetization of the deep source is 1.5 A/m. The inclination and declination of the body and the earth's magnetic field are 70.3°C and -10.4°C.

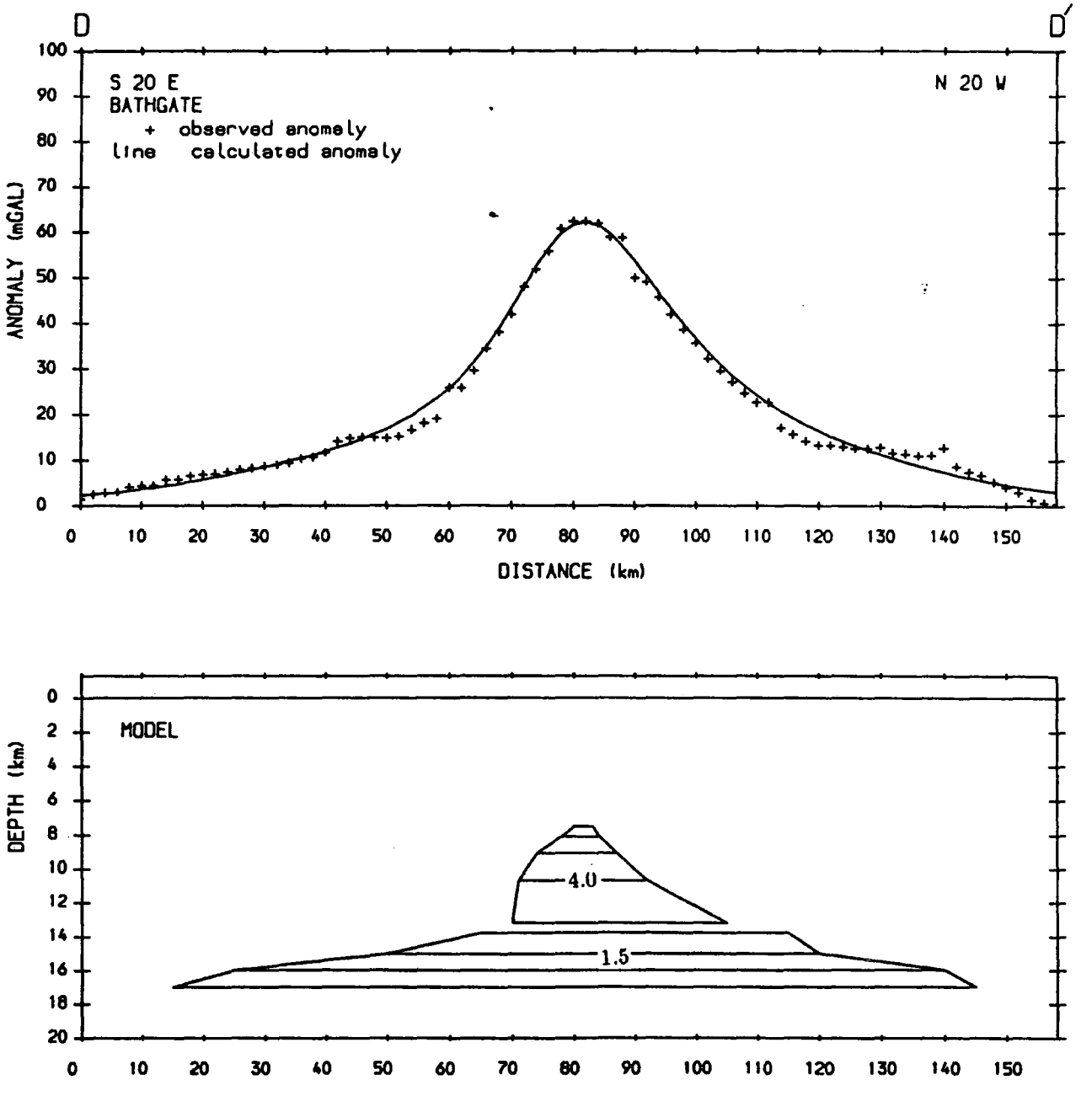

Figure 5.19b Pseudogravimetric modelling along profile DD′ using the same sources as in figure 5.19a. The density (kg/m^3) to magnetization (A/m) ratio is 150:1.0.

5.10 Discussion

The igneous activity which may have given rise to the main magnetic character of the Midland Valley occurred during the Lower Palaeozoic, late Silurian to Lower Devonian, Carboniferous and Tertiary. The Lower Palaeozoic ophiolitic complexes mainly occur along the boundary fault and caused elongated magnetic anomalies. Comparison of the outcrop of the late Silurian to Lower Devonian lavas to the aeromagnetic anomaly suggests that they do not produce large amplitude magnetic anomalies. In general, they can be assumed to be weakly magnetized. The most obvious source of the high amplitude short wavelength magnetic anomalies within the Midland Valley are the Carboniferous lavas. Some of the short wavelength anomalies are also caused by the numerous strongly magnetized dykes and sills within the regions. The major Tertiary igneous activity occurred in Arran and caused a slightly elongated magnetic anomaly.

The modelling of the magnetic and pseudogravimetric highs along profile CC′ over the Clyde Plateau lavas indicates that the source consists of the outcropping Clyde Plateau lavas and a deep crustal source (magnetic basement) which give rise to a long wavelength component. This long wavelength anomaly can also be clearly observed on the pseudogravimetric profile DD′ (figure 5.14) over the Bathgate region. The pseudogravimetric (figure 5.2) and upward continued magnetic maps (figure 5.3) reveal the basement feature as an elongated long wavelength anomaly traversing the region slightly oblique to the boundary fault. The depth of the basement cannot be constrainted by the modelling.

The magnetic basement as modelled is broader beneath the eastern Midland Valley than to the west (compare figures 5.16-5.19 to figures 5.11 and 5.12). The northern end of the magnetic basement as modelled on both profiles CC′ (Clyde Plateau) and DD′ (Bathgate) terminates just north of the Highland Boundary fault. The LIPSB profile (Bamford et al. 1977) similarly indicates a crustal change north

of the fault. Along profile CC′ the southern end of the magnetic basement ends within the Midland Valley and along profile DD′ it ends just under the Southern Uplands. The magnetic basement does not appear to be affected by the boundary faults which probably suggests that it is within the deeper crust. The magnetic basement (interface of the amphibolites and the granulites) as modelled by Powell (1978a) from the smoothed magnetic map of Hall and Dagley (1970) has its top at about 11 km depth.

The local Bathgate anomaly has been modelled as either due to shallow lavas with the top at about 800 metres or a circular intrusive body with a wide base and a narrower top. The lavas are observed in the Rashiehill Farm borehole at a depth greater than 800 metres. Its lateral extent is probably not large as shown by the borehole Salsburgh no. 1A. The lavas here only start at about 1200 metres depth. The base of the lavas is not known. The lava body modelled using a magnetization value of 2.7 A/m similar to the value modelled for the Clyde Plateau lavas requires a lava body which has its base at about 5.5 km depth. The base of the lavas is deeper than the top crystalline basement observed in the seismic studies of Conway et al. (1987) and Davidson et al. (1984). The modelled lava body thickness is about twice that of Clyde Plateau lavas. The near-circular shaped Bathgate anomaly differs from that of the irregular shape anomalies due to the outcropping lavas. These probably suggest that the lavas are not the major source of the local Bathgate anomaly. The circular shaped anomaly is similar to that of Arran which has been modelled as a concealed basic body. Comparison of the pseudogravimetric map with the regional gravity map of Hussain and Hipkin (1981) shows that the local Bathgate gravity anomaly has a similar size and shape, and is approximately coincident with that of the local Bathgate pseudogravimetric anomaly. The pseudogravimetric and gravity profiles along DD′ (figure 5.20) show the peaks of both the anomalies occur at the same place. This indicates that the source of the magnetic anomaly is probably identical to the high density source of the gravity anomaly. The Lower Carboniferous lavas, over the Clyde Plateau, do not produce strong gravity anomalies of the same

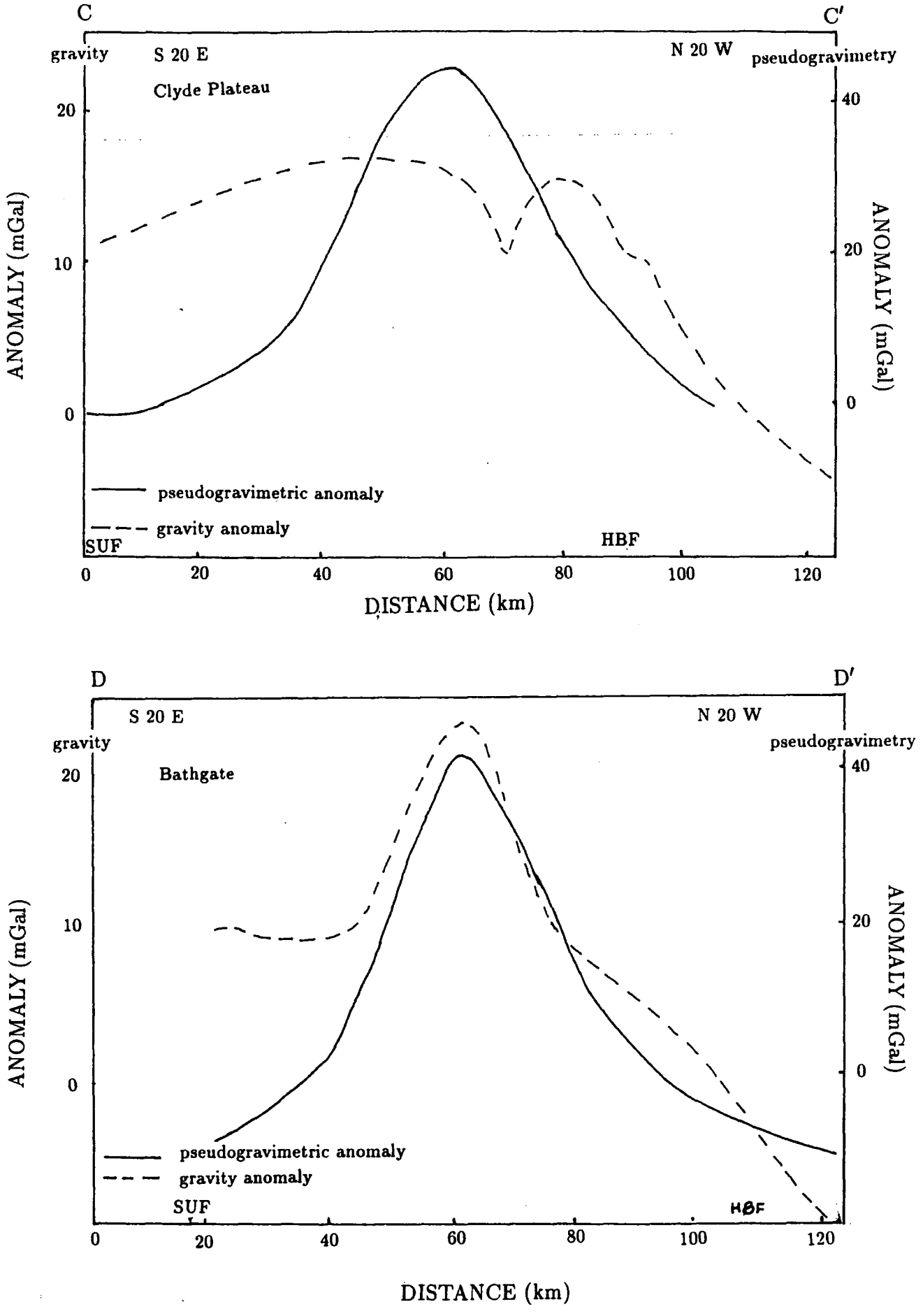

Figure 5.20 Comparison of the smoothed gravity and pseudogravimetric profiles along CC′ and DD′ from the regional gravity map of Hussain and Hipkin (1981) and the pseudogravimetric map in figure 5.2. The gravity anomaly has a true amplitude. The amplitude of the pseudogravimetric anomaly depends on the density (kg/m^3 to magnetization (A/m) ratio used in the transformation which is 150:1.0.

order of magnitude as the Bathgate anomaly. The pseudogravimetric and gravity profiles along CC′ (figure 5.20) are distinctly different. The second model, a circular basic intrusive body with a wide base and a narrower top is probably the more likely source of the local Bathgate anomaly. This differs from Conway et al. (1987) who suggested that the local Bathgate anomaly is caused by weathered and vesicular lavas but agrees with the basic intrusion of Powell (1978a).

CHAPTER 6

Summary and conclusion

6.1 Development of the modelling

An iterative procedure to upward continue magnetic anomalies observed on an irregular surface onto a horizontal plane has been developed. This is necessary because the aeromagnetic data acquired from the British Geological Survey is at variable absolute height. Subsequent pseudogravimetric transformation requires anomalies on a horizontal plane. Use of data observed on a surface of variable height by such a procedure would introduce errors in particular to the shorter wavelength components which vary substantially with change in height.

The iterative procedure uses the Fourier transform method to carry out upward continuation of a magnetic anomaly observed on an irregular surface onto a horizontal plane. The Fourier method has been applied because it is simple and computationaly fast when used with the fast Fourier transform particularly when applied to large data sets. The iterative continuation procedure is a further development of the upward and downward continuation of magnetic anomaly from a horizontal plane onto an irregular surface by Cordell (1985). In the upward continuation procedure, the anomalies observed on the horizontal plane are upward continued to a number of horizontal levels. The anomaly on the irregular surface between the highest and the lowest continuation level can then be obtained by interpolation. The procedure gives an exact upward continued anomaly on the irregular surface. A similar procedure can be used to downward continue an anomaly from a horizontal plane onto an irregular surface. The upward continuation of an anomaly observed on an irregular surface onto a horizontal level is based on a series of these upward and downward continuations. An upward continuation level above the observation surface is first defined.

The anomaly observed on an irregular surface is then assumed to be on a horizontal plane. Using the difference in heights between the irregular observation plane and the continuation level at every point, an irregular surface, the inverse of the observation surface, can be defined above the assumed horizontal plane. The observed anomaly is then upward continued onto this irregular surface using the procedure of Cordell. This upward continued anomaly is taken to be the initial estimate for the horizontal continuation level. This solution is then downward continued onto the observation surface using the procedure of Cordell above. This anomaly should be equal to the observed anomaly if the upward continued anomaly is the correct solution. If the residuals are large the residual value at each point is upward continued as has been done for the observed anomaly. The upward continued residual anomaly is added to the solution to obtain a new solution. This is again downward continued onto the observation surface and compared to the observed anomaly. This series of upward and downward continuations is carried out until the residual anomaly is negligible.

The procedure has been tested for magnetic anomalies of specified wavelengths observed on a topographic surface represented by one or more sinusoid calculated on a 2x2 km^2 grid. The tests indicate that the procedure succesfully upward continues magnetic anomalies produced by spherical sources with the centre of gravity greater than about 2 km depth calculated on a topographic surface exceeding about 5 km wavelength provided that the maximum continuation height is less than 2 km. Tests using continuation levels greater than this indicate that short wavelength instability is prominent. The aeromagnetic data digitised at 10 nT interval by the BGS contains anomaly components less than about 5 km but the gridding on a 2x2 km^2 grid using the radial averaging procedure has removed the wavelength components shorter than 4 km. Furthermore, this work deals with medium and long wavelength magnetic anomalies. The smoothed topographic data used to upward continue the aeromagnetic data obtained from Woollett (1988) contains only wavelength component greater than 4 km. The smoothed topographic data has a maximum height of less than 2 km. The application of the iterative continuation procedure on the

aeromagnetic data is thus not expected to cause severe errors. This procedure is also applicable to gravity anomalies.

The pseudogravimetric transformation is based on the Poisson relation stating that the magnetic potential is proportional to the derivative of the gravity potential provided that the ratio of density to magnetization is constant and the magnetization is in a constant direction. A new programme has been written using the Numerical Analysis Group fast Fourier transformation subroutine but otherwise following Tantrigoda (1982).

The advantages of using the pseudogravimetric data for interpretating a magnetic anomaly as compared to the direct use of magnetic methods are: (a) the transformation suppresses the short wavelength components and enhances the long wavelength components. This is useful for studying broad features and deep structures. (b) The dipole nature of the magnetic property produces mixed positive and negative anomalies. The relation to the source is complex and depends on the direction of magnetization and the earth's magnetic field. The pseudogravimetric anomaly is monopole in nature and is generally centred over the causative body. It has a simple anomaly-source relationship. (c) The pseudogravimetric anomaly can be interpreted using the simpler gravity methods. For example, the pseudogravimetric anomaly can be used to give a rapid estimate of the product of the magnetization and thickness of the causative body using the simple slab formula.

Tests on the transformation procedure indicate that it produces erroneous results only when the inclination of the magnetization of the body and the earth's magnetic field are small (less than about 20^o). The inclination of the earth's magnetic field in the regions of study are high and the effective magnetization of the body has been assumed to be mainly induced along the earth's field direction in all cases. A problem which arises from the three dimensional transformation is that magnetic sources close to each other may result in superposition of their anomalies and make the

isolation of the anomalies due to the different sources difficult. The two-dimensional transformation gives erroneous results when used on a body of limited strike length.

Two-dimensional interpretation has been carried out using the existing techniques and modelling routines available in Durham. Modelling using an end-correction factor has been used where necessary. Non-linear optimization routines have been used to obtain a rapid and improve fit of calculated and observed anomalies.

A new modelling approach applying a combined use of pseudogravimetric and magnetic interpretation has been introduced. The scheme is as follows. A model which satisfies the observed pseudogravimetric anomaly is first obtained. The magnetic anomaly of the model is then calculated and compared to the observed magnetic anomaly. The model is modified to obtain a satisfactory fit. A fit to the observed pseudogravimetric anomaly is again obtained. These steps are repeated until the body satisfies both the observed magnetic and pseudogravimetric anomalies within acceptable limits. This approach is particularly useful for a major magnetic body with superimposed short wavelength features due to shallow part of the body or interfering feature. The initial pseudogravimetric modelling is able rapidly to define the broad feature and the detail can be further improved by the magnetic modelling.

6.2 Interpretation of the Great Glen anomaly

The linear positive anomaly along the Great Glen fault (refered to as Great Glen anomaly) has its sharp apex correlating closely with the line of the fault. The pseudogravimetric anomaly also shows a similar close correlation. This suggests that the source is related to the fault. The Great Glen anomaly is not due to the outcropping rocks which are mainly weakly magnetized Moine rocks.

Two profiles have been used to study the source of the Great Glen anomaly:

(1) a profile AA′ which crosses the region where the magnetic and pseudogravimetric anomalies are least affected by the neighbouring anomalies, and (2) a profile BB′ northwest of Inverness where the change in gradient at the apex is shaperst.

Two basic types of source have been considered: (1) a strongly magnetized triangular region with outward dipping sides and a horizontal base, and (2) a strongly magnetized basinal feature with a horizontal top near the surface and inward dipping sides. Magnetic modelling using a high magnetization value of 2.5 A/m shows that the inward dipping basin-like feature cannot satisfactorily simulate the sharp apex of the observed magnetic anomaly. This is because the feature causing the apex is too deep. However, an outward dipping feature with the top at a relatively shallow depth is able to produce an anomaly which simulates the sharp apex of the observed magnetic anomaly. It is, therefore, the more satisfactory model and is taken to be the geometry of the magnetized body causing the Great Glen anomaly.

A minimum estimate of the magnetization value of about 0.8 A/m for the outward dipping feature has been obtained by modelling with the top at the surface and the base at the Moho (about 30 km depth). The actual magnetization is probably similar to the crustal rock exposed in northern Scotland. The measured magnetization of the surface rocks and values used in modelling by previous workers are less than 3.0 A/m. An estimate of the depth to the top of the outward dipping feature has therefore been obtained by magnetic modelling using magnetizations ranging from 1.0 to 2.5 A/m. Modelling along profile AA′ yields a depth of 2.5 to 5.5 km and along profile BB′ yields a depth of about 1 km to less than 2.5 km for magnetization values of 1.0 to 2.5 A/m respectively. The source clearly lies at least partly in the upper crust.

Pseudogravimetric modelling along profile AA′ has been used to determine realistic models that can explain the Great Glen anomaly. The pseudogravimetric profile has a gentler slope northwest of the fault and a background anomaly higher

here than to the southeast. It has been initially modelled using a single outward dipping body of homogenous magnetization which passes into a semi-infinite slab at the northwestern end. It is, however, more realistic to assume that the feature associated with the Great Glen fault is localised near the fault (Great Glen feature) and the higher background value northwest of the fault is caused by a magnetized crustal slab having a higher magnetization than the crust southeast of the fault. Modelling has been carried out based on this two-body feature. A magnetization range of 1.0-2.5 A/m and depth to the top of the Great Glen feature of 1-5 km were used. The magnetized slab was assumed to have either (1) a thickness similar to the Great Glen feature or (2) a constant thickness of 19 km with the top at 1 km depth. Similar modelling has been carried out using a three-body model where the magnetization of the Great Glen fault northeast of the fault is superimposed on the magnetization of the crustal slab. The apex modelled using a magnetized slab of the same thickness as the Great Glen feature is slightly to the north of the line of the Great Glen fault. The Great Glen feature in some of the models obtained with a magnetized slab thickness of 19 km is symmetrical about the apex and has the apex on the fault plane. The thickness of the Great Glen feature depends on the assumed depth to the top. Estimates range from about 7 to 18 km. The width is about 80-90 km at the base.

The models presented differ from the simple sloping step model of Hall and Dagley (1970) and the amphibolite/granulite interface of Powell (1978a). The simple step model cannot explain the pseudogravimetric high along the line of the fault. The model by Powell is constrained within the mid-crustal layer of LIPSB and is thus too deep. Both these studies were carried out on the smoothed aeromagnetic data of Hall and Dagley (1970). The present model gives a much better fit and is more realistic geologically.

The origin of the Great Glen feature may possibly be associated with symmetrical temperature rise on both sides of the fault resulting in the formation of

magnetite by appropriate metamorphic processes. One such process is the breakdown of the metamorphic chlorites and biotites in greenschists and amphibolites at temperatures greater than 520^0C due to progressive temperature increase. Temperature increase symmetrical about the fault may be caused by frictional heating or hot fluid channelled into the fault. The fluid flow hypothesis explains the temperature rise by movement of hot fluid into the fault from adjacent lower crustal regions and increases the temperature relative to the surroundings. The temperature increase is highest on the fault and broadens with increase in depth, following the fluid flow pattern rising into the fault. It is, however, difficult to model. The frictional heating hypothesis has been demonstrated by carrying out thermal modelling using the finite difference method. In the thermal modelling, it has been assumed that the shear stress along the active transcurrent fault was high (100-150 MPa). The problem with this assumption is that the heat generation along an active transcurrent fault may be low as inferred by some workers from the low heat flow anomaly along San Andreas fault. This has been used to indicate that shear stress along active transcurrent fault is low. Laboratory studies based on the coefficient of friction of crustal rocks predicted that the peak shear stress can be greater than calculated from the heat flow data. A likely reason given by previous workers to support the coincidence of high shear stress and the low heat flow anomaly is that the heat is redistributed by hydrothermal fluid circulations. Another problem is related to the horizontal displacement of about 400 km required to produce sufficient heat. This is near the upper limit of the possible Great Glen fault movement. A possible 600 km displacement has been inferred based on palaeomagnetic data while the geological evidence favours smaller movement of about 100-200 km. Furthermore, the Great Glen anomaly is restricted to mainland Scotland. The linear anomaly is about 200-250 km in length. This may suggest that the formation of magnetite occurred only at the end of the heat generating period or after the transcurrent movements. The fluid flow hypothesis has the advantage of being independent of the magnitude of the displacement. It is dependent on the temperature of the source fluid and an effective fluid transport mechanism within the crust.

The Great Glen magnetic anomaly appears to be ristricted to mainland Scotland. The Great Glen fault extends northeastwards beneath Moray Firth and southwestwards to the south of Mull. It is possible that the Great Glen magnetic anomaly does extend seawards in one or both direction but it may be masked by the anomalies due to other structure such as the Mull Tertiary igneous rocks and the magnetic effects of basement topography beneath the Moray Firth basin. Further work on these two areas may help resolve the problem of the apparent limited length of the Great Glen feature.

6.3 Interpretation of magnetic anomalies over the Midland Valley of Scotland

The Midland Valley of Scotland is traversed by a chain of positive magnetic anomalies. Over the Isle of Arran a slightly elongated magnetic anomaly occurs over the Tertiary volcanic centre. To its east, prominent short wavelength anomalies are caused by the outcropping Clyde Plateau lavas. An almost circular positive anomaly occurs over Bathgate region. This anomaly does not have any surface representation. The pseudogravimetric transformation smooths the short wavelength anomalies over the Clyde Plateau lavas into an elongated medium wavelength feature. The positive anomalies over Bathgate and Arran are distinct on the pseudogravimetric map.

A prominent feature of the pseudogravimetric map of the Midland Valley of Scotland is the long wavelength elongated anomaly traversing the region. It is slightly oblique to the Highland boundary and Southern Upland faults which forms the boundaries of the Midland Valley. This elongated anomaly is not obvious on the aeromagnetic map but is clear on the upward continued aeromagnetic map.

Modelling has been carried out over the Clyde Plateau lavas. A profile across the Midland Valley crossing the Clyde Plateau where the thickness of the lavas is

quite well defined has been used. The pseudogravimetric profile clearly shows the presence of a central medium wavelength anomaly superimposed on a long wavelength anomaly. This is not obvious on the magnetic profile where the magnetic anomaly defines the boundary of the lavas with the less magnetic rocks distinctly. Magnetic modelling along the profile with the lavas constrained by the outcrop and known depth extent gave a body which can only explain the central high of the pseudogravimetric anomaly. The magnetization of the body is about 2.7 A/m. This suggests that the long wavelength components observed on the pseudogravimetric anomaly is caused by a deeper crustal source. The pseudogravimetric anomaly has been used to estimate the deep source. There is, however, no definite constraint on the depth to the top and magnetization of the deep crustal source. The two bodies were combined to form a composite model and modified to obtain a satisfactory fit to both the magnetic and the pseudogravimetric anomalies. The modelling requires the presence of a deep source underlying the Midland Valley.

The pseudogravimetric profile traversing the Bathgate anomaly is made up of both long and medium wavelength components. These are attributed to the crustal source described above and a local Bathgate feature respectively. The magnetic anomaly along the same profile shows the local Bathgate feature as a prominent positive anomaly. It occurs over the Carboniferous sediments. The strongly magnetized Carboniferous lavas in the region occurs mainly within the Calciferous Sandstone Measures. The BGS Rashiehill Farm borehole indicates that the top of the lavas is at about 800 metres. The lavas may not be laterally extensive because the nearby Salsbury no. 1A borehole indicates that the volcanics only start at a depth of about 1200 meters. The source of Bathgate anomalies has been firstly modelled using the strongly magnetized lavas with a magnetization of about 2.7 A/m similar to the value modelled for the Clyde Plateau lavas. The modelling gives a lava body which has its base at about 5.5 km. The Bathgate anomaly is almost circular and this differs from the irregular shaped anomaly of the exposed lavas. The great depth of the base of the weathered and vesicular lavas and the differences in the shape of the anomalies

probably suggest that the lavas are not the source. Furthermore, the source of the Bathgate anomaly produces a strong positive gravity anomaly. This is not observed over the Clyde Plateau lavas. The almost circular shape of the Bathgate anomaly is similar to that of the anomaly over Arran which has been modelled as due to a concealed basic intrusive body also displaying a strong positive gravity anomaly. The second model of a basic intrusive body with a large base and narrow top seems to be a more likely source of the local Bathgate anomaly.

The chain of positive anomalies over the Midland Valley extends into northern Ireland. The long wavelength anomaly modelled over the Midland Valley is oblique to the boundary faults and does not extend northeastwards. Work on the Irish region based on similar line of studies, followed by comparative study of both regions would give a better understanding as to whether the similarities are surficial or extend within the crust.

6.4 Further potential of the modelling approach

The modelling approach applied in this work has been successful for interpretating some major magnetic anomalies of the Scottish mainland. A similar modelling approach could be applied to the other large magnetic anomalies in Great Britain observed in figures 1.1. This approach could readily be extended to interpret magnetic anomalies in other countries. However, the pseudogravimetric transformation of magnetic anomalies is only successful provided that either the inclination angle of the earth's magnetic field or of the magnetization is greater than about 20^o. Development of a method to overcome the present restriction to higher latitude is a prior step to using the approach in low latitude regions.

REFERENCES

Al-Chalabi, M., 1971. Some studies relating to nonuniqueness in gravity and magnetic inverse problems (Polygons optimisation nonlinear modelling). *Geophysics*, **36**, 835-855.

Allsop, J. M., 1985. Geophysical investigation into the extent of the Devonian rocks beneath East Anglia. *Proceeding Geological Association*, **96**, 371-379.

Anderson, T. B. and Oliver, G. J. H., 1986. The Orlock Bridge fault: a major Late Caledonian sinistral fault in the Southern Uplands Terrane, British Isles. *Transactions of the Royal Society of Edinburgh: Earth Sciences*, **77**, 203-222.

Arkani-Hamed, J. and Celetti, G., 1989. Effects of thermal remanent magnetization on the magnetic anomalies of intrusives, *Journal of Geophysical Research*, **94**, 7364-7378.

Bamford, D., Nunn, K., Prodehl, C. and Jacob. B., 1977. LISPB-III. Upper crustal structure of northern Britain. *Journal of the Geological Society, London*, **133**, 481-488.

Bamford, D., Nunn, K., Prodehl, C. and Jacob. B., 1978. LISPB-IV. Crustal structure of northern Britain. *Geophysical Journal of the Royal Astronomical Society*, **54**, 43-60.

Barakat, H. Z. and Clark, J. A., 1966. On the solution of the diffusion equations by numerical methods. *Journal of Heat Transfer*, **88**, 421-427.

Baranov, V., 1957. A new method for interpretation of aeromagnetic maps: Pseudo-gravimetric anomalies. *Geophysics*, **22**, 359-383.

Barraclough, D. R. and Malin, S. R. C., 1971. *Synthesis of international geomagnetic reference field values.* Institute of Geological Sciences, Report No. 71/1.

Båth, M., 1974. *Spectral analysis in geophysics.* Elsevier Science Publishing Company. Amsterdam, 563 pp.

Beach, A., 1976. The interrelations of fluid transport, deformation, geochemistry and heat flow in early Proterozoic shear zones in the Lewissian complex. *Philosophical Transactions of the Royal Society, London*, **A 280**, 569-604.

Bhattachryya, B. K. and Chan K. C., 1977. Reduction of magnetic and gravity

data on an arbitrary surface acquired in a region of high topographic relief. *Geophysics*, **42**, 1411-1430.

Bluck, B. J., 1983. Role of the Midland Valley of Scotland in Caledonian orogeny. *Transactions of the Royal Society Edinburgh: Earth Sciences*, **74**, 119-136.

Bluck, B. J., 1985. The Scottish paratectonic Caledonides. *Scottish Journal of Geology*, **21**, 437-464.

Bott, M. H. P., 1969. Computation of the magnetic anomalies caused by two-dimensional bodies. *Geophysical Journal of the Royal Astrononical Society*, **18**, 251-256.

Bott, M. H. P., 1973. Inverse methods in the interpretation of magnetic and gravity anomalies. *In*: Bolt, B. A., (ed.) *Methods in Computational Physics*, **13**, Academic Press, 133-162.

Bott, M. H. P., 1982. *The interior of the earth: its structure, constitution and evolution, second edition.* Edward Arnold, 402 pp.

Bott, M. H. P., 1984 GRAVEND, Durham geophysics computer program.

Bott, M. H. P., 1986 GRAV, Durham geophysics computer program.

Bott, M. H. P., 1988. MAG, Durham geophysics computer program

Bott, M. H. P. and Browitt, C. W. A., 1975. Interpretation of geophysical observations between the Orkney and Shetland Islands. *Journal of the Geological Society, London*, **131**, 353-371.

Bott, M. H. P., Holland, J. G., Storry, P. G. and Watts, A. B., 1972. Geophysical evidence concerning the structure of the Lewisian of Sutherland, N.W. Scotland. *Journal of the Geological Society, London*, **128**, 599-612.

Bott, M. H. P. and Ingles A., 1972. Matrix methods for joint interpretation of two dimensional gravity and magnetic anomalies with application to Iceland-Faeroe Ridge. *Geophysical Journal of the Royal Astronomical Society*, **30**, 55-57.

Bott, M. H. P. and Smith, R. A., 1958. The estimation of the limiting depth of gravitating bodies. *Geophysical Prospecting*, **6**, 1-10.

Bott, M. H. P., Smith, R. A. and Stacey, R. A., 1966. Estimation of the direction of magnetization of a body causing a magnetic anomaly using the pseudo-gravity

transformation. *Geophysics*, **31**, 803-811.

Brewer, J. A., Matthews, D. H., Warner, M. R., Hall, J., Smythe, D. K. and Whittington, R. J., 1983. BIRPS deep seismic reflection studies of the British Caledonides. *Nature*, **305**, 206-210.

Briden, J. C., Turnell, H. B. and Watt, D. R., 1984. British palaeomagnetism, Iapetus ocean and the Great Glen fault. *Geology*, **12**, 428-431.

Brook, M., Brewer, M. S. and Powell, D., 1977. Grenville events in Moine rocks of the Northern Highlands, Scotland. *Journal of the Geological Society, London*, **133**, 489-496.

Brown, P. E., 1983. Caledonian and early magmetism. *In*: Craig, G. Y. (ed.) *Geology of Scotland,* second edition. Scottish Academic Press, Edinburgh, 67-194.

Brown, G. C., Francis, E. H., Kennan, P. and Stillman, C. J., 1985. Caledonian igneous rocks of Britain and Ireland. *In*: Harris, A. L (ed)., *The nature and timing of orogenic activity in the Caledonian rocks of the British Isles.* Geological Society of London, Memoir, 9, 1-15.

Brown, G. C. and Locke, C. A., 1979. Space-time variation in British Caledonian granites: some geophysical correlations. *Earth and Planetary Science Letters*, **45**, 69-79.

Buddington, A. F. and Lindsley, D. H., 1964. Iron-titanium oxide mineral and synthetic equivalents. *Journal of Petrology*, **5**, 310-357.

Cameron, I. B. and Stepheson, D., 1985. *British regional geology: The Midland Valley of Scotland,* third edition. British Geological Survey, 172 pp.

Cardwell, R. K., Chinn, D. S., Moore, G. F. and Turcotte, D. L., 1978. Frictional melting on a fault zone with finite thickness. *Geophysical Journal of the Royal Astronomical Society*, **52**, 525-530.

Cermak, V. and Rybach, L., 1989. Vertical distribution of heat production in the continental crust. *Tectonophysics*, **159**, 217-230.

Chan, K. C., 1989. Reply on: Bhattacharyya and Chan, 1977. *Geophysics*, **54**, 665.

Conway, A., Dentith, M. C., Doody, J. J. and Hall, J., 1987. Preliminary interpretation of upper crustal structure across the Midland Valley of Scotland from two east-west seismic refraction profiles. *Journal of the Geological Society, London,*

144, 865-870.

Cooley, J. W. and Tukey, 1965. An algorithm for machine calculation of complex Fourier series. *Mathematics of Computation*, **19**, 297-301

Cordell, L. and Taylor, P. T., 1971. Investigation of magnetisation and density of a north Atlantic seamount using Poisson's theorm. *Geophysics*, **36**, 919-937.

Cordell, L., 1985. Technique, application and problems of analytical continuation of New Mexico aeromagnetic data between arbitrary surfaces of very high relief. International meeting on: *Potential field on rugged topography*, Institut de Geophysique Universite De Lausanne, Switzerland.

Cotton, W. R., 1968. *A geophysical survey of the Campsie and Kilpatrick Hills.* Unpublished PhD thesis, University of Glasgow.

Courtillot, V. E., Ducruix, J. and Le Mouel, J. L., 1973. Le prolongment d'un champ de potentiel d'un contour quelconque sur un contour horizontal., *Annales Geophysicae,* **29**, 361-366.

Courtillot, V. E., Ducruix, J. and Le Mouel, J. L., 1974. A solution of some inverse problems in geomagnetism and gravimetry. *Journal of Geophysical Research*, **79**, 4933-4940.

Craig, G. Y., 1983. *Geology of Scotland,* second edition. Scottish Academic Press, Edinburgh, 472 pp.

Crampin, S., Jacob, A. W. B., Miller, A. and Neilson, A., 1970. The LOWNET radio-linked seismometer network in Scotland. *Geophysical Journal of the Royal Astronomical Society*, **21**, 207-216.

Crawford, M. L. and Hollister, L. S., 1986. Metamorphic fluids: the evidence from fluid inclusions. *In*: Walther, J. V. and Wood, J. B. (eds.). *Fluid-rock interactions during metamorphism.* Advances in Physical Geochemistry, **5**, 1-35.

Dampney, C. N. G., 1969. The equivalent source technique. *Geophysics*, **34**, 39-53.

Davidson, K. A. S., Sola, M., Powell, D. W. and Hall, J., 1984. Geophysical model for the Midland Valley of Scotland. *Transactions of the Royal Society Edinburgh: Earth Science*, **75**, 175-181.

Dempster, T. J. and Bluck, B. J., 1989. Short paper: The age and origin of boulders in the Highland Border Complex: constraints on terrane movements. *Journal*

of the Geological Society, London, **146**, 377-379.

Dewey, J. F., 1971. A model for the Lower Palaeozoic evolution of the southern margin of the southern Caledonides of Scotland and Ireland. *Scottish Journal of Geology*, 7, 219-240.

Dimitropoulos, K., 1981. Caledonian granites as a cause of uncertainty in LISPB interpretation in the Grampian Highland area. *Geophysical Journal of the Royal Astronomical Society*, **65**, 695-702.

Dimitropoulos, K. and Donato, J. A., 1981. The inner Moray Firth Central Ridge, a geophysical interpretation. *Scottish Journal of Geology*, **17**, 27-38.

Donovan, R. N., Archer, R., Turner, P. and Tarling, D.H., 1976. Devonian palaeogeography of the Orcadian Basin and the Great Glen fault. *Nature*, **259**, 550-551.

Downing, R. A. and Gray, D. A., 1986. *Geothermal energy: The potential in United Kingdom.* British Geological Survey. 187 pp

Ducruix, J., Le Mouel, J. L. and Courtillot, V, 1974. Continuation of three-dimensional potential fields measured on an uneven surface. *Geophysical Journal of the Royal Astronomical Society*, **38**, 299-314.

Elders, C. F., 1987. The provenance of granite boulders in conglomerates of the Northern and Central Belts of the Southern Uplands of Scotland. *Journal of the Geological Society, London*, **144**, 853-860.

Emeleus, C.H., 1983. Tertiary igneous activity. *In*: Craig, G. Y.(ed.), *Geology of Scotland,* second edition. Scottish Academy Press, Edinburgh, 357-390.

Emilia, D. A., 1973. Equivalent sources used as an analytic base for processing total magnetic-field profile . . . *Geophysics*, **38**, 339-348

Engles, A. E. J. and Engles, C. E., 1962. Hornblende formed during progressive metamorphism of amphibolite, north-west Adirandack mountain New York. *Bulletin of the Geological Society of America*, **73**, 1499-1514.

Etheridge, M. A., Wall, V. J. and Vernon, R. H., 1983. The role of the fluid phase during regional metamorphism and deformation. *Journal of Metamorphic Geology*, **1**, 205-226.

Ferry, J. M., 1986. Reaction progress: a monitor of fluid-rock interaction during metamorphic and hydrothermal events. *In*: Walther, J. V. and Wood, J. B.

(eds.). *Fluid-rock interactions during metamorphism.* Advances in Physical Geochemistry, **5**, 60-88.

Fettes, D. J., Long, C. B., Bevins, R. E., Max, M. D., Oliver, G. J. H, Primmer, T. J., Thomas, L. J. and Yardly, B. W. D., 1985. Grade and time of metamorphism in the Caledonide orogen of Britain and Ireland. *In*: Harris, A. L., (ed.), *The nature and timing of orogenic activities in the Caledonian rocks of the British Isles.* Geological Society of London, Memoir, 9, 41-45.

Fletcher, R., 1970. A new approach to variable metric algorithm. *Computer Journal*, **13**, 317-322.

Floyd, J. D. and Trench, A., 1988. Magnetic susceptibility contrasts in Ordovician greywackes of the Southern Uplands of Scotland. *Journal of Geological Society, London*, **145**, 77-83.

Fountain, D. M., Furlong, K. P. and Salisbury, M. H., 1987. A heat production model of a shield area and its implications for the heat flow-heat production relationship. *Geophysical Research Letters*, **14**, 283-286.

Francis, E. H., 1983. Carboniferous-Permian igneous rocks. *In*: Craig, G. Y. (ed.) *Geology of Scotland*, second edition. Scottish Academy Press, Edinburgh, 253-291.

Freeman, B., Klemperer, S. L. and Hobbs, R. W., 1988. The deep structure of northern England and Iapetus suture zone from BIRPS deep seismic reflection profiles. *Journal of the Geological Society, London*, **145**, 727-740.

Frost, B. R. and Chacko, T., 1989. The granulite uncertainty principle: limitations on thermobarometry in granulites. *Journal of Geology*, **97**, 435-450.

Frost, B. R. and Frost, C. D., 1987. CO_2, melts and granulite metamorphism. *Nature*, **327**, 503-505.

Garson, M. S. and Plant, J., 1972. Possible dextral movements on the Great Glen and Minch Faults, Scotland. *Nature, Physical Science*, **240**, 31-35.

Gates, A. E. and Gundersen, L. C. S., 1989. Role of ductile shearing in the concentration of radon in the Brookneal zone, Virginia. *Geology*, **17**, 391-394.

Gebhart, B., 1971. *Heat transfer*, second edition. McGraw-Hill Book Company, New York, 596 pp.

Graham, A. M. and Upton, B. G. J., 1978 . Gneisses in diatremes, Scottish Midland Valley: petrology and tectonic implications. *Journal of the Geological Society, London*, **135**, 219-228.

Granser, H., 1983. Comments on: Syberg 1972. *Geophysical Prospecting*, **31**, 992-994.

Gunn, P. J., 1972. Application of Wiener filters to transformations of gravity and magnetic fields. *Geophysical Prospecting*, **20**, 860-871.

Gupta, V. K. and Ramani, N., 1978. A note on convolution and padding for two dimensional data. *Geophysical Prospecting*, **26**, 214-217

Hagiwara, Y., 1966. Three dimensional distribution of real Bouguer anomalies from gravity values observed at various elevation. *Bulletin of the Earthquake Research Institute Tokyo Imperial University*, **48**, 519-530.

Hall, J., 1974. A seismic reflection survey of the Clyde Plateau lavas in northern Ayrshire and Renfrewshire. *Scottish Journal of Geology*, **9**, 252-279.

Hall, D. H. and Dagley, P., 1970. *Regional magnetic anomalies. An analysis of the smoothed aeromagnetic map of Great Britain and Northern Ireland.* Institute of Geological Sciences, Report No. 70/10.

Hall, J., 1985. Geophysical constrains on crustal structure of Dalradian region of Scotland. *Journal of the Geological Society, London*, **142**, 149-155.

Hall, J., 1986, Geophysical lineaments and deep continental structure. *Philosophical Transactions of the Royal Society London*, **A 317**, 33-44.

Hansen R. O., 1985. Variable elevation using equivalent source. International meeting on: *Potential field on rugged topography.* Institut de Geophysique Universite De Lausanne, Switzerland.

Hansen, R. O. and Miysaki, Y., 1984. Continuation of potential fields between arbitrary surfaces (equivalent source algorithm). *Geophysics*, **49**, 787-795.

Harris, A. L, 1983. The growth and structure of Scotland *In:* Craig, G. Y. (ed.) *Geology of Scotland,* second edition. Scottish Academy Press, Edinburgh, 1-21.

Henderson, R. G. and Cordell, L., 1971. Reduction of unevenly spaced potential field data to a horizontal plane by means of finite harmonic series. *Geophysics*, **36**, 856-866.

Hickman, S. H., Zoback, M. D. and Healy, J. H., 1988. Continuation of a deep borehole stress measurement profile near the San Andreas fault. 1. Hydraulic fracturing stress measurements at Hi Vista, Mojave Desert, California. *Journal of Geophysical Research*, **93**, 15183-15195.

Hipkin, R. G. and Hussain, A. 1983. *Regional gravity anomalies. 1 Northern Britain.* Institute Geological Sciences, Report No. 82/10.

Holgate, N. ,1969. Palaeozoic and Tertiary transcurrent movements on the Great Glen fault. *Scottish Journal of Geology*, **5**, 97-139.

Holliday, D. W., 1986. Devonian and Carboniferous basin. *In*: Downing, R. A. and Gray, D. A. (eds). *Geothermal energy: the potential in the United Kingdom.* British Geological Survey, 84-110.

Hossain, M. M. A., 1976. *Analysis of the major gravity and magnetic anomalies centered about Bathgate, Central Scotland.* Unpublished M.Sc. thesis, University of Glasgow.

Hussain, A. and Hipkin, R. G., , 1981. Regional gravity map of the British Isles, North sheet. *In*: Hipkin, R. G. and Hussain, A. (1983) *Regional gravity anomalies. 1 Northern Britain.* Institute of Geological Sciences, Report No. 82/10.

Hutton, D. H. W., 1987. Strike-slip terranes and a model for the evolution of the British and Irish Caledonides. *Geological Magazine*, **124**, 405-425.

Ivan, M., 1986. On the upward continuation of potential field data between irregular surfaces. *Geophysical Prospecting*, **34**, 735-742.

James, F. and Roos, M., 1969. *Minuit: A program to minimise a function of n variables, compute the covariance matrix, and find the true error.* Unpublished Long write up, CERN Computer 6000 series Program Library, 47 pp.

Johnson, M. R. W., 1983a. Torridonian-Moine. *In*: Craig, G. Y.(ed.) *Geology of Scotland*, second edition. Scottish Academy Press, Edinburgh, 49-70.

Johnson, M. R. W., 1983b. Dalradian. *In*: Craig G. Y. (ed.) *Geology of Scotland*, second edition. Scottish Academy Press, Edinburgh, 77-104.

Kelling, G., 1961. The stratigraphy and structure of the Ordovician rocks of Rhinns of Galloway. *The Quarterly Journal of the Geological Society, London*, **117**, 107-137.

Kennedy, W. Q., 1946. The Great Glen Fault. *Quarterly Journal of the Geological Society, London,* **102**, 41-72.

Kerrich, R., La Tour, T. E. and Willmore, L., 1984. Fluid participation in deep fault zones: Evidence from geological, geochemical, and $^{18}O/^{16}O$ relations. *Journal of Geophysical Research,* **89**, 4331-4343.

Kerrich, R., 1986. Fluid transport in lineaments. *Philosophical Transactions of the Royal Society of London,* **A 317**, 219-251.

Kremenetsky, A. A., Milanovsky, S. Yu. and Ovchinnikov, L. N., 1989. A heat generation model for continental crust based on deep drilling in the Baltic Shield. *Tectonophysics,* **159**, 231-246.

Lachenbruch, A. H. and Sass, J. H., 1980. Heat flow and energetics of the San Andreas fault zone. *Journal of Geophysical Research,* **85**, 6185-6222.

Lachenbruch, A. H., 1980. Frictional heating, fluid pressure, and the resistance to fault motion. *Journal of Geophysical Research,* **85**, 6097-6112.

Lamb, W. M. and Valley, J., 1984. Metamorphism of reduced granulites in low-CO2 vapour free environment. *Nature,* **312**, 56-58.

Lambert, R. St. J. and McKerrow, W. S., 1976. The Grampian orogeny. *Scottish Journal of Geology,* **12**, 271-292.

Lee, T. C. and Delaney, P. T., 1987. Frictional heating and pore pressure rise due to a fault slip. *Geophysical Journal of the Royal Astronomical Society, London,* **88**, 569-591.

Leggett, J. K., McKerrow, W. S. and Soper, N. J., 1983. A model for the crustal evolution of southern Scotland. *Tectonics,* **2**, 187-210.

Longman, C. D., Bluck, B. J. and van Breeman, O., 1979. Ordovician conglomerates and the evolution of the Midland Valley. *Nature,* **280**, 578-581.

MacDonald, R., 1975. Petrochemistry of the early Carboniferous (Dinantian) lavas of Scotland. *Scottish Journal of Geology,* **11**, 269-314.

Mayhew, M. A., Johnson, B. D. and Wasilewski, 1985. A review of problems and progress in studies of satellite magnetic anomalies. *Journal of Geophysical Research,* **90**, 2511-2522.

Mbipom, E. W. and Hutton, V. R. S., 1983. Geoelectromagnetic measurements across the Moine thrust and Great Glen in northern Scotland. *Geophysical Journal of the Royal Astronomical Society, London*, **74**, 507-524.

McCaig, A. M., 1988. Deep fluid circulation in fault zones. *Geology*, **16**, 867-870.

McGarr, A., Zoback, M. D. and Hanks, T. C., 1982. Implications of an elastic analysis of in situ stress measurements near the San Andreas fault. *Journal of Geophysical Research*, **87**, 7797-7806.

McKenzie, D. P. and Brune, J. N., 1972. Melting of fault plane during large earthquake. *Geophysical Journal of the Royal Astronomical Society*, **29**, 65-78.

McLean, A. C. and Qureshi, I. R., 1966. Regional Gravity anomalies in the western Midland Valley of Scotland. *Transactions of the Royal Society of Edinburgh: Earth Sciences*, **66**, 267-283.

McLean. A. C. and Walker, J., 1978. Gravity and magnetic surveys of the upper Firth of Clyde and Bute *In*: McLean, A. C. and Deegan, C. E. (eds.). *The solid geology of the Clyde Sheet (55° N/6° W)*. Institute of Geological Sciences, Report No. 78/9, 29-42.

McLean, A. C. and Wren, A. E., 1978. Gravity and magnetic studies of lower Firth of Clyde. *in*: McLean, A. C. and Deegan, C. E. (eds.) *The solid geology of the Clyde sheet (55°N/6° W)*. Institute of Geological Sciences. Report No. 78/9, 7-27.

Morgan, P., Wayne, N. S. and Kelvin, P. F., 1987. Background and implication of the linear heat-flow production. *Geophysical Research Letters*, **14**, 248-251.

Morris, P., 1989. A composite magnetic map of Ireland. Communications of the Dublin Institute for advance studies. *Geophysical Bulletin*, Series D, **42**

Munro, M., 1973. Structures in the south-eastern portion of the Strontian granitic complex, Argyllshire. *Scottish Journal of Geology*, **9**, 99-108.

Murrell, S. A. F., 1985. Aspects of relationship between deformation and prograde metamorphism that cause evolution of water. *In*: Thompson, A. B. and Rubie, D. C. (eds). *Metamorphic reactions, kinetic, texture and deformation.* Advances in Physical Geochemistry, **4**, 211-241.

Murrell, S. A. F., 1986. The role of deformation, heat, and thermal processes in the formation of the lower continental crust. *In*: Dawson, J. B., Carswell, D. A.,

Hall, J. and Wedepohl, K. H. (eds). *The nature of the lower Continental Crust.* Geological Society of London, Special Publication, **24**, 107-117.

Mutton, A. J. and Shaw, R.D., 1979. Physical property measurement as an aid to magnetic interpretation in basement terrains. *Bulletin of Australian Society Exploration Geophysicist*, **10**, 79-91.

Mykura, W., 1975. Possible large scale sinistral displacement along the Great Glen fault in Scotland. *Geological Magazine*, **112**, 91-93.

Mykura, W., 1983. Old Red Sandstone. *In*: Craig, G. Y. (ed.) *Geology of Scotland,* second edition. Scottish Academy Press, Edinburgh, 205-251.

Nagata, T., 1939. A 'free-air' reduction of local magnetic anomalies. *Bulletin of the Earthquake Research Institute Tokyo Imperial university*, **17**, 411-421.

Nakatsuka, T., 1981. Reduction of magnetic anomalies to and from an arbitrary surface. *Butsuri-Tanko (Geophysical Exploration)*, **34**, 6-12.

Nelder, J. A. and Mead, R., 1965. A simplex method for function minimization. *Computer Journal*, **7**, 308-313 .

Nesbitt, B. E. and Muehlenbachs, K., 1989. Origin and movements of fluids during deformation and metamorphism in the Canadian Cordillera. *Science*, **245**, 733-736.

Nettleton, L. L., 1940. *Geophysical prospecting for oil.* McGraw-Hill New York and London, 444 pp.

Nicolas, A., Bouchez, J. L., Blaise, J. and Poirier, J. P., 1977. Geophysical aspects of deformation in continental shear zones. *Tectonophysics*, **42**, 55-73.

Nur, A., and Walder, J. (in press, see page 149).

Ofoegbu, C. O., 1982. *Methods of interpreting magnetic anomalies with application to the Minch Dyke and magnetic anomalies over the lower and upper Benue Trough of Nigeria.* Unpublished Ph.D. thesis, University of Durham.

Ord, A. and Christie, J. M., 1984. Flow stresses from microstructures in mylonitic quartzite of the Moine Thrust Zone, Assynt Area, Scotland. *Journal of Structural Geology*, **6**, 639-654.

O'Neil, J. R., and Hanks, T. C., 1980. Geochemical evidence for water-rock interaction along San Andreas and Garlock fault of California. *Journal of Geophysical Research*, **85**, 8286-6292.

ODP Leg 110 Scientific Party , 1987. Explusion of fluids from depth along a subduction-zone decollement horizon. *Nature*, **326**, 785-788.

Pankhurst, R. J., 1979. Isotope and trace element evidence from origin and evolution of Caledonian granites in the Scottish Highlands. *In:* Atherton, M. P. and Tarner (eds). *Origin of granite batholiths: geochemical evidence*, Shiva, 18-33.

Park, R. G., 1961. A vertical force magnetic survey over part of the Dusk Water Fault of north Ayrshire. *Transactions of the Geological Society, Glasgow*, **24**, 154-168.

Parker, R. L. and Kiltgord, K. D., 1972. Magnetic upward continuation from an uneven track(Schwarz-Christoffel transformation on deep-tow). *Geophysics*, **37**, 662-668.

Parry, W. T. and Bruhn, R. L., 1986. Pore fluid and seismogenic characteristic of fault rock at depth on the Wasatch fault, Utah. *Journal of Geophysical Research*, **91**, 730-744.

Passchier, 1982. Pseudotactyte and the development of ultramylonite bands in the Saint-Barthelemy massif, French Pyrenees. *Journal of Structural Geology*, **4**, 69-79.

Paterson, I. B. and Hall, I. H. S., 1986. *Lithostatigraphy of the late Devonian and early Carboniferous rocks in the Midland Valley of Scotland.* British Geological Survey, Report No. 18/3.

Pavlis, T. L., 1986. Role of strain heating in evolution of megathrust. *Journal of Geophysical Research,* **91** , 120-142 .

Pedersen, L. B.,1989. Discussion on: Bhattachryya and Chan, 1977. *Geophysics,* **54**, 664-665.

Piaseki, M. A. J. and van Breemen, O., 1979. The Central Highland Granulites - cover-basement tectonics in the Moine. *In*: Harris, A. L., Holland, C. L. and Leak, B. E.,(eds.) *The Caledonides of the British Isles* - reviewed. Geological Society of London, Special Publication, **8**, 139-144.

Piper, J. D. A., 1979. The palaeomagnetism of the central zone of the Lewisian foreland, north-west Scotland. *Geophysical Journal of the Royal Astrononical Society*, **59**, 101-122.

Plant, J. A., Simpson, P. R., Green, P. M., Watson, J. V. and Fowler, M. B., 1983.

Metalliferous and mineralized Caledonian granites in relation to regional metamorphism and fracture systems in northern Scotland. *Transactions Institute of Mining and Metallurgy*, **92**, 33-41.

Powell, D and Phillips, W. E. A, 1985. Time of deformation in the Caledonide Orogeny of Britain and Ireland. *In*: Harris, A. L.(ed.) *The nature and the timing of orogenic activities in the Caledonian rocks of the British Isles*, Geological Society of London, Memoir, 9, 17-39.

Powell, D. W., 1970. Magnetised rocks within the Lewisian of Western Scotland and under the Southern Uplands. *Scottish Journal of Geology*, **6**, 353-369.

Powell, D. W., 1978a. Gravity and magnetic anomalies attributable to basement sources under Britain. In Bowes, D. R. and Leak (eds) *Crustal evolution in northwestern Britain and adjacent regions.* Geological Journal Special Issue, 10, 107-144.

Powell, D. W. , 1978b. Geology of a continental margin 3: gravity and magnetic anomaly interpretaion of Girvan-Ballentrae district. *In*: Bowes, D. R. and Leak (eds) *Crustal evolution in northwestern Britain and adjacent regions.* Geological Journal Special Issue, 10, 177-182.

Ramberg, H., 1948. Titanic iron ore formed by dissociation of silicates in granulite facies. *Economic Geology*, **43**, 553-570.

Ray, R. D. and Friedberg, J. L., 1985. Continuation as an aid in compilation of draped aeromagnetic survey. International meeting on: *Potential field on rugged topography*, Institut de Geophysique Universite De Lausanne, Switzerland.

Read, H. H., 1961. Aspects of Caledonian magmatism in Britain. *Liverpool and Manchester Geological Journal*, **2**, 653-683.

Ricard, Y. and Blakely, R. J., 1988. A method to minimise edge effects in two-dimensional discrete Fourier transforms. *Geophysics*, **53**, 1113-1117.

Richardson, S. W. and Powell, R., 1976. Thermal causes of the Dalradian metamorphism in the central Highlands of Scotland. *Scottish Journal of Geology*, **12**, 237-268.

Rogers, D. A., Marshall, J. E. A and Astin, T. R., 1989. Short paper: Devonian and later movements on the Great Glen fault system, Scotland. *Journal of the Geological Society, London*, **146**, 369-372.

Roy, A., 1962. Ambiguity in geophysical interpretation. *Geophysics*, **27**, 90-99.

Roy, R. F., Blackwell, D. D. and Birch, F., 1968. Heat generation of plutonic rocks and continental heat flow provinces. *Earth Planetary Science Letters*, **5**, 1-12.

Sampson, R. J., 1975. Surface II graphic system. Kansas Geological Survey, 239 pp.

Schatz, J. F. and Simmons, G., 1972. Thermal conductivity of earth materials at high temperatures. *Journal of Geophysical Research*, **77**, 6966-6973.

Schlinger, C. M., 1985. Magnetization of lower crust and interpretation of regional magnetic anomalies: Example from Lofoten and Vesteralen Norway. *Journal of Geophysical Research*, **90**, 11484-11504.

Scholz, C. H., Beavan, J. and Hanks, T. C., 1979. Frictional metamorphism, argon depletion, and tectonic stress on the Alpine Fault, New Zealand. *Journal of Geophysical Research*, **84**, 6770-6782.

Shive, P. N., 1989. Can remanent magnetization in the deep crust contribute to long wavelength magnetic anomalies?, *Geophysical Research Letters*, **16**, 89-92.

Shuey, R. T., 1972. Application of Hilbert transforms to magnetic profiles (Pseudo-gravity reduction-to-pole). *Geophysics*, **37**, 1043-1045.

Sibson, R. H., 1983. Continental fault structure and the shallow earthquake source. *Journal of the Geological Society, London*, **140** 40, 741-767.

Sibson, R. H., 1986. Earthquakes and rock deformation in crustal fault zone. *Annual Review of Earth Planet Science*, **14**, 149 -175.

Smith, D. I. and Watson, J., 1983. Scale and timing of movements on the Great Glen Fault, Scotland. *Geology*, **11**, 523-526.

Smith, R. A., 1959a. On the depth of bodies producing local magnetic anomalies. *Quarterly Journal of Mechanics and Applied Mathematics*, **12**, 354-364.

Smith, R. A., 1959b. Some depth formulae for local magnetic and gravity anomalies. *Geophysical Prospecting*, **7**, 55-63.

Smith, R. A., and Bott, M. H. P., 1975. Structure of the crust beneath the Caledonian foreland and Caledonian belt of north Scottish shelf region. *Geophysical Journal of the Royal Astronomical Society*, **40**, 187-205.

Spector, A. and Grant, F. S., 1970. Statistical models for interpreting aeromagnetic data. *Geophysics*, **35**, 293-302 .

Stock, J. M. and Healy, J. H., 1988. Hydraulic fracturing stress measurements at Black Butte, Mojave Desert, California. Continuation of a deep borehole stress measurement profile near the San Andreas fault. *Journal of Geophysical Research*, **93**, 15196-15206.

Storetvedt, K. M. and Torsvik, T. H., 1983. Palaeomagnetic reexamination of the basal Caithness Old Red Sandstone: aspects of local and regional tectonics. *Tectonophysics*, **98**, 151-164.

Storetvedt, K. M., 1974. Possible large scale sinistral displacement along the Great Glen fault in Scotland. *Geological Magazine*, **111**, 23-36.

Storetvedt, K. M., 1975. Possible large scale sinistral displacement along the Great Glen fault in Scotland (reply). *Geological Magazine*, **112**, 93-94.

Storetvedt, K. M., 1987. Major late Caledonian and Hercynian shear movements on the Great Glen Fault. *Tectonophysics,* **143**, 253-267.

Syberg, F. J. R., 1972. Potential field continuation between general surfaces. *Geophysical Prospecting*, **20**, 267-282 .

Tantrigoda, D. A., 1982. *Interpretation of magnetic anomalies using the pseudogravimetric transformation and other methods, with application to Tertiary volcanic centres in N-W Scotland*, Unpublished Ph.D. thesis, University of Durham, 95 pp.

Thirlwall, M. F., 1989. Short paper: Movement on proposed terrane boundaries in northern Britain: constraints from Ordovician-Devonian igneous rocks. *Journal of the Geological Society, London*, **146**, 373-376.

Torgersen, T., 1990. Crustal-scale fluid transport. *Eos, Transactions, American Geophysical Union*, **71**, 1,4,13.

Torsvik, T. H., Lyse, O., Atteras, G. and Bluck, B. J., 1989. Paleozoic paleomagnetic results from Scotland and their bearing on the British apparent polar wander path. *Physics of the Earth and Planetary Interiors*, **55**, 93-105.

Trench, A., Bluck, B. J. and Watts, D. R., 1988. Palaeomagnetic studies within the Ballantrae Ophiolite; southwest Scotland: magnetotectonic and regional tectonic implications. *Earth and Planetary Science Letters*, **90**, 431-448.

Tsay, L. J., 1975. The use of Fourier series method in upward continuation with new improvements. *Geophysical Prospecting*, **23**, 1-28.

Tsay, L. J., 1976. Continuation of total intensity anomaly on aeromagnetic profiles with constant elevation change. *Geophysical Prospecting*, **24**, 70-78.

Tsirulskiy, A. V. and Ospishcheva, L. Y., 1968. An algorithm for the reduction of observed potential value to a common level. *Physics of the Solid Earth*, 226-270

Tsuboi. C., 1965. Calculation of Bouguer anomalies with due regard to anomaly in the vertical gradient. *Japan Academy Proceedings,* **41**, 386-391.

Turcotte, D. L. and Schubert, G., 1982. *Geodynamics: application of continuum physics to geological problems.* John Wiley and sons, New York, Chichester, Brisbane, Toronto, Singapore. 450 pp.

Turcotte, D. L., Tag, P. H. and Cooper, R. F., 1980. A steady state model for the distribution of stress and temperature on the San Andreas fault, *Journal of Geophysical Research*, **85**, 6224-6230.

Turner, J. F., 1968. *Metamorphic petrology, mineralogical and field aspect.* McGraw-Hill Book company, 403 pp.

Upton, B. J. G., Aspen, P. and Chapman, N. A., 1983. The upper mantle and deep crust beneath the British Isles: evidence from inclusions in volcanic rocks. *Journal of the Geological Society, London*, **140**, 105-121.

Van der Voo, R. and Scotese, C., 1981. Palaeomagnetic evidences for a large scale (2000km) sinistral offset along the Great Glen fault during Carboniferous time. *Geology*, **9**, 583-589.

Wasilewski, P. J., Thomas, H. H. and Mayhew, M. A., 1979. The Moho as a magnetic boundary. *Geophysical Research Letters*, **6**, 541-544.

Watson, J. 1983. Lewisian. *In* Craig, G. Y. (ed.), *Geology of Scotland*, second edition. Scottish Academy Press, Edinburgh, 23-47.

Watson, J., 1984. The ending of the Caledonian orogeny in Scotland. *Journal of the Geological Society, London*, **141**, 193-214.

Watts, A. B., 1971. Geophysical investigations on the continental shelf and slope north of Scotland. *Scottish Journal of Geology*, **7**, 189-218.

Webb, P. C. , Lee, M. K. and Brown, G. C. 1987. Heat flow-heat production relationships in the UK and the vertical distribution of heat production in granite batholiths. *Geophysical Research Letters*, **14**, 279-282.

Wendorff, L., 1985. The Schawrz Christoffel transformation applied to upward continuation of potential field data from uneven track. International meeting on: *Potential field on rugged topography*, Institut de Geophysique Universite De Lausanne, Switzerland.

Westbrook, G. K., 1973. *Crust and upper mantle structure in the region of Barbados and the Lesser Antilles.* Unpublished Ph.D thesis, University of Durham, 277 pp.

Wheildon, J. and Rollin, K. E., 1986. Heat flow. *In*: Downing, R. A. and Gray, D. A., (eds) *Geothermal energy: The potential in United Kingdom.* British Geological Survey, 8-20.

Williams, C. F. and Narasimhan, T. N., 1989. Hydrogeologic constraints on heat flow along the San Andreas fault: a testing of hypotheses. *Earth and Planetary Science Letters*, **92**, 131-143.

Williams, D. M. and Harper, D. A. T., 1988. A basin model for the Silurian of the Midland Valley of Scotland and Ireland. *Journal of the Geological Society, London*, **145**, 741-748.

Winchester, J. A., 1973. Pattern of regional metamorphism suggests a sinistral displacement of 160 km along the Great Glen fault. *Nature, Physical Science*, **246**, 81-84.

Wintsch, R. P., 1985. The possible effect of deformation on chemical processes in metamorphic zone. *In*: Thompson, A.B. and Rubie, D.C. (eds). *Metamorphic reactions: kinetic, textures and deformation.* Advances in Physical Geochemistry, 4, 291 pp.

Woollett, R. W. 1988. *Digital image processing and isotatic studies of the regional gravity field of Great Britain and adjacent marine regions.* Unpublished Ph.D thesis, University of Durham.

Worm, H. U., 1989. Comment on: Shive 1989. *Geophysical Research Letters*, **16**, 595-597.

Zhou, Xixiang. et. al., 1985. The equivalent source technique for potential field continuation and conversion in rugged topography. International meeting on:

Potential field on rugged topography, Institut de Geophysique Universite De Lausanne, Switzerland

Zoback, M. D., Tsukahara, H. and Hickman, S., 1980. Stress measurements at depth in the vicinity of the San Andreas fault: implications for the magnitude of shear stress at depth. *Journal of Geophysical Research*, **85**, 6157-6173.

Nur, A. and J. Walder, (in press 1989). Time dependent hydraulics of the Earth's crust in The role of fluids in crustal processes, National Academy Press, Washington, D.C.

APPENDICES

The following appendices are programmes used in this work. The programmes are largely self explanatory. The appendices are given in the following order:

Appendix	Program name
2.1	REDUCE
2.2	SPHEREM
2.3	PROFIL
3.1	PSGRA3D
3.2	PSGRA2D
3.3	SPHEREGM
4.1	FDHEAT

```
*
*                        APPENDIX   2.1
*
*
*                      PROGRAM       REDUCE
*
************************************************************************
*    THIS PROGRAMME CARRIES OUT AN UPWARD CONTINUATION OF MAGNETIC
*    ANOMALIES  OBSERVED ON AN IRREGULAR SURFACE ONTO A HORIZONTAL PLANE.
*    THE ROUTINE USES THE NUMERICAL ANALYSIS FFT SUBROUTINE C06FJF.
*    IT TAKES THE MAXIMUM HEIGHT OF THE DATA POINT  AS THE CONTINUATION
*    LEVEL  IF THE INPUT CONTINUATION LEVEL IS SMALLER THAN THE MAXIMUM
*    HEIGHT.
****
*
*     INPUT GRIDDED DATA :   UNIT 7
**      Input data are in free format i.e. data items separated by a blank
*       or comma
**      Distances are in arbitrary units
*
*     LINE 1  NX,NY
*             NX  Number of data points  in x direction
*             NY  Number of data points  in y direction
*             (NX=NY and  MUST BE EVEN)
*     LINE 2  DELX,DELY,XMIN,XMAX,YMIN,YMAX
*             DELX,DELY Sampling interval along x and y directions
*             XMIN,XMAX  minimum and maximum  value  in x  directions.
*             YMIN,YMAX  minimum and maximum  value  in y  directions.
*     LINE 3  Z,A,XC,YC
*      .      Z  Absolute topographic/observation height or
*                continuation distances from the irregular surface
*                to the upward continuation level.
*      .      A  Anomaly, x and y coordinates
*      .      XC,YC  x and y coordinates
*      .      (REPEAT NX*NY TIMES)
*
****
*     INPUT PARAMETER FILE:  UNIT 5 (or interactive and prompted)
*     LINE 1  INFILE
*           File name containing the magnetic anomalies, 7 characters
*     LINE 2  ZCL
*           Continuation level (absolute height above zero level)
*     LINE 3 IYESH
*           IYESH=1  If input is in absolute hight (topographic height)
*           IYESH=1  If input in continuation distance (difference between
*                    ZCL and the absolute height)
*     LINE 4 IYESI
*           IYESI=1  Repeat  repeat 1's for n number of
*                    iterations. Use a value of 0 to    write the
*                    results in the file read in LINE 5.
*                    e.g.  1 1 1 1 1 0 (five iterations and write)
```



```
*     LINE  5 OUTFILE
*           File name for the output. Seven characters only.(eg. 'RESFILE')
*           Output:  UNIT 8
*              NX,NY,DELX,DELY,XMIN,XMAX,ZMIN,ZMAX (2I10,/,6F10.2)
*              Z,AC,XC,YC                          (F10.2,E15.5,2F10.2)
*
*     LINE 6 ITER
*           ITER=1 RETURN TO LINE 4
*           ITER=0 STOP
*
*
*     Compile in MTS:  RUN *FORTRANVS SCARDS=REDUCE
*     Run           :  Run -load+*ig+*nag
*
*
      IMPLICIT REAL*8 (A-H,O-Z)
      DIMENSION A( 64, 64),Z( 64, 64),AAA( 64, 64),AAB( 64, 64),
     +AAC( 64, 64),AAD( 64, 64),AAE( 64, 64),AAF( 64, 64),AC( 64, 64)
      DIMENSION  AR( 64, 64),AI( 64, 64),DK( 64, 64),
      CHARACTER*7 INFILE,OUFILE,REFIL
      WRITE(6,*)' DATA FILE :'
      READ(5,15)INFILE
   15 FORMAT(A7)
      OPEN(7,FILE=INFILE,STATUS='OLD')
      READ(7,*)NX,NY,DELX,DELY,XMIN,XMAX,YMIN,YMAX
      ZMIN=10000000.
      ZMAX=-10000000.
      DO 1 J=1,NY
      DO 1 I=1,NX
C***  CLEAN ARRAY FIRST
      AC(I,J)=0.0D0
      AR(I,J)=0.0D0
      A(I,J)=0.0D0
      AAA(I,J)=0.0D0
      AAB(I,J)=0.0D0
      AAC(I,J)=0.0D0
      AAD(I,J)=0.0D0
      AAE(I,J)=0.0D0
      AAF(I,J)=0.0D0
      DK(I,J)=0.0D0
      READ(7,*)Z(I,J),A(I,J),XC,YC
      AR(I,J)=A(I,J)
      IF (Z(I,J).LT.0)Z(I,J)=0.
      IF (ZMIN.GT.Z(I,J)) ZMIN=Z(I,J)
      IF (ZMAX.LT.Z(I,J)) ZMAX=Z(I,J)
    1 CONTINUE
      DO 100 IJ=1,3*NX
      WORK(IJ)=0.D0
  100 CONTINUE
      WRITE(6,*)'           ZMIN ',ZMIN ,'  ZMAX ',ZMAX
      WRITE(6,*)' CONTINUATION HEIGHT ?'
```

```
      READ(5,*)ZCL
      ZMAXH=ZMAX
      IF (ZCL.LE.ZMAX) ZMAX=ZMAX
      IF (ZCL.GT.ZMAX) ZMAX=ZCL
      WRITE(6,*)' HIGHT INVERSION  IYESH = 1 '
      READ(5,* )IYESH
      WRITE(6,*)' NO OF CONTINUATION LEVELS (MAX 6)'
      READ(5,*)ILL
C***  SET HEIGHT FROM BASE  HEIGHT TO CONTINUATION HEIGHT
      IF (IYESH.NE.1)GOTO 30
      DO 17 J=1,NY
      DO 17 I=1,NX
      Z(I,J)=ZMAX-Z(I,J)-ZMIN
   17 CONTINUE
      ZMAX=ZMAX-ZMIN
      ZMIN=ZMIN-ZMIN
C***  DIVIDE THE RANGE INTO  ILL LEVEL
 30   ZSCALE=ZMAX/(FLOAT(ILL-1))
      WRITE(6,*)'           ZMIN ',ZMIN ,'  ZMAX ',ZMAX
      DO 2  I=1,ILL
      ZL(I)=ZSCALE*(I-1)
      WRITE(6,*)' CONTINUATION HEIGHT ZL(I) :',ZL(I)
    2 CONTINUE
C***  CALCULATE THE WAVE NUMBER
C***  PARAMETERS FOR THE NAG FFT ROUTINE
C***  RENEW ITERATION FROM HERE
      NIT=1
 999  CONTINUE
      WRITE(6,*)' NO OF ITERATIONS  ==',NIT,'  TIMES'
      NIT=NIT+1
      CALL TIME(0)
C***    SET ARRAY FOR THE DIFF. LEVEL
      CALL DKXDKY(DK,NX,NY,DELX,DELY)
      DO 4 J=1,NY
      DO 4 I=1,NX
      AAA(I,J)=AR(I,J)
      AAB(I,J)=AR(I,J)
      AAC(I,J)=AR(I,J)
      AAD(I,J)=AR(I,J)
      AAE(I,J)=AR(I,J)
      AAF(I,J)=AR(I,J)
C     WRITE(2,*)I,J,DK(I,J)
      AI(I,J)=0.D0
    4 CONTINUE
C***            CONTINUATION
      ND(1)=NX
      ND(2)=NY
      LWORK=NX*3
      NDIM=2
      IXY=NX*NY
      IFAIL=0
      UP=-1.
```



```
CL1
      CALL C06FJF(NDIM,ND,IXY,AAA,AI,WORK,LWORK,IFAIL)
      DO 31 J=1,NY
      DO 31 I=1,NX
      AAA(I,J)= AAA(I,J)* EXP(DK(I,J)*ZL(1)*UP)
      AI(I,J)= AI(I,J)* EXP(DK(I,J)*ZL(1)*UP)
   31 CONTINUE
      CALL C06GCF(AI,IXY,IFAIL)
      CALL C06FJF(NDIM,ND,IXY,AAA,AI,WORK,LWORK,IFAIL)
      CALL C06GCF(AI,IXY,IFAIL)
      DO 32 J=1,NY
      DO 32 I=1,NX
      AI(I,J)=0.D0
   32 CONTINUE
CL2
      CALL C06FJF(NDIM,ND,IXY,AAB,AI,WORK,LWORK,IFAIL)
      DO 33 J=1,NY
      DO 33 I=1,NX
      AAB(I,J)= AAB(I,J)* EXP(DK(I,J)*ZL(2)*UP)
      AI(I,J)= AI(I,J)* EXP(DK(I,J)*ZL(2)*UP)
   33 CONTINUE
      CALL C06GCF(AI,IXY,IFAIL)
      CALL C06FJF(NDIM,ND,IXY,AAB,AI,WORK,LWORK,IFAIL)
      CALL C06GCF(AI,IXY,IFAIL)
      DO 34 J=1,NY
      DO 34 I=1,NX
      AI(I,J)=0.D0
   34 CONTINUE
CL3
      CALL C06FJF(NDIM,ND,IXY,AAC,AI,WORK,LWORK,IFAIL)
      DO 35 J=1,NY
      DO 35 I=1,NX
      AAC(I,J)= AAC(I,J)* EXP(DK(I,J)*ZL(3)*UP)
      AI(I,J)= AI(I,J)* EXP(DK(I,J)*ZL(3)*UP)
   35 CONTINUE
      CALL C06GCF(AI,IXY,IFAIL)
      CALL C06FJF(NDIM,ND,IXY,AAC,AI,WORK,LWORK,IFAIL)
      CALL C06GCF(AI,IXY,IFAIL)
      DO 36 J=1,NY
      DO 36 I=1,NX
      AI(I,J)=0.D0
   36 CONTINUE
CL4
      CALL C06FJF(NDIM,ND,IXY,AAD,AI,WORK,LWORK,IFAIL)
      DO 37 J=1,NY
      DO 37 I=1,NX
      AAD(I,J)= AAD(I,J)* EXP(DK(I,J)*ZL(4)*UP)
      AI(I,J)= AI(I,J)* EXP(DK(I,J)*ZL(4)*UP)
   37 CONTINUE
      CALL C06GCF(AI,IXY,IFAIL)
      CALL C06FJF(NDIM,ND,IXY,AAD,AI,WORK,LWORK,IFAIL)
      CALL C06GCF(AI,IXY,IFAIL)
```

```
      DO 38 J=1,NY
      DO 38 I=1,NX
      AI(I,J)=0.D0
   38 CONTINUE
CL5
      CALL C06FJF(NDIM,ND,IXY,AAE,AI,WORK,LWORK,IFAIL)
      DO 39 J=1,NY
      DO 39 I=1,NX
      AAE(I,J)= AAE(I,J)* EXP(DK(I,J)*ZL(5)*UP)
      AI(I,J)= AI(I,J)* EXP(DK(I,J)*ZL(5)*UP)
   39 CONTINUE
      CALL C06GCF(AI,IXY,IFAIL)
      CALL C06FJF(NDIM,ND,IXY,AAE,AI,WORK,LWORK,IFAIL)
      CALL C06GCF(AI,IXY,IFAIL)
      DO 40 J=1,NY
      DO 40 I=1,NX
      AI(I,J)=0.D0
   40 CONTINUE
CL6
      CALL C06FJF(NDIM,ND,IXY,AAF,AI,WORK,LWORK,IFAIL)
      DO 41 J=1,NY
      DO 41 I=1,NX
      AAF(I,J)= AAF(I,J)* EXP(DK(I,J)*ZL(6)*UP)
      AI(I,J)= AI(I,J)* EXP(DK(I,J)*ZL(6)*UP)
   41 CONTINUE
      CALL C06GCF(AI,IXY,IFAIL)
      CALL C06FJF(NDIM,ND,IXY,AAF,AI,WORK,LWORK,IFAIL)
      CALL C06GCF(AI,IXY,IFAIL)
C***
C***  GATHER  THE  6 CONTINUATION VALUES FOR EACH POINT INTO AN ARRAY AND
C***  CARRIES OUT THE INTERPOLATION AT  THE POINT Z(I,J)
C***  ONE BY ONE
      DO 6 J=1,NY
      DO 6 I=1,NX
C*    GET THE HEIGHT AT WHICH THE INTERPOLATION IS NEEDED
      ZI=Z(I,J)
      S=0.D0
C-    WRITE(6,*)' ZI :',ZI
C*   GATHER ANOMALY FROM THE CONTINUED LEVEL
      AL(1)=AAA(I,J)
      AL(2)=AAB(I,J)
      AL(3)=AAC(I,J)
      AL(4)=AAD(I,J)
      AL(5)=AAE(I,J)
      AL(6)=AAF(I,J)
C***  INTERPOLATION ROUTINE
C***  S THE INTERPOLATED VALUE
      CALL GET(ZI,ZL,ZU,AL,AU,S,ZSCALE,ILL)
C***  AC(I,J) IS THE ARRAY OF THE CALCULATED ANOMALY ON THE HORIZONTAL
C***  LEVEL
      AC(I,J)=AC(I,J)+S
    6 CONTINUE
```



```
      WRITE(6,*)' UPCON  ENDS AND STARTS DOWNCON'
C*** THE ANOMALY IS NOW TAKEN TO BE ON A HORIZONTAL PLANE AS IT SHOULD
C*** BE, DOWNWARD CONTINUED TO THE NECESSARY LEVELS. THE ANOMALY ON THE
C*** IRREGULAR SURFACE IS THEN INTERPOLATED FROM THESE LEVELS. THIS
C*** ANOMALY SHOULD BE EQUAL TO THE OBSERVED ANOMALY IF THE
C*** CONTINUATION IS SUCCESSFUL.
C***
C*** SET THE INTERPOLATED ANOMALIES TO THE ARRAY FOR DIFFERENT LEVEL SO
C*** AS THE CONTINUATION  CAN BE DONE DIRECTLY ON TO THE LEVEL
      DO 7 J=1,NY
      DO 7 I=1,NX
       AAA(I,J)=AC(I,J)
       AAB(I,J)=AC(I,J)
       AAC(I,J)=AC(I,J)
       AAD(I,J)=AC(I,J)
       AAE(I,J)=AC(I,J)
       AAF(I,J)=AC(I,J)
       AI(I,J)=0.D0
    7 CONTINUE
CL1
      CALL C06FJF(NDIM,ND,IXY,AAA,AI,WORK,LWORK,IFAIL)
      DO 43 J=1,NY
      DO 43 I=1,NX
      AAA(I,J)= AAA(I,J)* EXP(DK(I,J)*ZL(1))
      AI(I,J)= AI(I,J)* EXP(DK(I,J)*ZL(1))
   43 CONTINUE
      CALL C06GCF(AI,IXY,IFAIL)
      CALL C06FJF(NDIM,ND,IXY,AAA,AI,WORK,LWORK,IFAIL)
      CALL C06GCF(AI,IXY,IFAIL)
      DO 44 J=1,NY
      DO 44 I=1,NX
      AI(I,J)=0.D0
   44 CONTINUE
CL2
      CALL C06FJF(NDIM,ND,IXY,AAB,AI,WORK,LWORK,IFAIL)
      DO 45 J=1,NY
      DO 45 I=1,NX
      AAB(I,J)= AAB(I,J)* EXP(DK(I,J)*ZL(2))
      AI(I,J)= AI(I,J)* EXP(DK(I,J)*ZL(2)  )
   45 CONTINUE
      CALL C06GCF(AI,IXY,IFAIL)
      CALL C06FJF(NDIM,ND,IXY,AAB,AI,WORK,LWORK,IFAIL)
      CALL C06GCF(AI,IXY,IFAIL)
      DO 46 J=1,NY
      DO 46 I=1,NX
      AI(I,J)=0.D0
   46 CONTINUE
CL3
      CALL C06FJF(NDIM,ND,IXY,AAC,AI,WORK,LWORK,IFAIL)
      DO 47 J=1,NY
      DO 47 I=1,NX
      AAC(I,J)= AAC(I,J)* EXP(DK(I,J)*ZL(3))
```

```
      AI(I,J)= AI(I,J)* EXP(DK(I,J)*ZL(3))
   47 CONTINUE
      CALL C06GCF(AI,IXY,IFAIL)
      CALL C06FJF(NDIM,ND,IXY,AAC,AI,WORK,LWORK,IFAIL)
      CALL C06GCF(AI,IXY,IFAIL)
      DO 48 J=1,NY
      DO 48 I=1,NX
      AI(I,J)=0.D0
   48 CONTINUE
CL4
      CALL C06FJF(NDIM,ND,IXY,AAD,AI,WORK,LWORK,IFAIL)
      DO 49 J=1,NY
      DO 49 I=1,NX
      AAD(I,J)= AAD(I,J)* EXP(DK(I,J)*ZL(4))
      AI(I,J)= AI(I,J)* EXP(DK(I,J)*ZL(4))
   49 CONTINUE
      CALL C06GCF(AI,IXY,IFAIL)
      CALL C06FJF(NDIM,ND,IXY,AAD,AI,WORK,LWORK,IFAIL)
      CALL C06GCF(AI,IXY,IFAIL)
      DO 50 J=1,NY
      DO 50 I=1,NX
      AI(I,J)=0.D0
   50 CONTINUE
CL5
      CALL C06FJF(NDIM,ND,IXY,AAE,AI,WORK,LWORK,IFAIL)
      DO 51 J=1,NY
      DO 51 I=1,NX
      AAE(I,J)= AAE(I,J)* EXP(DK(I,J)*ZL(4))
      AI(I,J)= AI(I,J)* EXP(DK(I,J)*ZL(4))
   51 CONTINUE
      CALL C06GCF(AI,IXY,IFAIL)
      CALL C06FJF(NDIM,ND,IXY,AAE,AI,WORK,LWORK,IFAIL)
      CALL C06GCF(AI,IXY,IFAIL)
      DO 52 J=1,NY
      DO 52 I=1,NX
      AI(I,J)=0.D0
   52 CONTINUE
CL6
CL6
      CALL C06FJF(NDIM,ND,IXY,AAF,AI,WORK,LWORK,IFAIL)
      DO 53 J=1,NY
      DO 53 I=1,NX
      AAF(I,J)= AAF(I,J)* EXP(DK(I,J)*ZL(6))
      AI(I,J)= AI(I,J)* EXP(DK(I,J)*ZL(6))
   53 CONTINUE
      CALL C06GCF(AI,IXY,IFAIL)
      CALL C06FJF(NDIM,ND,IXY,AAF,AI,WORK,LWORK,IFAIL)
      CALL C06GCF(AI,IXY,IFAIL)
C***

C***  COLLECT THE  6 CONTINUATION VALUES FOR EACH POINT INTO AN ARRAY AND
C***  CARRIED OUT THE INTERPOLATION FOR THE HEIGHT AT THE POINT Z(I,J)
```



```
C***  ONE BY ONE
      DO 8 J=1,NY
      DO 8 I=1,NX
C*    GET THE HEIGHT AT WHICH THE INTERPOLATION IS NEEDED
      ZI=Z(I,J)
      S=0.D0
C*   GATHER ANOMALY FROM THE CONTINUED LEVEL
      AL(1)=AAA(I,J)
      AL(2)=AAB(I,J)
      AL(3)=AAC(I,J)
      AL(4)=AAD(I,J)
      AL(5)=AAE(I,J)
      AL(6)=AAF(I,J)
C***  INTERPOLATION ROUTINE
      CALL  GET(ZI,ZL,ZU,AL,AU,S,ZSCALE,ILL)
C*    USE AR(I,J) FOR THE ARRAY OF THE DOWN CONTINUED  VALUES
      AR(I,J)=S
    8 CONTINUE
C*** DETERMINE THE RESIDUAL VALUE OF THE OBSERVED AND THE CONTINUED FROM
C*** THE REDUCED ANOMALY. SHOULD BE SMALL IF THE REDUCED ANOMALY IS
C*** CORRECT
      SUM=0.0
      DO 9 J=1,NY
      DO 9 I=1,NX
      AR(I,J)=A(I,J)-AR(I,J)
       SUM=SUM+ABS(AR(I,J))
       SUM=ABS(SUM)
    9 CONTINUE
      WRITE(6,*)' SUM OF RESIDUAL :',SUM
      WRITE(6,*)'MORE ITER ? IYESI = 1'
      READ(5,*)IYESI
      IF(ABS(SUM).LT.5   )GOTO 998
      IF(IYESI.EQ.1)          GOTO 999
998   WRITE(6,*)' RESULT    FILE :'
      READ(5,15)OUFILE
      OPEN(8,FILE=OUFILE,STATUS='NEW')
      WRITE(8,10)NX,NY,DELX,DELY,XMIN,XMAX,YMIN,YMAX
   10 FORMAT(2I10,/,6F10.1)
      DO 11 J=1,NY
      DO 11 I=1,NX
      WRITE(8,13)Z(I,J),AC(I,J),XMIN+DELX*(I-1),YMIN+DELY*(J-1)
C***  SET ESTIMATED ANOMALY FOR NEXT ITERATION
   13 FORMAT(F10.2,E15.5,2F10.1)
   11 CONTINUE
      CLOSE(8)
      CLOSE(9)
      CLOSE(10)
      WRITE(6,*)' WRITE MORE ITERATION=1   NO=0  '
      READ(5,*) ITER
      IF (ITER.EQ.1) GOTO 999
   12 STOP
      END
```

```
C***
C***
      SUBROUTINE GET(ZI,ZL,ZU,AL,AU,S,ZSCALE,ILL)
C*    ~~~~~~~~~~~~~~~~~~~~~~~~~~~~~~~
      IMPLICIT REAL*8 (A-H,O-Z)
C***  ROUTINE TO GATHER THE 3 DATA VALUES NEEDED FOR INTERPOLATION
      DIMENSION ZL(6),AL(6),ZU(3),AU(3),A(3,3)
      ZUMIN=100000.
      IK=0
      ZSCAL=ZSCALE+ZSCALE/100.
      DO 16 K=1,ILL
      AB=     ZI-ZL(K)
      IF(AB.LT.0)AB=-AB
C     WRITE(6,*)' AB,ZI,ZL(K) ,K: ',AB,ZI,ZL(K),K,AL(K)
      IF (AB.LE.ZSCAL)THEN
      IK=IK+1
      ZU(IK)=ZL(K)
      AU(IK)=AL(K)
C     WRITE(6,*)'  IK ,ZU,AU :', IK ,ZU(IK),AU(IK)
      IF (IK.EQ.3)GOTO 16
      GOTO 16
      ENDIF
      IF (ZUMIN.GT.AB) THEN
      ZUMIN=AB
      ZU(3)=ZL(K)
      AU(3)=AL(K)
      KK=K
      ENDIF
   16 CONTINUE
C     WRITE(6,*)'  K  ,ZU,AU :', KK   ,ZU(3),AU(3)
C***  SORT THE DATA IN ACCENDING ORDER
      DO 6 J=1,2
      DO 6 I=1,2
      IF (ZU(I+1).LT.ZU(I)) THEN
      ZTEM=ZU(I)
      ATEM=AU(I)
      ZU(I)=ZU(I+1)
      AU(I)=AU(I+1)
      ZU(I+1)=ZTEM
      AU(I+1)=ATEM
      ENDIF
    6 CONTINUE
      CALL QUARD(ZU,AU,ZI,S,ZSCALE)
    5 RETURN
      END
C***
      SUBROUTINE QUARD(ZU,AU,ZI,S,ZSCALE)
C*    ~~~~~~~~~~~~~~~~~~~~~~~~~~~~~~~~~~
C***  INTERPOLATE  FROM 3 EQUALLY SPACE DATA
C***  AU = AA + AB * ZU + AC * ZU**2
      IMPLICIT REAL*8(A-H,O-Z)
      DIMENSION ZU(3),AU(3)
```



```
      ZMIN=10000.
      DO 1 I=1,3
      IF(ZMIN.GT.ZU(I))ZMIN=ZU(I)
    1 CONTINUE
      ZT=ZSCALE
      ZI=(ZI-ZMIN)/ZT
      AA=AU(1)
      AC=  AU(3)/2. -AU(2)+AU(1)/2.
      AB=AU(2)-AU(1)-AC
      S=AA+AB*ZI+AC*ZI**2
      DO 3 I=1,3
    3 CONTINUE
      RETURN
      END
C
C***
C***
      SUBROUTINE DKXDKY(DK,NX,NY,DELX,DELY)
C***  ~~~~~~~~~~~~~~~~~~~~~~~~~~~~~~~~~~~
      IMPLICIT REAL*8 (A-H,O-Z)
      DIMENSION DK(NX,NY)
C***  THIS ROUTINE CALCULATES THE WAVE NUMBERS FOR AN ARRAY
      IF(MOD(NX2,2).EQ.1.OR.MOD(NY2,2).EQ.1)STOP
      NX2=NX/2
      NY2=NY/2
      PI2=2.D0*4.D0*DATAN(1.D0)
      WRITE(6,*)PI2,NX,NY,DELX,DELY
      DO 5 J=1,NY
      DO 6 I=1,NX
      DXX =DFLOAT(I-1)
      IF(I.GT.NX2)DXX =DFLOAT((NX-I)+1)
      DYY=DFLOAT(J-1)
      IF(J.GT.NY2)DYY =DFLOAT((NY-J)+1)
      DKN=DSQRT(DXX**2+DYY**2)
      DK(I,J)=PI2*DKN/(DELX*(NX-1))
    6 CONTINUE
    5 CONTINUE
      RETURN
      END
```

```
*
*                       APPENDIX   2.2
*
*
*
                        PROGRAM   SPHEREM
*
**********************************************************************
*    THIS ROUTINE CALCULATES MAGNETIC ANOMALY OF A SYSTEM OF SPHERES
*    WITH CENTRES AS SPECIFIED. THE ANOMALY IS CALCULATED ON A
*    SQUARE AREA. THE INTERVALS IN BOTH DIRECTIONS ARE SET AT 2 UNIT
*    DISTANCE. UNIT FOR DISTANCES IS ARBITRARY
*
*    x, y and z axes are normally taken as north, east and downwards
*    respectively
* ~~~~~~~~~~~~~~~~~~~~~~~~~~~~~~~~~~~~~~~~~~~~~~~~~~~~~~~~~~~~~~~~~~~~
*  $RUN *FORTRANVS SCARDS=SPHEREM
*  $RUN -LOAD 7=DATAFILE 5=*SINK*  8=OUTPUTFILE
*
***   INPUT DATAFILE:  UNIT 7
*                      All input is in free format
*   LINE 1  ED,EI  Earths' field declination and inclination degrees
*   LINE 2  WD,WI  Body declination and inclination  degrees
*                      note: declination is measured from x axis
*   LINE 3  W      Magnetization (A/m)
*   LINE 4  IW,WID,AMP
*                  (1) IW=0 calculates anomaly on a horizontal plane at
*                      height   WID above the  reference level,AMP=0
*                  (2) IW.EQ.1 calculates the anomaly on sinusoid
*                      2-D surface. WID is the wavelength.
*                      AMP is the peak to peak  amplitude.
*                  (3) IW.EQ.2 calculates the anomaly on an irregular
*                      2-D surface having 3 different wavelength). WID
*                      is the smallest wavelength. The program increament
*                      the wavelength to wavelength of WID+ (1/3)WID and
*                      WID+ (2/3)WID at (1/3) and (2/3) distance away
*                      from the origin
*                      AMP is the peak to peak amplitude ot the surface.
*   LINE 5  NO     no of data points along each side of the square
*   LINE 6  ZM,R   Depth of the centre and radius of the sphere
*   LINE 7  XMM,YMM   X and Y coordinates of the sphere
*     note: Repeat line 6 and 7 for the number of spheres used.
*           The program stops input using END= atatement
*
*
*   OUTPUT: UNIT 8
*   LINE 1 and 2
*           NO,NO,xINT,yINT,xMIN,xMAX,yMIN,yMAX (2I10,/,6F10.2)
*            INT - sampling interval
*            MIN,MAX - minimum and maximum in the along respective axes
*   LINE 3 to NO*NO+2
*     observation height,anomaly (nT), x and y coordinates
```



```
*
* ****************************************************************
      REAL G(64,64),F(64,64),F1(64,64),HIG(64,64)
      CHARACTER*7 INFILE,OUFILE
C     INFILE='INDATA'
C     OUTFILE='OUTDAT'
C     OPEN(7,FILE=INFILE,STATUS='OLD')
C     OPEN(8,FILE=OUFILE,STATUS='OLD')
      READ(7,*)ED,EI
      READ(7,*)WD,WI
      READ(7,*)W
      READ(7,*)IW,WID,AMP
      READ(7,*)NO

      DO 11 I=1,NO
      DO 11 J=1,NO
      F(I,J)=0.0
      F1(I,J)=0.0
  11  CONTINUE

      PI=ATAN(1.)*4.
*    CONVERT A/m  TO GAMMA
      W=W*4.*PI*100.
      PI=ATAN(1.)*4.
      RPI=PI/180.
*
      WD=WD*RPI
      WI=WI*RPI
      ED=ED*RPI
      EI=EI*RPI

*     X,Y,Z-POSITION OF MODEL w.r.t ORIGIN
  5   READ(7,*,END=55)ZM,R
      READ(7,*)XMM,YMM
      XM=XMM
      YM=YMM
      XINT=2.0
      YINT=2.0
      XMIN=0.
      XMAX= (NO-1)* XINT
      YMIN=0.
      YMAX= (NO-1)* YINT
*                    PARAMETERS
      EY=COS(ED)*COS(EI)
      EX=COS(EI)*SIN(ED)
      EZ=SIN(EI)
*
      WY=W*COS(WD)*COS(WI)
      WX=W*COS(WI)*SIN(WD)
      WZ=W*SIN(WI)
*
```

```
      PER=1.
      PAM=(PER*(R**3))/3.
*
      NX=(INT(XMAX-XMIN)/XINT) +1
      NY=(INT(YMAX-YMIN)/YINT) +1
      ZZ=  ZM
      M=1
      NYW1=NY/3
      NYW2=NY/2
      DO 35 I=1,NX
      DO 30 J=1,NY
      XX=XMIN+((I-1)*XINT)-XM
      XC=XMIN+FLOAT(I-1)*XINT
      YC=YMIN+FLOAT(J-1)*YINT
      YY=YMIN+((J-1)*YINT)-YM
      RR=SQRT(XX**2+YY**2+ZZ**2)
*
      IF (IW.EQ.1) THEN
*     calculate irregular surface  with WAVELENGTH  WID unit
*
       AJ=FLOAT(I-1)
       ZZZ=SIN(2.* PI*2.  *AJ/ WID)
       ZZ=(ZZZ+1.)*(AMP/2.)+ZM
      ELSEIF (IW.EQ.2) THEN
*     calculate irregular surface  with FUNDAMENTAL
*     WAVELENGTH  WID unit
*
       IF(I.GT.NYW1) WID=WID+(WID/3)
       IF(I.GT.NYW2) WID=WID+(WID/2)
       AJ=FLOAT(I-1)
       ZZZ=SIN(2.* PI*2.  *AJ/ WID)
       ZZ=(ZZZ+1.)*(AMP/2.)+ZM
*
*
       ELSEIF (IW.EQ.0) THEN
*     SET  horizontal surface  with HIGH  above or below observation level
*
       HIGH = WID
       ZZ=HIGH  +ZM
       ENDIF

       HIG(I,J)=ZZ
       FF1=EX*WX*(3*XX**2-RR**2)
       FF2=EY*WY*(3*YY**2-RR**2)
       FF3=EZ*WZ*(3*ZZ**2-RR**2)
       FF4=3*(EX*WY+EY*WX)*XX*YY
       FF5=3*(EX*WZ+EZ*WX)*XX*ZZ
       FF6=3*(EY*WZ+EZ*WY)*YY*ZZ
*
      F(I,J)=(PAM/(RR**5))*(FF1+FF2+FF3+FF4+FF5+FF6)
      F1(I,J)=F1(I,J)+F(I,J)
*
```



```
      M=M+1

 30 CONTINUE
 35 CONTINUE
      GOTO 5
 55 CONTINUE
      WRITE(8,16)NX,NY,XINT,YINT,XMIN,XMAX,YMIN,YMAX
 16 FORMAT(2I10,/,6F10.2)
      WRITE(8,40)(((HIG(I,J)-ZM),F1(I,J),FLOAT(I-1 )*(XINT)
     +,FLOAT(J-1  )* (XINT), I=NX,1,-1),J=NY,1,-1 )
 40 FORMAT( F10.1,E15.5,2F10.1)
      STOP
      END
```

```
*
*                       APPENDIX 2.3
*
*
*                       PROGRAM PROFIL
*
*
*
*
*  This routine draws a profile across any rectangular area.  A line
*  is first define by  a  starting  and  an  ending  coordinates.  A
*  specified  band  (window)  of  data  on both sides of the line is
*  obtained.  Radial averaging is then carried out on equal interval
*  points along the line with a specified radius.  The coordinates are
* (eastward point, northward point). The starting
*  coordinates must have the eastward coordinates value smaller than
*  the ending coordinates.  If the starting coordinates is XS,YS and
*  ending coordinate is XE,YE then XS < XE.
*
*  NOTE: the data must be input sequentially eastwards.
*  The unit for distance  are arbitrary
*    INPUT UNITS = OUTPUT UNITS
*
*  The profile is plotted using the GHOST80 subroutines
*
****
*  INPUT DATAFILE IN UNIT 7
*  All input in free format
*
*  LINE 1 NX,NY
*             No of data points in the eastwards and northwards
*             direction
*  LINE 2 DELX,DELY,XMIN,XMAX,YMIN,YMAX
*             Sampling intervals, minimum and maximum coordinates
*             along  the eastwards and northwards  directions
*  LINE 3 DATA1,DATA2,X,Y
*             DATA1 AND DATA2 input data for  profiling, eastwards
*             and northwards coordinates
*
****
*  INPUT PARAMETER FILE IN UNIT 5 (OR iterative and prompted)
*
*  LINE 1   ITOP (1 OR 2)
*                1 for DATA1 and 2 for DATA2 profile to be obtained
*  LINE 2   MENU (1 OR 2)
*                1 To get a new profile from the same data
*                2 Exit from the program
*         note:: the program exit here. If new profile is needed,
*                repeat the following
*  LINE 3   XS,YS    Starting coordinates (eastwards and northwards)
*  LINE 4   XE,YE    Ending coordinates (eastwards and northwards)
*  LINE 5   SPACE    Intervals along the output profile
```



```
*  LINE 6   WL       Half length of the window or band perpendicular
*                    to the line. Generally this value is larger
*                    than the radius below
*  LINE 7   RADIUS   Radius of capture around the point where the z
*                    value is to be determine.
*  LINE 8   IWIG   (1 TO 6)
*                  Choise of weighting given to distant data points
*                     1  1/ R
*                     2  1/ R**2
*                     3  1/ R**3
*                     4  1/ R**4
*                     5  1/ R**5
*                     6  1/ R**6
*  LINE 9   'TITLE'  The title used on the plotfile
*  LINE 10  'UNIT'   The unit of the Z values
*  LINE 11  IR       IR=1 Reverse the profile in the plot and OUTPUT
*                    i.e point XE,YE becomes the first point
*
**** output in unit 8
*  LINE 1    NINT,SPACE,XMIN,XMAX
*               no. of data points, spacing, start and end value
*               along the profile
*  LINE 2 - NINT+1   X(I),DUMMY, Y(I)
*               distance along profile,dummy value, anomaly value
*
*      run *fortranvs scards=reduce
*      r -load+*ig+*ghost80 7=datafile 8=outputfile
*~~~~~~~~~~~~~~~~~~~~~~~~~~~~~~~~~~~~~~~~~~~~~~~~~~~~~~~~~~~~~~~~~~~~~~~
*
      IMPLICIT REAL*8 (A-H,O-Z)
      DIMENSION Z(65536),XC(65536),YC(65536),RTD(65536),RD(1000),
     +ZR(65536),XCR(65536),YCR(65536)
      CALL PAPER(1)
      CALL PSPACE(0.2,0.95,0.4,0.8)
      CALL CSPACE(0.2,0.8,0.2,0.40)
      READ(7,*)NX,NY,DELX,DELY,XMIN,XMAX,YMIN,YMAX
      IXY=1
      WRITE(6,*)' TOPOGRAPHY  1  OR  ANOMALY 2'
      READ(5,*)ITOP
    2 CONTINUE
      IF (ITOP.EQ.2)READ(7,*,END=1)DFLAG,Z(IXY),XC(IXY),YC(IXY)
      IF (ITOP.EQ.1)READ(7,*,END=1)Z(IXY),DFLAG,XC(IXY),YC(IXY)
      IXY=IXY+1
      GOTO 2
    1 IXY=IXY-1
C***
   35 WRITE(6,34)XMIN,YMIN,XMAX,YMAX
   34 FORMAT('XMIN  ',F10.1,'  YMIN  ',F10.1,/,
     +       'XMAX  ',F10.1,'  YMAX  ',F10.1)
      WRITE(6,33)
   33 FORMAT('MENU           ',/,
     +       '    1.  Plot profile',/,
```

```
     +       '&   2.  Return      ')
      READ(5,*) MENU
      IF (MENU.EQ.2) RETURN
      WRITE(6,3)
    3 FORMAT('&Input start XS,YS coord. of profile ')
      READ(5,*)XS,YS
      WRITE(6,4)
    4 FORMAT('&Input start XE,YE coord. of profile ')
      READ(5,*)XE,YE
      IF (XS.EQ.XE) XE=XS+0.000000001
      IF (YS.EQ.YE) YE=YS+0.000000001
      WRITE(6,15)
   15 FORMAT('&Input spacing along retrieved line  ')
      READ(5,*)SPACE
C***  Distance between the start and and point
      RRR=DSQRT((YE-YS)**2+(XE-XS)**2)
      ITD=INT(RRR/SPACE)+1
      CALL LINE(IXY,Z,XC,YC,ITD,ZR,XCR,YCR,SPACE,XS,XE,YS,YE,RD,ZZMI)
C**   Create X points for plotting
      GRAD=(YE-YS)/(XE-XS)
      TETA=DATAN(GRAD)
      DO 6 I=1,ITD
      X=(I-1)*SPACE
      ZR(I)=X
    6 CONTINUE
      CALL LPLOT(RD,ZR,ITD,SPACE,1,XS,XE,YS,YE,ZZMI,Z,SPACE)
      GOTO 35
   39 CALL GREND
   38 RETURN
      END
C***
      SUBROUTINE LINE(IXY,Z,XC,YC,ITD,ZR,XCR,YCR,SPACE,XS,XE,YS,YE,RD,
     +                ZZMI)
C*    ~~~~~~~~~~~~~~~~~~~~~~~~~~~~~~~~~~~~~~~~~~~~~~~~~~~~~~~~~~~~~~~~~~
C***  Retrieve profile
      IMPLICIT REAL*8 (A-H,O-Z)
      DIMENSION Z(IXY),XC(IXY),YC(IXY),ZR(IXY),XCR(IXY),YCR(IXY)
     +,RD(ITD),DFLAG(300),WD(30),ZD(30)
C     DIMENSION Z(65536),XC(65536),YC(65536),RTD(65536),RD(1000),
C    +ZR(65536),XCR(65536),YCR(65536)
C     COMMON /BL1/ Z(65536),XC(65536),YC(65536)
C     COMMON /BL2/ ZR(65536),XCR(65536),YCR(65536)
      YEYS=YE-YS
      IF(YE.EQ.YS)YEYS=0.000001
      XEXS=XE-XS
      IF(XE.EQ.XS)YEYS=0.000001
      GRAD=YEYS/XEXS
C     GRAD=(YE-YS)/(XE-XS)
      TETA=DATAN(GRAD)
      C=YE-GRAD*XE
      WRITE(6,1)
    1 FORMAT('&Window length along X axis ')
```



```
      READ(5,*)WL
      WRITE(6,5)
    5 FORMAT('&       radius used  ')
      READ(5,*)      RADIUS
      WRITE(6,*)'WEIGHTING '
      WRITE(6,14)
   14 FORMAT(' 1- 1/W',/,' 2-1/W**2',/,'  3-1/W**3',/,'  4-1/W**4'
     +,/,'  6-1/W**6'
     +,/,' 7- 1 / (1-((RR/1.1+RRMAX)**2) / ((RR/1.1+RRMAX)**2)'   )
      READ(5,*)IWIG
      CU=C+WL
      CL=C-WL
      WRITE( 6,10)XS,YS,XE,YE,SPACE,RADIUS
   10 FORMAT('Start point ',2F10.1,/,
     +       'End point   ',2F10.1,/,
     +'Spacing along line  ',F10.1,/,'Radius of capture  ',F10.1)
       WRITE( 6,11) CL,C,CU,GRAD,TETA
   11  FORMAT('Limits on intersection :lower  , intersect , upper ',/,
     +3F10.1,/,'Gradient of line ',F13.3,'Angle ',F10.4)
C***  Collect data within window area
      IC=1
      ZZMI=10000000
      DO 2 I=1,IXY
      IF (ZZMI.GT.Z(I)) ZZMI=Z(I)
C***  Calculate intersection and keep data
      CC=YC(I)-GRAD*XC(I)
      IF (CC.GT.CL.AND.CC.LT.CU)THEN
      XCR(IC)=XC(I)
      YCR(IC)=YC(I)
      ZR(IC)=Z(I)
      IC=IC+1
      ENDIF
    2 CONTINUE
      DO 4 I=1,ITD
C***  Determine points on the line
      X=(I-1)*SPACE*DCOS(TETA)+XS
      Y=(I-1)*SPACE*DSIN(TETA)+YS
      SUM=0.0
      IT=0
      DFLAG(I)=0.0
      IDFL=0
      RDI=0.D0
      RRMAX=0.D0
      DO 13 J=1,IC
      RR=DSQRT((Y-YCR(J))**2+(X-XCR(J))**2)
      IF (RR.LE.RADIUS.OR.RR.EQ.0)THEN
      IF (RR .EQ.0.0) RR=0.0000001
      IF (RRMAX.LT.RR)RRMAX=RR
      ENDIF
   13 CONTINUE
C***  Search within the radius required
      DO 6 J=1,IC
```

```
*
      RR=DSQRT((Y-YCR(J))**2+(X-XCR(J))**2)
      IF (RR.LE.RADIUS.OR.RR.EQ.0)THEN
      IT=IT+1
      IF (RR .EQ.0.0) RR=0.0000001
C     WD(IT)=1/(RR**4)
      IF (IWIG.EQ.1)WD(IT)=1/(RR   )
      IF (IWIG.EQ.2)WD(IT)=1/(RR**2)
      IF (IWIG.EQ.3)WD(IT)=1/(RR**3)
      IF (IWIG.EQ.4)WD(IT)=1/(RR**4)
      IF (IWIG.EQ.6)WD(IT)=1/(RR**6)
      RRD=(RR/(1.1*RRMAX))
      IF (IWIG.EQ.7)WD(IT)=((1-RRD)**2/RRD**2)
      SUM=SUM+WD(IT)
      ZD(IT)=ZR(J)
      ENDIF
    6 CONTINUE
      IF (IT.EQ.0) THEN
      RD(I)=0.0
      DFLAG(I)=1.0
      IDFL=IDFL+1
      WRITE(6,*)'HOLE IN    ',I
      GOTO 8
    9 ENDIF
C***  Average of values within search area
      ZDD=0.0
      DO 7 KK=1,IT
C     ZD(KK)=ZD(KK)*(WD(KK)/SUM)
      ZDD   =ZD(KK)*(WD(KK)/SUM)
      RDI   =RDI+ZDD
    7 CONTINUE
      RD(I)=RDI
    8 CONTINUE
    4 CONTINUE
      WRITE(6,*)'Line retrival end  !!!!'
      RETURN
      END
C***
      SUBROUTINE LPLOT(YY,XX,NINT,SINT,NWICH,XS,XE,YS,YE,ZZMI,Z,SPACE)
      REAL*8    YY(NINT),XX(NINT),SINT,Z(NINT)
      REAL Y(500),X(500),XMIN,XMAX,YMIN,YMAX
      CHARACTER   AS*200,BS*15
      WRITE(6,6)
    6 FORMAT('& Title                ')
      READ(5,7)AS
    7 FORMAT(A200    )
      WRITE(6,8)
    8 FORMAT('& Unit                 ')
      READ(5,9)   BS
    9 FORMAT(    A15)
      WRITE( 6,3)
    3 FORMAT(/,'Plotting report ',/,'----------------'   )
      YMIN=1.E10
```



```
*
      YMAX=-1.E10
      XMIN=1.E10
      XMAX=-1.E10
      WRITE(6,*)' Reverse profile ?   YES=1       '
      READ(5,*) IR
      DO  1 J=1,NINT
      IF(IR.EQ.1) THEN
      X(J)=REAL(XX(J    ))/1000.
      Y(J)=REAL(YY(NINT-J+1  ))
      ELSE
      X(J)=REAL(XX(J))/1000.
      Y(J)=REAL(YY(J))
      ENDIF
      IF(YMIN.GT. Y(J)) YMIN= Y(J)
      IF(YMAX.LT. Y(J)) YMAX= Y(J)
      WRITE (6,*)X(J),Y(J) ,J,NINT
    1 CONTINUE
      XMIN=X(1)
      XMAX=X(NINT)
      WRITE( 6,*)' NO OF STATION POINTS ',NINT
      WRITE( 6,4)XMIN,XMAX,YMIN,YMAX
    4 FORMAT('Xmin      ',E10.3,'  Xmax    ',E10.3,/,
     +       'Ymin      ',E10.3,'  Ymax    ',E10.3,/,
     +       ' X values     Y values ' )
      WRITE(8,55)NINT,SPACE,X(1),X(NINT)
   55 FORMAT(I10,3F15.3)
      WRITE( 8,5) (      X(I),0.0 ,Y(I),I=1,NINT)
    5 FORMAT(    3F15.3)
      IF (NWICH.EQ.1)THEN
      YMIP=YMIN-YMAX*0.1
      YMAP=YMAX+YMAX*0.1
      CALL MAP(XMIN,XMAX,YMIP,YMAP)
      CALL CTRMAG(15)
      CALL AXES
      CALL BORDER
      CALL CURVEO(X ,Y ,1,NINT)
      CALL PTPLOT(X ,Y ,1,NINT,342  )
      CALL CSPACE(0.2,0.8,0.2,0.38)
      CALL PLACE(20,1)
      CALL TYPECS('DISTANCE (km)')
      AINT=FLOAT(NINT)
      CALL PLACE(40,3)
      CALL TYPECS(' TOTAL STN PT IS ')
      CALL TYPENF(AINT,1)
      CALL PLACE(5,5)
      CALL TYPECS('Starting coordinate :')
      CALL TYPENF(XS,1 )
      CALL TYPENF(YS,1 )
      CALL PLACE(5,6)
      CALL TYPECS('Ending   coordinate :')
      CALL TYPENF(XE,1 )
      CALL TYPENF(YE,1 )
```

```
*
      CALL CSPACE(0.2,0.8,0.40,0.80)
      CALL PLACE( 2,1)
      CALL TYPECS(AS)
      CALL CTRORI(90.)
      CALL CSPACE(0.10,0.17,0.5,0.8)
      CALL PLACE(1,1)
      CALL TYPECS(BS)
      CALL CTRORI(0.)
      CALL FRAME
C     CALL GREND
      ENDIF
      RETURN
      END
```

```
*
*                       APPENDIX    3.1
*
*
*                       PROGRAM    PSGRAV3D
*****************************************************************
*  This routine carries out  pseudogravimetric  transformation using
*  NAG  FFT subroutines (CO6FJF). Two input files are required (1) a
*  gridded data and    (2)  a   parameter  file  containing the
*  inclination  and declination of the  earth's magnetic field  and
*  the body, the   fictitious density contrast, magnetization and
*  the required level. The data must be input in the east to west
*  sequence.
*
*  x, y and z are normally  north, east and downwards.
*****************************************************************
*    FILES : 7 gridded  data file, 8 output file and  5 parameter file
***
*    note: all input in free format
*    INPUT :   UNIT 7
*    Line 1  NXO,NYO
*            NXO     No of data in X  directions
*            NYO     No of data in Y  directions
*            (NXO=NYO and must be  EVEN)
*    LINE 2  DELX,DELY,XMIN,XMAX,YMIN,YMAX  (m)
*            DELX,DELY  Sampling interval in X and Y  directions
*            XMIN,XMAX  Minimum and maximum coordinates in X direction
*            YMIN,YMAX  Minimum and maximum coordinates in Y direction
*    LINE 3  X(I),XC(I),(YC(I)
*            X(I)       Magnetic anomaly (nT)
*            XC(I)      X coordinate (m)
*            YC(I)      Y coordinate (m)
*                REPEAT LINE 3 NXO*NYO TIMES
*                (Input data terminated by END= ind the read command)
*
*
***   INPUT :  UNIT 5.
*               (Read in subroutine  INCDEC)
*    LINE 1   ED,EI
*             ED,EI  Field declination, and inclination from x (degrees)
*    LINE 2   WD,WI
*             WD,WI  Field declination, and inclination from x (degrees)
*    Line 3   RC,HC
*             RC       Fictious density (kg/m3)
*             HC       Magnetization (A/m)
*    Line 4   Z
*             Z    The required height(m) above  0  observation level
*
***   OUTPUT :  UNIT 8   (all output units are the same as input unit)
*    LINE 1 and 2     NX,NY,  DELX,DELY,XMIN,XMAX,YMIN,YAX
*                     (2F10,/,6F10.1)
*    LINE 3 TO NX*NY+2  X(I), XC(I), XC(I)
*                     (F15.3,2F10.1)
```



```
*                    X(I) pseudogravimetric anomaly (mGal)
***
*
*    compile: r *fortranvs scards=psgrav3d
*    run:     r -load+*nag 7=datafile 5=parameterfile  8=output
*****************************************************************
***  Double pre.
      IMPLICIT REAL*8 (A-H,O-Z)
      DIMENSION  X (65536),Y (65536),WORK(131072),XC(65536),YC(65536)
*     Integers
      INTEGER IFAIL,ND(2),RES,NDIM,IXY,N,LWORK
*     Data
      DATA  LWORK,NDIM,IFAIL/131072,2,0/
*
*     Reading data file ,header first
      READ(7,*)NXO,NYO,DELX,DELY,XMIN,XMAX,YMIN,YMAX
      WRITE( 6,11) NXO,NYO,DELX,DELY,XMIN,XMAX,YMIN,YMAX
   11 FORMAT('Data read from the header of file',/,
     +       '-----------------------------------',/,
     +       'Dimension NXO,NYO                  ',2I5,/,
     +       'Smpling interval (must be equal)  X,Y  ',2F10.1,/,
     +       'Boarders of  area                 ',4F10.1,/)
       IF (DELX.NE.DELY) THEN
       WRITE(6,*)'Interval not equal'
       STOP
       ENDIF
      NNXY=NXO*NYO
      NX=NXO
      NY=NYO
      IXY=0
    3 IXY=IXY+1
*     Read in data
      READ(7,*,END=4) X(IXY),XC(IXY),YC(IXY)
      GOTO 3
    4 IXY=IXY-1
      IF(NNXY.NE.IXY) THEN
      WRITE(6,*)'INPUT data ',IXY,'not equal to declared ',NNXY
      STOP
      ENDIF
   22 CONTINUE
C***  CONVERT DISTANCES TO cm
      DELX=DELX*100.
      DELY=DELY*100.
      XMIN=XMIN*100.
      YMIN=YMIN*100.
      XMAX=XMAX*100.
      YMAX=YMAX*100.
      DO 24 I=1,NX*NY
      XC(I)=XC(I)*100.
      YC(I)=YC(I)*100.
   24 CONTINUE
      NW= NX* NY *2
```

```
*
      NTP=0
      DFLAG=1.
      IXY=NX*NY
C***  Clear array
      DO 25 I=1,IXY
      Y(I)=0.D0
      WORK(I+IXY)=0.D0
   25 CONTINUE
      WRITE(6 ,*)'++ FFT    STARTED ++'
      ND(1)=NX
      ND(2)=NY
      IXY=NX*NY
      IFAIL=0
      LWORK=3*ND(1)
      CALL TIME(0)
      WRITE(6,12)NDIM,IXY,LWORK
   12 FORMAT('Parameters for FFT            ',/,
     +       '-----------------------------',/,
     +       'Dimension                    ',I5,/,
     +       'Number of data point used    ',I5,/,
     +       'Work space                   ',I5)
      CALL C06FJF(NDIM,ND,IXY,X,Y,WORK,LWORK,IFAIL)
      WRITE(6,*)'++ FFT        ENDS ++'
*
*     Read in the parameter file
      CALL INCDEC(Z,ED,EI,WD,WI,RH)
      WRITE(6,111)Z,ED,EI,WD,WI,RH
  111 FORMAT('Values used  are :',/,
     +       '    Obs. level   Z  :',F10.2 ,/,
     +       '    Earth       dec :',F10.2 ,'  inc :',F10.2 ,/,
     +       '    Mass        dec :',F10.2 ,'  inc :',F10.2 ,/,
     +       '    Den. Mag. ratio :',F10.5 )
C
*     Modify data
      DEL=DELX
      CALL MODIFY (X,Y,NX,NY,RH,ED,EI,WD,WI,Z,DELX)
      WRITE(6,*)'++  COMPLETED MODIFY ROUTINE ++'
*
*     Calculate the inverse transform
      WRITE(6,*)'++  IFFT     starts ++'
      CALL C06GCF(Y,IXY,IFAIL)
      CALL C06FJF(NDIM,ND,IXY,X,Y,WORK,LWORK,IFAIL)
      CALL C06GCF(Y,IXY,IFAIL)
      WRITE(6,*)'++  IFFT     ends ++'
*
      CALL TIME(1,0,RES)
      WRITE(6,13)RES
   13 FORMAT('FFF > Modify > IFFT   Time = ',I5)
*
*  Write  output   to unit 8
      WRITE(8,14)NX,NY,DELX/100.,DELY/100.,XMIN/100.,XMAX/100.
     +,YMIN/100.,YMAX/100.
```



```
   14 FORMAT(2I10,/,6F10.1)
*
*     CONVERT TO milligal
      CON=1000.
      DO 16  I=1,IXY
      X(I)=X(I)*CON
      WRITE(8,15)       X(I)    , XC(I)/100., YC(I)/100.
   15 FORMAT (F15.3,2F10.1)
   16 CONTINUE
      STOP
      END
*
      SUBROUTINE INCDEC(Z,ED,EI,WD,WI,RH)
*     ***********************************
      REAL*8 Z,ED,EI,WD,WI,RH,RHO,RMAG,PI,RPI,RC,HC
*             EARTH            ED,EI   in degrees        D-DECLINATION
      READ(5,*)ED,EI
*             BODY             WD,WI   in degrees        I-INCLINATION
      READ(5,*)WD,WI
*                    Density, Magnetization        kg/m3  A/M
      READ(5,*) RC,HC
*                    Required level (m)
      READ(5,*) Z
*
      PI=4.D0*DATAN(1.D0)
*     CONVERT to cm
      Z=Z*100.
*     CONVERT TO gm/cm3
      RC=RC/1000.
*     CONVERT TO GAMMA
      HC=HC*4.D0 * PI * 100.D0
      RH=RC/HC
      WRITE(6,2)Z,ED,EI,WD,WI,RH
    2 FORMAT('Input values are :',/,
     +       '    Obs. level   Z  :',F10.2 ,/,
     +       '    Earth       dec :',F10.2 ,'  inc :',F10.2 ,/,
     +       '    Mass        dec :',F10.2 ,'  inc :',F10.2 ,/,
     +       '    RHO/MAG           ',F10.6 )
      RPI=PI/180.0D0
      WD=WD*RPI
      WI=WI*RPI
      ED=ED*RPI
      EI=EI*RPI
      RETURN
      END
*
      SUBROUTINE MODIFY (FR,FI,NX,NY,RH,ED,EI,WD,WI,Z,DEL)
*     ****************************************************
*     This routine sets the correct array for calculating the
*     transformation operator
*     FR and FI  Real and imaginary value array
      REAL*8 SE,SW,WD,WI,ED,EI,PKK,EX2,Z,DENOM,RPI,AR,AI,A,B,PI
```

```
      REAL*8  FR(NX,NY),FI(NX,NY),DK1,DK2,PI2,RH,DEL
      WRITE(6,*)'+++++   MODIFY STARTS '
      PI=DATAN(1.0D0)*4.0D0
      AN=FLOAT(NX)
      PI2=2.0D0*PI/DBLE(AN)
*     Calculate for k1=1,NX/2   , K2=0 and NX/2
      DO 22 K1=1,NX/2-1
      DO 21 K2=0,NX/2,NX/2
      I=K1+1
      J=K2+1
      JR=K2+1
      IR=NX-K1+1
      DK1=DBLE(K1)
      DK2=DBLE(K2)
      CALL   CALC(DK1,DK2,WD,WI,ED,EI,I,J,IR,JR,FR,FI,NX,NY,RH,DEL)
   21 CONTINUE
   22 CONTINUE
*
      DO 24 K2=1,NY/2-1
      DO 23 K1=0,NX/2,NX/2
      DK1=DBLE(K1)
      DK2=DBLE(K2)
      I=K1+1
      J=K2+1
      IR=K1+1
      JR=NY-K2+1
      CALL   CALC(DK1,DK2,WD,WI,ED,EI,I,J,IR,JR,FR,FI,NX,NY,RH,DEL)
   23 CONTINUE
   24 CONTINUE
*
      DO 26 K1=1,NX/2-1
      DO 28 K2=1,NX/2-1
      I=K1+1
      J=K2+1
      IR=NX-K1+1
      JR=NY-K2+1
      DK1=DBLE(K1)
      DK2=DBLE(K2)
      CALL   CALC(DK1,DK2,WD,WI,ED,EI,I,J,IR,JR,FR,FI,NX,NY,RH,DEL)
*
      I=K1+1
      J=NY-K2+1
      IR=NX-K1+1
      JR=K2+1
      DK1=DBLE(K1)
      DK2=DBLE(-K2)
      CALL   CALC(DK1,DK2,WD,WI,ED,EI,I,J,IR,JR,FR,FI,NX,NY,RH,DEL)
   28 CONTINUE
   26 CONTINUE
*     Calculate     FR,FI  for  NX/2 ,NY/2
      DO 20 K1=0,NX/2,NX/2
      DO 25 K2=NY/2,0,-NY/2
```



```
      I=K1+1
      J=K2+1
      IR=1
      JR=1
      IF (K1.EQ.0.AND.K2.EQ.0) THEN
      GOTO 25
      ENDIF
      DK1=DBLE(K1)
      DK2=DBLE(K2)
      CALL   CALC(DK1,DK2,WD,WI,ED,EI,I,J,IR,JR,FR,FI,NX,NY,RH,DEL)
*     Set FI for NX/2 & NY/2 for even NX,NY
      FI(I,J)=0.0D0
*     Set FR & FI for k1,k2=0 to 0
      FR(IR,JR)=0.0D0
      FI(IR,IR)=0.0D0
   25 CONTINUE
   20 CONTINUE
      RETURN
      END
*
      SUBROUTINE CALC(DK1,DK2,WD,WI,ED,EI,I,J,IR,JR,FR,FI,NX,NY,RH,DEL)
*     ~~~~~~~~~~~~~~~~~~~~~~~~~~~~~~~~~~~~~~~~~~~~~~~~~~~~~~~~~~~~~~~~~~~~
*     Actual calculation for  the pg.  coefficient.
*      g(k1,k2)= f(k1,k2) * A' * operator
*************************************************************************
*                                                  3             2      *
*                  4xPIxG  RHO       1          P -P(S1xS2)-i(P (S1+S2))   Pz *
* g(k1,k2)=f(k1,k2)x------x----x-------------x-------------------------x e   *
*                    mu     J  Sin(WI)Sin(EI)     2    2   2    2         *
*                                                (P + S1 )(P + S2 )       *
*             2*PI                                   Cos(I)               *
*         S = ---        x( k1 COS(D) + k2 SIN(D) ) x -----               *
*             NX * DEL                               Sin(I)               *
*                                                                         *
*             2xPI          2     2   1/2                                 *
*         P = ----    x( k1  + k2  )                                      *
*             NX *DEL                                                     *
*                                                                         *
*************************************************************************
*
      REAL*8 DK1,DK2,WD,WI,ED,EI,RH,FR(NX,NY),FI(NX,NY),PI2
      REAL*8 PKK,SW,SE,DENOM,EXZ,A,B,CON,ASIN
*
      PI2=DATAN(1.0D0)*4.0D0*2 / (NX*DEL)
      PI =DATAN(1.0D0)*4.0D0
      PKK=PI2*DSQRT(DK1**2+DK2**2)
      SW=PI2*(DK1*DSIN(WD)+DK2*DCOS(WD))*(DCOS(WI)/DSIN(WI))
      SE=PI2*(DK1*DSIN(ED)+DK2*DCOS(ED))*(DCOS(EI)/DSIN(EI))
      DENOM=(PKK**2+SE**2)*(PKK**2+SW**2)
      EXZ=DEXP(PKK*Z)
*     Assuming CON is the fictitious density contrast
      CON=4.0D0*PI*6.672E-8*RH
```

```
ASIN=1/(DSIN(WI)*DSIN(EI))
AR=(PKK**3-PKK*SW*SE)/DENOM
AI=((SW+SE)*PKK**2)/DENOM
A=(FR(I,J)*AR-FI(I,J)*AI)*EXZ*ASIN*CON
B=(FR(I,J)*AI+FI(I,J)*AR)*EXZ*ASIN*CON
FR(I,J)=A
FI(I,J)=B
FR(IR,JR)=FR(I,J)
FI(IR,JR)=-FI(I,J)
RETURN
END
```

```
*                          APPENDIX    3.2
*
*
*                       PROGRAM    PSGRAV2D
*                       --------------------
*
*
****************************************************************
*  Two-dimensional pseudogravimetric transformation program using
*  the NAG FFT  subroutine C06FCF
*
*   x, y and z axes are along the profile, strike of body and
*                    downwards respectively
****************************************************************
***          Variables for NAG routine
*    DWORK    Work space used by NAG
*    X        Array  containing real values
*    Y        Array  containing  imaginary values
*    N        Total no of data values NX
*    IFAIL    Recommended value =0
***
*             Input data file. READ in UNIT 7.
*    LINE 1          NX,DELX,XMIN,XMAX
*          no of data, sampling interval (km), min. and max. dist.
*    LINE 2,NX+2     XC,  DUMMY, X
*          x distance (km), Dummy value, magnetic anomaly (nT)
*    LINE NX+2+1     EI,ED
*          inclination and declination of earth's field w.r.t
*         positive x axis
*    LINE NX+2+3     WI,WD
*          inclination and declination of body  w.r.t positive
*         x axis
*    LINE NX+2+4     RHO,MAG
*          density (kg/m3), magnetizatiom of the body (A/m)
*    LINE NX+2+5      LTX
*          Number of data point to be tapered on each end
*    LINE NX+2+6      BG
*         (BG.LT.0) - INPUT DATA only for transformation
*         (BG.GT.0) - Used only for testing the routine
*                     READ in GRAVITY data (e.g. calculated from GRAV.U)
*                     from test model used to calculate magnetic data
*                     (e.g. calculated from MAG.U) INPUT above.
*                     BG - THE BACKGROUND value added to the
*                     pseudogravimetric anomaly. (suggests BG=0 if
*                     background value is not known)
*    LINE NX+2+7       REPEAT NX    times
*                       XC,DUMMY,GR(I) gravity anomaly
*
*
***              Output data file: WRITE in UNIT  8
*    LINE 1  NX,DELX,XMIN,XMAX    (I10,3F10.2)
```



```
*    LINE 2  XC, GR, X           (F10.2,2F15.3)
*                  X - pseudogravimetric anomaly (mGal)
*                 GR - gravity anomaly (mGal) or dummy value
*
*    compile: run *fortranvs scards=psgrav2d
*    run    : r -load+*nag+*ghost80 7=datafile  8=outputfile
*****************************************************************
***  Double pre.
      IMPLICIT REAL*8 (A-H,O-Z)
      DIMENSION  X(1024),Y(1024),DWORK(1310),XC(1024)
***   Real   (array for plotting)
      REAL   XX(1024),YY(1024),GR(1024),XB(1024),XTAP(1024)
***   Integers
      INTEGER IFAIL ,RES ,IXY
      DATA IFAIL/0/
*
*     Read  data file, header first  and set to even numbered data
      READ(7,*)NX,DELX
      NXO=NX
      WRITE( 6,11) NX,DELX
   11 FORMAT('Data read from the header of file',/,
     +       '--------------------------------',/,
     +       'Dimension NX           ', I5,/,
     +       'Smpling interval  X    ', F10.1,/)
*     Read in data
      IXY=0
    3 IXY=IXY+1
      READ(7,*,END=4)     XC(IXY),DUN,X(IXY)
*     convert to cm.
      XC(IXY)=XC(IXY)*1000.*100.
      Y(IXY)=0.D0
      XB(IXY)=REAL(X(IXY))
      IF(IXY.EQ.NX)GOTO 5
      GOTO 3
    4 IXY=IXY-1
*     Taper the data
    5 WRITE(6,*)' LENGTH OF DATA TO TAPER '
      READ(7,*)LTX
      CALL TAPER(X,IXY,LTX)
      DO 54 I=1,IXY
      XTAP(I)=REAL(X(I))
   54 CONTINUE
*     Convert distances to cm
      DELX=DELX*100.*1000.
      XMIN=XMIN*100.*1000.
      XMAX=XMAX*100.*1000.
      NNX=MOD(NX,2)
*     Set to even number data
      IFLAG=0
      IF(NNX.NE.0)THEN
      NX=NX+1
      X(NX)=X(NX-1)
```

```
      XC(NX)=XC(NX-1)+DELX
      WRITE(6,*)' NO OF DATA IS NOW ',NX
      IFLAG=1
      ENDIF
      IXY=NX
      IF(NX.LT.128) THEN
      NO=NX
      NX=256
      ELSEIF(NX.GT.128.AND.NX.LT.256) THEN
      NO=NX
      NX=256
      ENDIF
      IFAIL=0
      CALL TIME(0)
      WRITE(6,12)NX  ,IXY,IFAIL
   12 FORMAT('Parameters for transformation ',/,
     +       '-------------------------------',/,
     +       'Dimension                      ',I5,/,
     +       'Number of data point used      ',I5,/,
     +       'IFAIL                          ',I5)
      NOX=NX-NO
      NOX=NOX/2
      NE=NO+NOX
      NN=NO
*     Padd extended data points with zeros
      DO 33 I=NE,NOX+1,-1
      X(I)=X(NN)
      Y(I)=0.D0
      NN=NN-1
   33 CONTINUE
      DO 34 I=1,NOX
      X(I)=0.0
      Y(I)=0.D0
      X(NX+1-I)=0.0
      Y(NX+1-I)=0.0
   34 CONTINUE
      WRITE(6 ,*)' Start transformation  IXY',IXY
C     WRITE(16,67)             (I,  X(I),Y(I),I=1,NX)
   67 FORMAT(I10,  2F15.8)
      CALL C06FCF(X,Y,NX ,DWORK,IFAIL)
      WRITE(16,* )'out 1 st FFT'
C     WRITE(16,66)                (X(I),Y(I),I=1,NX)
   66 FORMAT(      2F15.8)
      WRITE(6,*)' End   transformaton'
*     Read in the angles, fictious density and magnetisation
      CALL INCDEC(ED,EI,WD,WI,RMAG,RHO,BETA)
      WRITE(6,111)ED,EI,WD,WI,BETA
  111 FORMAT('Values used  are :',/,
     +       '    Earth       inc :',F10.2 ,'  dec :',F10.2 ,/,
     +       '    Mass        inc :',F10.2 ,'  dec :',F10.2 ,/,
     +       '    BETA              :',F10.5 )
*
```



```
C     Modify using the transform operator
      CALL MODIFY (NX,X,Y,ED,EI,WD,WI,RHO,RMAG,BETA,DELX)
      WRITE(6,*)'+++++++  COMPLETED MODIFY ROUTINE'
*
*     Calculate the inverse transform
C     WRITE(16,66)(X(I),Y(I),I=1,NX)
      WRITE(6,*)' Start  inverse  FFT  '
      CALL C06GCF(Y,NX ,IFAIL)
      CALL C06FCF(X,Y,NX ,DWORK,IFAIL)
      CALL C06GCF(X,NX ,IFAIL)
C     WRITE(16,66)(X(I),Y(I),I=1,NX)
      CALL TIME(1,0,RES)
      WRITE(6,13)RES
   13 FORMAT('Transform >modify>Inverse Transform Time = ',I5)
*
*     Write header   to unit 8
*
      WRITE(8,14)NX,DELX/100.,XMIN/100.,XMAX/100.
   14 FORMAT( I10,/,3F10.1)
*
*     Restore data, output and plot
      NX=NO
      DO 35 I=1,NX
      X(I)=X(NOX+I)
   35 CONTINUE
      IF (IFLAG.EQ.1)NX=NX-1
      YMAX=-100000
      YMIN=100000
      XMAX=-100000
      XMIN=+100000
      XBMAX=-100000
      XBMIN=+100000
      WRITE(6,*)'INPUT BACKGROUND'
      READ(7,*)BG
      DO 16  I=1,NX
      GR(I)=FLOAT(I)
      IF (BG.LT.0.) READ(7,*)A,B,GR(I)
*     Convert PG anomaly to milligal
      CON=1000.
      X(I)=-X(I)*CON + BG
      XX(I)=X(I)
      YY(I)=XC(I)/100000.
      WRITE(8,15) XC(I)/100   , GR(I) , XC(I)
   15 FORMAT(  F10.1,E15.3,2F10.1)
      IF(XMAX.LT.X (I))XMAX=X (I)
      IF(XMIN.GT.X (I))XMIN=X (I)
      IF(XMAX.LT.GR(I))XMAX=GR(I)
      IF(XMIN.GT.GR(I))XMIN=GR(I)
      IF(YMAX.LT.XC(I))YMAX=XC(I)/100000.
      IF(YMIN.GT.XC(I))YMIN=XC(I)/100000.
      IF(XBMAX.LT.XB(I))XBMAX=XB(I)
      IF(XBMIN.GT.XB(I))XBMIN=XB(I)
```

```
   16 CONTINUE
      CALL PAPER(1)
      CALL MAP(YMIN,YMAX,XMIN,XMAX)
      CALL PSPACE(0.1,0.9,0.55,0.9)
      CALL CSPACE(0.1,0.9,0.50,0.88)
      CALL PLACE(2,1)
      CALL TYPECS(' 2-D Pseudogravimetric test')
      CALL PLACE(2,2)
      CALL TYPECS('    +  - transformed anomaly ')
      CALL PLACE(2,3)
      CALL TYPECS('  line - cal. gravity anomaly ')

      CALL CTRMAG (17)
      CALL CSPACE(0.4,0.9,0.40,0.51)
      CALL PLACE(1,1)
      CALL TYPECS('DISTANCE (km)')
      CALL CSPACE(0.03,0.1,0.25,0.50)
      CALL CSPACE(0.4,0.9,0.00,0.15)
      CALL PLACE(1,1)
      CALL TYPECS('DISTANCE (km)')
      CALL CSPACE(0.03,0.1,0.25,0.50)
      CALL CTRORI (90.)
      CALL PLACE(1,1)
      CALL TYPECS('ANOMALY (nT)')
      CALL CSPACE(0.03,0.9,0.60,0.90)
      CALL PLACE(1,1)
      CALL TYPECS('ANOMALY (mGal)')
      CALL CTRORI (0.)
      CALL SCALES
      CALL BORDER
C     CALL AXORIG(0.0,0.0)
      CALL CTRMAG (10)
      WRITE(16,*)XMIN,XMAX,YMIN,YMAX,NX
      WRITE(16,66)(XX(I),YY(I),I=1,NX)
*     OBSERVED ANOMALY
      CALL PTPLOT(YY,XX,1,NX,0)
*  PG ANOMALY
C     CALL PTPLOT(YY,GR,1,NX,250)
      CALL CURVEO(YY,GR,1,NX)
      WRITE(16,*)XMIN,XMAX,YMIN,YMAX
      CALL MAP(YMIN,YMAX,XBMIN,XBMAX)
      CALL PSPACE(0.1,0.9,0.20,0.47)
      CALL CSPACE(0.1,0.9,0.20,0.47)
      CALL PLACE(2,2)
      CALL TYPECS('Magnetic anomaly')
      CALL SCALES
      CALL BORDER
*      MAGNETIC ANOMALY
      CALL CURVEO(YY,XB,1,NX)
      CALL PTPLOT(YY,XTAP,1,NX,250)
      CALL CSPACE(0.1,0.9,0.0,0.15)
      CALL CTRMAG(15)
```



```
      PI=   4.*DATAN(1.D0)/180.
      AW1=DTAN(WI)
      AW2=DCOS(WD)
      AWI=DATAN(AW1/AW2)
      WD=WD/PI
      WI=WI/PI
      ED=ED/PI
      EI=EI/PI
      AWI=AWI/PI
      CALL PLACE(1,2)
      CALL GREND
      RETURN
      END
C***
      SUBROUTINE INCDEC(ED,EI,WD,WI,RMAG,RHO,BETA )
*     **********************************
      IMPLICIT REAL*8 (A-H,O-Z)
      READ( 7,*)ED,EI
      READ( 7,*)WD,WI
      READ( 7,*) RHO,RMAG
*
      PI=4.D0*DATAN(1.D0)
*     CONVERT TO gm/cm3
      RHO=RHO/1000.
*     Convert to mGal
      RMAG=RMAG*4.D0 * PI * 100.D0
      RH=RHO/RMAG
      WRITE(16,2)ED,EI,WD,WI,RH
    2 FORMAT('Input values are :',/,
     +       '    Earth       inc :',F10.2 ,'  dec :',F10.2 ,/,
     +       '    Mass        inc :',F10.2 ,'  dec :',F10.2 ,/,
     +       '    RHO/MAG           ',F10.6 )
      RPI=PI/180.0D0
      WD=WD*RPI
      WI=WI*RPI
      ED=ED*RPI
      EI=EI*RPI
*     BETA= MU + SIGMA
*        MU angle of dip of the magnetisation vector in the plane of profile.
*        SIGMA angle of dip of the earth magnetisation in plane of profile
      IF(EI.EQ.(90.*RPI))THEN
      SIGMA=EI
      GOTO 320
      ENDIF
      SIGMA=DATAN(DSIN(EI)/(DCOS(EI)*DCOS(ED)))
  320 IF(WI.EQ.(90.*RPI))THEN
      AMU=WI
      GOTO 340
      ENDIF
      AMU=DATAN(DSIN(WI)/(DCOS(WI)*DCOS(WD)))
      WRITE(16,*)'MU      ',AMU,WD,WI
  340 BETA=AMU+SIGMA
```

```
      RETURN
      END
***
1     SUBROUTINE MODIFY (NX,FR,FI,ED,EI,WD,WI,RHO,RMAG,BETA,DEL)
*     ***********************************************************
*    The transformation formula
*          4 * Pi * G  RHO      [Cos(BETA)   iSin(BETA)]
*   G  = - ----------  ---    * [-------- + ----------]  * F
*     k       mu * f    RMAG     [ ABS(k)          k    ]     k
*
*   G  Pseudogravimetric coeff.
*   F  Magnetic coeff.
*   G  Gravitational constant
*   mu 1 cgs or 4 * pi * 1E-07 H/m
*   J  Intensity of magnetisation
*   RHO Density contrast
*   f = SQRT(Cos(EI)**2 * Cos(ED)**2+Sin(EI)**2)
*       *  SQRT(Cos(WI)**2 * Cos(WD)**2+Sin(WI)**2)
*   k  wave number(2*Pi m /wavelength)
      IMPLICIT REAL*8 (A-H,O-Z)
      DIMENSION FR(NX),FI(NX)
      PI=DATAN(1.0D0)*4.D0
      IR=NX
      DO 400 I=2,NX/2 +1
      DK=2.D0*PI*DFLOAT(I-1)/( DFLOAT(NX-1)*DEL)
      WRITE(16,*)'DK,NX,DEL ', DK,NX,DEL
      A=DCOS(BETA)/ABS(DK)
      B=DSIN(BETA)/DK
      FJ = SQRT(COS(EI)**2 * COS(ED)**2+SIN(EI)**2)
     +*    SQRT(COS(WI)**2 * COS(WD)**2+SIN(WI)**2)
      FA=-6.67D-8*RHO/(RMAG*FJ)*4.D0*PI
      A=A*FA
      B=B*FA
      AR   =A*FR(I)-B*FI(I)
      AI   =B*FR(I)+A*FI(I)
      FR(I )=AR
      FI(I )=AI
      FR(IR)=FR(I)
      FI(IR)=-FI(I)
      IR=IR-1
 400  CONTINUE
      FI(1)=0.D0
      FR(1)=0.D0
      FI(NX/2+1 )=0.D0
C     WRITE(16,10)(I,FR(I),FI(I),I=1,NX)
  10  FORMAT(I10,2E15.5)
      RETURN
      END
***
      SUBROUTINE TAPER(FR,NX,   LX   )
*     ~~~~~~~~~~~~~~~~~~~~~~~~~~~~~~~
*      ROUTINE TO TAPER THE REAL DATA
```



```
*     LX=TAPER LENGTH
*     NX=NO OF DATA POINT
      IMPLICIT REAL*8 (A-H,O-Z)
      DIMENSION FR(NX   )
      PI=4.D0*DATAN(1.D0)
      DNX=DFLOAT(NX)
      DLX=DFLOAT(LX)
      DO 2 I=1,NX
      H=1.0D0
      IF(I.LE.LX)THEN
      PIL=(PI*DFLOAT(I-1))/DLX
      H=H*0.5D0*(1.0D0-COS(PIL))
      ELSEIF(I.GT.(NX-LX))THEN
      PIL=(PI*(DNX-DFLOAT(I)))/DLX
      H=H*0.5D0*(1.0D0-COS(PIL))
      ENDIF
      FR(I)=FR(I)*H
    2 CONTINUE
      RETURN
      END
```

```
*                        APPENDIX 3.3
*
*
*                     PROGRAM    SPHEREGM
*
*
* THIS ROUTINE CALCULATES  GRAVITY AND MAGNETIC ANOMALIES OF A SYSTEM
* OF SPHERE WITH CENTRES AS SPECIFIED. THE ANOMALIES ARE CALCULATED ON
* A SQUARE AREA. THE DECLINATION FOR CALCULATING THE MAGNETIC ANOMALY
* IS w.r.t  THE X AXIS.

*     X, Y and Z  are normally north, east and down
*
* ~~~~~~~~~~~~~~~~~~~~~~~~~~~~~~~~~~~~~~~~~~~~~~~~~~~~~~~~~~~~~~~~~~~~~~~~
*  $RUN *FORTRANVS SCARDS=SPHEREGM
*  $RUN -LOAD 7=DATAFILE     8=MAGNETICFILE  10=GRAVITYFILE
*
***      INPUT DATAFILE :  UNIT 7
* LINE 1   ED,EI      inc. and dec. of earth's field in degrees
* LINE 2   WD,WI          "              body in degrees
* LINE 3   RHO,W    density(kg/m),magnetization(A/m)
* LINE 4   XINT,NO  sampling interval (km) and number of data points
*                   along each side.
* LINE 5   ZM,R     depth(km) to the centre and radius(km) of sphere
* LINE 6   XMM,YMM  x and y coordinates of the centre of spheres (km)
*   note: REPEAT line 5 and 6 for as many spheres needed
*         The input stops by the program using END= command.

*** OUTPUT:
*          MAGNETIC ANOMALY IN UNIT 8
*   LINE 1 AND 2  NO,NO,XINT,XINT,XMIN,XMAX,YMIN,YMAX
*                 (2I10,/,6F10.2)
*   LINE 3 TO (NO*NO)+2
*             DUMMY,F1(magnetic anomaly nT), X and Y coordinates (km)
*                 (F10.2,F15.3,2F10.2)
*
*          GRAVITY  ANOMALY IN UNIT 10
*   LINE 1 AND 2  NO,NO,XINT,XINT,XMIN,XMAX,YMIN,YMAX
*                 (2I10,/,6F10.2)
*   LINE 3 TO (NO*NO)+2
*             DUMMY,G1(gravity anomaly mGal), X and Y coordinates (km)
*                 (F10.2,F15.3,2F10.2)
* ********************************************************************************

      REAL G( 64, 64),F( 64, 64),G1( 64, 64),F1( 64, 64)
      READ(7,*)ED,EI
      READ(7,*)WD,WI
      READ(7,*)RHO,W
      READ(7,*)XINT,NO
      DO 11 J=1,NO
      DO 11 I=1,NO
```



```
*
      G(I,J)=0.0
      F(I,J)=0.0
      G1(I,J)=0.0
      F1(I,J)=0.0
   11 CONTINUE

      PI=ATAN(1.)*4.
*    CONVERT A/m  TO gamma
      W=W*4.*PI*100.
*    CONVERT kg/m3  gm/m3
*     all distances in cm
      RHO=RHO/1000
      PI=ATAN(1.)*4.
      RPI=PI/180.
*
      WD=WD*RPI
      WI=WI*RPI
      ED=ED*RPI
      EI=EI*RPI
*
    5 READ(7,*,END=55)ZM,R
      ZM=ZM*1000.*100.
      R=R*1000. *100.
*
*     X,Y,Z-POSITION OF MODEL w.r.t ORIGIN IN KM.
*     WRITE(6,*)' X AND Y POSITION OF SPHERE '
      READ(7,*)XMM,YMM
      XM=XMM  *1000.   *100.
      YM=YMM  *1000.   *100.
*     YINT,XINT-SAMPLE INTERVAL / MAX,MIN FOR X,Z
      XINT=XINT   *1000. *100.
      YINT=XINT   *1000. *100.
      XMIN=0.
      XMAX=(NO-1)*XINT  *1000. *100.
      YMIN=0.
      YMAX=(NO-1)*XINT  *1000. *100.
      WRITE(6,14)
   14 FORMAT('   ZM,R,ED,EI,W,WD,WI,RHO')
      WRITE (6,80)ZM,R,ED,EI,W,WD,WI,RHO
   80 FORMAT(8F8.2)
      WRITE (6,81)XM,YM,ZM,XINT,XMIN,XMAX,YINT,YMIN,YMAX
   81 FORMAT(9F8.2)
*     TO CALCULATE THE GRAVITY AND MAGNETIC ANOMALY
*     FOR GRAVITY PARAMETERS
      PARA=(4./3.)*PI*R**3.*RHO*6.672E-8
*     FOR MAGNETIC PARAMETERS
      EY=COS(ED)*COS(EI)
      EX=COS(EI)*SIN(ED)
      EZ=SIN(EI)
*
      WY=W*COS(WD)*COS(WI)
      WX=W*COS(WI)*SIN(WD)
```

```
*
      WZ=W*SIN(WI)
*
      PER=1.
      PAM=(PER*(R**3))/3.
*
      NX=INT(XMAX-XMIN)/XINT
      NY=INT(YMAX-YMIN)/YINT
      ZZ=   (ZM)
      M=1
      DO 35 J=1,NY
      DO 30 I=1,NX
      XX=XMIN+((I-1)*XINT)-XM
      XC=XMIN+FLOAT(I-1)*XINT
      YC=YMIN+FLOAT(J-1)*YINT
      YY=YMIN+((J-1)*YINT)-YM
      RR=SQRT(XX**2+YY**2+ZZ**2)

*     THE GRAVITY ANOMALY
*     CONVERT TO MILLIGAL
      G(I,J)=PARA*(ABS(ZZ)/(RR*RR*RR))
      G(I,J)=G(I,J)*1000.0
      G1(I,J)=G1(I,J)+G(I,J)

*     MAGNETICS
       FF1=EX*WX*(3*XX**2-RR**2)
       FF2=EY*WY*(3*YY**2-RR**2)
       FF3=EZ*WZ*(3*ZZ**2-RR**2)
       FF4=3*(EX*WY+EY*WX)*XX*YY
       FF5=3*(EX*WZ+EZ*WX)*XX*ZZ
       FF6=3*(EY*WZ+EZ*WY)*YY*ZZ
*     MAGNETIC ANOMALY
      F(I,J)=(PAM/(RR**5))*(FF1+FF2+FF3+FF4+FF5+FF6)
      F1(I,J)=F1(I,J)+F(I,J)
*
      M=M+1
   30 CONTINUE
    35 CONTINUE
      GOTO 5
   55  CONTINUE
      DCON=1000.*100
      WRITE(6,*)' FILE FOR MAGNETIC DATA '
      WRITE(8,16)NX,NY,XINT/DCON,YINT/DCON,XMIN/DCON,XMAX/DCON,
     +YMIN/DCON,YMAX/DCON
      WRITE(6,*)' FILE FOR GRAVITY  DATA '
      REWIND 16
      WRITE(10,16)NX,NY,XINT/DCON,YINT/DCON,XMIN/DCON,XMAX/DCON,
     +YMIN/DCON,YMAX/DCON
    16 FORMAT(2I10,/,6F10.2)
      WRITE(8,40)(( FLOAT(M-1),F1(I,J),FLOAT(I-1 )*(XINT/DCON)
     +,FLOAT(J-1  )* (XINT/DCON), I=1,NX),J=1,NY)
      WRITE(10,40)(( FLOAT(M-1),G1(I,J),FLOAT(I-1 )*(XINT/DCON)
     +,FLOAT(J-1  )* (XINT/DCON), I=1,NX),J=1,NY)
```



```
*
   40 FORMAT( F10.2,F15.3,2F10.2)
      STOP
      END
```

```
*                       APPENDIX  4.1
*
*
*                       PROGRAM  FDHEAT
*
*     A FINITE DIFFERENT ROUTINE TO CALCULATE THE CRUSTAL TEMPERATURE
*     DISTRIBUTION  DUE TO FRICTIONAL HEATING ON A FAULT  USING THE
*     TIME DEPENDENT HEAT   CONDUCTION  EQUATION.
*     STEADY HEAT GENERATION ON THE FAULT IS ASSUMED.
*     THE ROUTINE FIRST CALCULATES
*     (1) THE NORMAL   TEMPERATURE DITRIBUTION IN THE CRUST
*         USING THE EQUATION OF TURCOTTE AND  SCHUBERT 1982, THEN
*     (2) THE TEMPERATURE RISE ON THE FAULT PLANE  USING GEBHART (1971)
*         PROCEDURE AND
*     (3) CALCULATES THE TEMPERATURE DISTRIBUTION USING BARAKAT (1966)
*         EXPLICIT FINITE DIFFERENCE METHOD.
*
**** Input:   UNIT 7 (the file name has been set to INDAT)
*           All input  are in free format.
*
*  LINE 1 SPAN,SINT
*          SPAN        The total time of fault movement.
*          SINT        The time increament  for each iterations
*                   The no of iteration is the integer of  (SPAN/SINT)
*  LINE 2 XL,ZMAX
*          XL and ZMAX  max. distance in x and z direction where the
*                       temperature increase after each time increament is
*                       not expected to affect the boundary conditions (km)
*                       The sampling interval is set at 1x1 km square grid.
*  LINE 3 ICHO,ICHO1
*            ICHO   1    Use a linear temperature increase of 20 degrees C/km
*            ICHO   3    Use an exponential crustal temperature distribution
*            ICHO1  0    Use ICHO temperature  distribution as the initial
*                        temperature condition
*            ICHO1  1    The initial temperature distribution is set to zero
*                        ICHO=2
*  LINE 4 QS, D, HS
*            QS          Surface heat flow  (mW/m2)
*            D           Characteristic depth  (km)
*            HS          Heat   production   (microW/m3)
*  LINE 5 SH, RHO, TK
*            SH          Specific heat  (kJ/kg K)
*            RHO         Density        (kg/m3)
*            TK          Thermal conductivity  (W/m K)
*  LINE 6 RM, STMAX, ZKB
*            RM          Rate of fault movement    (m/year)
*            STMAX       Maximum shear stress   (MPa)
*            ZKB         The depth where  the shear stress is small
*                        (may be assumed to be the Moho)
*
```



```
*  LINE 7 TO,GR
*            TO          Surface temperature in degrees C
*            GR          The value of linear geothermal gradient
*                        if ICHO=1 else
*
*
**** Output:  UNIT  8
*
*   LINE 1  IX,KZ
*             IX         No of data points in x direction
*             KZ         No of data points in z direction (depth)
*   LINE 2 DELX,DELZ,XMIN,XMAX,ZMIN,ZMAX
*             DELX       Sampling interval in x direction
*             DELZ       Sampling interval in z direction
*             XMIN,XMAX  Minimum and maximum in x direction
*             ZMIN,ZMAX  Minimum and maximum in y direction
*   LINE 3  TO  LINE IX*IZ
*           T(I), X, Z
*             T(I)      The crustal temperature distribution in
*                       (degree C) at point (X,Z)
*
*      The results  are  plotted using Ghost80.
*
*
*      Compile: r *fortranvs scards=FDHEAT
*      run    : r -load+*Ghost 7=INDAT   8=OUTPUTFILE
*

      DIMENSION TT(8100),W(8100),TPO(90),CL25(10),CL100(8)
      COMMON
     1 /VAR1/UU(8100),UL(8100),VU(8100),VL(8100),T(8100)
     2 /VAR2/IX,KZ,TD,DELX,DELT,QS,QD,D
     3 /VAR3/TP(8100)
     4 /VAR4/SH,RHO,ST,RM,DELZ,STMAX,ZKL,ZKB,HS,ICHO
     5 /VAR5/CTSEC,CMIL ,CDIST,IA,TK
     6 /VAR6/ZP(100),TG20(100),TG25(100),TPP(100)
     7 /VAR7/SP(100)

      INTEGER  RES
      CHARACTER*7 RESUL

       DATA CL25/25.,50.,75.,100.,125.,150.,175.,200.,225.,250./
       DATA CL100/100.,200.,300.,400.,500.,600.,700.,800./

      OPEN(7,FILE='INDAT')

*     SET PARAMETERS

      CALL TIME(0)
*    conversion to million
      CMIL=1000000.
```

```
*
*    conversion year to sec
      CYSEC=   356.25 * 24.* 60.* 60.
*    conversion from 1 My to sec
      CTSEC  =     CYSEC * CMIL
*    time interval, total time and no of time increament
      READ(7,*)SPAN,SINT
      DELT=SINT   *CTSEC
      SPAN =SPAN  *CTSEC
      NTIME=INT(SPAN/DELT)+2
      ATIME=DELT

*   distances  conversion   km to  m
      CDIST=1000.
      READ(7,*)XL,ZMAX
*   depth , sampling depth
      ZMAX=ZMAX *CDIST
      DELZ=1.*CDIST
*     distance away from the fault, sampling distance.
      XL=XL *CDIST
      DELX=1.*CDIST

*   pressure conversion  from MegaPa to kg/m2/s2
      CPRES=1.E+6

*   nodes  determine no of nodes
      IX=INT(XL/DELX)
      KZ=INT(ZMAX/DELZ)


*   plot  limits
      XMIN=0.0
      ZMIN=0.0
      XMAX=XL
      ZMAX=ZMAX

      READ(7,*)ICHO,ICHO1
      READ(7,*)QS,D,HS
*     convert milli W/m to W/m
      CHF=1.E-3
      QS=QS*CHF
*     convert km to m  metre
      D=CDIST*D
*     convert micro W/m to W/m
      HS=HS*1.E-6
*
      READ(7,*) SH,RHO,TK
*     specific heat in m2/s2 K
      SH=SH*1.E+3
*    thermal diffusivity
      TD=(TK/(RHO*SH))
      FFF=DELX**2/(4.*TD)
*
```



```
*
      READ(7,*)RM,STMAX,ZKB
*     rate / sec
      RM=RM/CYSEC
*    maximum pressure  STMAX   AT ZKL (determine in prog.
*    and exponential decrease to ZKB
*     km to m
      ZKB=ZKB*CDIST
*     MegaPa to  kg/m/s2
      STMAX=STMAX*CPRES
      READ(7,*)TO, GR
*    conversion   to cent. / metre
      GR=GR/CDIST

*     initialised array for TIME=0
*     set all arrays to initial condition (temperature distribution)
*
      IK=0
      WRITE(11,*)IX,KZ,DELX,DELZ,0.,IX*DELX,0.,DELZ*KZ
      DO 1 I=1,IX
      DO 1 K=1,KZ
      IK=IK+1
*     Linear crustal temperature distribution  (only for testing)
*         TZ = TO + GR* Z
*              Z    depth (metres)
*              TZ   Temperature in degrees C
      Z=FLOAT(K-1)*DELZ
*    The  crustal   tempeature distribution using Turcotte and Schubert
*    1982 formula  assumes that the radiogenic heat decays exponentially
*    with depth
*
*                 QD*Z    (QS-QD)*D*(1 - exp(-(Z/D)))
*     TZ = TO +  ----  +  ---------------------------     where  (QS-QD) = HS D
*                  K                  K
*
*
*    choose crustal temperature distribution
      IF(ICHO.EQ.1)   T00= TO + GR*Z
      IF(ICHO.EQ.3)T00=TO+(QS-HS*D)*Z/TK+(HS*D*D*(1.-EXP(-(Z/D))))/TK
      W(IK)=T00
      WRITE(11,100)FLOAT(IK),W(IK),FLOAT(I),FLOAT(K)
      IF (ICHO1.EQ.0) THEN
      TT(IK)=T00
      T(IK)=T00
      UL(IK)=T00
      VL(IK)=T00
      UU(IK)=T00
      VU(IK)=T00
      ELSEIF (ICHO1.EQ.1) THEN
*     Initial temperature condition set to zero
      T00=0.0
      TT(IK)=T00
      T(IK)=T00
```

```
      UL(IK)=T00
      VL(IK)=T00
      UU(IK)=T00
      VU(IK)=T00
      ELSEIF (ICHO1.NE.0.OR.ICHO1.NE.1) THEN
      WRITE(6,*) ' Wrong ICHO1 '
      STOP
      ENDIF
      ZP(K)= Z /CDIST
      TPP(K)=T00
    1 CONTINUE
*     Barakat' formula is
*
*   Forward iteration
*     UU(i,j)=a UL(i,j) + b (UU(i-1,j) + UL(i+1,j)) + c (UU(i,j-1) + UL(i,j+1))
*
*   Backward iteration
*     VU(i,j)=a VL(i,j) + b (UL(i-1,j) + VU(i+1,j)) + c (VL(i,j-1) + VU(i,j+1))
*
*     VL,UL - temperature at time  TIME
*     VU,UU - temperature at time  TIME+DELT
*                            --    1           1    --              1 - CONST
*     CONST= TD * DELT *     |   -----    +  -----   |          A = ---------
*                            |       2           2  |              1 + CONST
*                            --   DELX        DELZ  --
*
*           TD * DELT    /                              TD * DELT    /
*     B =   ---------   /  (1 + CONST)           C =    ---------   /  (1 + CONST)
*                 2    /                                      2    /
*             DELX    /                                     DELZ    /
*
*   grid system
*        1 2 3 4 5 . . . . .    IX
*      1  -------------------------XL      1  9----------------------
*      2 |                                 2 10
*      3 |                                 3 11   IK nodes
* k    . |                 transform to    4 12
*      . |                                 5 13
*        |                                 6 14
*     KZ |                                 7 15
*       ZMAX                               8 16
*
*   set up constants
      CONST= TD  * DELT * ((1/DELX**2)+(1/DELZ**2))
      A=(1-CONST)/(1+CONST)
      B=((TD*DELT)/DELX**2)/(1+CONST)
      C=((TD*DELT)/DELZ**2)/(1+CONST)

*   loop for total  time
      ATIME=0.
      IFIL=0
```



```
      DO  7 ITIME=1,NTIME
*   TIME lapse DELT*ITIME, evaluate  the temperature distribution at ITIME
*   temperature increase. Call routine BAR4 :to calculate and add
*   the temperature increase after DELT increament.
      NPT= INT(SPAN/SINT)
C     NPT=400
            IA=MOD(ITIME,NPT)
      IF (IA.EQ.0)WRITE (6,*)'TIME ',ATIME/CTSEC,' MOD TIME  ',IA,
     1' NO OF ITER. ', ITIME
      CALL BAR4
*   only temperatures at the internal nodes will be calculate (temperatures at
*   the boundaries at level TIME and TIME+DELT are known
*   First calculate the FORWARD algorithm
      IK=KZ-1
      DO 4 I=2,IX-1
      IK=IK+2
      DO 4 K=2,KZ-1
      Z=FLOAT(K-1)*DELZ
      IK=IK+1
      IF (ICHO1.EQ.1)
     1UU(IK)=A*UL(IK)+B*(UU(IK-KZ)+UL(IK+KZ))+C*(UU(IK -1)+UL(IK+1))
      IF (ICHO1.EQ.0)
     2UU(IK)=A*UL(IK)+B*(UU(IK-KZ)+UL(IK+KZ))+C*(UU(IK -1)+UL(IK+1))
     3 +HS*EXP(-(Z/D))*TD* DELT/TK
    4 CONTINUE
*   then calculate the BACKWARD algorithm
      IK= IX*KZ-KZ +2
      DO 5 I=IX-1,2,-1
      IK=IK-2
      DO 5 K=KZ-1,2,-1
      Z=FLOAT(K-1)*DELZ
      IK=IK-1
      IF (ICHO1.EQ.1)
     1VU(IK)=A*VL(IK)+B*(VL(IK-KZ)+VU(IK+KZ))+C*(VL(IK-1)+VU(IK+1))
      IF (ICHO1.EQ.0)
     2VU(IK)=A*VL(IK)+B*(VL(IK-KZ)+VU(IK+KZ))+C*(VL(IK-1)+VU(IK+1))
     3 +HS*EXP(-(Z/D))*TD* DELT/K
    5 CONTINUE
      IK=0
      DO 6 I=1,IX
      DO 6 K=1,KZ
      IK=IK+1
      Z=FLOAT(K-1)*DELZ
*   only then calculate the true temperature distribution (average of the
*   forward  and  backward solution)
      T(IK)=(VU(IK)+UU(IK))/2.
*     Reset the values of array at time TIME  using present temperature
      VL(IK)=T(IK)
      UL(IK)=T(IK)
*     ARRAY TO CHECK THE TEMP AT  XMAX.
      T20(K)= T(IK)
    6 CONTINUE
```

```
*
      CALL TIME(1,0,RES)
      WRITE (6,*)'I  ',ITIME
*   Only for ploting the result
      ATIME=ATIME+DELT
      IF (IA.EQ.0) THEN

*     Rearange data for plotting the calculated   temperature

      IFIL=IFIL+1
      IXN=INT(IX*1.)
      XLL=IXN*DELX
      CALL PAPER(1)
      CALL MAP(0.0,XLL/CDIST,-ZMAX/CDIST,0.0)
      CALL PSPACE(.1,.9,0.0,.1)
      CALL CTRMAG(15)
      CALL XAXISI(10.)
      CALL PSPACE(.1,.9,.1,.9)
      CALL BORDER
      CALL YAXISI(10.0)

      KI=0
      KIA=0
      WRITE(8,101)IX,KZ,DELX,DELZ,0.,IX*DELX,0.,KZ*DELZ
 101  FORMAT(2I10,/,6F10.2)
      DO 9 I=1,IX
      DO 9 K=1,KZ
      KIA=KIA+1
      WRITE(10,100)T(KIA),FLOAT(I),FLOAT(K)
 100  FORMAT(4F15.3)
      IF(I.GT.IXN)GOTO     9
      KI=KI+1
      IK=IXN*(KZ-K)+I
      TP(IK)=T(KI)
      W(IK)=TT(KI)
    9 CONTINUE
      NW=IX*KZ * 2
      XLLX=XLL/1000.
      ZMAXZ=ZMAXZ/1000.
      IF (ICHO1.EQ.0) THEN
      CALL CONTRA(W,1,IXN,IXN,1,KZ,KZ,CL100,1,8)
      CALL CONTRA(TP,1,IXN,IXN,1,KZ,KZ,CL100,1,8)

      ELSEIF (ICHO1.EQ.1) THEN

      CALL CONTRA(TP,1,IXN,IXN,1,KZ,KZ,CL25,1,10)
      ENDIF
*     Rearange data for plotting the geothermal gradient
      KI=0
      DO 13 I=1,IX
      DO 13 K=1,KZ
      KI=KI+1
      IK=IX*(KZ-K)+I
```



```
*
      TP(IK)=TT(KI)
      TPO(KI-1)=T(KI-1 )
       TMAX=AMAX1(TMAX,T(K))
CCC   WRITE(7,*)IK,KI
   13 CONTINUE

      CALL CTRMAG(18)
      CALL CSPACE(0.0,0.6,0.4,0.8)
      CALL CTRORI(90.)
      CALL PLACE(1,1)
      CALL TYPECS(' DEPTH  (km)')
      CALL CTRORI(0.0)
      CALL CSPACE (0.35,1.0,0.0,0.045)
      CALL PLACE(1,1)
      CALL TYPECS('DISTANCE  (km)       ')
      CALL TIME(1,0,RES)
      CALL TYPENI(RES)
      CALL CTRMAG(16)
      CALL TYPECS('  millisec')
      CALL FRAME
      CALL GREND
      ENDIF
       TMAX=AMAX1(TMAX,T(I))
    7 CONTINUE
*     Rearange plot data for plott IN GHOST  to  check first initial values
      KI=0
      IXN=INT(IX*1.0)
      XLL=IXN*DELX
      XLLL=XLL/1000.
      ZMAXL=ZMAX/1000.
      DO 99 I=1,IX
      DO 99 K=1,KZ
      IF (I.GT.IXN) GOTO 99
      KI=KI+1
      IK=IXN*(KZ-K)+I
      TP(IK)=TT(KI)
   99 CONTINUE

*    set arrays for  plot IN GHOST80
      TMAX=0.
      DO 8 K=1,KZ
      Z=FLOAT(K-1)*DELZ
      TG20(K)=FLOAT(K-1)*20
      TG25(K)=FLOAT(K-1)*25
      ZP(K)=Z
      IF(ICHO.EQ.1)   T00= TO + GR*Z
      IF(ICHO.EQ.3)T00=TO+(QS-HS*D)*Z/TK+(HS*D*D*(1.-EXP(-(Z/D))))/TK
      TPP(K)=T00
    8 CONTINUE
```

```
*
*     GHOST 80 PLOT
      CALL PAPER(1)
       ZKB=ZKB/CDIST
       ZKL=ZKL/CDIST
       STMAX=STMAX/CPRES
       ZMA=ZMAX/CDIST
       DO   55 K=1,KZ
       ZP(K)=ZP(K)/CDIST
       SP(K)=SP(K)/CPRES/100.
   55  CONTINUE
C     IF(ICHO.EQ.3)   QD=QS/CHF-HS*1.E+6 *D/CDIST
      CALL PSPACE(.1,.65,.35,.95)
C     CALL MAP(0.,TMAX,ZKB,0.)
      CALL MAP(0.,700.,ZMA,0.)
      CALL CTRMAG(15)
      CALL CSPACE(.11,.95,.30,.50)
      CALL PLACE(1,1)
      CALL TYPECS( 'Crustal temp. dist.')
      CALL PLACE(1,3)
      CALL TYPENC(248)
      CALL TYPECS( '  20 degree/km')
      CALL PLACE(1,4)
      CALL TYPENC(232)
      CALL TYPECS( '  25 degree/km')
      CALL PLACE(1,5)
      CALL TYPENC(176)
      CALL TYPECS( '  Expnoential ')
      CALL PLACE(45,5)
      CALL TYPECS( ' Shear stress')
      CALL BORDER
      IF (ICHO1.EQ.1) CALL CURVEO(TPO,ZP,1,KZ)
      IF (ICHO1.EQ.0) CALL CURVEO(TPP,ZP,1,KZ)
      CALL PTPLOT(TG20,ZP,1,KZ,248)
      CALL CURVEO(TG20,ZP,1,KZ)
      CALL PTPLOT(TG25,ZP,1,KZ,232)
      CALL CURVEO(TG25,ZP,1,KZ)
      CALL AXESSI(100.,2.)
      CALL CSPACE(.25,.65,.95,1.0)
      CALL CTRMAG(18)
      CALL TYPECS(' degree C ')
      CALL CSPACE(.00,.07,.5,.9)
      CALL CTRORI(90.)
      CALL TYPECS('  DEPTH  (km)        ')
      CALL CTRORI(0.)
      CALL PSPACE(.65,.9,.35,.95)
      STTT=STMAX/100.
C     CALL MAP(0.,STTT,ZKB,0. )
      CALL MAP(0.,STTT,ZMA,0. )
      CALL FULL
      CALL CSPACE(.7,.9,.95,1.0)
      CALL CTRMAG(15)
      CALL TYPECS(' x100 MPa     ')
```



```
*
      CALL CTRMAG(12)
      CALL CURVEO(SP,ZP,1,KZ)
      CALL BORDER
      CALL XAXISI(1.)
      CALL CSPACE(.1,.9,.10,.33)
      CALL PLACE(1,2)
      CALL TYPECS('  D =')
      D=D/CDIST
      CALL TYPENF(D,1)
      IF (ICHO.EQ.3)THEN
      CALL TYPECS(' km,  HS =')
      HS=HS*1.E+6
      CALL TYPENF(HS,1)
C     CALL TYPECS('  {qd =')
C     CALL TYPENF(QD,1)
C     CALL TYPECS(' m/m2)')
      ENDIF
      CALL TYPECS(' miW/m2,  QS =')
      QS=QS/CHF
      CALL TYPENF(QS,1)
      CALL TYPECS(' mW/m2,')
      CALL PLACE(1,6)
      CALL TYPECS('  STMAX =')
      CALL TYPENF( STMAX,1)
      CALL TYPECS(' MPA,  RM =')
      RM=RM*CYSEC
      CALL TYPENF(  RM,3)
C     CALL TYPECS(' m/year, BASE =')
      CALL TYPECS(' m/year'        )
      CALL TYPENF(ZKB,1)
C     CALL TYPECS(' km,')
      CALL PLACE(1,4)
      CALL TYPECS('  RHO=')
      CALL TYPENF( RHO,1)
      CALL TYPECS(' kg/m3,')
      CALL TYPECS('  C =')
      SH=SH/1.E+3
      CALL TYPENF( SH,2)
      CALL TYPECS(' kJ/kg K,  K =')
      CALL TYPENF(TK,2)
      CALL TYPECS(' W/m  K.')
      CALL FRAME
      CALL GREND
      STOP
      END

       SUBROUTINE BAR4
*      Routine to calculate
*      (1) heat generated on a fault plane due to frictional heating
*      (2) the temperature rise on the fault due to this excess heat.
*
*      ST = stress at the fault [kg/m/s2]
```

```
*     RM = rate of fault movement [m/s]
*     AZ  = heat generation  [J/m2/s  ]   (J = kg m2/s2)
*     SH = specific heat [ m2/s2/degree K]
*     RHO= density       [kg/ m3]
*     DELT=              [s].
*                        .
*   -X             x=0 . DELY      +X
*                  Td.
*              A    |    D
*               . . | . .
*               .   |   .              Ta-Tb=2*DELX
*         Ta - - - To- - - Tb           Tc-Td=2*DELY
*               .   |   .
*               . . | . .
*              B    |    C
*                   Tc
*                  FAULT
*
*
*     Heat generation   A = ST * RM
*     Total heat generation in time DELT  along surface DELY * DELZ is
*                       A = ST * RM * DELT * (DELY * DELZ)
*
*     Total heat in   DELX *   DELY * DELZ  m3  (block ABCD)
*                       TI =   DELX * DELY * DELZ * RHO * SH * del T
*              del T = ave. temp.  diff. in block ABCD
*
*     Temperature rise due energy produce by fault movement is
*                                          DELT
*                       Tz =  STz   * RM  ---------------        EQUATION 1
*                                          DELX * RHO * SH
*           2    2     2    2
*     In   d T/dx  +  d T/dx  + A/K = (1/k)(dT/dt), A   is the energy
*     generated to cause the above temperature rise. Using the finite
*     difference procedure the temperature  along the fault  is
*
*     t+DELT                    t                    2
*     To     = F(Ta+Tb+Tc+Td) + To(1-4F) + (A'''/K) DELX  F          EQUQTION 2
*                          2
*          F= k * DELT / DELX
*                                                          2
*    The rise in temperature due to heat generated, (A/K) DELX  F = Tz
*
*     Total heat generated in   DELZ * DELY in DELT is
*                                Atot = ST * RM *   DELZ * DELY * DELT   [J]
*     This energy is contained in volume    ABCD
*                                 V =   DELX *   DELZ * DELY
*     i.e. Energy per unit volume and time is
*                 A = Atot / (V * DELT) = ST * RM  / DELX
*
*
```



```
*
**************************************************************************
      COMMON
     1 /VAR1/UU(8100),UL(8100),VU(8100),VL(8100),T(8100)
     2 /VAR2/IX,KZ,TD,DELX,DELT,QS,QD,D
     4 /VAR4/SH,RHO,ST,RM,DELZ,STMAX,ZKL,ZKB,HS,ICHO
     5 /VAR5/CTSEC,CMIL ,CDIST,IA,TK
     7 /VAR7/SP(100)
*    determine the  depth for the maximum shear stress assuming the depth is at
*    the transition brittle/ductile zone (300-350 degrees C). Use 325
      TZL=325.
      TZZ=0.
      TO=0
      DO 2 K=1,KZ
      ZK=FLOAT(K-1)*DELZ
     IF(ICHO.EQ.3)TZZ=TO+(QS-HS*D)*ZK/TK+(HS*D*D*(1.-EXP(-(ZK/D))))/TK
C    IF(ICHO.EQ.1)TZZ=TO+(QS-HS*D)*ZK/TK+(HS*D*D*(1.-EXP(-(ZK/D))))/TK
      IF (TZZ.LE.TZL)  ZKL=ZK
    2 CONTINUE
*   determine parameters for exponential decrease of shear stress assuming thet
*   the shear stress below the moho is small (at Moho assumed to be 0.1*STMAX
      ALPHA=ZKB/ZKL
      ST2=STMAX*0.1
      BETA=STZ/STMAX
      ANN=ALOG(1.-ALOG(BETA))/ALOG(ALPHA)
*    loop for points of increasing depth at fault plane
      I=1
C     IF (ICHO.EQ.1) ZKL=19.
      DO 1 K=2,KZ-1
*    set the depth
      ZK=FLOAT(K-1)*DELZ
*    calculate stress at depth Zk assuming maximum stress on transcurrent fault
*  of STMAX (DEGREES) with linear increase to ZKL linear decrease to ZKB (Moho)
      IF (ZK.LE.ZKL) THEN
      G20=STMAX/ZKL
*    stress between surface to ZKL
      ST=ZK*G20
C****  assume ST=STMAX  as in Scholtz   FOR TEST
C     IF(ICHO.EQ.1)  ST=STMAX
      ELSEIF (ZK.GT.ZKL) THEN
*    stress between ZKL to ZBL
      IF(ICHO.NE.1) ST=STMAX*EXP(1.-(ZK/ZKL)**ANN)
C****  assume ST=0    as in Scholtz      FOR TEST
C     IF(ICHO.EQ.1) ST=0.
      ENDIF
      SP(1)=0.0
      SP(KZ)=STZ
      SP(K)=ST
*    calculate heat produced
      AZ=  ST * RM
*    time-distance constant relationship FF<=4 for 2-D case for spacing x=z
      FF=TD*DELT *(1./DELX**2)
*                   USE CONDUCTIVITY-DISTANCE-F function  for method 2
```

```
*
      TI = DELX * FF/ (TK      )
      TII = AZ * TI
*     calculation of temperature at the fault using EQUATION 2
*     index for Ta,Tb,Tc,Td (Ta=Tb) and To
       ITB=K+KZ
        ITC=K+1
        ITD=K-1
        ITO=K
        TABCD=(T(ITB)*2 + T(ITC)+T(ITD))*FF
        TOF=((1.0-4.*FF)*T(ITO))
*     NEW  temperature at x(0)  AFTER time DELT
       T1= TABCD+TOF+TII
 10    FORMAT(8E10.3,/,8E10.3,/,E10.3)
*     reset temperature  USE IN THE ITERATION at X(0)
*     to accomodate increase  in temp.
      UU(K  )=T1
      VU(K  )=T1
    1  CONTINUE
       RETURN
       END
```